THERMODYNAMICS OF METAL HYDRIDES FOR HYDROGEN STORAGE APPLICATIONS USING FIRST PRINCIPLES CALCULATIONS

A **Thesis**

Presented to

The Academic Faculty

by

Ki Chul Kim

In Partial Fulfillment

of the Requirements for the Degree

DOCTOR OF PHILOSOPHY in the

School of Chemical and Biomolecular Engineering

Georgia Institute of Technology

August 2010

THERMODYNAMICS OF METAL HYDRIDES FOR HYDROGEN STORAGE APPLICATIONS USING FIRST PRINCIPLES CALCULATIONS

Approved by:

Dr. David S. Sholl, Advisor
School of Chemical and Biomolecular Engineering
Georgia Institute of Technology

Dr. Martha Grover
School of Chemical and Biomolecular Engineering
Georgia Institute of Technology

Dr. Tom Fuller
School of Chemical and Biomolecular Engineering
Georgia Institute of Technology

Dr. Seung Soon Jang
School of Materials Science and Engineering
Georgia Institute of Technology

Dr. Paul A. Kohl
School of Chemical and Biomolecular Engineering
Georgia Institute of Technology

Date Approved: [06. 24, 2010]

To my parents,

For their love and support.

To my sister,

Somi,

For always being with parents instead of me.

ACKNOWLEDGEMENTS

First of all, I would like to thank my advisor, Professor David S. Sholl for his most invaluable guidance and assistance for the past four years. Professor Sholl was a mentor for my life as well as an advisor for my research to me. I could rigorously learn how I would be a real research scientist through his advice and thus the past four years for which I have studied here would be the happiest moment in my entire life.

I would also like to thank many friends in our group, department, South Korea for their kindness. Especially, I would like to thank Byoungnam Park and Sung Gu Kang for their excellent research discussions and invaluable friendship. I will not forget every happy memory that they gave me. I would also like to thank Taku Watanabe, Ji Zang, and my office mate, Emmanuel Haldoupis for many happy memories and friendship. I would also like to thank Hyung Suk Kim who is my best friend in South Korea. He was always pleased whenever I visited South Korea.

Special thanks to Professor J. Karl Johnson at University of Pittsburgh and Dr. Mark D. Allendorf at the Sandia National Lab. for their excellent discussions in my research. I would also like to Professor Tom Fuller, Professor Paul Kohl, Professor Martha Grover, and Professor Seung Soon Jang for their helpful comments and questions as my Ph.D thesis committee.

Finally, the successful completion of my Ph.D study would have been not possible without the continuous support and love of my parents and sister. I am grateful to God that makes it possible that they were, are, and will be always with me. I would like to thank to my parents and sister for their love.

TABLE OF CONTENTS

LIST OF TABLES

Page

LIST OF FIGURES

Page

SUMMARY

Metal hydrides are promising candidates for H_2 storage, but high stability and poor kinetics are the important challenges which have to be solved for vehicular applications. Most of recent experimental reports for improving thermodynamics of metal hydrides have been focused on lowering reaction enthalpies of a metal hydride by mixing other compounds. However, finding out metal hydride mixtures satisfying favorable thermodynamics among a large number of possible metal hydride mixtures is inefficient and thus a systematic approach is required for an efficient and rigorous solution. Our approaches introduced in this thesis allow a systematic screening of promising metal hydrides or their mixtures from all possible metal hydrides and their mixtures. Our approaches basically suggest two directions for improving metal hydride thermodynamics. First, our calculations for examining the relation between the particle size of simple metal hydrides and thermodynamics of their decomposition reactions provide that the relation would depend on the total surface energy difference between a metal and its hydride form. It ultimately suggests that we will be able to screen metal hydride nanoparticles having favorable thermodynamics from all possible metal hydrides by examining the total surface differences. Second, more importantly, we suggest that our thermodynamic calculations combined with the grand canonical linear programming method and updated database efficiently and rigorously screen potential promising bulk metal hydrides and their mixtures from a large collection of possible combinations. The screened promising metal hydrides and their mixtures can release H_2 via single step or multi step. Our additional free energy calculations for a few selected promising single step reactions and their metastable paths show that we can identify the most stable free energy paths for any selected reactant mixtures. In this thesis, we also demonstrate that a total free energy minimization method can predict the possible evolution of impurity other than H_2 for several specified mixtures. However, it is not ready to predict reaction thermodynamics from a large number of compounds.

CHAPTER 1

INTRODUCTION

1.1 Hydrogen Energy as Alternative Energy

Hydrogen energy is one of the alternative energy candidates which are being considered as a replacement for fossil fuels. Hydrogen can be produced from a various sources including coals, natural gases, and ultimately water. It is non-toxic and environmentally clean energy as water would only remain after the cyclic usage of the energy.

The automobile industry, one of the main potential applications of hydrogen energy, requires stored hydrogen for mobile applications. Therefore, methods to store H_2 with appropriate weight and volume are important for successful applications.[1] The development of a hydrogen storage device having light weight and high capacity is necessary condition to enable fuel cell vehicles to replace fossil fuel vehicles. More importantly, the developed vehicle should be operated at temperatures of 50 ~ 150 °C and pressures of 1 ~ 100 bar.[2-6] The vehicle should also have a fast recharge/discharge cycle.[7-12]

1.2 Hydrogen Storage System

1.2.1 Metal Hydrides as Promising Hydrogen Storage Method

H_2 can be stored as compressed gas or liquid, but these methods are not suitable for automobile applications.[1, 13, 14] Unlike these storage methods, metal hydrides storing H_2 in an atomic form in a solid state material have high gravimetric and volumetric densities.[1, 15, 16] The mechanism for metal hydrides storing/releasing H_2 is defined by solid-state hydrogenation/dehydrogenation reactions, so favorable thermodynamics and fast kinetics of the reactions involving metal hydrides are key factors for practical applications.[2-6, 9-12, 17-22] Favorable reaction thermodynamics would ideally allow reversibility of the reaction at

appropriate temperature (50 ~ 150 ˚C) and pressure (1 ~ 100 bar) ranges.[2-6] On the other hand, kinetics of a reaction can (at least in principle) be enhanced by the appropriate catalysts such as V or Ti if the metal hydrides have favorable thermodynamics.[8, 12] Therefore, the reaction thermodynamics of metal hydrides have been studied extensively.[2-6, 18, 23, 24] Representative materials which have been studied are $LiBH_4$ and $Mg(BH_4)_2$.[18, 23, 24] These materials are good candidates for the hydrogen storage in the sense that they have high H_2 capacity of 18.5 wt.% and 14.9 wt.%.[18, 23, 24] However, they are limited by their unfavorable thermodynamics. For example, the temperatures required for desorption of H_2 from $LiBH_4$ and $Mg(BH_4)_2$ are 470 ˚C and 323 ˚C.[18, 23, 24]

1.2.2 Methods for Enhanced Metal Hydride Thermodynamics

One way to alter metal hydride reaction thermodynamics is to reduce the particle size of the metal hydride. There are reports that it could improve the reaction thermodynamics.[20, 25, 26] Wagemans et al.[25] and Cheung et al.[26] predicted that a reduction of the equilibrium temperature for H_2 release relative to bulk MgH_2 for MgH_2 clusters containing up to 50 Mg atoms. Li and Chen experimentally examined hydrogen release from MgH_2 nanowires of radii 20, 45, and 80 nm.[20] In this experiment, there was a little improvement in the reaction temperature for H_2 release.

Another more widely explored approach for improving the reaction thermodynamics of metal hydrides is to destabilize metal hydrides by reacting them with other materials.[2-6, 18, 27-29] Vajo et al. experimentally identified the destabilization reaction of $LiBH_4$ using MgH_2.[27, 28] They obtained a destabilization reaction having the reaction temperature of 543 ~ 613 K that is 100 K lower than the values of the decomposition reaction of $LiBH_4$. Pinkerton et. al.[29] and Aoki et al.[18] examined the destabilization reaction of $LiBH_4$ with $LiNH_2$ and identified a reaction produced $Li_4BN_3H_{10}$ as an intermediate material. Motivated by these observations, Alapati, Johnson, and Sholl identified a number of the destabilization reactions of complex metal hydrides using first principles calculations.[2-6] They examined all possible reactions which are obtained from a

database of 212 crystalline compounds, and identified 43 promising reactions that satisfy screening criteria expressed in terms of the 0 K reaction enthalpy (15 kJ/mol $H_2 \leq \Delta U_0 \leq 75$ kJ/mol H_2) and H_2 capacity (≥ 6.0 wt.%).[6]

1.3 Impurity Gases in Metal Hydride System

The reversibility of metal hydride reactions is a challenge in H_2 storage that is as serious as the problem of the reaction thermodynamics stated above. An irreversible reaction can potentially occur due to the evolution of an impurity gas such as N_2 or CH_4, or the production of a refractory material such as BN or TiB_2.[6, 30, 31] When H_2 is repeatedly discharged and charged in a metal hydride system, if an impurity gas (N_2, NH_3, CH_4, boranes, etc.) sourced from the metal hydride is evolved with H_2 in each cycle, the metal will be eventually exhausted and the new metal will have to be supplied into a vehicle for continuous operation. Some experimental reports show the evolution of such problematic impurity gases.[32, 33] Chen et al. observed that $LiNH_2$ decomposes to produce Li_2NH with NH_3.[32] Gross et al. detected small amounts of methane in the decomposition reaction of $LiBH_4$ within a carbon aerogel.[33]

Experimental observations of the possible evolution of the impurity gases in several interesting systems would be the first step to deal with this issue. $LiNH_2$, $LiBH_4$, and $Mg(BH_4)_2$ are good examples for the observation in the sense that most of the metal hydrides include N, C, or B having a potential for evolving impurity gases such as N_2, NH_3, CH_4, or boranes. As stated early, some experimental reports showed that lithium amide evolved NH_3 during its decomposition reaction.[32, 34-47] Another reports showed that a mixture of $LiNH_2$ and LiH did not evolve NH_3 during heating, concluding that LiH exothermically reacted with NH_3 evolved from $LiNH_2$ decomposition reaction.[32, 34-36, 43-46] Gross et al. experimentally observed small amounts of methane in decomposition of $LiBH_4$ within a carbon aerogel.[33] However, these observations need an additional effort for further understanding. At this point, the thermodynamic examination through computational method would be the next step for understanding the thermodynamic sources related to the evolution of the impurity gases.

1.4 Thesis Summary

The main purpose of this thesis is to predict dehydrogenation reaction schemes which release sufficient amounts of H_2 at appropriate temperature without the evolution of any impurity gases. We discuss two methods to accomplish this purpose. First, we examine the possibility for the positive or negative effect of the metal hydride particle size on its reaction temperature.[48] The computational details and the resulting effect are detailed in Chapter 2. Second, we focus on identifying promising metal hydride mixtures which have favorable thermodynamics and high H_2 capacity.[49-51] To examine the potentially promising reactions, we use a computationally efficient strategy developed by Alapati, Johnson, and Sholl[6] instead of calculating the thermodynamic quantities and H_2 capacity for every possible reaction scheme. This grand potential approach automatically identifies the minimum energy path for every possible mixture, and then screens potentially promising reaction mixtures having favorable thermodynamics from the identified reaction schemes. Chapter 3 describes the computational details of the approach and the promising single-step reactions involving $LiK(BH_4)_2$, KBH_4, or $NaBH_4$ that are identified by the method.[49] Our effort for predicting the promising single-step reactions is extended from $LiK(BH_4)_2$, KBH_4, or $NaBH_4$ involving reaction mixtures to a much larger number of mixtures in Chapter 4.[50] We carry out all of the examinations after updating the database of the crystal compounds constructed by Alapati, Johnson, and Sholl.[4, 6]

We examine promising single-step and multi-step reactions from large collection of crystalline compounds in Chapter 4. The grand potential approach described in Chapter 3 is used to predict promising single-step reactions. We use a modified grand potential approach to predict promising multi-step reactions. The modified approach is developed on the idea that an initial mixture partially releases H_2 at several different temperatures in a multi-step reaction scheme. That is, the approach traces sequential changes of the initial mixture with H_2 releases during one cycle of temperature from 0 K to 1000 K. Some of the predicted promising single-step and multi-step reactions are interesting in the sense that they release H_2 without producing any undesirable compounds. The computational details and the resulting reaction schemes are described in

Chapter 4.

The promising single-step reactions predicted in Chapter 4 are based on the grand potential approach which describes the most stable paths based on the reaction enthalpy changes at 0 K.[50] It is therefore possible that the predicted reaction thermodynamics may be not correct if the H_2 pressure is changed or the vibrational and entropic contributions are fully considered. For this reason, we are interested in identifying other reaction mechanisms having slightly higher 0 K reaction enthalpy than the original reaction scheme.[51] We refer the other reaction mechanisms as metastable reactions in the sense that they are metastable under the condition of 0 K reaction enthalpies.[51] We develop the new thermodynamic method modified from the original grand potential approach to examine all possible metastable paths of thirteen chosen promising single-step reactions.[51] We finally identify the minimum free energy paths of the promising single-step reactions by comparing the van't Hoff plots of all identified reaction paths.[51] The details of the computational method and result are described in Chapter 5.

The possible evolution of gases other than H_2 is another concern in our calculations.[52] Our grand potential approach is not available for the purpose, since it is based on the assumption that H_2 gas is the only gaseous phase in the system.[49-51] Instead, we use the FactSage program, which is a free energy minimization code designed to examine the thermodynamic equilibrium under the condition of the multiple gaseous phases. Specifically, we examine the possible evolution of impurity gases for N, C, or B containing metal hydride mixtures. We can understand the thermodynamic equilibrium relation of $N_2/H_2/NH_3$ mixture and the possible kinetic limitation of N_2 evolution through the decomposition reaction of $LiNH_2$. The details of the examination are described in Chapter 6.

1.5 REFERENCES

1. L. Schlapbach and A. Züttel, *Nature*, 2001, **414**, 353.
2. S. V. Alapati, J. K. Johnson and D. S. Sholl, *J. Phys. Chem. B*, 2006, **110**, 8769-8776.
3. S. V. Alapati, J. K. Johnson and D. S. Sholl, *J. Alloys Compd.*, 2007, **446**, 23-27.
4. S. V. Alapati, J. K. Johnson and D. S. Sholl, *Phys. Chem. Chem. Phys.*, 2007, **9**, 1438-1452.
5. S. V. Alapati, J. K. Johnson and D. S. Sholl, *J. Phys. Chem. C*, 2007, **111**, 1584-1591.
6. S. V. Alapati, J. K. Johnson and D. S. Sholl, *J. Phys. Chem. C*, 2008, **112**, 5258-5262.
7. B. Bogdanovíc and M. Schwickardi, *J. Alloys Compd.*, 1997, **253-254**, 1.
8. W. Luo and K. J. Gross, *J. Alloys Compd.*, 2004, **385**, 224.
9. J. Graetz, J. J. Reilly, J. G. Kulleck and R. C. Bowman, *J. Alloys Compd.*, 2007, **446**, 271-275.
10. F. E. Pinkerton, *J. Alloys Compd.*, 2005, **400**, 76-82.
11. A. Sudik, J. Yang, D. Halliday and C. Wolverton, *J. Phys. Chem. C*, 2007, **111**, 6568-6573.
12. T. Vegge, *Phys. Chem. Chem. Phys.*, 2006, **8**, 4853-4861.
13. *A Multiyear plan for the Hydrogen R&D Program: Rationale, Structure, and Technology Roadmaps; U.S. Department of Energy; http://www.eere.energy.gov/hydrogenandfuelcells/pdfs/bk28424.pdf*, 1999, 32.
14. *National Hydrogen Energy Roadmap; US Department of Energy; http://www.eere.energy.gov/hydrogenandfuelcells/pdfs/hydrogen_posture_plan.pdf*, 2002, 17.
15. H. Imamura, K. Masanari, M. Kusuhara, H. Katsumoto, T. Sumi and Y. Sakata, *J. Alloys Compd.*, 2005, **386**, 211-216.
16. M. Fichtner, J. Engel, O. Fuhr, O. Kircher and O. Rubner, *Mater. Sci. Eng. B*, 2004, **108**, 42-47.
17. J. Graetz and J. J. Reilly, *Scripta Materialia*, 2007, **56**, 835-839.
18. M. Aoki, K. Miwa, T. Noritake, G. Kitahara, Y. Nakamori, S. Orimo and S. Towata, *Appl. Phys. A*, 2005, **80**, 1409.
19. S. Li, P. Jena and R. Ahuja, *Phys. Rev. B*, 2006, **74**, 132106-132104.
20. W. Li, C. Li and H. M. J. Chen, *J. Am. Chem. Soc.*, 2007, **129**, 6710-6711.
21. O. M. Løvvik and S. M. Opalka, *Phys. Rev. B*, 2005, **71**, 054103.
22. J. Lu, Z. Z. Fang and H. Y. Sohn, *Inorg. Chem.*, 2006, **45**, 8749-8754.
23. K. Miwa, N. Ohba, S. Towata, Y. Nakamori and S. Orimo, *Phys. Rev. B*, 2004, **69**, 245120.
24. N. Ohba, K. Miwa, M. Aoki, T. Noritake, S.-i. Towata, Y. Nakamori, S.-i. Orimo and A. Zuttel, *Phys. Rev. B*, 2006, **74**, 075110-075117.
25. R. W. P. Wagemans, J. H. van Lenthe, P. E. de Jongh, A. J. van Dillen and K. P. de Jong, *J. Am. Chem. Soc.*, 2005, **127**, 16675 -16680.
26. S. Cheung, W.-Q. Deng, A. C. T. van Duin and W. A. Goddard, *J. Phys. Chem. A*, 2005, **109**, 851-859.
27. J. J. Vajo, S. L. Skeith and F. Meters, *J. Phys. Chem. B*, 2005, **109**, 3719.

28. J. J. Vajo, F. Mertens, C. C. Ahn, J. Robert C. Bowman and B. Fultz, *J. Phys.Chem B*, 2004, **108**, 13977.
29. F. E. Pinkerton, G. P. Meisner, M. S. Meyer, M. P. Balogh and M. D. Kundrat, *J. Phys. Chem. B*, 2005, **109**, 6.
30. Y. Nagahara, S. Sugawara and K. Shinohara, *J. Power Sources*, 2008, **182**, 422-428.
31. R. Halseid, P. J. S. Vie and R. Tunold, *J. Power Sources*, 2006, **154**, 343-350.
32. P. Chen, Z. Xiong, J. Luo, J. Lin and K. L. Tan, *J. Phys. Chem. B*, 2003, **107**, 10967.
33. A. F. Gross, J. J. Vajo, S. L. Van Atta and G. L. Olson, *J. Phys. Chem. C*, 2008, **112**, 5651-5657.
34. J. H. Yao, C. Shang, K. F. Aguey-Zinsou and Z. X. Guo, *J. Alloys Compd.*, 2007, **432**, 277-282.
35. L. L. Shaw, R. Ren, T. Markmaitree and W. Osborn, *J. Alloys Compd.*, 2008, **448**, 263-271.
36. S. Orimo, Y. Nakamori, G. Kitahara, K. Miwa, N. Ohba, T. Noritake and S. Towata, *Appl. Phys. A*, 2004, **79**, 1765-1767.
37. Y. Song and Z. X. Guo, *Phys. Rev. B*, 2006, **74**, 195120.
38. J. F. Herbst and J. L. G. Hector, *Phys. Rev. B*, 2005, **72**, 125120.
39. S. Isobe, T. Ichikawa, K. Tokoyoda, N. Hanada, H. Leng, H. Fujii and Y. Kojima, *Thermochimica Acta*, 2008, **468**, 35-38.
40. M. Gupta and R. P. Gupta, *J. Alloys Compd.*, 2007, **446-447**, 319-322.
41. H. Y. Leng, T. Ichikawa, S. Hino and H. Fujii, *J. Alloys Compd.*, 2008, **463**, 462-465.
42. Y. Nakamori and S. Orimo, *Mater. Sci. Eng. B*, 2004, **108**, 48-50.
43. T. Ichikawa, N. Hanada, S. Isobe, H. Leng and H. Fujii, *J. Phys. Chem. B*, 2004, **108**, 7887-7892.
44. J. Z. Hu, J. H. Kwak, Z. Yang, W. Osborn, T. Markmaitree and L. L. Shaw, *J. Power Sources*, 2008, **181**, 116-119.
45. K. F. Aguey-Zinsou, J. Yao and Z. X. Guo, *J. Phys. Chem. B*, 2007, **111**, 12531-12536.
46. S. Ikeda, N. Kuriyama and T. Kiyobayashi, *Inter. J. Hydrogen Energy*, 2008, **33**, 6201-6204.
47. T. Kar, S. Scheiner and L. Li, *J. Mol.Struc. THEOCHEM*, 2008, **857**, 111-114.
48. K. C. Kim, B. Dai, J. K. Johnson and D. S. Sholl, *Nanotechnology*, 2009, **20**, 204001.
49. K. C. Kim and D. S. Sholl, *J. Phys. Chem. C*, 2010, **114**, 678-686.
50. K. C. Kim, A. D. Kulkarni, J. K. Johnson and D. S. Sholl, *in preparation*.
51. K. C. Kim, A. D. Kulkarni, J. K. Johnson and D. S. Sholl, *in preparation*.
52. K. C. Kim, M. D. Allendorf, V. Stavila and D. S. Sholl, *Phys. Chem. Chem. Phys.*, **in press**.

CHAPTER 2

ASSESSING NANOPARTICLE SIZE EFFECTS ON METAL HYDRIDE THERMODYNAMICS USING THE WULFF CONSTRUCTION

2.1 Introduction*

The high gravimetric and volumetric capacities of light metal hydrides make them appealing candidates for reversible H_2 storage in vehicular applications[1, 2]. However, as discussed in Chapter 1, the performance of metal hydrides for H_2 storage is limited by thermodynamic and kinetic factors. For many hydrides, the equilibrium conditions required for H_2 release and uptake lie outside those appropriate for fuel-cell powered vehicles. This situation has spurred searches for materials with more appropriate thermodynamic properties[3-8]. Aside from these thermodynamic factors, the kinetics of H_2 uptake and release by metal hydrides are often much slower than would be desirable.

As stated in Chapter 1, the concept of improving the performance of metal hydrides for H_2 storage by using nanoparticles has received considerable attention.[9-14] This work is most often motivated by the idea that the kinetics of H_2 uptake and release may be improved by decreasing the particle size of the relevant solid phases. This expectation is reasonable if reaction kinetics is controlled by diffusion through a bulk phase. It is not yet clear in most light metal hydrides what the rate limiting steps in H_2 uptake or release are, so anticipating the effects of nanosizing on the kinetics of these reactions remains difficult. It is useful to note in this chapter that examples are known in studies of metal films used as membranes for H_2 purification where reducing the film thickness below a critical thickness yields a limited return in terms of improved device performance because processes other than bulk diffusion become rate limiting[15, 16].

In addition to changing reaction kinetics, using nanoparticles instead of bulk metal

*The contents of this chapter have also appeared in <K. C. Kim, B. Dai, J. K. Johnson, and D. S. Sholl, *Nanotechnology*, 2009, **20**, 204001>.

hydrides may can also alter the thermodynamics of H_2 uptake and release[17, 18]. Conceptually, the thermodynamics of these processes is governed by energy differences between the metal and metal hydride. Because the energies (on a molar basis) of both materials change in going from bulk materials to nanoparticles, the reaction thermodynamics of these materials must be affected by particle size[19]. The aim of this chapter is to estimate the size of this effect for a number of simple metal hydrides. The ultimate aim of work on metal hydride nanoparticles is to generate reliable experimental data with robust materials. Because the reactions of many metal hydrides have severe kinetic limitations, unambiguously decoupling kinetic and thermodynamic effects in experimental studies of nanoparticles is challenging. This situation means that estimates of the thermodynamic effects associated with nanoparticles from theoretical methods can play a useful role in understanding the overall properties of these materials.

One useful theoretical approach to examining the energy of nanoparticles is a "bottom up" method in which detailed calculations are performed for clusters where every atom is represented. This approach has been used extensively to explore the geometry of very small metal clusters[20]. Two studies have explored Mg and MgH_2 nanoclusters in this way[19, 21]. Wagemans et al. used density functional theory (DFT) to examine clusters with < 60 Mg atoms, with most of their calculations focusing on clusters with < 20 Mg atoms[19]. Cheung et al. used DFT calculations of small clusters and bulk materials to parameterize a classical force field for Mg-H interactions and subsequently applied this force field to study cluster containing up to 101 Mg atoms[21]. Both of these studies provided clear indications that nanoclusters containing < 50 Mg atoms could show deviations in their heats of formation from bulk materials, an observation that implies that the reaction thermodynamics of these clusters differ from bulk materials. An important limitation of this "bottom up" approach is that the computational expense associated with examining clusters grows rapidly with the cluster size. Clusters of Mg with radii of 2 nm and 5 nm contain ~1500 and ~23000 atoms, respectively, and the relevant MgH_2 clusters contain three times as many atoms. These system sizes lie far beyond those that are accessible with contemporary DFT calculations, and even using a force field approach, such as the one introduced by Cheung et al.,

these system sizes are daunting. Calculations based on classical force fields face the additional complication that a large amount of effort must be expended for each new material of interest.

In this chapter, we explore the thermodynamics of metal hydride nanoparticles from an alternate "top down" viewpoint.[22] In this approach, the crystal structure of each nanoparticle is assumed to be identical to the bulk crystal and differences in energy between nanoparticles and bulk materials arise because of the presence of well defined surfaces. For each surface exposed on a nanoparticle, this energy difference is characterized by a surface energy. We have used DFT calculations to compute the surface energies, including the effects of surface relaxation, of a large number of potentially relevant surfaces for seven elemental metals and their hydrides. The equilibrium crystal shape (ECS) of a material can be predicted using the calculated surface energies and the Wulff construction[23-25]. This makes it possible to calculate the net surface energy of the nanoparticle. In the next section, we describe the influence of nanoparticle size on reaction thermodynamics for nanoparticles formed in this way.

2.2 Theoretical Approach

A useful way to characterize the thermodynamics of hydrogen release or uptake by metal hydrides is to determine the temperature at which the metal hydride is in equilibrium with the metal when the H_2 pressure is 1 bar[26]. Under these conditions the free energy, or equivalently, the grand potential, of the two systems are equal[7]. For bulk samples, the grand potential can be estimated using DFT calculations by

$$\Omega(T) = E - \frac{1}{2}\left(E_{H_2} + E_{ZPE,H_2} + \tilde{\mu}\right) \tag{2.1}$$

where E is the total energy for the solid of interest computed from DFT, the quantities inside the parentheses are the energy, zero point energy (ZPE), and chemical potential of molecular H_2, and n^H is the number of H atoms per metal atom in the solid[27-29]. This expression neglects ZPE in the solid and temperature dependent vibrational contributions to the solid's free energy; we return to these approximations below. From this expression for the grand potential, it follows that the bulk

metal hydride and metal are in equilibrium when

$$\tilde{\mu}\quad\quad =1\text{ bar})=\beta=\frac{2}{n^H}\left(E_{MH}^{bulk}-E_M^{bulk}\right)-\left(E_{H_2}+E_{ZPE,H_2}\right). \tag{2.2}$$

Here, MH and M denote the metal hydride and metal, respectively. To extend this expression to solid particles of finite size, the influence of surface energy on the overall energy of the solids must be included. Using quantities accessible via DFT calculations based on slab geometries, the surface energy is

$$\gamma=\left[E^{slab}-NE^{bulk}\right]/A \tag{2.3}$$

where E^{slab} is the total energy of the slab containing N metal atoms, E^{bulk} is the total energy of the bulk material per metal atom, and A is the total surface area exposed by both sides of the slab[24, 25, 30]. Here, the slab energy is defined using a slab that has been geometry optimized to include the effects of surface relaxation. Nanoparticles of a metal and its metal hydride are in equilibrium when $\tilde{\mu}\quad\quad =1\text{bar})=\beta+\alpha/N$, where

$$\alpha=\frac{2}{n^H}\left(\sum_i\left(A_{MH,i}^{surf}\gamma_{MH,i}^{surf}\right)-\sum_j\left(A_{M,j}^{surf}\gamma_{M,j}^{surf}\right)\right)=\frac{2}{n^H}\Delta\left(A^{surf}\gamma^{surf}\right). \tag{2.4}$$

The summations are necessary here to allow for particles that expose multiple surfaces. Once $\tilde{\mu}\quad\quad)$ is known from either Eq. (2.2) or (2.4), the temperature at which the metal and metal hydride are in equilibrium, T_{eq}, is defined. In calculating T_{eq}, we assume that H_2 is an ideal gas.

An alternative way to describe the thermodynamic effects of nanosizing is to use the change in enthalpy between the reaction involving a nanoparticle and the reaction for the bulk materials,

$$\Delta\Delta H=\Delta H(N)-\Delta H(\infty). \tag{2.5}$$

In terms of the quantities defined above, this enthalpy change is simply

$$\Delta\Delta H=-\frac{\alpha}{N}. \tag{2.6}$$

To make use of the formalism above, we need to determine the areas and surface energies

of the surfaces exposed by each nanoparticle of interest. If the surface energies of each possible surface are known, the Wulff construction can be used to predict the equilibrium crystal shape (ECS) of the material[23-25]. To apply the Wulff construction, we used DFT to calculate the surface energy of each low index surface of seven elemental metals and their hydrides, as summarized in Table 2.1. A complete list of the surface energies from our calculations is given in the Table 2.2. A convenient feature of these low index surfaces for all the hydrides we considered is that each layer normal to the surface has the same stoichiometry as the bulk hydride. This means that there is no ambiguity in defining the termination of these surfaces[31].

2.3 Computational Details

All of our DFT calculations were performed with the PW91 generalized gradient approximation functional[32] using the Vienna *ab initio* simulation package[33, 34]. The core electrons of each atom were described by ultrasoft pseudopotentials[35], and an energy cutoff of 300 eV was used for all calculations. During geometry optimization, all atoms were relaxed until the forces on all atoms were less than 0.03 eV/Å. All surface calculations used supercells defined by the DFT-optimized bulk lattice constant in the plane of the surface and a vacuum spacing of at least 10.8 Å. All surfaces were modeled by using (1×1) surface unit cells with six layers in which all atoms are allowed to relax freely. Calculations on the surface unit cells were performed with a $12\times12\times1$ Monkhorst-Pack mesh in *k*-space. Reciprocal space for the bulk materials was sampled using 8×8×8 *k*-points for NaH, LiH, ScH_2, TiH_2, and VH_2, 8×8×12 *k*-points for MgH_2, 12×12×4 *k*-points for AlH_3, 12×12×12 *k*-points for Na, Li, and V, 15×15×10 *k*-points for Ti and Sc, 20×20×12 *k*-points for Mg and 20×20×20 *k*-points for Al. All bulk materials were modeled by using $(1\times1\times1)$ supercell.

2.4 ECS Based on the Surface Energies of Low Index Surfaces

Using the surface energies calculated from DFT, we applied the Wulff construction for the seven metals and metal hydrides we considered. Two examples of the resulting equilibrium

crystal shapes are shown in Fig. 2.1. We examined five low index surfaces for Sc, and all of these surfaces appear on the ECS shown in Fig. 2.1(a), with the $\left(10\bar{1}1\right)$ and $\left(11\bar{2}1\right)$ surfaces defining about 70% of the entire surface area. The $\left(11\bar{2}0\right)$ surface is predicted to only account for 0.4% of the particle's total surface area. The same set of five surfaces was considered for Ti, whose predicted ECS is shown in Fig. 2.1(c). For Ti, only four surfaces are present on the ECS, and the $\left(11\bar{2}1\right)$ surfaces defines about half of the total surface area. Our calculated surface energies for Ti differ in several respects from the values reported by Wang, Zhang, and Xu using calculations with the modified embedded atom method (MEAM)[36]. For example, our calculations indicate that the $\left(11\bar{2}1\right)$ surface has the lowest surface energy, while Wang et al.'s calculations suggested that the $\left(11\bar{2}0\right)$ surface has a lower surface energy than $\left(11\bar{2}1\right)$. Although DFT calculations do not give exact results for surface energies, it seems likely that our DFT results are more reliable than results from the semi-empirical MEAM. The ECS of ScH_2 and TiH_2 are much simpler than their metal counterparts, an observation that can be understood by noting that the partially ionic nature of these materials makes their surface energies much more anisotropic than the surface energies of elemental metals. As shown in Fig. 2.1(b) and (d), these hydrides have only $\left(111\right)$ surfaces on their ECS. The contribution of each surface to the total surface area on the ECS of each of the seven metals and hydrides we have considered is summarized in Table 2.1.

Table 2.1: Summary of the surfaces examined for each material in applying the Wulff construction to form the ECS. The final column indicates the fraction of the total surface area on the ECS associated with each surface.

Space group	Material(s)	Surfaces examined	Surfaces on ECS
$Im\bar{3}m$	V	$(111),(110),(100)$	$(110)-70\%,(100)-24\%,(111)-6\%$
	Li	$(111),(110),(100)$	$(110)-53\%,(100)-39.3\%,(111)-7.7\%$
	Na	$(111),(110),(100)$	$(110)-78.1\%,(100)-21.2\%,(111)-0.7\%$
$P6_3/mmc$	Sc	$(0001),(10\bar{1}0),(10\bar{1}1),(11\bar{2}0),(11\bar{2}1)$	$(10\bar{1}1)-38.7\%,(11\bar{2}1)-33\%,(0001)-15.8\%,$ $(10\bar{1}0)-12.1\%,(11\bar{2}0)-0.4\%$
	Ti	$(0001),(10\bar{1}0),(10\bar{1}1),(11\bar{2}0),(11\bar{2}1)$	$(11\bar{2}1)-55.5\%,(10\bar{1}1)-24.5\%,(0001)-17.2\%,$ $(10\bar{1}0)-2.8\%$
	Mg	$(0001),(10\bar{1}0),(10\bar{1}1),(11\bar{2}0),(11\bar{2}1)$	$(10\bar{1}1)-38\%,(10\bar{1}0)-37.8\%,(0001)-24.2\%$
$Fm\bar{3}m$	Al	$(111),(110),(100)$	$(111)-75.5\%,(100)-24.5\%$
$Fm\bar{3}m$	VH_2	$(111),(110),(100)$	$(111)-100\%$
	LiH	$(111),(110),(100)$	$(100)-100\%$
	NaH	$(111),(110),(100)$	$(100)-100\%$
	ScH_2	$(111),(110),(100)$	$(111)-100\%$
	TiH_2	$(111),(110),(100)$	$(111)-100\%$
$P4_2/mnm$	MgH_2	$(111),(110),(101),(100),(001)$	$(101)-45\%,(110)-38.1\%,(100)-16.4\%,$ $(001)-0.5\%$
$R\bar{3}c$	AlH_3	$(0001),(10\bar{1}0),(10\bar{1}1),(11\bar{2}0),(11\bar{2}1)$	$(11\bar{2}1)-100\%$

Table 2.2: The calculated surface energy of each surface considered in our DFT calculations and predictions of the equilibrium crystal shape via the Wulff construction.

Surface	Surface energy (J/m^2)	Surface	Surface energy (J/m^2)
VH_2		**V**	
(111)	1.159	(110)	2.479
(110)	1.874	(100)	2.539
(100)	2.797	(111)	2.775
LiH		**Li**	
(100)	0.328	(100)	0.467
(110)	0.769	(110)	0.503
(111)	2.446	(111)	0.558
ScH_2		**Sc**	
(111)	0.858	$(11\bar{2}1)$	1.272
(110)	1.310	$(10\bar{1}0)$	1.284
(100)	2.211	$(10\bar{1}1)$	1.303
		$(11\bar{2}0)$	1.331
		(0001)	1.336
TiH_2		**Ti**	
(111)	1.322	$(11\bar{2}1)$	1.858
(110)	1.736	$(11\bar{2}0)$	2.009
(100)	2.573	$(10\bar{1}1)$	2.010
		(0001)	2.021
		$(10\bar{1}0)$	2.080
AlH_3		**Al**	
$(11\bar{2}1)$	0.355	(111)	0.782
$(10\bar{1}0)$	0.444	(100)	0.885
$(11\bar{2}0)$	0.564	(110)	0.982
$(10\bar{1}1)$	0.937		
(0001)	2.403		
NaH		**Na**	
(100)	0.199	(110)	0.208
(110)	0.472	(100)	0.217
(111)	1.519	(111)	0.247
MgH_2		**Mg**	
(110)	0.531	(0001)	0.523
(100)	0.592	$(10\bar{1}0)$	0.581
(101)	0.621	$(10\bar{1}1)$	0.635
(001)	0.709	$(11\bar{2}0)$	0.705
(111)	0.764	$(11\bar{2}1)$	0.744

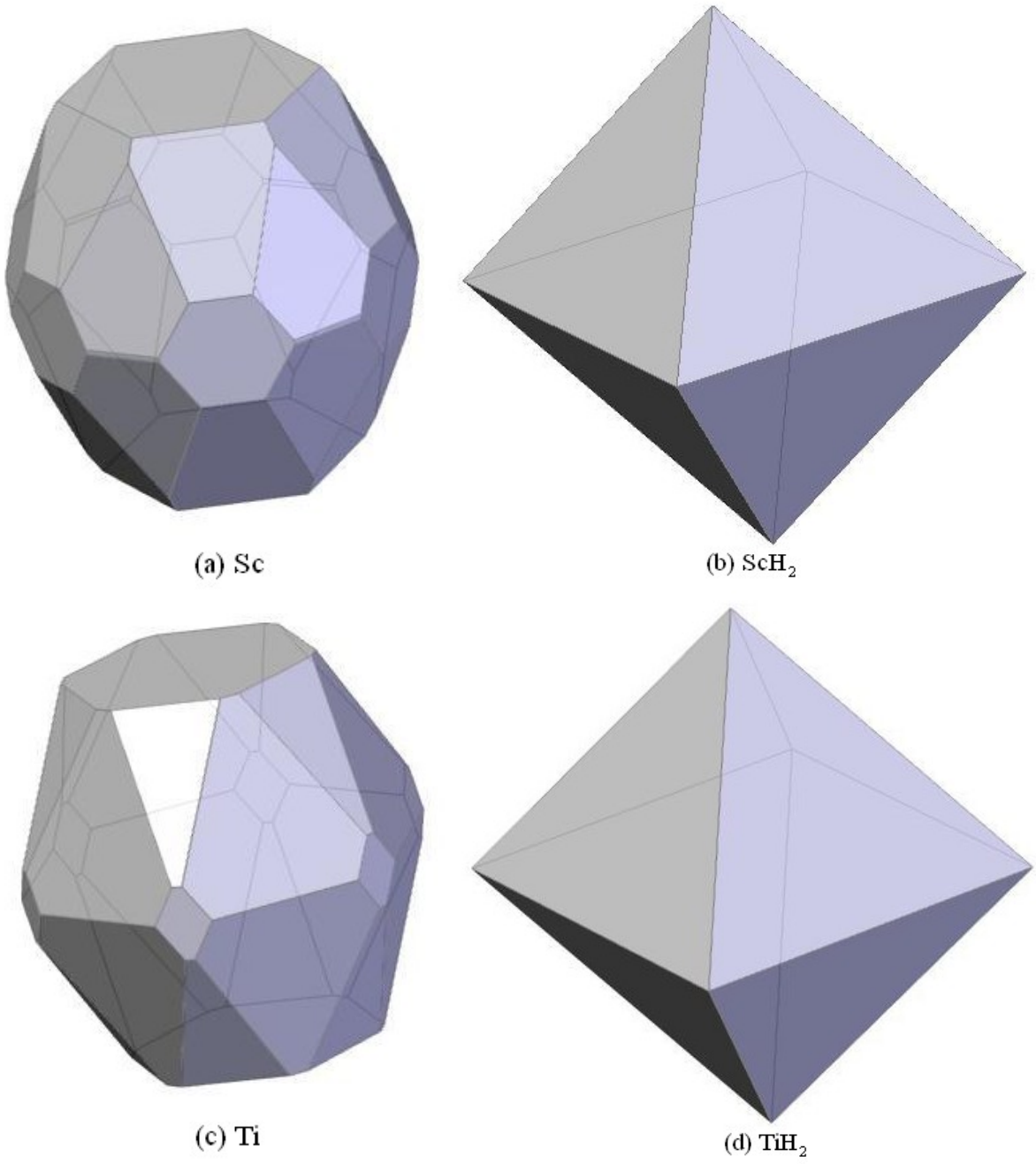

Figure 2.1: The predicted equilibrium crystal shapes of Sc, Ti, and their hydrides determined from the Wulff construction as described in the text.

2.5 Effect of Particle Size on Thermodynamics of Hydrogen Release

From the calculated surface energies and ECS, we used Eq. (2.4) to describe the

influence of particle size on the thermodynamics of hydrogen evolution. Our results are summarized in Fig. 2.2, which shows the difference between the equilibrium temperature, T_{eq}, for a nanoparticle and a bulk material. In this figure, the size of the metallic nanoparticle is shown by converting the volume of the nanoparticle with the predicted Wulff ECS to a spherical particle with the same bulk density. The numerical values of α for each metal/metal hydride pair are listed in Table 2.3. An initial observation from Fig. 2.2 and Table 2.3 is that both positive and negative deviations of the transition temperature with respect to the bulk material exist. For MgH_2/Mg and NaH/Na, the sign of α is positive, so the transition temperature decreases as the particle size is reduced. The opposite trend is seen for the other five metal/metal hydride pairs.

A second observation from Fig. 2.2 is that the changes in the transition temperature relative to the bulk materials are, on the whole, small. For metal particles with radius 10 nm, the effects from the exposed surfaces change the transition temperature by less than 20 K for every material. For the two cases where the transition temperature is lower for nanoparticles than for the bulk material, the temperature is only reduced by 33 (16) K for MgH_2/Mg (NaH/Na) for the extreme case of a nanoparticle having a radius of 1 nm. The largest effect of nanoparticle size is predicted for VH_2/V. If we consider a V nanoparticle with radius 5 nm as an example, the transition temperature in this case is only 30 K larger than for the bulk system. We note that for most systems it is desirable to reduce the transition temperature or heat of reaction. However, for AlH_3, it would be useful to increase the transition temperature (or equivalently, the heat of reaction) because at equilibrium, AlH_3 decomposes at temperatures that are too low for practical applications[37]. The nanoparticle transition temperature does indeed increase for the AlH_3/Al system, as seen in Fig. 2.2, but the effect is extremely small, increasing T_{eq} by only 13 K for the extreme case of a metal nanoparticle 1 nm in radius.

Our results are shown in Fig. 2.3 in terms of the enthalpy instead of temperature. As has already been discussed by focusing on the transition temperatures for these materials, the enthalpy changes associated with even very small nanoparticles are small.

To consider the physical source of the trends in α listed in Table 2.3, we calculated the charge associated with the H atoms in each metal hydride we examined using a Bader charge decomposition[38]. The resulting charges are shown in Fig. 2.4. With the exception of LiH, there is a distinct correlation between α and the H atom Bader charge in the hydride, with the most (least) ionic materials being associated with positive (negative) values of α.

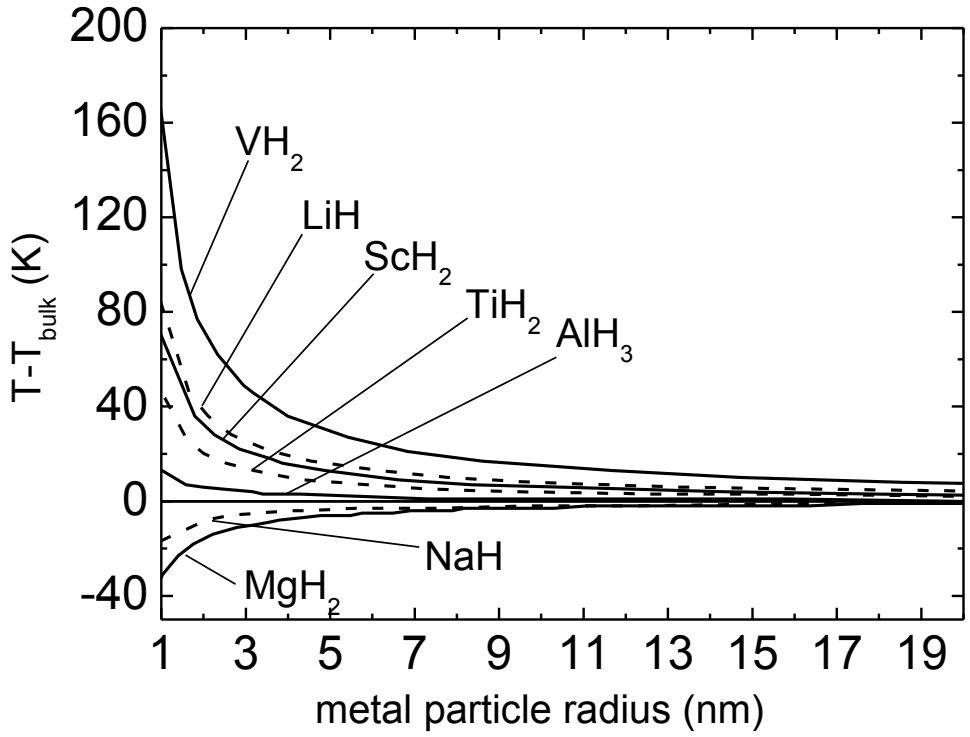

Figure 2.2: The variation in the metal/metal hydride transition temperature relative to the result for a bulk material determined as described in the text.

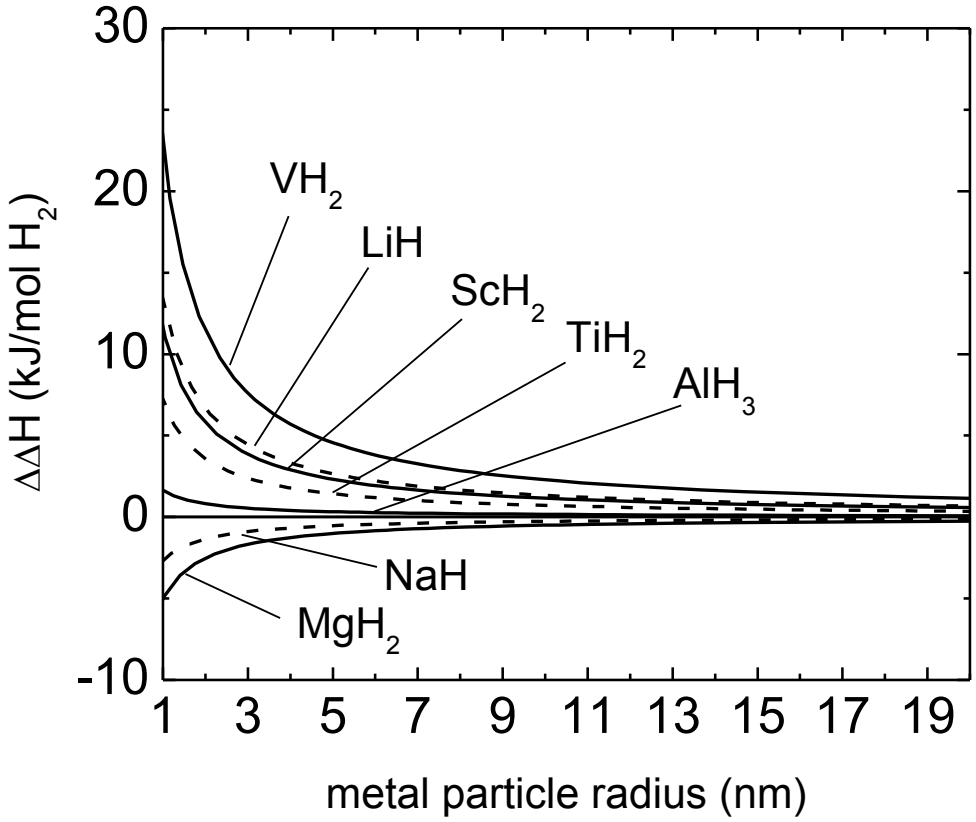

Figure 2.3: The variation in the metal/metal hydride reaction enthalpy relative to the result for a bulk material determined as described in the text.

Table 2.3: The numerical coefficient, α, that controls nanoparticle thermodynamic effects for the seven systems we have considered, where *N* is the number of metal atoms in the nanoparticle.

System	$\alpha N^{-2/3}$ (eV)
VH_2/V	-1.608
LiH/Li	-0.822
ScH_2/Sc	-0.667
TiH_2/Ti	-0.461
AlH_3/Al	-0.107
NaH/Na	0.134
MgH_2/Mg	0.296

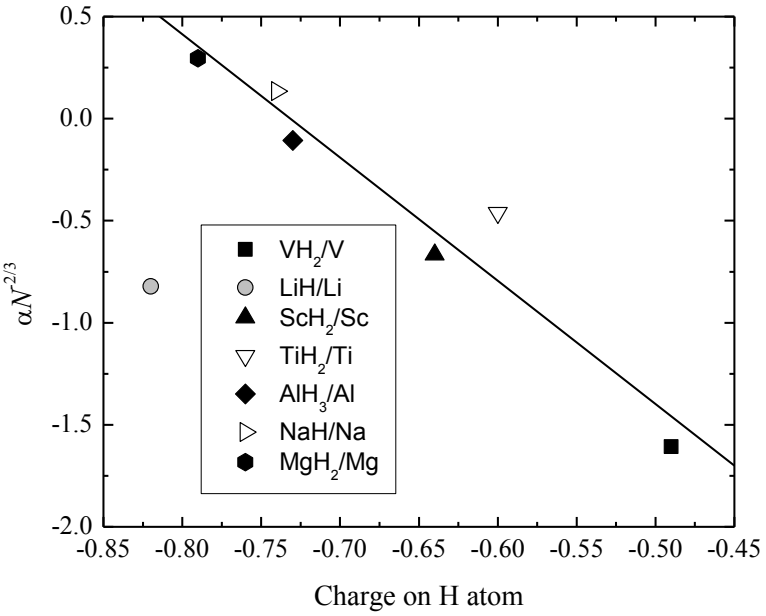

Figure 2.4: Plot of $\alpha N^{-2/3}$ as a function of the charge on the H atom in the bulk hydride as computed by Bader charge analysis, where α is the parameter that controls nanoparticle thermodynamic effects and N is the number of metal atoms in the nanoparticle. The line is a linear fit to all systems except LiH/Li.

2.6 Examination of Zero Point Energy Contribution to the Surface Energies

The results discussed above relied on surface energies calculated without accounting for zero point energies. Calculating the zero point energy contributions to surface energies is time consuming, so we have only examined the strength of these effects for three representative examples. In each case, we considered the equilibrium between a two dimensional slab of a metal hydride that exposes one surface facet to a two dimensional slab of metal that also exposes a single surface facet. We estimated the zero point energy contribution to the surface energy of each surface using $\gamma + \gamma^{ZP} = \left[E^{slab} - NE^{bulk} \right] / A + \left[E^{slab,ZP} - NE^{bulk,ZP} \right] / A$. The zero point energies on the right hand side of this expression were calculated using harmonic normal mode frequencies calculated within DFT with finite displacements of each atom in an appropriate

supercell. In principle, this treatment could be made more precise by computing the full vibrational density of states[28, 39] for the bulk material and a slab model of a surface, but we have not pursued calculations of this kind.

The zero point energy contributions to the surface energies of the six surfaces we have examined are listed in Table 2.4. As should be expected, the zero point energy effects are larger in magnitude for the metal hydrides than for the metals. Similarly, the zero point energy for the Li surface is larger than for Mg or V. An interesting observation from these results is that values of γ^{ZP} with both negative and positive signs are found, the former for $VH_2(111)$ and the latter for $MgH_2(101)$ and LiH(100). Figure 2.5 shows the change of the transition temperatures after considering the zero point energy in terms of the thickness of metal film about $MgH_2(101)$/Mg(0001) and $VH_2(111)$/V(110) films. As shown in Fig. 2.5, the transition temperatures of $MgH_2(101)$/Mg(0001) and $VH_2(111)$/V(110) systems are changed by just 30 ~ 40 K from the values before the consideration of the zero point energy at the film thickness of even 1 nm.

The effect of surface energy on the transition temperature for equilibrium between the metal hydride and metal surfaces listed in Table 2.4 is controlled by $\alpha = \frac{2}{n_p}\Delta\left(A^{surf}[\gamma^{surf} + \gamma^{ZP}]\right)$. The importance of the zero point energy effects can therefore be quantified by the dimensionless ratio $\frac{\alpha^{ZP}}{\alpha} = \frac{\Delta\left(A^{surf}\gamma^{ZP}\right)}{\Delta\left(A^{surf}\gamma^{surf}\right)}$. For $MgH_2(101)/Mg(0001)$, $LiH(100)/Li(100)$, and $VH_2(111)/V(110)$ films, this ratio is 0.36, 0.01, and 0.34 respectively. These values indicate that it is reasonable to think of the zero point energy contributions as a correction to the results calculated without zero point energies. This observation supports the idea that our calculations for the full ECS of the seven materials considered above that did not include zero point energies give useful estimates for the influence of nanoparticle size on reaction thermodynamics.

Table 2.4: Surface energies of MgH_2(101)/Mg(0001), LiH(100)/Li(100), and VH_2(111)/V(110) films computed using DFT with and without zero point energy.

Materials	Without ZPE	With ZPE	Materials	Without ZPE	With ZPE
MgH_2(101)	0.62 J/m^2	0.79 J/m^2	**Mg(0001)**	0.52 J/m^2	0.57 J/m^2
LiH(100)	0.33 J/m^2	0.45 J/m^2	**Li(100)**	0.47 J/m^2	0.55 J/m^2
VH_2(111)	1.16 J/m^2	0.84 J/m^2	**V(110)**	2.48 J/m^2	2.65 J/m^2

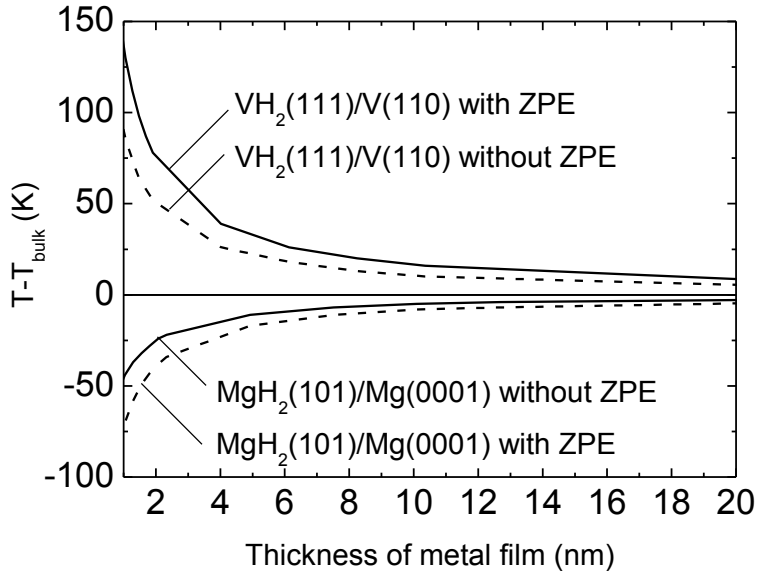

Figure 2.5: The change of film thickness on the transition temperatures of MgH_2(101)/Mg(0001) and VH_2(111)/V(110) films, showing the effects of zero point energy.

2.7 Discussion

In this chapter, we discussed the effect of the particle size of seven simple metal hydrides on the reaction thermodynamics. Our results for MgH_2 nanoclusters provide a useful way to compare our methods to other approaches and to consider the strengths and limitations of our

calculations. Possibly the most direct comparison we can make with experimental data is via the experiments of Li and Chen, who examined hydrogen evolution from MgH_2 nanowires of radii 20, 45, and 80 nm[11]. In these experiments, no noticeable difference in the temperatures associated with H_2 evolution was observed between the nanowires of different radii, although the thinner nanowires had better reaction kinetics. Our results are consistent with these observations; the data in Fig. 2.2 suggests that the transition temperature for MgH_2 varies only by a few degrees over the size range examined in these experiments. The calculations discussed in the Introduction by Wagemans et al.[19] and Cheung et al.[21] for MgH_2 clusters containing up to 50 Mg atoms both predicted a reduction in the equilibrium temperature for H_2 evolution relative to bulk MgH_2, but found that this reduction was small once clusters containing ~100 Mg atoms were considered. These predictions are consistent in both sign and magnitude with our results.

The experimental results of Aguey-Zinsou et al.[14], which exhibit H_2 evolution from Mg nanoparticles near room temperature, appear superficially to contradict our theoretical predictions. It is crucial to note however, that the colloidal particles in these experiments are not Mg nanoparticles in isolation, instead the metal cores of these particles are coated in tetrabutylammonium bromide and only ~1/5 of the total mass of the colloidal particles comes from Mg, limiting the hydrogen storage capacity of these particles to less than 1.5 wt.%. Because the physical environment in which the Mg and MgH_2 in these particles is so different from the isolated environment considered in our model and in other theoretical calculations[19, 21], it is not surprising that our calculations are unable to describe the outcome of these experiments.

There are a number of reasons why our calculations define only an approximate description of metal hydride nanoparticle thermodynamics. To discuss these issues, we first consider the case of nanoparticles that are isolated from a support or surrounding matrix material. Our description is based on the concept of an equilibrium crystal shape (ECS) as predicted for a pure material. It is important to note, however, that the presence of impurities during crystal growth can substantially alter crystal shapes relative to the ECS of the pure material. This phenomenon is frequently used to control particle morphology in crystal growth[40, 41]. These

effects may be relevant to the crystal shape in particular experiments, but they are unlikely to change the overall conclusion of our calculations that the effect of nanosizing on reaction thermodynamics in simple metal hydrides is relatively small because the magnitude of α in Eq. (2.2) is not especially sensitive to the precise surface areas of the surfaces making up each crystal. Our treatment of the ECS is also approximate because we neglected the contributions of edge and kink sites defined by the intersections between atomically flat surfaces on the crystal. Examples are known from studies of heterogeneous catalysis on metal nanoparticles where these sites dominate the catalytic properties of practical nanoparticles when the reactivity of these sites greatly exceeds that of sites on flat surfaces[42]. Because applications for nanoparticles in hydrogen storage require removing or adding hydrogen to all sites in a nanoparticle, not just those that might be most reactive, the influence of these undercoordinated sites will be minimal for moderate and large particles. For very small particles, however, where the fraction of all surfaces sites that are edge sites becomes appreciable, then including these sites in assessing reaction thermodynamics may become important. To give a sense of the number of these edge sites, we consider the TiH_2 crystal shown in Fig. 2.1. For the hydride particle associated with a metal particle of radius 10 or 5 nm, approximately 4.5 or 9% of the surface atoms are edge sites, respectively. If the radius of the metal nanoparticle is reduced to 2 nm, 22% of the surface sites on the ECS shown in Fig. 2.1 are edge sites. The Wulff construction is only valid if the internal crystal structure of the particle being considered is identical to the bulk material. For nanoparticle containing 20 or fewer atoms, many examples are known where the coordination of atoms in a nanoparticle is not related in a simple way to the material's bulk crystal structure[20]. For nanoparticles in the size range we have considered above, however, treating the crystal structure of the bulk and an isolated nanoparticle as being the same appears to be a reasonable approach.

In practical applications, metal or metal hydride nanoparticles cannot be isolated entities, instead they must be in contact with an appropriate support material or matrix. This situation creates a number of complications that have not been included in our calculations or in previous

"bottom-up" calculations of metal hydride nanoparticle properties. First, when nanoparticles are in contact with a support, even if that support is relatively inert, some of the surface energy contributions to the nanoparticle free energy must be replaced by interfacial energies. These energies can be calculated using DFT, but typically only for examples where the support is highly ordered and there is little strain between the material and the support[31] or, alternatively, for very small nanoparticles[43]. When particle/support interactions create significant strain within a nanoparticle, these effects can play an important role in the nanoparticle's properties[17, 18]. Finally, in hydrogen storage applications where long term cycling of a material between the hydrogenated and dehydrogenated states is envisioned, the possibility of chemical interactions between the nanoparticle and a support material cannot always be ignored. For example, reversible reactions involving $LiBH_4$ and graphitic carbon with favorable thermodynamics have been identified in theoretical calculations[6]. It is possible that reactions of this kind could play a role in the cycling of $LiBH_4$ when this material is contained in a nanoporous carbon. The role of chemical interactions of this kind can clearly not be examined by considering isolated nanoparticles.

2.8 REFERENCES

1. A. Züttel, *Naturwissenschaften*, 2004, **91**, 157-172.
2. W. Grochala and P. P. Edwards, *Chem. Rev.*, 2004, **104**, 1283.
3. S.-i. Orimo, Y. Nakamori, J. R. Eliseo, A. Züttel and C. M. Jensen, *Chem. Rev.*, 2007, **107**, 4111-4132.
4. S. V. Alapati, J. K. Johnson and D. S. Sholl, *J. Phys. Chem. B*, 2006, **110**, 8769-8776.
5. S. V. Alapati, J. K. Johnson and D. S. Sholl, *Phys. Chem. Chem. Phys.*, 2007, **9**, 1438-1452.
6. S. V. Alapati, J. K. Johnson and D. S. Sholl, *J. Phys. Chem. C*, 2008, **112**, 5258-5262.
7. A. Akbarzadeh, V. Ozoliņš and C. Wolverton, *Adv. Mat.*, 2007, **19**, 3233.
8. C. Wolverton, D. J. Siegel, A. R. Akbarzadeh and V. Ozolins, *J. Phys. Condens. Matter*, 2008, **20**, 064228.
9. M. Fichtner, J. Engel, O. Fuhr, O. Kircher and O. Rubner, *Mater. Sci. Eng. B*, 2004, **108**, 42-47.
10. H. Imamura, K. Masanari, M. Kusuhara, H. Katsumoto, T. Sumi and Y. Sakata, *J. Alloys Compd.*, 2005, **386**, 211-216.
11. W. Li, C. Li and H. M. J. Chen, *J. Am. Chem. Soc.*, 2007, **129**, 6710-6711.
12. J. J. Vajo and G. L. Olson, *Scripta Materialia*, 2007, **56**, 829-834.
13. V. Bérubé, G. Radtke, M. Dresselhaus and G. Chen, *Int. J. Energy Research*, 2007, **31**, 637-663.
14. K.-F. Aguey-Zinsou and J.-R. Ares-Fernández, *Chem. Mater.*, 2008, **20**, 376-378.
15. T. L. Ward and T. Dao, *J. Membrane Sci.*, 1999, **153**, 211-231.
16. C. Ling and D. S. Sholl, *J. Membrane Sci.*, 2007, **303**, 162.
17. A. Pundt, *Adv. Eng. Mat.*, 2004, **6**, 11-21.
18. A. Pundt and R. Kirchheim, *Ann. Rev. Materials Res.*, 2006, **36**, 555-608.
19. R. W. P. Wagemans, J. H. v. Lenthe, P. E. d. Jongh, A. J. v. Dillen and K. P. d. Jong, *J. Am. Chem. Soc.*, 2005, **127**, 16675 -16680.
20. L.-L. Wang and D. D. Johnson, *Phys. Rev. B*, 2007, **75**, 235405.
21. S. Cheung, W.-Q. Deng, A. C. T. vanDuin and W. A. Goddard, *J. Phys. Chem. A*, 2005, **109**, 851-859.
22. K. C. Kim, B. Dai, J. K. Johnson and D. S. Sholl, *Nanotechnology*, 2009, **20**, 204001.
23. G. Wulff, *Z. Krist. Mineral.*, 1901, **34**, 449-530.
24. H. Q. Shi and C. Stampfl, *Phys. Rev. B*, 2008, **77**, 094127.
25. A. Soon, L. Wong, B. Delley and C. Stampfl, *Phys. Rev. B*, 2008, **77**, 125423.
26. A. Züttel, *Mater. Today*, 2003, **6**, 24.
27. P. Raybaud, J. Hafner, G. Kresse, S. Kasztelan and H. Toulhoat, *J. Catal.*, 2000, **189**, 129-146.
28. S. V. Alapati, J. K. Johnson and D. S. Sholl, *J. Phys. Chem. C*, 2007, **111**, 1584-1591.
29. C. Stampfl, *Catal. Today*, 2005, **105**, 17-35.
30. R. B. Rankin and D. S. Sholl, *J. Chem. Phys.*, 2006, **124**, 074703.
31. A. Asthagiri and D. S. Sholl, *J. Chem. Phys.*, 2002, **116**, 9914-9925.
32. J. P. Perdew, J. A. Chevary, S. H. Vosko, K. A. Jackson, M. R. Pederson, D. J. Singh and C. Fiolhais, *Phys. Rev. B*, 1992, **46**, 6671.

33. G. Kresse and J. Furthmüller, *Phys. Rev. B*, 1996, **54**, 11169.
34. G. Kresse and D. Joubert, *Phys. Rev. B*, 1999, **59**, 1758.
35. D. Vanderbilt, *Phys. Rev. B*, 1990, **41**, 7892-7895.
36. D.-D. Wang, J.-M. Zhang and K.-W. Xu, *Surf. Sci.*, 2006, **600**, 2990-2996.
37. J. Graetz, J. J. Reilly, J. G. Kulleck and R. C. Bowman, *J. Alloys Compd.*, 2007, **446**, 271-275.
38. G. Henkelman, A. Arnaldsson and H. Jonsson, *Comp. Mat. Sci.*, 2006, **36**, 354-360.
39. G. J. Ackland, *J. Phys.: Condens. Matter*, 2002, **14**, 2975.
40. D. H. Chen, L. Y. Zhu, H. P. Zhang, K. Xu and M. C. Chen, *Mat. Chem. Phys.*, 2008, **109**, 224-229.
41. S. K. Poomachary, P. S. Chow and R. B. H. Tan, *J. Crystal Growth*, 2008, **310**, 3034-3041.
42. K. Honkala, A. Hellman, I. N. Remedeiakis, Á. Logadóttir, A. Carlsson, S. Dahl, C. H. Christensen and J. K. Nørskov, *Science*, 2005, **307**, 555-558.
43. L.-L. Wang and D. D. Johnson, *J. Am. Chem. Soc.*, 2007, **129**, 3658-3664.

CHAPTER 3

CRYSTAL STRUCTURES AND THERMODYNAMIC INVESTIGATIONS OF $LIK(BH_4)_2$, KBH_4, AND $NABH_4$

3.1 Introduction*

In the last chapter, we showed that controlling the particle size of metal hydrides can affect the reaction thermodynamics of the metal hydrides. For MgH_2 and NaH, we predicted that the transition temperatures to release H_2 decreased as the particle size was reduced. An alternative way to obtain favorable thermodynamics of the dehydrogenation reactions of metal hydrides is to destabilize a metal hydride by reacting with other crystal compounds, as stated in Chapter 1. Much of the ongoing research associated with the destabilization reactions of metal hydrides is based on complex metal hydrides such as alanates, borohydrides, and amides due to higher thermodynamic stability of the simple metal hydrides discussed in Chapter 2.[1-9] Among the complex metal hydrides, borohydrides are good candidates because of their high H_2 capacity.[5-7] For example, Zuttel *et al*. obtained a H_2 capacity of 18.5 wt.% from $LiBH_4$[5] and Orimo's group obtained a H_2 capacity of ~15 wt.% from $Mg(BH_4)_2$.[6] A great need remains to identify new materials whose thermodynamic properties improve upon these and other known materials.[5, 6] Therefore, considerable efforts have been focused on discovering new borohydrides with the aim of creating materials with favorable thermodynamics.[10, 11]

Nickels *et al.* recently reported a new bialkali borohydride, $LiK(BH_4)_2$ that was experimentally obtained by ball-milling a mixture of $LiBH_4$ and KBH_4.[11] They examined the crystal structure through X-ray diffraction data and explored the relationship between the decomposition temperature and the Pauling electronegativity of the metals in borohydrides. Unfortunately, this work did not identify the reaction products of this decomposition reaction.

*The contents of this chapter have also appeared in < K. C. Kim and D. S. Sholl, *J. Phys. Chem. C*, 2010, **114**, 678-686>.

Xiao *et al.*[12] have reported a first-principles study of $LiK(BH_4)_2$ based on the experimental results of Nickels *et al.* This work described the optimized structure and formation energy of $LiK(BH_4)_2$ through Density Functional Theory (DFT) calculations, but did not examine the thermodynamics of any reaction involving this compound. In this chapter, we extend these previous studies by considering the reaction thermodynamics of $LiK(BH_4)_2$.[13]

In the past several years, work by our group[14-18] and Wolverton, Ozolins, and co-workers[19-21] have shown that DFT calculations of crystalline materials can be combined with rigorous thermodynamic methods to efficiently search very large numbers of possible reaction mixtures to identify reaction mechanisms for reactions involving hydrogen release and uptake by metal hydrides. These calculations rely on having a database of crystal materials that is as complete as possible. Our previous reports from this approach were based on a database that included $LiBH_4$[15] but not KBH_4. Because KBH_4 is the source material for the experimental synthesis of $LiK(BH_4)_2$, we have performed DFT calculations for this material to allow us to consider the reaction thermodynamics of $LiK(BH_4)_2$. Our earlier reports did not also include $NaBH_4$, a structural analog of KBH_4. $NaBH_4$ is interesting as a possible material (in combination with other materials) for hydrogen storage, so we have also performed DFT calculations for $NaBH_4$. In this chapter, we examine the crystal structures and reaction thermodynamics of both KBH_4 and $NaBH_4$.[13]

This chapter is organized as follows. In section 3.2, we describe our DFT calculations and then discuss the DFT-optimized crystal structures of $LiK(BH_4)_2$, KBH_4 and $NaBH_4$. Both KBH_4 and $NaBH_4$ exist in several crystal structures.[22-24] These results appear to be the first report systematically examining the multiple possible structures of the two materials with DFT. In addition to describing structural aspects of the crystals, we report predictions for the bulk modulus and elastic constants of KBH_4 and $NaBH_4$ and compare these results with previous experimental observations. In section 3.3, we examine the stability of $LiK(BH_4)_2$. Our DFT calculations indicate that at room temperature this material is unstable with respect to decomposition into $LiBH_4$ and KBH_4, suggesting that the experimental observations by Nickel *et*

al. may correspond to a metastable material. We also predict the reaction products of heating this material (or more precisely, mixture of materials) to temperatures high enough that hydrogen is released. Finally, section 3.4 examines whether reaction mixtures exist involving KBH_4, $NaBH_4$, or $LiK(BH_4)_2$ and other compounds whose reaction thermodynamics are more favorable than the borohydrides alone. We found multiple two step reactions in which $LiK(BH_4)_2$ could release useful amounts of hydrogen in combination with other reactants after decomposition into $LiBH_4$ and KBH_4. We also identify several reaction mixtures involving either KBH_4 or $NaBH_4$ that have reaction thermodynamics within the range of values that would make future experimental studies of these reaction mixtures worthwhile.

3.2 Crystal Structures of Materials

3.2.1 Computational Details

All of our DFT calculations were performed with the PW91 generalized gradient approximation (GGA) functional using the Vienna *ab initio* simulation package.[25-28] The core electrons of each atom were described by the projector augmented wave (PAW) method.[29] We used a conjugate gradient method for optimization of all materials. A cutoff energy of 425 eV was used in all calculations. Geometries were relaxed until the forces on all atoms were less than 0.03 eV/Å.

We carried out bulk optimization for supercells comprised of 1×1×1 unit cells of $LiK(BH_4)_2$, KBH_4 and $NaBH_4$. The optimization of $LiK(BH_4)_2$ was carried out using a 6×12×4 Monkhorst-Pack mesh of *k*-points. The calculations for γ-KBH_4 and β-$NaBH_4$ were performed using a 9×9×6 and 8×8×6 Monkhorst-Pack mesh of *k*-points, respectively. The calculations for α-KBH_4 and α-$NaBH_4$ used a 6×6×6 Monkhorst-Pack mesh of *k*-points. We examined the Vibrational Density of States (VDOS) of two phases for KBH_4 and $NaBH_4$ using the PHONON code developed by Parlinski to identify the relative stability between two phases at finite temperatures.[30]

$B_{12}H_{12}$ species have been observed as intermediate materials in a variety of reactions associated with metal borohydrides.[31-36] To include species of this type in our study, we used DFT to optimize the structure of $Li_2B_{12}H_{12}$, $MgH_{12}H_{12}$, $CaB_{12}H_{12}$, and $K_2B_{12}H_{12}$ using supercells comprised of 1 × 1 × 1 unit cells. For these materials, the initial structures for geometry relaxations were obtained from the previous experimental data and computational calculations.[31, 37] These calculations used a Monkhorst-Pack mesh of 8 × 8 × 8, 5 × 7 × 8, 9 × 5 × 6, and 8 × 8 × 8 *k*-points, respectively.

3.2.2 $LiK(BH_4)_2$

Nickels *et al.* synthesized $LiK(BH_4)_2$ having an orthorhombic structure with a = 7.91 Å, b = 4.49 Å, c = 13.84 Å, cell volume V = 492.0 Å^3, and space group Pnma (No. 62).[11] More recently, a DFT optimized structure of $LiK(BH_4)_2$ was reported by Xiao *et al*.[12] They optimized $LiK(BH_4)_2$ using the PW91-GGA functional. In our calculations, optimizing the structure with DFT starting from the experimental structure gives us an orthorhombic structure with a = 7.78 Å, b = 4.43 Å, c = 13.72 Å, and cell volume V = 473.4 Å^3. Table 3.1 shows the results of our DFT-optimized structures and experimental structures of $LiK(BH_4)_2$. Our cell volume is 3.78% smaller than the experimentally observed value, and very similar to the cell volume of the structure optimized by Xiao *et al*., which is 3.82% smaller than the experimentally observed one.[12] The results from DFT for other borohydrides are helpful for assessing our optimized structure. Dai *et al.* optimized $Mg(BH_4)_2$ using the PW91 functional from its experimentally observed structure, finding a cell volume 2.13% smaller than experiment.[38] Vajeeston *et al.* performed similar calculations for the orthorhombic (hexagonal) structures of $LiBH_4$ using the PW91 functional, and calculated cell volumes that differed from experimental observations by −1.41% (-8.55%).[23] Miwa *et al.* investigated the orthorhombic structure of $LiBH_4$ using the PBE functional, finding a cell volume 1.8% smaller than the experimental value.[39] The deviation between our DFT-optimized cell volume for $LiK(BH_4)_2$ is therefore similar to results for other borohydrides.

The calculated Li – B distances in the DFT-optimized structure are 2.46, 2.49, and 2.59 Å, which are 0.77 ~ 3.49% shorter than the experimental values of 2.51, 2.58, and 2.61 Å. The calculated B – Li – B angles are 102, 104, 114 and 118˚, in good agreement with the experimental values of 101, 102, 115, and 119˚.

Table 3.1: Lattice constants and unit cell volumes for $LiK(BH_4)_2$, KBH_4, and $NaBH_4$ from DFT calculations and experiments[11, 22-24].

Material		DFT-calculated values		Experimental values	
		Lattice constants (Å)	Volume (Å^3)	Lattice constants (Å)	Volume (Å^3)
$LiK(BH_4)_2$		*a* = 7.78 *b* = 4.43 *c* = 13.72	473.4	*a* = 7.91 *b* = 4.49 *c* = 13.84	492.0
KBH_4	α phase	*a* = 6.69	299.3	*a* = 6.71	302.1
	γ phase	*a* = 4.71 *c* = 6.61	146.5	*a* = 4.68 *c* = 6.57	143.9
$NaBH_4$	α phase	*a* = 6.02	218.2	*a* = 6.15	232.6
	β phase	*a* = 4.31 *c* = 5.82	108.1	*a* = 4.35 *c* = 5.86	110.9

3.2.3 KBH_4

Renaudin *et al.* reported that KBH_4 has a phase transition from γ-KBH_4 (the low temperature structure) to α-KBH_4 (the high temperature structure) at 66 K.[22] This work also indicated that that α-KBH_4 has space group $Fm\bar{3}m$ (No. 225) with lattice parameter *a* = 6.71 Å and V=302.1 Å^3 and γ-KBH_4 has space group $P4_2/nmc$ (No. 137) with *a* = 4.68 Å, *c* = 6.57 Å and V=143.9 Å^3. Table 3.1 contains the results of the DFT-optimized structures and experimental structures of KBH_4. The DFT-optimized structure of γ-KBH_4 has *a* = 4.71 Å and *c* = 6.61 Å, giving a cell volume 1.81% larger than the experimental value.[22]

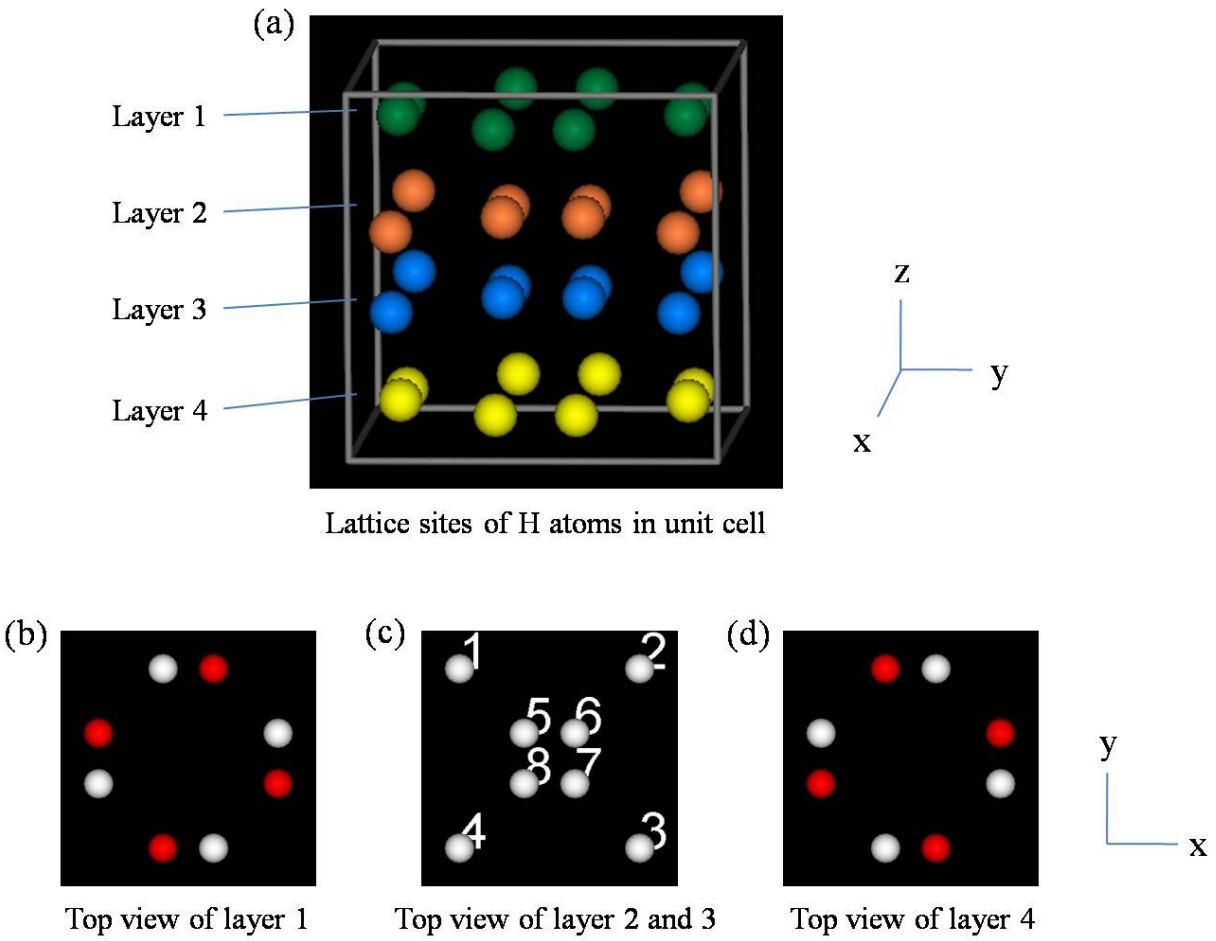

Figure 3.1: (a) The possible lattice sites for H atoms in α-KBH_4 and α-$NaBH_4$ with H atoms of half occupancy. (b) - (d) Top views of layer 1, 2, 3, and 4 from (a). In (b) and (d), the red circles are the lattice sites occupied by H atoms in the structures examined in our initial calculations.

Table 3.2: The initial positions of H atoms and the relative energies for α-KBH_4 and α-$NaBH_4$. The second and third columns represent the initial positions of H atoms in the layer 2 and layer 3 expressed using the labels in Fig.3.1(c).

α-KBH_4	H position (Layer 2)	H position (Layer 3)	E_{diff} (α-KBH_4) (eV/f.u.)
Case 1	2, 4, 5, 7	1, 3, 6, 8	0
Case 2	1, 3, 4, 6	2, 5, 7, 8	0
Case 3	1, 2, 3, 4	2, 5, 7, 8	0.11
Case 4	1, 3, 4, 6	5, 6, 7, 8	0.11
Case 5	1, 3, 4, 6	2, 4, 5, 7	0.11
Case 6	2, 4, 5, 7	3, 5, 6, 8	0.11
Case 7	1, 3, 4, 6	1, 2, 3, 8	0.16
Case 8	2, 5, 7, 8	4, 5, 6, 7	0.16
Case 9	1, 2, 3, 4	2, 3, 4, 5	0.40
Case 10	2, 5, 7, 8	5, 6, 7, 8	0.53
Case 11	1, 2, 3, 4	5, 6, 7, 8	2.06
Case 12	1, 2, 3, 4	2, 4, 5, 7	2.19
Case 13	2, 4, 5, 7	5, 6, 7, 8	2.19
Case 14	1, 2, 3, 4	1, 2, 3, 4	4.11
Case 15	5, 6, 7, 8	5, 6, 7, 8	4.11
α-$NaBH_4$	H position (Layer 2)	H position (Layer 3)	E_{diff} (α-$NaBH_4$) (eV/f.u.)
Case 1	2, 4, 5, 7	1, 3, 6, 8	0
Case 2	1, 3, 4, 6	2, 5, 7, 8	0
Case 3	1, 2, 3, 4	2, 5, 7, 8	0
Case 4	1, 3, 4, 6	5, 6, 7, 8	0
Case 5	1, 3, 4, 6	2, 4, 5, 7	0
Case 6	2, 4, 5, 7	3, 5, 6, 8	0
Case 13	2, 4, 5, 7	5, 6, 7, 8	0
Case 12	1, 2, 3, 4	2, 4, 5, 7	0.01
Case 7	1, 3, 4, 6	1, 2, 3, 8	0.06
Case 8	2, 5, 7, 8	4, 5, 6, 7	0.06
Case 10	2, 5, 7, 8	5, 6, 7, 8	0.38
Case 9	1, 2, 3, 4	2, 3, 4, 5	0.39
Case 11	1, 2, 3, 4	5, 6, 7, 8	1.98
Case 14	1, 2, 3, 4	1, 2, 3, 4	3.84
Case 15	5, 6, 7, 8	5, 6, 7, 8	3.85

α-KBH_4 includes lattice sites for H atoms with half occupancy, as shown in Fig. 3.1. In a DFT calculation, it is necessary to specify each site as either occupied or unoccupied; it is not possible to directly examine partial occupancies. In our initial calculations, we considered structures in which half of the sites in layers 1 and 4 in each unit cell were occupied by

alternating positions within these adjacent layers (see Fig.3.1). Fifteen independent structures were then examined corresponding to different orderings of H atoms in layers 2 and 3. The initial positions of the occupied H atoms in the layer 2 and 3, and the relative energies after minimization for all cases are shown in Table. 3.2 and the optimized positions of the occupied H atoms after optimization for all cases are shown in Table 3.3. In case 9 and 10, the optimized positions of H atoms are not located at the numbered positions, so it is difficult to describe the optimized position using the numbered positions (See Table 3.4). Of these fifteen structures, two have equivalent energies that are lower than all of the others. The remaining structures have energies that are at least 0.11 eV/formula unit higher in energy. The two lowest energy structures from this list are not completely isotropic. That is, they do not have the identical orderings of H atoms in the ±x, ±y, and ±z directions and, after optimization, cubic unit cells. It is possible, however, to rearrange the H atoms within the unit cell into a structure that has the same total energy and is identical in the six lattice directions (±x, ±y, and ±z). This structure is shown in Fig. 3.2. The optimized structure of α-KBH_4 with this ordering of the H atoms has a lattice constant of a = 6.69 Å, giving a cell volume 0.93% smaller than the experimental value.[22]

Table 3.3: The optimized positions of H atoms for α-KBH_4 and α-$NaBH_4$. For the case 9 and 10, it is difficult to describe the position of H atoms using the numbered H atoms since the optimized atoms are not located at the numbered positions.

α-KBH_4	H position (Layer 2)	H position (Layer 3)
Case 1	2, 4, 5, 7	1, 3, 6, 8
Case 2	2, 4, 5, 7	1, 3, 6, 8
Case 3	2, 3, 7, 8	1, 2, 5, 8
Case 4	1, 4, 5, 6	3, 4, 6, 7
Case 5	1, 4, 5, 6	3, 4, 6, 7
Case 6	3, 4, 5, 8	2, 3, 5, 6
Case 7	1, 2, 6, 7	1, 4, 7, 8
Case 8	1, 2, 6, 7	1, 4, 7, 8
Case 11	1, 2, 3, 4	5, 6, 7, 8
Case 12	1, 2, 3, 4	2, 4, 5, 7
Case 13	2, 4, 5, 7	5, 6, 7, 8
Case 14	1, 2, 3, 4	1, 2, 3, 4
Case 15	5, 6, 7, 8	5, 6, 7, 8
α-$NaBH_4$	H position (Layer 2)	H position (Layer 3)
Case 1	2, 4, 5, 7	1, 3, 6, 8
Case 2	2, 4, 5, 7	1, 3, 6, 8
Case 3	2, 4, 5, 7	1, 3, 6, 8
Case 4	2, 4, 5, 7	1, 3, 6, 8
Case 5	2, 4, 5, 7	1, 3, 6, 8
Case 6	2, 4, 5, 7	1, 3, 6, 8
Case 13	2, 4, 5, 7	1, 3, 6, 8
Case 12	2, 4, 5, 7	1, 3, 6, 8
Case 7	1, 4, 6, 7	1, 2, 7, 8
Case 8	1, 2, 7, 8	1, 4, 6, 7
Case 11	1, 2, 3, 4	5, 6, 7, 8
Case 14	1, 2, 3, 4	1, 2, 3, 4
Case 15	5, 6, 7, 8	5, 6, 7, 8

Table 3.4. The fractional coordinates of the optimized positions of H atoms for configurations 9 and 10 of α-KBH_4 and α-$NaBH_4$.

α-KBH_4	H position (Layer 2)	H position (Layer 3)
Case 9	(0.13, 0.24, 0.86) (0.31, 0.58, 0.64) (0.15, 0.85, 0.56) (0.74, 0.84, 0.56)	(0, 0.37, 0.54) (0.4, 0.37, 0.53) (0.03, 0.03, 0.49) (0.92, 0.8, 0.31)
Case 10	(0.14, 0.29, 0.67) (0.62, 0.37, 0.58) (0.13, 0.82, 0.55) (0.4, 0.47, 0.5)	(0.9, 0.79, 0.41) (0.6, 0.6, 0.39) (0.07, 0.02, 0.34) (0.5, 0.28, 0.28)
α-$NaBH_4$	H position (Layer 2)	H position (Layer 3)
Case 9	(0.68, 0.82, 0.67) (0.77, 0.94, 0.66) (0.16, 0.02, 0.63) (0.34, 0.57, 0.59)	(0.51, 0.33, 0.48) (0.93, 0.13, 0.48) (0.09, 0.88, 0.37) (0.27, 0.44, 0.33)
Case 10	(0.05, 0.74, 0.66) (0.63, 0.56, 0.64) (0.16, 0.02, 0.55) (0.41, 0.41, 0.5)	(0.96, 0.84, 0.41) (0.52, 0.69, 0.39) (0.69, 0.17, 0.31) (0.57, 0.27, 0.3)

To assess the optimized structure of α-KBH_4, we calculated the elastic constants, C_{11}, C_{12}, and C_{44}, and bulk modulus, B.[40-42] In these calculations, a small volumetric strain is applied to a crystal to obtain C_{11} and C_{12} from the relation between the normal strain and normal stress.[40] For C_{44}, a small shear strain is applied to the crystal, and C_{44} is obtained from the relation between the shear strain and the shear stress.[40] We calculated the bulk modulus, B, in two ways. First, we used the definition $B=(C_{11}+2C_{12})/3$ from the elastic constants described above. Second, we determined B by fitting energy-volume data for isotropic deformations of the unit cell to the third order Birch-Murnaghan equation of state.[24, 41, 43] Table 3.5 shows our calculated elastic constants and bulk modulus and the experimental measurements by Kumar *et al.*[44] for α-KBH_4. Our two calculations of the bulk modulus yield almost identical results, and this result is ~ 11% higher than the experimental value. There may be some contribution to the elasticity in the real material due to disorder in the H positions, but our calculation is not capable of estimating the strength of this effect. Kumar *et al.* also reported a value of the bulk modulus from Car-Parrinello molecular

dynamics (CPMD) calculations performed using DFT with a local density approximation (LDA) functional.[44, 45] This calculation gave the bulk modulus of 15.4 GPa. It seems likely that the difference between our DFT result and this earlier theoretical result is mainly due to the different functionals used in the two calculations.

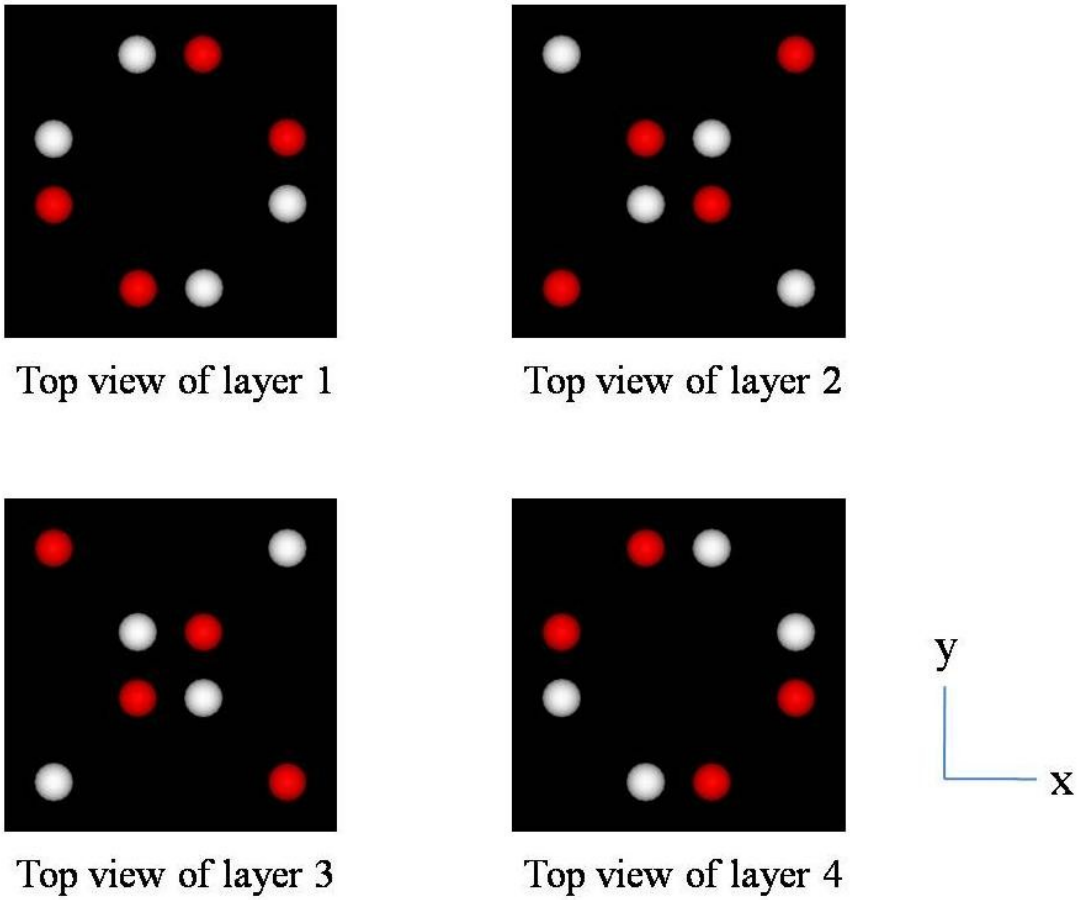

Figure 3.2: The lattice sites for H atoms in the optimized structures of α-KBH_4 and α-$NaBH_4$. In the figures, the red circles are the lattice sites occupied by H atoms.

Table 3.5: The elastic constants and bulk modulus of α-KBH_4. There is no experimental result for the elastic constants, C_{11}, C_{12}, and C_{44}.[44]
[a]Data obtained from $B=(C_{11}+2C_{12})/3$.
[b]Data obtained from the Birch-Murnaghan equation of state.

	Calculated value (GPa)	Experimental value (GPa)
B	18.7[a] (18.8[b])	16.8
C_{11}	35.3	N/A
C_{12}	10.5	N/A
C_{44}	8.9	N/A

We examined the relative stability between the two phases of KBH_4 by considering the vibrational and entropic contributions obtained from the calculated VDOS for the DFT-optimized ordered structures described above. This calculation yields $\Delta(H_\gamma - H_\alpha)_{300\ K}$ = -1.4 kJ/mol and $\Delta(S_\gamma - S_\alpha)_{300\ K}$ = 2.9 J/K/mol, giving $\Delta(G_\gamma - G_\alpha)_{300\ K}$ = -2.3 kJ/mol. It is also appropriate to include the configurational entropy associated with the disordered H in α-KBH_4 in this description.[46-48] Treating the H atoms as completely disordered over the available sites with half occupancy gives a configurational entropy for α-KBH_4 of 46.1 J/K/mol. This value should be regarded as an upper bound on the material's true configurational entropy, since the DFT calculations described showed that some combinations of H positions are enthalpically unfavorable. Including this configurational entropy in our description gives $\Delta(G_\gamma - G_\alpha)_{300\ K}$ = 11.6 kJ/mol. Figure 3.3 shows the relative Gibbs free energies for two phases of KBH_4 as a function of temperature. A striking feature of this figure is that it indicates that no phase transition would occur if configurational entropy in the α phase was neglected. Recalling that our calculated configurational entropy is an upper bound, the phase transition temperature from γ-KBH_4 to α-KBH_4 obtained from Fig. 3.3, 39 K, is in good agreement with the experimentally reported temperature, 66 K.[22]

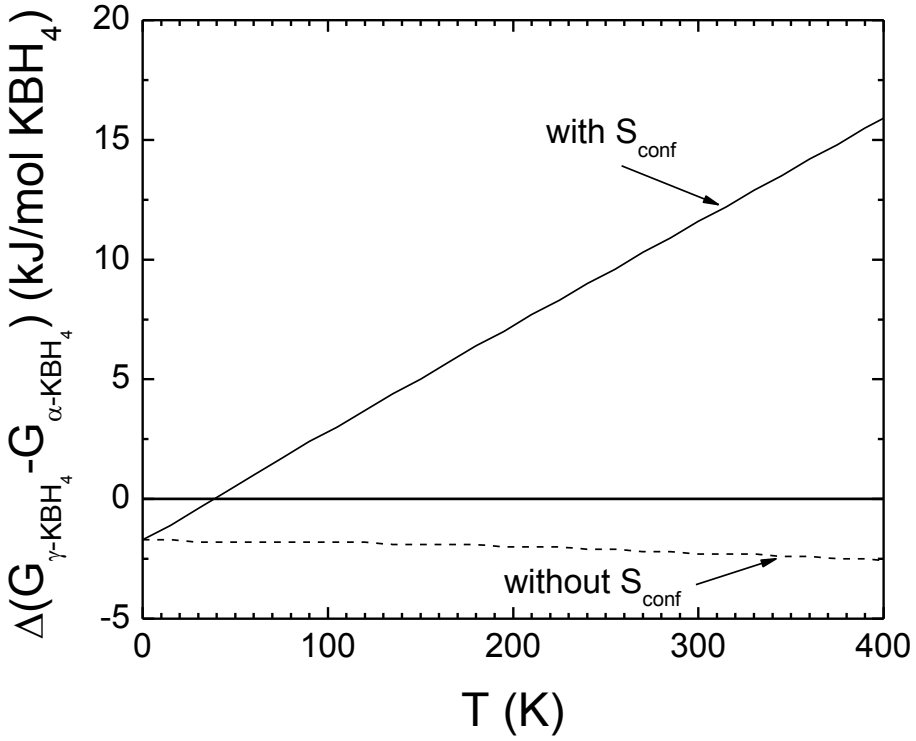

Figure 3.3: The relative Gibbs free energies of γ-KBH_4 and α-KBH_4. The solid (dashed) curve represents the case where the configurational entropy for α-KBH_4 is included (neglected).

3.2.4 $NaBH_4$

Allis *et al.* reported that $NaBH_4$ has a phase transition from β-$NaBH_4$ (the low temperature structure) to α-$NaBH_4$ (the high temperature structure) at 189.9 K.[49] α-$NaBH_4$[24] has lattice parameters a = 6.15 Å and cell volume V=232.6 $Å^3$ with space group $Fm\bar{3}m$ (No. 225) and β-$NaBH_4$[23] has lattice parameters a = 4.35 Å, c = 5.86 Å, cell volume V=110.9 $Å^3$ with space group of $P42_1c$ (No. 114).

As shown in Table 3.1, the DFT-optimized structure of β-$NaBH_4$ has lattice parameters of a = 4.31 Å and c = 5.82 Å, giving a cell volume 2.52% smaller than the experimental value. α-$NaBH_4$ is structurally similar to α-KBH_4, including H atoms of half occupancy, so the structure

of α-$NaBH_4$ was also examined by the procedure described above for α-KBH_4. The initial positions of the occupied H atoms in the layer 2 and 3, and the relative energies after minimization for all cases are shown in Table. 3.2 and the optimized positions of the occupied H atoms after optimization for all cases are shown in Table 3.3. In case 9 and 10, the optimized positions of H atoms are not located at the numbered positions, so it is difficult to describe the optimized position using these positions (See Table 3.4). Of these fifteen structures, eight have equivalent energies that are at least 0.05 - 0.06 eV/formula unit lower than all of the others. The eight lowest energy structures from this list are not completely isotropic. Similarly to our treatment of α-KBH_4, it is possible to rearrange the H atoms within the unit cell to give an isotropic structure without changing the material's total energy. The resulting optimized structure of α-$NaBH_4$ has lattice constant a = 6.02 Å, giving a cell volume 6.19% smaller than the experimental value.[24]

We calculated the elastic constants, C_{11}, C_{12}, and C_{44}, and bulk modulus B of α-$NaBH_4$ using the same methods described above for α-KBH_4.[40-42] Table 3.6 shows our calculated elastic constants and bulk modulus and the experimental measurements by Chernyshov *et al*.[33] for α-$NaBH_4$.[50] The calculated elastic constants are 14.3 and 6.3% lower for C_{11} and C_{12}, and 40.4% higher for C_{44} than the experimental values.[50] Our two calculations of the bulk modulus yield almost identical results, and this result is $\sim$ 14% lower than the experimental value.[50] As stated above, our calculations cannot estimate contributions to the elasticity in the real material due to disorder in the H positions. Kim *et al*. reported a value of the bulk modulus for this material from CPMD calculation performed using DFT with LDA functional.[51] This calculation gave the bulk modulus of 20.6 GPa. It seems likely that the difference between our DFT result and this earlier result is mainly due to the different functionals used in the two calculations.

Table 3.6: The calculated and experimental values for the elastic constants and bulk modulus of α-$NaBH_4$.
[a]Data obtained from $B=(C_{11}+2C_{12})/3$.
[b]Data obtained from the Birch-Murnaghan equation of state.

	Calculated value (GPa)	Experimental value (GPa)
B	13.5[a] (13.6[b])	15.8
C_{11}	22.7	26.5
C_{12}	8.9	9.5
C_{44}	13.2	9.4

The relative stability of the two phases of $NaBH_4$ was examined by the procedure described above for α-KBH_4. The calculation yields $\Delta(H_\beta - H_\alpha)_{300\ K}$ = -5.3 kJ/mol and $\Delta(S_\beta - S_\alpha)_{300\ K}$ = -9.4 J/K/mol, giving $\Delta(G_\beta - G_\alpha)_{300\ K}$ = -2.5 kJ/mol. The calculation for the configurational entropy associated with the completely disordered H in α-$NaBH_4$ gives the value of 46.1 J/K/mol (the same as α-KBH_4). As stated above for α-KBH_4, this value should be regarded as an upper bound on the material's true configurational entropy. Including the configurational entropy in our description gives $\Delta(G_\beta - G_\alpha)_{300\ K}$ = 11.3 kJ/mol. Figure 3.4 shows the relative Gibbs free energies for two phases of $NaBH_4$ as a function of temperature. A striking feature of this figure is that it indicates that the phase transition would occur at 525 K, that is, 335.1 K higher than the experimentally reported temperature, if configurational entropy in the □ phase was neglected. Recalling that our calculated configurational entropy is an upper bound, the phase transition temperature from β-$NaBH_4$ to α-$NaBH_4$ obtained from Fig. 3.4, 88 K, is in reasonable agreement with the experimental observation.

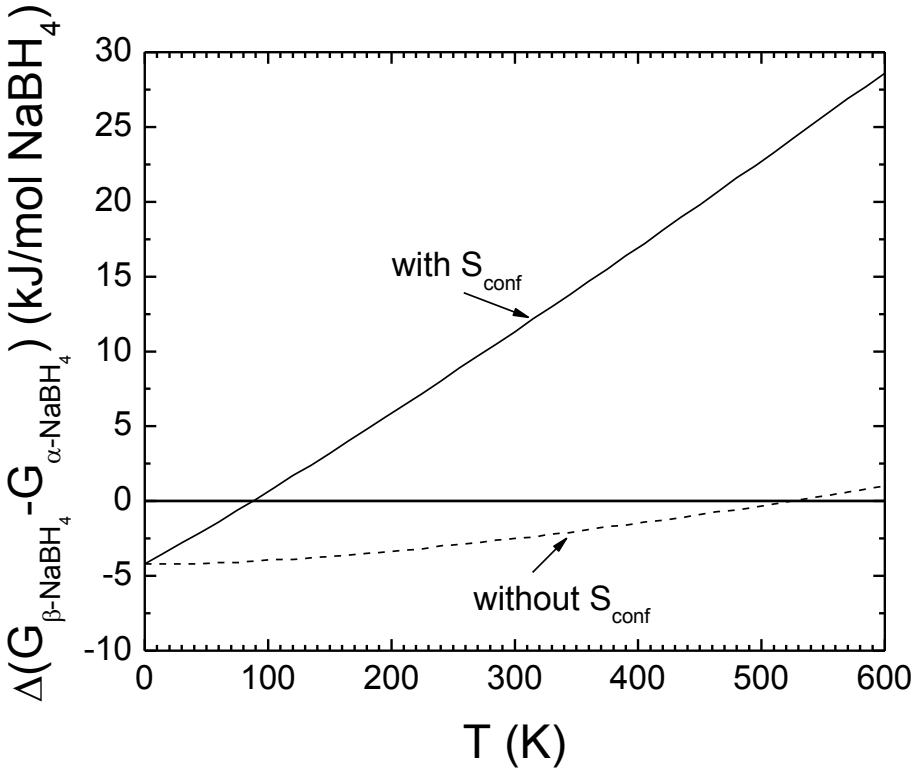

Figure 3.4: The relative Gibbs free energies of β-$NaBH_4$ and α-$NaBH_4$. The solid (dashed) curve represents the case where the configurational entropy for α-$NaBH_4$ is included (neglected).

3.3 Stability of $LiK(BH_4)_2$

Nickels *et al.* synthesized $LiK(BH_4)_2$ from an equimolar mixture of $LiBH_4$ and KBH_4.[11] We now turn to examining the thermodynamics of the reaction

$$LiBH_4 + KBH_4 \rightarrow LiK(BH_4)_2 \tag{3.1}$$

using the DFT results described above. The temperature dependent free energy change calculated from DFT including vibrational and configurational contributions to the free energy for this reaction is shown in Fig. 3.5. If the configurational entropy of KBH_4 is neglected, the bialkali material is predicted to be marginally stable at very low temperatures but marginally unstable at

room temperature. Specifically, our VDOS calculations yield $\Delta H_{300\,K}$ = -1.3 kJ/mol and $\Delta S_{300\,K}$ = -15.5 J/K/mol, giving $\Delta G_{300\,K}$ = 3.3 kJ/mol (neglecting configurational entropy). This prediction changes substantially when configurational entropy is included. Including the configurational entropy for α-KBH_4 of 46.1 J/K/mol gives $\Delta G_{300\,K}$ = 17.2 kJ/mol, and these calculations predict that the bialkali material is unstable against decomposition into KBH_4 and $LiBH_4$ at essentially all temperatures. As discussed above, the value we have used for the configurational entropy in α-KBH_4 is likely to overestimate this entropy because not all possible orderings of H atoms in the structure are equally likely. Nevertheless, the prediction of our DFT calculations is that the bialkali material synthesized by Nickel *et al*. is a metastable material. This situation is similar to the behavior of $Ca(AlH_4)_2$, which decomposes into reaction products with loss of hydrogen at low temperatures.[14, 15, 18, 52] This suggests that although $LiK(BH_4)_2$ is an interesting material for understanding the general properties of bi-alkali borohydrides, it is unlikely to be useful in practical schemes to store H_2 for vehicular applications.

We now address the experimental observations of Nickels *et al.*[11] for $LiK(BH_4)_2$. Their main observation is that the compound is synthesized by ball-milling the mixture of $LiBH_4$ and KBH_4, and then the compound is decomposed with weight loss at 653 K. The identity of the products of this decomposition was not reported. Our calculated result above gives a simple prediction for the decomposition products starting from the metastable bialkali material: first, the compound would decompose to the mixture of $LiBH_4$ and KBH_4 without weight loss, followed by decomposition of these separate species.

We predicted the reaction path for this combination of materials using the methods of Alapati et al.;[14-18] more information on this approach is given in Section 3.4. After including the $B_{12}H_{12}$ species listed in Section 3.2.1, our calculations predict

$$\mathrm{LiK(BH_4)_2} \rightarrow \mathrm{LiBH_4 + KBH_4} \rightarrow \mathrm{KBH_4} + \frac{5}{6}\mathrm{LiH} + \frac{1}{12}\mathrm{Li_2B_{12}H_{12}} + \frac{13}{12}\mathrm{H_2} \quad . \qquad (3.2)$$

This decomposition reaction for $LiBH_4$ differs from the reaction reported in a number of experiments[14-18] and in earlier theoretical calculations[14-18] these earlier sources indicated that

$LiBH_4$ decomposes into a mixture of LiH, B, and H_2. Recent NMR experiments by Hwang et al.,[14-18] however, support the idea that $Li_2B_{12}H_{12}$ appears as a decomposition product of $LiBH_4$. The decomposition temperature of 653 K reported by Nickels *et al.* is similar enough to previous reports of $LiBH_4$ decomposition[11] to indicate that this is a plausible description of the reaction observed by in these experiments.

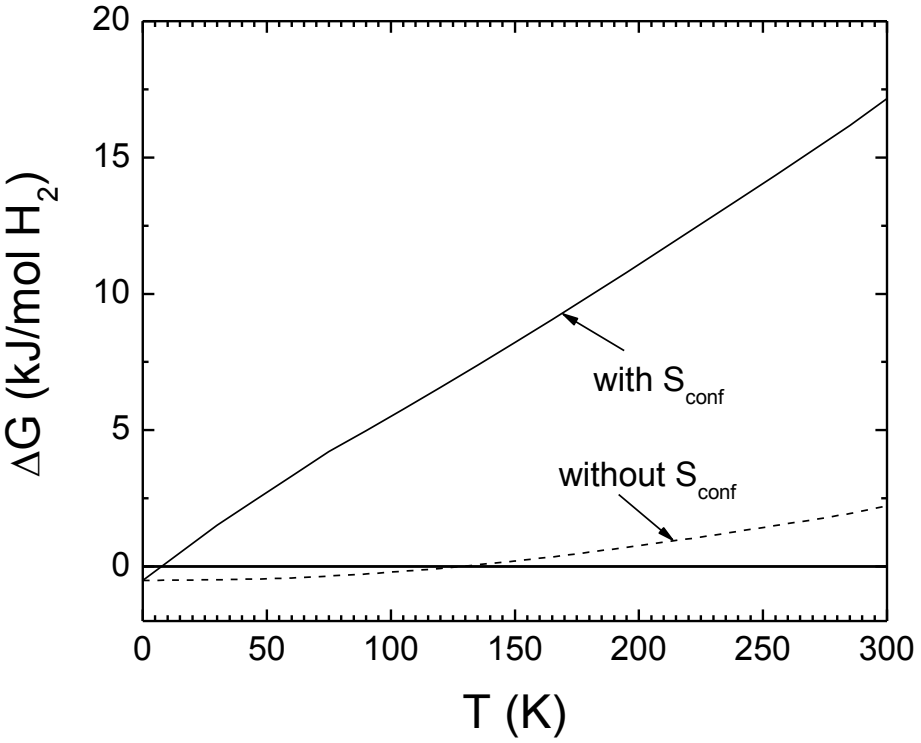

Figure 3.5: The change of the Gibbs free energies for the reaction (1) as a function of temperature. The solid (dashed) curve represents the case where the configurational entropy is included (neglected).

3.4 Destabilization Reactions Involving KBH_4, $NaBH_4$, or $LiK(BH_4)_2$

3.4.1 Theory for the Thermodynamic Calculations

We now turn to the prediction of destabilization reactions that involve $LiK(BH_4)_2$, KBH_4, or $NaBH_4$. Our calculations are based on the methods of Alapati *et al.*[14-18, 46], which estimate reaction thermodynamics at finite temperatures using DFT total energies at 0 K. More precise information about reaction thermodynamics can be obtained from DFT-based calculations of the Gibbs' free energy of reaction, as was done above to examine the stability of $LiK(BH_4)_2$.[14-17, 46] Comparisons between calculations with these two approaches have shown that the approach based on 0 K enthalpies gives reliable predictions.[14-17, 46] The main advantage of using the 0 K enthalpy approach is that a large database of materials can be developed without performing computationally demanding VDOS calculations for every material.

We followed the approach of Alapati *et al.*, which uses a database of DFT-calculated energies for 212 crystalline compounds containing Al, B, C, Ca, K, Li, Mg, N, Na, Sc, Si, Ti, V, and H.[14-18] We added our DFT results for $LiK(BH_4)_2$, KBH_4, $NaBH_4$, $Li_2B_{12}H_{12}$, $MgB_{12}H_{12}$, $K_2B_{12}H_{12}$, and $CaB_{12}H_{12}$ to this database. For a specified chemical mixture, H_2 pressure, and temperature, the equilibrium composition of the mixture among all possible combinations of materials in the database can be found rigorously and efficiently by solving a linear program following the methods introduced by Ozolins, Wolverton, and co-workers.[19-21]

The caveats associated with this computational approach to predict chemical reaction paths have been discussed previously by Alapati *et al.*[14-18] Briefly, these calculations cannot give information about the existence of materials not included in the database or about situations where kinetic limitations dictate some details of the reactions observed experimentally. The only gaseous species included in these calculations is H_2, so we cannot comment on the possible formation of other gaseous species.

One difference between our calculations and the methods of Alapati *et al.* is that our database includes two materials, KBH_4, and $NaBH_4$, for which configurational entropy plays an

important role. For these materials, we performed thermodynamic calculations where the estimate for the configurational entropy given in section 3.2.3 and 3.2.4 was incorporated into the grand potential used by Alapati *et al.* in determining the equilibrium composition of each system of interest. These calculations predict a reaction temperature based on external H_2 pressure of 1 bar, so in situations where configurational entropy plays a role in the reaction, we report the contribution of the configurational entropy to the reaction free energy at the reaction temperature, $T_{rxn}\Delta S_{conf}$. It has been shown before that using the 0 K enthalpies defined above typically overestimates the finite temperature reaction free energy when this free energy is calculated including zero point energies and finite temperature vibrational effects.[14] As a result, the temperature of the reaction is typically overestimated by this method, meaning in turn that the magnitude of $T\Delta S_{conf}$ is overestimated in the results reported below. For specific reactions of significant interest, this uncertainty can be removed by performing VDOS calculations for all of the solids involved in the reaction.[14, 16, 17]

To examine the reaction thermodynamics of $LiK(BH_4)_2$, we considered five element spaces that are composed of Li-K-B-X-Y, where X, Y = Al, C, Ca, Mg, N, Na, Sc, Si, Ti, V. Similarly, the destabilization reactions for KBH_4 ($NaBH_4$) were predicted from the thermodynamic calculations with the four element spaces K(Na)-B-X′-Y′, where X′, Y′ = Al, C, Ca, Mg, N, Na(K), Sc, Si, Ti, V. Here the sum of the mole fractions of elements composing each element space is equal to 1. In each element space, distinct compositions filling the entire element space were defined using increments in the non-H mole fraction of 0.02.

3.4.2 Destabilization Reactions associated with KBH_4 and $NaBH_4$

We first describe reactant mixtures involving KBH_4 and $NaBH_4$ that can destabilize these borohydrides to allow H_2 release at moderate temperatures. Our thermodynamic calculations for the direct decomposition of these two borohydrides give 0 K reaction enthalpies, ΔU_0, (configurational entropy changes at the reaction temperature, $T_{rxn}\Delta S_{conf}$) of 117.5 (-27.8) kJ/mol H_2 and 101.5 (-25.4) kJ/mol H_2 for KBH_4 and $NaBH_4$, respectively, with the decomposition

reactions occurring as follows:

$$KBH_4 \rightarrow \frac{5}{6}K + \frac{1}{12}K_2B_{12}H_{12} + 1.5H_2 \quad (3.3)$$

$$NaBH_4 \rightarrow Na + B + 2H_2 \quad . \quad (3.4)$$

This 0 K reaction enthalpy for KBH_4 ($NaBH_4$) is 25.3 (4.5) kJ/mol H_2 lower than for a reaction mechanism that produces KH and B (NaH and B) as products. We expect from the predicted mechanisms of $LiBH_4$ and KBH_4 that the decomposition reactionof $NaBH_4$ might involve $Na_2B_{12}H_{12}$, but we do not have the structural information for $Na_2B_{12}H_{12}$ necessary to test this idea.

When seeking destabilized reactions involving KBH_4 or $NaBH_4$, we followed the criteria used by Alapati *et al.*[15], namely we only retained single step reactions with $15 \leq \Delta U_0 \leq 75$ kJ/mol H_2 and a H_2 capacity at completion $\geq$ 6.0 wt.%. After scanning the full range of reactant compositions defined above, these calculations predicted five destabilization reactions for KBH_4, as listed in Table 3.7. The analogous calculations for $NaBH_4$ yield the five reactions listed in Table 3.8. The first and third reactions involving KBH_4 and $Mg(BH_4)_2$ in Table 3.7 produce $K_2B_{12}H_{12}$, but not $MgB_{12}H_{12}$.

Table 3.7: The single step destabilization reactions involving KBH_4 satisfying the criteria described in the text. T_{rxn} and S_{conf} indicate the reaction temperature and the configurational entropy.

Reaction	wt.%	ΔU_0 (kJ/mol H_2)	$T_{rxn}\Delta S_{conf}$ (kJ/mol H_2)
$KBH_4 + 2.5Mg(BH_4)_2 + 1.25Si \rightarrow 1.25Mg_2Si + 0.5K_2B_{12}H_{12} + 9H_2$	8.1	37.3	-2.9
$KBH_4 + LiH + 2LiNH_2 \rightarrow Li_3BN_2 + KH + 4H_2$	7.48	43.6	-7.2
$KBH_4 + 2.5Mg(BH_4)_2 \rightarrow 2.5MgH_2 + 0.5K_2B_{12}H_{12} + 6.5H_2$	6.94	38	-4.0
$KBH_4 + 1.5LiNH_2 \rightarrow 0.5Li_3BN_2 + 0.5BN + KH + 3H_2$	6.84	41.6	-9.7
$KBH_4 + 0.75Mg(NH_2)_2 \rightarrow 0.25Mg_3N_2 + BN + KH + 3H_2$	6.29	46.9	-10.3

Table 3.8: Similar to Table 3.7 but for reactions involving $NaBH_4$.

Reaction	wt.%	ΔU_0 (kJ/mol H_2)	$T_{rxn}\Delta S_{conf}$ (kJ/mol H_2)
$NaBH_4 + 0.75Mg(NH_2)_2 \rightarrow NaH + 0.25Mg_3N_2 + BN + 3H_2$	7.55	34.4	-8.8
$NaBH_4 + LiH + C \rightarrow NaH + LiBC + 2H_2$	6.98	62.9	-19
$NaBH_4 + LiNH_2 \rightarrow NaH + LiH + BN + 2H_2$	6.63	19.4	-11.3
$NaBH_4 + 0.5ScH_2 \rightarrow NaH + 0.5ScB_2 + 2H_2$	6.58	67.5	-19.8
$NaBH_4 + 0.5TiH_2 \rightarrow NaH + 0.5TiB_2 + 2H_2$	6.42	40	-15.1

In terms of equilibrium thermodynamics, the reaction in Table 3.8 combining $NaBH_4$ and $LiNH_2$ is the most attractive, with ΔU_0 - $T_{rxn}\Delta S_{conf}$ = 30.7 kJ/mol H_2. As discussed above, this value is expected to overestimate the true reaction free energy for the reaction. It must be noted, however, that this reaction (and several of the other reactions in Tables 3.7 and 3.8) includes BN as a reaction product. BN is a refractory material, so it is reasonable to be concerned that the reaction kinetics of hydrogenation reactions involving mixtures of this material could be severely kinetically hindered even if the reaction thermodynamics are favorable. The reactions in Table 3.8 that combine $NaBH_4$ with ScH_2 or TiH_2 are analogous to destabilization reactions of the latter hydrides with $LiBH_4$ that have been previously predicted to have reasonable thermodynamic properties[14, 15] but which have not been observed to react, presumably due to kinetic limitations, in experimental studies.[53, 54] The reaction in Table 3.8 that combines $NaBH_4$, LiH, and C could also potentially react via the formation of CH_4 or other gaseous hydrocarbons, but even without this complication the relatively high value of ΔU_0 - $T_{rxn}\Delta S_{conf}$ for this reaction makes it of only limited interest.

To summarize our results for the destabilization of KBH_4 or $NaBH_4$, our calculations have identified 10 single step reactions that meet the criteria listed above. An important conclusion from calculations of this kind is that there are no other combinations of the large number of crystalline materials we have considered that meet these criteria. Although there are good reasons to suspect that it may be difficult to observe most of the reactions as they are

described above due to kinetic limitations, these results point out a number of specific reactant mixtures that would be worthwhile examining experimentally.

3.4.3 Destabilization Reactions associated with $LiK(BH_4)_2$

Our calculations above predicted that $LiK(BH_4)_2$ is unstable with respect to decomposition into $LiBH_4$ and KBH_4 at room temperature and above. Although the bialkali borohydride is therefore best described as a metastable material, it is nevertheless useful to consider when this material can be combined with other reactants to achieve a destabilized path to reversible hydrogen storage. To explore this possibility, we used the thermodynamic approach described above to examine a wide range of reactant mixtures in which $LiBH_4$ and KBH_4 are present in equimolar quantities. All reactions that are predicted involving these mixtures can be interpreted as involving $LiK(BH_4)_2$, with the initial step in the reaction starting from the bialkali borohydride being its decomposition into $LiBH_4$ and KBH_4.

There are two classes of reactions that exist including $LiK(BH_4)_2$. In the first class, the overall mixture reacts in two steps, with one step being a destabilized reaction involving $LiBH_4$ and the second a similar reaction but involving KBH_4. To give one example, an initial reactant mixture of $LiBH_4$, KBH_4, $Mg(BH_4)_2$, LiH, and $LiNH_2$ in the ratio 2:2:5:2:4 reacts in two steps:

$$LiBH_4 + 2.5Mg(BH_4)_2 \rightarrow 2.5MgH_2 + 0.5Li_2B_{12}H_{12} + 6.5\ H_2 \quad (3.5)$$

$$KBH_4 + LiH + 2LiNH_2 \rightarrow Li_3BN_2 + KH + 4H_2 \quad (3.6)$$

with a total H_2 capacity of 8 wt.%. Both of the individual reaction steps have 15 kJ/mol $H_2 \leq \Delta U_0 \leq$ 75 kJ/mol H_2. Almost all pairs of the reactions listed for KBH_4 in Table 3.7 and the analogous reactions for $LiBH_4$ predicted by Alapati *et al.*[14, 15] can be combined in this way, but this approach cannot be said to have identified any new reactions. The one interesting feature of combining reactions in this way is that single step reactions that do not release enough H_2 on their own to be useful can be combined with another single step reaction that releases a large amount of H_2 to yield a net system that still has a useful H_2 capacity. For example, an initial mixture of $LiBH_4$, KBH_4, VH_2, and C with the ratio of 2:2:3:2 produces 6.03 wt.% H_2 from the

two step reaction

$$LiBH_4 + C \rightarrow LiBC + 2H_2 \quad (3.7)$$

$$KBH_4 + 1.5VH_2 \rightarrow 0.5V_3B_2 + KH + 3H_2 \quad . \quad (3.8)$$

Here, the two steps have 0 K reaction enthalpies (configurational entropy changes at the reaction temperature) of 37 (0) kJ/mol H_2 and 40.5 (-9.6) kJ/mol H_2, respectively. If the second reaction in this sequence is considered alone, it only has a H_2 capacity of 4.53 wt.%, but the higher H_2 capacity of the first reaction raises the overall H_2 capacity of the reaction mixture.

A more interesting set of two step reactions occurs in mixtures where one of the reaction products of the first reaction is a reactant in the second reaction. As one example, an initial mixture of $LiBH_4$, KBH_4, $LiNH_2$, and N_4Si_3 with the ratio of 4:4:8:1 produces 7.07 wt.% H_2 from the two step reaction

$$LiBH_4 + 0.25N_4Si_3 \rightarrow LiH + 0.75Si + BN + 1.5H_2 \quad (3.9)$$

$$KBH_4 + LiH + 2LiNH_2 \rightarrow Li_3BN_2 + KH + 4H_2 \quad . \quad (3.10)$$

The two steps in this mechanism have ΔU_0 ($T_{rxn}\Delta S_{conf}$) of 38.6 (0) kJ/mol H_2 and 43.6 (-7.2) kJ/mol H_2, respectively. The LiH formed as a product in the reaction involving $LiBH_4$ acts as a reactant in the reaction of KBH_4. Our calculations identified 16 distinct two step reactions with similar properties to this example. The net reaction of each of these 16 reaction schemes is shown in Table 3.9, with the species that acts as both a product and a reactant indicated for each reaction. Nine of the reactions use LiH as the shared species by using the second reaction in Table 3.7 as the reaction that includes KBH_4, while the other seven reactions include Si, MgH_2, or $Li_2B_{12}H_{12}$ as the shared species. Of the 16 reactions listed in Table 3.9, the two reactions that use $TiSi_2$ and VSi_2 as reactants are perhaps the most interesting in the sense that the other fourteen reactions all involve reaction products such as BN or $B_{12}H_{12}$-containing materials that are likely to be associated with kinetic limitations, Sc-containing materials, which have obvious cost limitations, or C-containing materials, which have the possibility for the evolution of impurity gases such as methane. We emphasize, however, that our calculations predict all of the

two step reaction schemes shown in Table 3.9 correspond to minimum energy reaction paths within the large set of crystal structures we have considered and they have equilibrium reaction thermodynamics for each step satisfying 15 kJ/mol $H_2 \leq \Delta U_0 \leq 75$ kJ/mol H_2.

Table 3.9: Net reactions involving mixtures of $LiK(BH_4)_2$ and other reactants with 15 kJ/mol $H_2 \leq \Delta U_0 \leq 75$ kJ/mol H_2 for each reaction step and a total H_2 capacity ≥ 6.0 wt.%. Each reaction proceeds in two steps, as described in the text. The column labeled "Shared species" indicates the species that is a product in the first step of the overall reaction and a reactant in the second step.

Reaction	Shared species	wt.%
$LiBH_4 + KBH_4 + 2.5Mg(BH_4)_2 + 1.25Si + C \rightarrow LiBC + 1.25Mg_2Si + Li_3BN_2 + 0.5K_2B_{12}H_{12} + 11H_2$	$Li_2B_{12}H_{12}$	8.6
$LiBH_4 + KBH_4 + 2LiNH_2 + 0.5ScH_2 \rightarrow 0.5ScB_2 + Li_3BN_2 + KH + 6H_2$	LiH	8.33
$LiBH_4 + KBH_4 + 2LiNH_2 + \frac{1}{6}LiH \rightarrow \frac{1}{12}Li_2B_{12}H_{12} + Li_3BN_2 + KH + \frac{61}{12}H_2$	LiH	8.33
$LiBH_4 + KBH_4 + 2.5Mg(BH_4)_2 + 1.25Si \rightarrow \frac{5}{6}LiH + \frac{1}{12}Li_2B_{12}H_{12} + 1.25Mg_2Si + 0.5K_2B_{12}H_{12} + \frac{121}{12}H_2$	$Li_2B_{12}H_{12}$	8.27
$LiBH_4 + KBH_4 + 2.5Mg(BH_4)_2 + 0.5Si + 0.25N_4Si_3 \rightarrow LiH + BN + 1.25Mg_2Si + 0.5K_2B_{12}H_{12} + 10.5H_2$	Si	8.15
$LiBH_4 + KBH_4 + 2.5Mg(BH_4)_2 + 0.25Si + 0.5TiSi_2 \rightarrow LiH + 0.5TiB_2 + 1.25Mg_2Si + 0.5K_2B_{12}H_{12} + 10.5H_2$	Si	7.85
$LiBH_4 + KBH_4 + 2LiNH_2 + \frac{1}{3}TiN \rightarrow \frac{1}{3}TiB_2 + \frac{1}{3}BN + Li_3BN_2 + KH + 5.5H_2$	LiH	7.79
$LiBH_4 + KBH_4 + 2.5Mg(BH_4)_2 + C \rightarrow LiBC + 2.5MgH_2 + 0.5K_2B_{12}H_{12} + 8.5H_2$	$Li_2B_{12}H_{12}$	7.69
$LiBH_4 + KBH_4 + 2LiNH_2 + 0.5TiC \rightarrow 0.5C + 0.5TiB_2 + Li_3BN_2 + KH + 5.5H_2$	LiH	7.31
$LiBH_4 + KBH_4 + 2.5Mg(BH_4)_2 + 0.5TiH_2 \rightarrow 0.5Li_2B_{12}H_{12} + 0.5TiB_2 + 1.5MgH_2 + KMgH_3 + 8.5H_2$	MgH_2	7.27
$LiBH_4 + KBH_4 + 2.5Mg(BH_4)_2 \rightarrow \frac{5}{6}LiH + \frac{1}{12}Li_2B_{12}H_{12} + 2.5MgH_2 + 0.5K_2B_{12}H_{12} + \frac{91}{12}H_2$	$Li_2B_{12}H_{12}$	7.26
$LiBH_4 + KBH_4 + 2LiNH_2 + 0.25N_4Si_3 \rightarrow 0.75Si + BN + Li_3BN_2 + KH + 5.5H_2$	LiH	7.07
$LiBH_4 + KBH_4 + 2LiNH_2 + 0.5ScSi \rightarrow 0.5Si + 0.5ScB_2 + Li_3BN_2 + KH + 5.5H_2$	LiH	7.01
$LiBH_4 + KBH_4 + 2LiNH_2 + 0.5TiSi_2 \rightarrow Si + 0.5TiB_2 + Li_3BN_2 + KH + 5.5H_2$	LiH	6.38
$LiBH_4 + KBH_4 + 2LiNH_2 + 0.5VSi_2 \rightarrow Si + 0.5VB_2 + Li_3BN_2 + KH + 5.5H_2$	LiH	6.33
$LiBH_4 + KBH_4 + 2LiNH_2 + \frac{1}{6}V_6C_5 \rightarrow \frac{5}{6}C + VB + Li_3BN_2 + KH + 5.5H_2$	LiH	6.07

3.5 Conclusions

In this chapter, we have described the structures and reaction thermodynamics of $LiK(BH_4)_2$, KBH_4, and $NaBH_4$ using DFT calculations. Our calculations examined the multiple phases that are known to exist for KBH_4 and $NaBH_4$, and showed that the configurational entropy associated with H disorder plays an important role in determining which phase is stable at room temperature. Both KBH_4 and $NaBH_4$ have large enthalpies for direct decomposition, meaning that very high temperatures are needed to dehydrogenate these materials. We showed, however, that a small number of destabilization reactions exist in which KBH_4 or $NaBH_4$ can be combined with other reactants to greatly lower the enthalpy required for dehydrogenation in a single reaction step. A useful feature of these calculations is that they show that a very large number of other possible reaction mixtures involving these borohydrides cannot achieve this important goal. These calculations have identified a number of reactant mixtures involving KBH_4 or $NaBH_4$ that would be worthwhile examining experimentally.

The structural properties of $LiK(BH_4)_2$ calculated with DFT are in good agreement with earlier experimental studies of this material. Our DFT calculations predict that this bialkali borohydride is unstable at room temperature and higher temperatures with respect to decomposition into $LiBH_4$ and KBH_4, so previous experimental observations of this material may have been in a metastable state. Our thermodynamic calculations identified a number of two step reactions in which $LiK(BH_4)_2$, or more precisely, its constituent borohydrides, can be combined with other reactants to release appreciable amounts of H_2 with reaction enthalpies that are potentially of interest for practical applications. Many of these two step reactions are simply linear combinations of individual reactions already known for the individual borohydrides, but sixteen reaction schemes were identified in which a reaction product of the first reaction is used as a reactant in the subsequent reaction.

3.6 REFERENCES

1. B. Bogdanovic and M. Schwickardi, *J. Alloys Compd.*, 1997, **253-254**, 1-9.
2. J. Wang, A. D. Ebner and J. A. Ritter, *J. Am. Chem. Soc.*, 2006, **128**, 5949-5954.
3. M. Fichtner, O. Fuhr and O. Kircher, *J. Alloys Compd.*, 2003, **356-357**, 418-422.
4. J. J. Vajo, S. L. Skeith and F. Mertens, *J. Phys. Chem. B*, 2005, **109**, 3719-3722.
5. A. Zuttel, S. Rentsch, P. Fischer, P. Wenger, P. Sudan, P. Mauron and C. Emmenegger, *J. Alloys Compd.*, 2003, **356-357**, 515-520.
6. H. W. Li, K. Kikuchi, Y. Nakamori, N.Ohba, K. Miwa, S. Towata and S. Orimo, *Acta Mater.*, 2008, **56**, 1342-1347.
7. J. H. Kim, S. A. Jin, J. H. Shim and Y. W. Cho, *Scripta Mater.*, 2008, **58**, 481-483.
8. P. Chen, Z. Xiong, J. Luo, J. Lin and K. L. Tan, *Nature*, 2002, **420**, 302-304.
9. J. Lu and Z. Z. Fang, *J. Phys. Chem. B*, 2005, **109**, 20830-20834.
10. G. Soloveichik, J. H. Her, P. W. Stephens, Y. Gao, J. Rijssenbeek, M. Andrus and J.-C. Zhao, *Inorg. Chem.*, 2008, **47**, 4290-4298.
11. E. A. Nickels, N. O. Jones, W. I. F. David, S. R. Johnson, R. L. Lowton, M. Sommariva and P. P. Edwards, *Angew. Chem. Int. Ed.*, 2008, **47**, 2817-2819.
12. X.-B. Xiao, W.-Y. Yu and B.-Y. Tang, *J. Phys.: Condens. Matter*, 2008, **20**, 445210-445211 ~ 445210-445216.
13. K. C. Kim and D. S. Sholl, *J. Phys. Chem. C*, 2010, **114**, 678-686.
14. S. V. Alapati, J. K. Johnson and D. S. Sholl, *Phys. Chem. Chem. Phys.*, 2007, **9**, 1438-1452.
15. S. V. Alapati, J. K. Johnson and D. S. Sholl, *J. Phys. Chem. C*, 2008, **112**, 5258-5262.
16. S. V. Alapati, J. K. Johnson and D. S. Sholl, *J. Phys. Chem. C*, 2007, **111**, 1584-1591.
17. S. V. Alapati, J. K. Johnson and D. S. Sholl, *J. Alloys Compd.*, 2007, **446**, 23-27.
18. S. V. Alapati, J. K. Johnson and D. S. Sholl, *J. Phys. Chem. B*, 2006, **110**, 8769-8776.
19. D. J. Siegel, C. Wolverton and V. Ozoliņš, *Phys. Rev. B*, 2007, **76**, 134102-134101~134106.
20. A. R. Akbarzadeh, V. Ozolinš and C. Wolverton, *Adv. Mater.*, 2007, **19**, 3233-3239.
21. C. Wolverton and V. Ozolinš, *Phys. Rev. B*, 2007, **75**, 064101.
22. G. Renaudin, S. Gomes, H. Hagemann, L. Keller and K. Yvon, *J. Alloys Compd.*, 2004, **375**, 98-106.
23. P. Vajeeston, P. Ravindran, A. Kjekshus and H. Fjellvag, *J. Alloys Compd.*, 2005, **387**, 97-104.
24. R. S. Kumar and A. L. Cornelius, *Appl. Phys. Lett.*, 2005, **87**, 261916.
25. J. P. Perdew, J. A. Chevary, S. H. Vosko, K. A. Jackson, M. R. Pederson, D. J. Singh and C. Fiolhais, *Phys. Rev. B*, 1992, **46**, 6671-6687.
26. G. Kresse and J. Hafner, *Phys. Rev. B*, 1993, **47**, 558-561.
27. G. Kresse and J. Furthmuller, *Phys. Rev. B*, 1996, **54**, 11169-11186.
28. D. Vanderbilt, *Phys. Rev. B*, 1990, **41**, 7892-7895.
29. G. Kresse and D. Joubert, *Phys. Rev. B*, 1999, **59**, 1758.
30. K. Parlinski, *Software PHONON*, 2005.
31. J. H. Her, M. Yousufuddin, W. Zhou, S. S. Jalisatgi, J. G. Kulleck, J. A. Zan, S. J. Hwang, J. Robert C. Bowman and T. J. Udovic, *Inorganic Chemistry*, 2008, **47**, 9757-9759.

32. H. W. Li, K. Miwa, N. Ohba, T. Fujita, T. Sato, Y. Yan, S. Towata, M. W. Chen and S. Orimo, *Nanotechnology*, 2009, **20**, 204013.
33. V. Ozolins, E. H. Majzoub and C. Wolverton, *J. Am. Chem. Soc.*, 2009, **131**, 230-237.
34. S. J. Hwang, J. Robert C. Bowman, J. W. Reiter, J. Rijssenbeek, G. L. Soloveichik, J. C. Zhao, H. Kabbour and C. C. Ahn, *J. Phys. Chem. C*, 2008, **112**, 3164-3169.
35. A. Zuttel, A. Borgschultea and S. I. Orimo, *Scr. Mater.*, 2007, **56**, 823-828.
36. N. Ohba, K. Miwa, M. Aoki, T. Noritake, S. I. Towata, Y. Nakamori, S. Orimo and A. Zuettel, *Phys. Rev. B*, 2006, **74**, 075110.
37. J. A. Wunderlich and W. N. Lipscomb, *J. Am. Chem. Soc.*, 1960, **82**, 4427-4428.
38. B. Dai, D. S. Sholl and J. K. Johnson, *J. Phys. Chem. C*, 2008, **112**, 4391-4395.
39. K. Miwa, N. Ohba, S. Towata, Y. Nakamori and S.-i. Orimo, *Phys. Rev. B*, 2004, **69**, 245120-245121 ~ 245120-245128.
40. E. Menéndez-Proupin and A. K. Singh, *Phys. Rev. B*, 2007, **76**, 054117.
41. R. Zhu, E. Pan, P. Chung, X. Cai, K. M. Liew and A. Buldum, *Semicond. Sci. Technol.*, 2006, **21**, 906-911.
42. J. K. Baria, *Physica B*, 2006, **371**, 280-296.
43. F. Birch, *J. Geophys. Res.*, 1978, **83**, 1257-1268.
44. R. S. Kumar, E. Kim and A. L. Cornelius, *J. Phys. Chem. C*, 2008, **112**, 8452-8457.
45. R. Car and M. Parrinello, *Phys. Rev. Lett.*, 1985, **55**, 2471-2474.
46. S. V. Alapati, J. K. Johnson and D. S. Sholl, *Phys. Rev. B*, 2007, **76**, 104108.
47. S. S. Kapur and T. Sinno, *Appl. Phys. Lett.*, 2008, **93**, 221911.
48. S. S. Kapur, M. Prasad, J. C. Crocker and T. Sinno, *Phys. Rev. B*, 2005, **72**, 014119.
49. D. G. Allis and B. S. Hudson, *Chem. Phys. Lett.*, 2004, **385**, 166-172.
50. D. Chernyshov, A. Bosak, V. Dmitriev, Y. Filinchuk and H. Hagemann, *Phys. Rev. B*, 2008, **78**, 172104-172101~172104.
51. E. Kim, R. Kumar, P. F. Weck, A. L. Cornelius, M. Nicol, S. C. Vogel, J. Zhang, M. Hartl, A. C. Stowe, L. Daemen and Y. Zhao, *J. Phys. Chem. B*, 2007, **111**, 13873-13876.
52. C. Weidenthaler, T. J. Frankcombe and M. Felderhoff, *Inorg. Chem.*, 2006, **45**, 3849–3851.
53. J. Yang, A. Sudik and C. Wolverton, *J. Phys. Chem. C*, 2007, **111**, 19134-19140.
54. J. Purewal, S. J. Hwang, J. Robert C. Bowman, E. Rnnebro, B. Fultz and C. Ahn, *J. Phys. Chem. C*, 2008, **112**, 8481-8485.

CHAPTER 4

LARGE-SCALE SCREENING OF PROMISING METAL HYDRIDES BASED ON EQUILIBRIUM REACTION THERMODYNAMICS

4.1 Introduction

In Chapter 3, we have discussed the approach to search metal hydride mixtures having favorable reaction thermodynamics with releasing a sufficient H_2.[1] However, this discussion has been limited to only metal hydride mixtures involving $LiK(BH_4)_2$, KBH_4, or $NaBH_4$.[1] Under this limitation, it was not possible to find every possible promising metal hydride mixture. For example, even though Vajo et al.[2] reported that $LiBH_4$ was experimentally destabilized by MgH_2 and Ibikunle *et al.*[3] reported that $LiBH_4$ was experimentally destabilized by CaH_2, we could not predict these metal hydride mixtures. We therefore extend our discussion associated with the approach to large collection of possible metal hydride mixtures.

Several earlier efforts have been made to categorize metal hydride mixtures using the thermodynamic calculations based on the first-principles calculations and a database of crystal compounds.[4-9] The methodological basis of these calculations is the grand canonical linear programming method introduced by Ozolins and co-workers.[4-7, 9] This approach rigorously determines the thermodynamic state of a specified set of elements among a set of crystalline materials in equilibrium with gaseous H_2, subject to a number of caveats that are discussed in section 4.2. Ozolins *et al.* systematically predicted the thermodynamics of possible metal hydride mixtures in the Li-Mg-Ca-B-H system using this method[7]. They same group has reported results for the Li-B-N-H, Li-Mg-N-H and Li-Mg-Al-H systems.[4-6, 9] Calculations that explored a wider range of elements were performed by Alapati, Johnson, and Sholl, who analyzed the 715 four-element spaces available from thirteen elements and H atom with the same method.[8] Alapati et al. performed calculations based on 0 K reaction enthalpies predicted by DFT, an approach that

requires less computational effort for each solid than the free energy calculations used by Ozolins et al. The approximation inherent in this approach can readily be removed for specific reactions of interest by computing the DFT-based free energies of the solids involved in these reactions.[8, 10-12]

A key limitation of the linear programming approach is that it cannot make predictions about reactions that involve compounds that are not included in the database of materials used for the calculations. Because of the large amount of research that has been performed on metal hydrides and related materials in recent years, the studies cited above were based on databases that did not include many materials that have been characterized in more recent experiments. For example, the earlier work of Alapati et al. did not include the metal closoboranes (Li, Mg, Ca, K)$B_{12}H_{12}$ which since that time have been observed or predicted as intermediates in the decomposition reactions of the metal borohydrides.[1, 7, 13-16] One aim of this chapter is to update the comprehensive calculations of Alapati et al. using a database of materials that includes a large number of these recently described compounds. Specifically, we performed the necessary DFT calculations to add 147 new crystalline compounds (including but not limited to $B_{12}H_{12}$-based materials) to the 212 materials that were used earlier by Alapati et al. We then analyzed the reactions thermodynamics for all reaction mixtures defined by the 715 four-element spaces mentioned above.

The earlier work of Alapati et al. categorized the large number of distinct reactions that can occur for mixtures involving metal hydrides by focusing exclusively on reactions that occur in a single step. As discussed in section 4.2.2, however, there are well known examples of multi-step reactions that have properties that are interesting in H_2 storage applications that are not captured if one focuses solely on single step reactions. A second aim of this chapter is analyze the large number of reactive mixtures listed above to identify multi-step reactions with useful thermodynamic properties. Below, we introduce a straightforward method to achieve this goal and apply it to the 715 four-element spaces accessible via our thermodynamic calculations.

4.2 Theoretical Approach

4.2.1 Thermodynamic Calculations

Our calculations are based on the methods of Alapati *et al.*, which estimate reaction thermodynamics at finite temperatures using Density Functional Theory (DFT) total energies at 0 K.[8, 10-12, 17] We denote the reaction enthalpy based on 0 K DFT total energies by ΔU_0. More precise information about reaction thermodynamics can of course be obtained from DFT-based calculations of the Gibbs' free energy of reaction. Comparisons between calculations with these two approaches have shown that the approach based on 0 K enthalpies gives reliable predictions. The main advantage of using the 0 K enthalpy approach is that a large database of materials can be developed without performing computationally demanding vibrational density of states (VDOS) calculations for every material.

We followed the approach of Alapati *et al.*, which used a database of DFT-calculated energies for 212 crystal compounds containing Al, B, C, Ca, K, Li, Mg, N, Na, Sc, Si, Ti, V, and H.[8] We updated this database with 147 additional crystal compounds whose structures have been identified.[18] These 147 materials are identified in Table 4.1. A list of the complete set of 359 materials used in our thermodynamic calculations is given in the Table 4.2. For a specified chemical mixture, H_2 pressure (1 bar), and temperature, the equilibrium composition of the mixture among all possible combinations of materials in the database can be found rigorously and efficiently by solving a linear program.[5-9]

Table 4.1: 147 crystalline compounds whose total energies were calculated with DFT in this work.

Two-element compounds				
AlB_{12}	Al_4C_3	Al_4Ca	$Al_{14}Mg_{13}$	$Al_{30}Mg_{23}$
$Al_{23}V_4$	$Al_{45}V_7$	B_4C	$B_{13}C_2$	$(B_{10}H_{13})_2$
$B_{13}N_2$	C_2Ca	C_2N_2	C_3N_4	C_5N_4
$C_{12}N_6$	CaB_4	Ca_2Si	KC_8	KSi
K_8Si_{46}	LiB	LiMg	$Li_{12}Si_7$	$Li_{13}Si_4$
$Li_{15}Si_4$	NaB_{15}	Na_3B_{20}	Na_4Si_4	Na_8Si_{46}
$Sc_{15}C_{19}$	SiB_3	SiC	TiV	V_2N
V_5Si_3				
Three-element compounds				
$Al(BH_4)_3$	Al_2MgC_2	$Al_{18}Mg_3Ti_2$	BC_2N	$C_2H_4N_4$
$C_2H_{18}N_{18}$	$C_2N_2(NH)$	Ca_4Al_3Mg	CaAlSi	$Ca(BH_4)_2$
$CaB_{12}H_{12}$	CaC_4N_6	$Ca_4N_2(CN_2)$	$Ca_{11}N_6(CN_2)_2$	$CaSiN_2$
$Ca_2Si_5N_8$	$Ca_5(Si_2N_6)$	Ca_4TiN_4	H_9CN_9	KBH_4
$KB_{21}H_{18}$	$K_2B_6H_6$	$K_2(B_{10}H_{10})$	$K_2B_{12}H_{12}$	KC_4N_3
KNH_2	$(K(NH_2))(NH_3)_2$	$LiAlB_{14}$	$LiB_{13}C_2$	$Li_2B_{12}C_2$
LiBH	$Li(BH_2)$	$Li_2B_{12}H_{12}$	$Li_3(BH_6)$	$Li_2B_{12}Si_2$
$LiMgH_3$	Li_2MgSi	LiN_3Si_2	$LiNa_2N$	$LiNa_5N_2$
$Li_2Na_4N_2$	Li_2NaN	$Li_3Na_3N_2$	$Li_4Na_2N_2$	Li_5NaN_2
Li_3NaSi_6	$MgAl_2Si_2$	$MgB_{12}C_2$	$Mg_2B_{24}C$	$MgB_{12}H_{12}$
$MgB_{12}Si_2$	MgC_4N_6	Mg_7TiH_{16}	N_2BH_7	$N_2B_{10}H_{18}$
$N_3B_3H_6$	$N_3B_3H_{12}$	$N_4B_9H_{11}$	$N_4B_{10}H_8$	$N_4B_{10}H_{22}$
NH_3BH_3	$(NH_4)_2B_{12}H_{12}$	$(NH_2)CN$	NH_4HCN_2	$Na_5Al_3H_{14}$
$NaBH_4$	$Na_2(B_{10}H_{10})$	$Na_3(BN_2)$	$Na_3C_6N_9$	Sc_2AlC
Ti_2AlC	Ti_6Si_2B	$V_{12}Al_3C_8$	V_5SiB_2	
Four-element compounds				
$AlNC_3H_{10}$	BCH_5N_2	$B_{10}C_6H_{30}N_2$	$B_{20}C_3H_{30}N_2$	BC_4KN_4
$CH_3NH_2BH_3$	$Ca(NH_2BH_3)_2$	$KAl(NH_2)_4$	$K_5C_2HN_4$	$KCaN_3H_6$
$K(HCN_2)$	K_2LiAlH_6	$KLi_3(NH_2)_4$	$KLi_7N_8H_{16}$	$K_2Li(NH_2)_3$
$K_2Mg(NH_2)_4$	K_2NaAlH_6	$K_2Na(NH_2)_3$	$K_3Si_6N_{11}H_6$	$LiAlMg_{10}H_{24}$
$Li(B(CN)_4)$	$Li_2Ca(NH)_2$	$LiK(BH_4)_2$	$Li(NH_2BH_3)$	$(Li(NH_3)_4)_2(B_6H_6)(NH_3)_2$
$LiNa_2AlH_6$	$LiNa_2(NH_2)_3$	$LiSc(BH_4)_4$	$Mg(BH_4)_2(NH_3)_2$	$(NH_4)B(CN)_4$
$NaAl(NH_2)_4$	$NaB(CN)_4$	$Si_2C_7H_{18}N_2$	$VC_8H_{24}N_4$	
Five-element compounds				
$LiAlC_4H_{16}N_4$	$LiSi_3C_9H_{27}N_2$	$Si_2B_2C_{12}H_{37}N_5$		

Table 4.2: List of 359 compounds included in our database.

One-element compounds				
Al	B	C	Ca	K
Li	Mg	Na	Sc	Si
Ti	V			
Two-element compounds				
AlB_2	AlB_{12}	Al_4C_3	Al_2Ca	Al_4Ca
AlH_3	AlLi	Al_2Li_3	Al_3Li	Al_4Li_9
$Al_{12}Mg_{17}$	$Al_{14}Mg_{13}$	$Al_{30}Mg_{23}$	AlN	AlSc
$AlSc_2$	Al_2Sc	Al_3Sc	AlTi	$AlTi_3$
Al_2Ti	Al_3Ti	AlV	AlV_3	Al_3V
$Al_{10}V$	$Al_{23}V_4$	$Al_{45}V_7$	B_4C	$B_{13}C_2$
$B_3Ca_4LiN_6$	$(B_{10}H_{13})_2$	BN	$B_{13}N_2$	C_2Ca
C_2N_2	C_3N_4	C_5N_4	$C_{12}N_6$	CaB_4
CaB_6	CaH_2	$CaLi_2$	$CaMg_2$	CaN_6
Ca_2N	Ca_3N_2	$Ca_{11}N_8$	CaSi	$CaSi_2$
Ca_2Si	Ca_5Si_3	KB_6	KC_8	K_2C_2
KH	KN_3	K_3N	KSi	K_4Si_4
K_8Si_{46}	LiB	Li_5B_4	Li_2C_2	LiH
LiMg	LiN_3	Li_3N	LiSi	Li_2Si
Li_7Si_2	$Li_{12}Si_7$	$Li_{13}Si_4$	$Li_{15}Si_4$	MgB_2
MgB_4	MgB_7	MgC_2	Mg_2C_3	MgH_2
Mg_3N_2	MgSc	Mg_2Si	Mg_5Si_6	N_4Si_3
NaB_{15}	Na_3B_{20}	Na_2C_2	NaH	NaN_3
Na_3N	NaSi	Na_4Si_4	Na_8Si_{46}	ScB_2
ScB_{12}	ScC	Sc_2C	Sc_2C_3	Sc_3C_4
Sc_4C_3	$Sc_{15}C_{19}$	ScH_2	ScN	ScSi
$ScSi_2$	Sc_5Si_3	SiB_3	SiB_6	SiC
SiH	TiB	TiB_2	TiC	Ti_2C
Ti_8C_5	TiH	TiH_2	TiN	Ti_2N
TiSi	$TiSi_2$	Ti_5Si_3	Ti_5Si_4	TiV
VB	VB_2	V_2B_3	V_3B_2	VC
V_2C	V_6C_5	V_8C_7	VH_2	V_2H
VN	V_2N	VSi_2	V_3Si	V_5Si_3
V_6Si_5				
Three-element compounds				
$Al(BH_4)_3$	Al_5C_3N	$Al_6C_3N_2$	$Al_7C_3N_3$	$Al_8C_3N_4$
$Al_2Ca_3N_4$	Al_2CaSi_2	$Al_2Ca_3Si_2$	$AlLi_3N_2$	AlLiSi
$Al_3Li_8Si_5$	$Al_3Li_{12}Si_4$	Al_2MgC_2	$AlMg_4Si_6$	$Al_{18}Mg_3Ti_2$
$AlSc_2Si_2$	BC_2N	$C_2H_4N_4$	$C_2H_{18}N_{18}$	$C_2N_2(NH)$
$CaAlH_5$	$Ca(AlH_4)_2$	Ca_4Al_3Mg	Ca_3AlN_3	CaAlSi
CaB_2C_2	$Ca(BH_4)_2$	$CaB_{12}H_{12}$	Ca_3BN_3	$CaCN_2$
CaC_4N_6	Ca_2HN	CaLiN	$CaLiSi_2$	Ca_2LiSi_3
$CaMg_2N_2$	CaMgSi	$Ca_4N_2(CN_2)$	$Ca_{11}N_6(CN_2)_2$	Ca_2N_3V

Table 4.2 continued

Ca_3N_3V	$CaSiN_2$	$Ca_2Si_5N_8$	$Ca_5(Si_2N_6)$	Ca_4TiN_4
H_9CN_9	$KAlH_4$	K_3AlH_6	KBH_4	$KB_{21}H_{18}$
$K_2B_6H_6$	$K_2(B_{10}H_{10})$	$K_2B_{12}H_{12}$	KCN	KC_2N_3
KC_4N_3	K_2CN_2	$K_3C_6N_9$	K_3LiSi_4	K_7LiSi_8
$KMgH_3$	K_2MgH_4	KNH_2	$(K(NH_2))(NH_3)_2$	$KSiH_3$
$LiAlB_{14}$	$LiAlH_4$	Li_3AlH_6	LiBC	$LiB_{13}C_2$
$Li_2B_{12}C_2$	LiBH	$Li(BH_2)$	$LiBH_4$	$Li_2B_{12}H_{12}$
$Li_3(BH_6)$	Li_3BN_2	$Li_2B_{12}Si_2$	LiCN	Li_2CN_2
$LiMgH_3$	LiMgN	Li_2MgSi	$Li_{12}Mg_3Si_4$	$LiNH_2$
Li_2NH	Li_4NH	LiN_3Si_2	Li_5N_3Si	Li_7N_4V
$LiNa_2N$	$LiNa_5N_2$	$Li_2Na_4N_2$	Li_2NaN	$Li_3Na_3N_2$
$Li_4Na_2N_2$	Li_5NaN_2	Li_3NaSi_6	Li_3ScN_2	$MgAlH_5$
$Mg(AlH_4)_2$	MgAlSi	$MgAl_2Si_2$	MgB_2C_2	$MgB_{12}C_2$
$Mg_2B_{24}C$	$Mg(BH_4)_2$	$MgB_{12}H_{12}$	MgB_9N	Mg_3BN_3
$MgB_{12}Si_2$	MgC_4N_6	Mg(NCN)	$Mg(NH_2)_2$	$MgSiN_2$
Mg_7TiH_{16}	N_2BH_7	$N_2B_{10}H_{18}$	$N_3B_3H_6$	$N_3B_3H_{12}$
$N_4B_9H_{11}$	$N_4B_{10}H_8$	$N_4B_{10}H_{22}$	NH_3BH_3	$(NH_4)_2B_{12}H_{12}$
$(NH_2)CN$	NH_4HCN_2	$N(SiH_3)_3$	$NaAlH_4$	Na_3AlH_6
$Na_5Al_3H_{14}$	NaAlSi	$NaAlSi_4$	$NaBH_4$	$Na_2(B_{10}H_{10})$
$Na_3(BN_2)$	NaCN	NaC_4N_3	Na_2CN_2	$Na_3C_6N_9$
$NaMgH_3$	NaN_3C_2	$NaNH_2$	$ScAl_3C_3$	Sc_2AlC
Sc_3AlC	ScB_2C	ScB_2C_2	Sc_2BC_2	$Sc_2V_3Si_4$
SiCN	SiC_2N_4	Si_2CN_4	Ti_2AlC	Ti_3AlC
Ti_3AlC_2	Ti_2AlN	Ti_3AlN	Ti_4AlN_3	Ti_6Si_2B
Ti_3SiC_2	$V_{12}Al_3C_8$	V_5SiB_2		
Four-element compounds				
$AlNC_3H_{10}$	BCH_5N_2	$B_{10}C_6H_{30}N_2$	$B_{20}C_3H_{30}N_2$	BC_4KN_4
$CH_3NH_2BH_3$	Ca_2N_2BH	$Ca(NH_2BH_3)_2$	$KAl(NH_2)_4$	$K_5C_2HN_4$
$KCaN_3H_6$	$K(HCN_2)$	K_2LiAlH_6	$KLi_3(NH_2)_4$	$KLi_7N_8H_{16}$
$K_2Li(NH_2)_3$	$K_2Mg(NH_2)_4$	K_2NaAlH_6	$K_2Na(NH_2)_3$	$K_3Si_6N_{11}H_6$
$LiAlMg_{10}H_{24}$	$LiAl(NH_2)_4$	$Li(B(CN)_4)$	$Li_4BN_3H_{10}$	$Li_2Ca(NH)_2$
$LiK(BH_4)_2$	$Li_2Mg(NH)_2$	$Li(NH_2BH_3)$	$(Li(NH_3)_4)_2(B_6H_6)(NH_3)_2$	$LiNa_2AlH_6$
$LiNa_2(NH_2)_3$	$Li_3Na(NH_2)_4$	$LiSc(BH_4)_4$	$Mg(BH_4)_2(NH_3)_2$	$(NH_4)B(CN)_4$
$NaAl(NH_2)_4$	$NaB(CN)_4$	NaN_2CH	$Si_2C_7H_{18}N_2$	$VC_8H_{24}N_4$
Five-element compounds				
$LiAlC_4H_{16}N_4$	$LiSi_3C_9H_{27}N_2$	$Si_2B_2C_{12}H_{37}N_5$		

It is important to describe how the 147 new materials in our database were selected. In general, we aimed to include in our calculations all crystalline compounds made up of any of the elements listed above which were searched from the Inorganic Crystal Structure Database (ICSD).[18] Searching the ICSD identified 272 compounds that were not included in the previous

database of Alapati et al. $Li_2B_{12}H_{12}$ and $MgB_{12}H_{12}$, which have been stated as intermediates in the decomposition of $LiBH_4$ and $Mg(BH_4)_2$, respectively, but were not yet listed in the ICSD were identified from recent reports.[7, 13] Unfortunately, not all of these compounds are amenable to DFT calculations. We excluded four categories of materials from our calculations. First, materials for which the atomic positions of all atoms have not been determined were excluded. This includes, for example $NaCa(NH_2)_3$ and $Na_5N_6C_3H$, in which the positions of 96 and 2 H atoms are not yet determined, respectively. Second, we excluded compounds in which one or more lattice sites have partial occupancies. It is possible to examine materials like this with DFT, but this process is often time consuming.[1] An example of a material with partial occupancies is $Mg(CN)_2$, in which C and N atoms are positioned in half of eight possible sites. Third, we excluded compounds whose unit cells have ≥ 400 atoms because DFT calculations with this many atoms are challenging. This group of materials includes $K_{12}Si_{17}$ (464 atoms), $Li_2SiC_6H_{18}N_4$ (496 atoms), and $Si_{12}Al_3C_{45}H_{114}N_3$ (708 atoms). Finally, we excluded materials that are molecular crystals in which dispersion forces play a key role in forming stable crystal structures. DFT calculations using the approach outlined above cannot accurately describe the cohesive energy of materials of this kind.[19] Examples of these compounds include NH, NH_3, N_2H_4, B_2H_6, B_4H_{10},and HCN. Many species in this group exist as gas-phase species under mild conditions. We have recently described an extension of the thermodynamic approach used below that allows the possible role of gas-phase species of this kind in reactions of complex metal hydrides to be assessed once specific reactions of interest are identified.[20] Considering the four groups of compounds just discussed removes 127 compounds from the initial set of 272 materials identified from the ICSD.

The caveats associated with our computational approach to predict chemical reaction paths have been discussed previously by Alapati *et al.*.[8, 10-12, 17] Briefly, these calculations cannot give information about the existence of materials not included in the database or about situations where kinetic limitations dictate some details of the reactions observed experimentally. The only gaseous species included in these calculations is H_2, so we cannot directly comment on the

possible formation of other gaseous species. For specific mixtures of interest, methods have recently been demonstrated to predict the possible evolution of gases other than H_2 using the FactSage program, a free energy minimization code designed to model complex multi-phase equilibria.[20] The detailed discussion is given in Chapter 6. This approach cannot readily be applied to the large database of materials we consider here because it requires calculation of the VDOS for every solid that is considered.

One difference between our calculations and those of Alapati *et al.* is that our database includes two materials, KBH_4, and $NaBH_4$, for which configurational entropy plays a role. These are the only two materials we considered whose crystal structures include lattice sites with partial occupancies. For these materials, we performed thermodynamic calculations where an estimate for the configurational entropy was incorporated into the grand potential used by Alapati *et al.* in determining the equilibrium composition of each system of interest.[1] These calculations predict a reaction temperature based on an external H_2 pressure of 1 bar, so in situations where configurational entropy plays a role in the reaction, we report the contribution of the configurational entropy to the reaction free energy at the reaction temperature, $T\Delta S_{\text{conf}}$.

To examine the reaction thermodynamics of a large range of chemical mixtures, we considered 715 four element spaces that are composed of X_1-X_2-X_3-X_4, where X_1~X_4=Al, C, Ca, K, Mg, N, Na, Si, Ti, or V. Each element space satisfies $\sum\left(C_{X_1}+C_{X_2}+C_{X_3}+C_{X_4}\right)=1$, where C_a is the mole fraction of an element a. In these calculations, the method considered only compounds in our database that contain elements belonging to each element space. In each element space, distinct compositions filling the entire element space were defined using increments in the non-H mole fractions of 0.02.

4.2.2 Detecting the Existence of Multi-step Reactions

The decomposition of Li_3AlH_6 is experimentally well-known to occur via the following multi-step reaction:[21]

$$Li_3AlH_6 \rightarrow 3LiH+Al+(3/2)H_2 \qquad (4.1)$$

$$LiH+Al \rightarrow LiAl+(1/2)H_2 \quad (4.2)$$

Taken together, these two reactions release 7.49 wt% H_2. The grand potential calculations outlined above correctly predict this reaction mechanism and this is a useful example illustrating these methods. Thermodynamic calculations for this stoichiometry considered the crystalline compounds $LiAlH_4$, Li_3AlH_6, LiH, AlH_3, Li, Al, AlLi, Al_2Li_3, and Al_3Li, as these are the only compounds in our database that contain Li, Al, and/or H. Our calculations predict the mixture with a 3:1 ratio of Li:Al behaves as written in Eqs. (4.1) and (4.2); no other reaction or equilibrium products are predicted. The predicted temperature for the first reaction is 480 K, which is in a good agreement with the experimental value, 498 K,.[21] The second reaction is predicted to take place at 800 K, a somewhat larger value than 723 K, the experimental value.[21] Both of these predicted reaction temperatures are based on 0 K reaction enthalpies and a H_2 pressure of 1 bar. More precise estimates can be obtained from DFT calculations that include vibrational contributions.[10-12]

Although the calculation outlined above correctly predicts the two steps that occur during decomposition of Li_3AlH_6, the previous screening approach of Alapati *et al.* did not characterize this system as promising because that work considered only single step reactions.[8] When viewed as two single step reactions, neither of the reactions listed above satisfies the criterion that the H_2 capacity of a storage material is higher than 6.0 wt%. Taken jointly, however, the two reaction steps release enough H_2 to make Li_3AlH_6 an interesting material (as characterized by hydrogen content). Because it is likely that there are many other examples of this kind, we extended the earlier calculations of Alapati et al. by identifying promising multi-step reactions. Specifically, we identified any series of reactions in which each individual reaction satisfies the criterion that $15 \leq \Delta U_0 \leq 75$ kJ/mol H_2. We then calculated the total H_2 capacity of each series of reactions. Multi-step (or single step) reactions with a total H_2 capacity > 6.0 wt.% were retained for further examination.

4.3 Computational Details

All DFT calculations were performed with methods that are consistent with the earlier calculations of Alapati *et al.*[8, 10-12, 17] These DFT calculations used the Vienna *ab initio* Simulation Package (VASP) with the PW91 generalized gradient approximation (GGA) functional.[22-25] The projector augmented wave (PAW) method was used for describing the core electrons of each atom.[26] An energy cutoff of 425 eV was used for all calculations. Geometries were relaxed until the forces on all atoms were less than 0.03 eV/Å. Structural optimizations of all new crystal compounds in our database were performed by the conjugate gradient method. Calculations of compounds having cubic unit cells were performed with a Monkhorst-Pack mesh of 9×9×9 or 8×8×8 *k*-points. A smaller number of *k*-points were used for a few systems having the largest unit cells. The numbers of *k*-points for compounds having the non-cubic unit cells were determined by considering the shape of the unit cells so that the density of *k*-points in reciprocal space was similar to the value for materials with cubic unit cells.

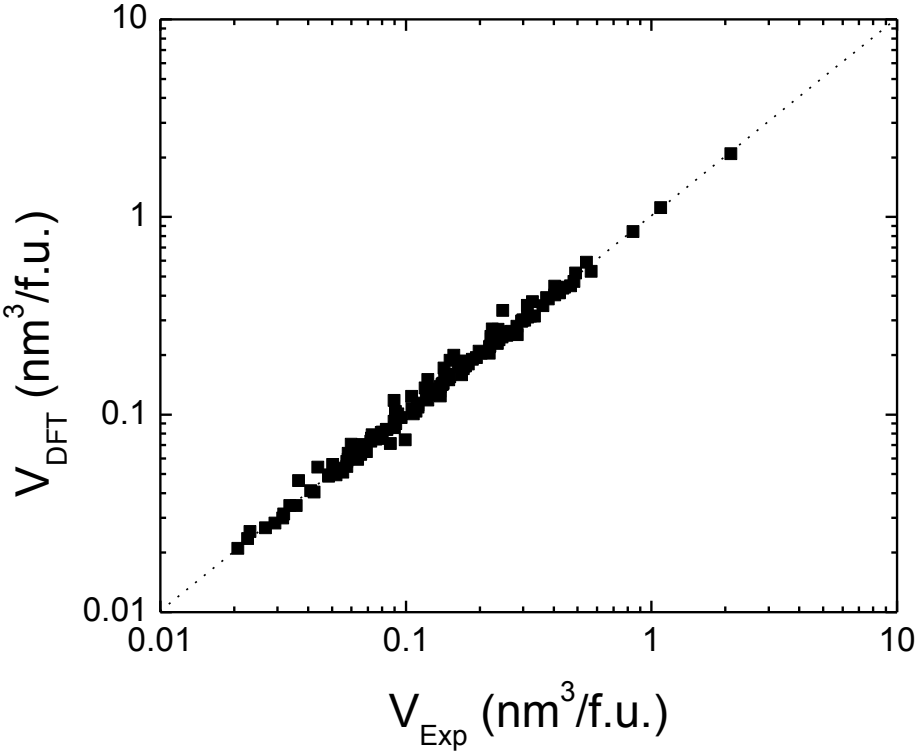

Figure 4.1: Comparison of the volume per formula unit between the experimental structure (V_{Exp}) and the optimized structure (V_{DFT}) for every compound listed in Table 4.1.

We used a supercell containing one unit cell to optimize the bulk crystal structure of each compound listed in Table 4.1. In general, the initial structures for geometry relaxations were obtained from the experimental data available from ICSD.[18] Optimization of $Li_2B_{12}H_{12}$ and $MgB_{12}H_{12}$ were started from the structures observed by Her *et al.*[13] and predicted by Ozolins *et al.*[7], respectively. The details of the optimized lattice parameters are reported in Table 4.3. One heuristic way to examine the reliability of our optimized structures is to compare the volume of the optimized structure with the experimental volume, as shown in Fig. 4.1. As expected, the agreement between the experimentally observed and DFT optimized volumes is in general very good. There are two compounds where the experimental and DFT optimized volumes differ by

more than 10%: $Si_2C_7H_{18}N_2$ (14% error) and Ti_2AlC (11% error). It is not clear what the source of these relatively large discrepancies is.

For two reactions described below we computed the VDOS of every solid compound in order to compute the reaction free energy. For these VDOS calculations, we used the PHONON code developed by Parlinski[27].

Table 4.3: Comparison of the experimental and the DFT calculated structural parameters for the 147 compounds listed in Table 4.1, with all distances in Å and angles in degrees.

Compound	Space group	Structural parameters (Å, degree)	
		Experimental	Calculated
AlB_{12}	$P4_12_12$	*a* = 10.17 *c* = 14.28	*a* = 11.41 *c* = 13.86
Al_4C_3	R-3mH	*a* = 3.335 *c* = 24.967 γ = 120	*a* = 3.349 *c* = 25.109 γ = 120
Al_4Ca	I4/mmm	*a* = 4.354 *c* = 11.18	*a* = 4.368 *c* = 11.19
$Al_{14}Mg_{13}$	Im-3m	*a* = 10.44	*a* = 10.2
$Al_{30}Mg_{23}$	R-3H	*a* = 12.825	*a* = 12.787
$Al_{23}V_4$	P63/mmc	*a* = 7.6928 *c* = 17.04 γ = 120	*a* = 7.6809 *c* = 17.04 γ = 120
$Al_{45}V_7$	C2/m	*a* = 25.604 *b* = 7.6213 *c* = 11.081 β = 128.92	*a* = 25.655 *b* = 7.6076 *c* = 11.086 β = 128.88
B_4C	R-3mH	*a* = 5.6 *c* = 12.12 γ = 120	*a* = 7.4 *c* = 8.77 γ = 120
$B_{13}C_2$	R-3mH	*a* = 5.633 *c* = 12.164 γ = 120	*a* = 5.656 *c* = 12.12 γ = 120
$(B_{10}H_{13})_2$	Pbca	*a* = 10.66 *b* = 10.55 *c* = 14.56	*a* = 10.83 *b* = 10.69 *c* = 14.78
$B_{13}N_2$	R-3m	*a* = 5.45 *c* = 12.26	*a* = 5.49 *c* = 12.41

Table 4.3 continued

C_2Ca	C2/m	*a* = 7.2076 *b* = 3.8283 *c* = 7.3677 β = 107.193	*a* = 7.1698 *b* = 3.8325 *c* = 7.4162 β = 106.961
C_2N_2	Pcab	*a* = 6.31 *b* = 7.08 *c* = 6.19	*a* = 6.72 *b* = 6.38 *c* = 6.06
C_3N_4	P-6m2	*a* = 4.742 *c* = 6.7205 γ = 120	*a* = 4.766 *c* = 6.4004 γ = 120
C_5N_4	R3cH	*a* = 9.062 *c* = 11.625 γ = 120	*a* = 8.912 *c* = 11.416 γ = 120
$C_{12}N_6$	Pa-3	*a* = 10.781	*a* = 10.746
CaB_4	P4/mbm	*a* = 7.1 *c* = 4.14	*a* = 7.17 *c* = 4.1
Ca_2Si	Pnma	*a* = 7.69 *b* = 4.82 *c* = 9.05	*a* = 7.65 *b* = 4.83 *c* = 9.09
KC_8	Fddds	*a* = 4.92 *b* = 8.51 *c* = 21.39999	*a* = 4.97 *b* = 8.61 *c* = 21.36525
KSi	P-43n	*a* = 12.62	*a* = 12.72
K_8Si_{46}	Pm-3n	*a* = 10.3	*a* = 10.36
LiB	PNMA	*a* = 6.4 *b* = 3 *c* = 5.6	*a* = 6.2251 *b* = 3.0727 *c* = 5.589
LiMg	Im-3m	*a* = 3.484	*a* = 3.434
$Li_{12}Si_7$	Pnma	*a* = 8.6 *b* = 19.755 *c* = 14.336	*a* = 8.54 *b* = 19.631 *c* = 14.32
$Li_{13}Si_4$	Pbam	*a* = 7.99 *b* = 15.21 *c* = 4.43	*a* = 7.902 *b* = 15.022 *c* = 4.432
$Li_{15}Si_4$	I-43d	*a* = 10.69	*a* = 10.6
NaB_{15}	Imam	*a* = 5.847 *b* = 8.415 *c* = 10.298	*a* = 5.848 *b* = 8.426 *c* = 10.295
Na_3B_{20}	Cmmm	*a* = 18.695 *b* = 5.701 *c* = 4.151	*a* = 18.636 *b* = 5.693 *c* = 4.158
Na_4Si_4	C2/c	*a* = 12.1534 *b* = 6.545 *c* = 11.1323 β = 118.9	*a* = 12.1512 *b* = 6.5632 *c* = 11.1085 β = 90
Na_8Si_{46}	Pm-3n	*a* = 10.19	*a* = 12.31

Table 4.3 continued

$Sc_{15}C_{19}$	P-42_1c	*a* = 7.5 *c* = 15	*a* = 7.51 *c* = 14.612
SiB_3	Imma	*a* = 8.3915 *b* = 12.568 *c* = 6.2134	*a* = 8.381 *b* = 12.588 *c* = 6.2233
SiC	F-43m	*a* = 4.36	*a* = 4.38
TiV	Im-3m	*a* = 3.159	*a* = 3.103
V_2N	P-31m	*a* = 4.917 *c* = 4.568 γ = 120	*a* = 4.899 *c* = 4.522 γ = 120
V_5Si_3	I4/mcm	*a* = 9.429 *c* = 4.756	*a* = 9.393 *c* = 4.715
$Al(BH_4)_3$	Pna2_1	*a* = 18.02 *b* = 6.14 *c* = 6.2	*a* = 17.99 *b* = 6.12 *c* = 6.2
Al_2MgC_2	P-3m	*a* = 3.377 *c* = 5.817 γ = 120	*a* = 3.385 *c* = 5.82 γ = 120
$Al_{18}Mg_3Ti_2$	Fd-3ms	*a* = 14.7875	*a* = 14.775
BC_2N	Pmm2	*a* = 2.528 *b* = 2.5024 *c* = 3.5871	*a* = 2.56 *b* = 2.5327 *c* = 3.6373
$C_2H_4N_4$	P21/c	*a* = 3.7913 *b* = 12.4117 *c* = 9.1125 β = 91.49	*a* = 3.6509 *b* = 12.0116 *c* = 9.1886 β = 91.32
$C_2H_{18}N_{18}$	P-1	*a* = 4.6208 *b* = 8.5854 *c* = 9.2705 α = 108.486 β = 95.29 γ = 102.991	*a* = 4.5006 *b* = 8.415 *c* = 9.1743 α = 109.353 β = 95.17 γ = 103.087
$C_2N_2(NH)$	Cmc2_1	*a* = 7.57 *b* = 4.44 *c* = 4	*a* = 7.63 *b* = 4.48 *c* = 4.04
Ca_4Al_3Mg	Pbcm	*a* = 6.1792 *b* = 24.2113 *c* = 5.8864	*a* = 6.1906 *b* = 24.2483 *c* = 5.9045
CaAlSi	P-6m2	*a* = 4.2 *c* = 4.4	*a* = 4.21 *c* = 4.41
$Ca(BH_4)_2$	F2dd	*a* = 8.78 *b* = 13.02 *c* = 7.41	*a* = 8.75 *b* = 12.94 *c* = 7.37

Table 4.3 continued

$CaB_{12}H_{12}$	C2/c	*a* = 14.3283 *b* = 7.1642 *c* = 11.017 α = β = 89.8353 γ = 122.0687	*a* = 14.3069 *b* = 7.1522 *c* = 11.0012 α = β = 89.8472 γ = 122.0691
CaC_4N_6	C2/c	*a* = 12.446 *b* = 6.08 *c* = 7.898 β = 145.2	*a* = 12.855 *b* = 6.261 *c* = 7.674 β = 149.86
$Ca_4N_2(CN_2)$	Pnma	*a* = 11.44 *b* = 3.58 *c* = 13.84	*a* = 11.51 *b* = 3.58 *c* = 13.92
$Ca_{11}N_6(CN_2)_2$	P42/MNM	*a* = 14.523 *c* = 3.6083	*a* = 14.5506 *c* = 3.6221
$CaSiN_2$	Pbca	*a* = 5.123 *b* = 10.207 *c* = 14.823	*a* = 5.163 *b* = 10.279 *c* = 14.933
$Ca_2Si_5N_8$	Pbca	*a* = 10.584 *b* = 9.652 *c* = 13.663	*a* = 10.6163 *b* = 9.6748 *c* = 13.6685
$Ca_5(Si_2N_6)$	C12/C1	*a* = 9.836 *b* = 6.0519 *c* = 12.757 β = 100.2	*a* = 9.899 *b* = 6.094 *c* = 14.736 β = 121.155
Ca_4TiN_4	P-1	*a* = 5.98 *b* = 6.01 *c* = 8.99 α = 71.57 β = 79.47 γ = 68.26	*a* = 6.01 *b* = 6.04 *c* = 9.02 α = 71.62 β = 79.32 γ = 68.07
H_9CN_9	$P2_1/c$	*a* = 6.679 *b* = 7.722 *c* = 13.143 β = 95.44	*a* = 6.555 *b* = 7.546 *c* = 12.901 β = 95.71
KBH_4	Fm-3m	*a* = 6.71	*a* = 6.69
KBH_4	$P4_2/nmc$	*a* = 4.68 *c* = 6.57	*a* = 4.71 *c* = 6.61
$KB_{21}H_{18}$	C2	*a* = 12.49 *b* = 7.11 *c* = 16.94 β = 93.81	*a* = 12.71 *b* = 7.22 *c* = 17.04 β = 94.1
$K_2B_6H_6$	Fm-3m	*a* = 8.839	*a* = 8.897
$K_2(B_{10}H_{10})$	P121/n1	*a* = 12.8554 *b* = 11.1784 *c* = 6.8227 β = 93.357	*a* = 11.9928 *b* = 9.7475 *c* = 9.0276 β = 91.93

Table 4.3 continued

$K_2B_{12}H_{12}$	Fm-3	a = 10.629	a = 10.639
KC_4N_3	P-1	a = 8.665 b = 8.873 c = 3.89 α = 86.7 β = 90.1 γ = 105	a = 8.827 b = 9.296 c = 4.009 α = 83.8 β = 90.9 γ = 104.3
KNH_2	$P2_1/m$	a = 4.586 b = 3.904 c = 6.223 β = 95.8	a = 4.458 b = 3.745 c = 6.111 β = 94.958
$(K(NH_2))(NH_3)_2$	$C222_1$	a = 6.8386 b = 9.9525 c = 6.5903	a = 6.8342 b = 9.6806 c = 6.5711
$LiAlB_{14}$	Imam	a = 5.8469 b = 8.1429 c = 10.3542	a = 5.852 b = 8.142 c = 10.353
$LiB_{13}C_2$	Imma	a = 5.6677 b = 10.8201 c = 8.0399	a = 5.842 b = 9.661 c = 8.923
$Li_2B_{12}C_2$	AMM2	a = 4.706 b = 5.318 c = 5.318 α = 115.798	a = 4.663 b = 5.5534 c = 5.5534 α = 100.47
LiBH	PNMA	a = 6.2 b = 3 c = 6.3	a = 5.6458 b = 3.0758 c = 6.5051
$Li(BH_2)$	PNMA	a = 8.1 b = 3 c = 5.9	a = 8.3217 b = 3.0367 c = 5.4851
$Li_2B_{12}H_{12}$	Pa3	a = 9.5771	a = 9.5804
$Li_3(BH_6)$	R3-H	a = 5.1824 α = β = γ = 91.1141	a = 5.3562 α = β = γ = 94.1637
$Li_2B_{12}Si_2$	Cmce	a = 6.106 b = 10.979 c = 8.405	a = 6.118 b = 11.012 c = 8.43
$LiMgH_3$	R3c	a = 4.96 c = 13.34	a = 4.94 c = 13.24
Li_2MgSi	Fm-3m	a = 12.83	a = 12.748
LiN_3Si_2	$Cmc2_1$	a = 9.222 b = 5.296 c = 4.78	a = 9.277 b = 5.329 c = 4.812
$LiNa_2N$	P6/mmm	a = 4 c = 4.2 γ = 120	a = 4.37 c = 3.838 γ = 120

Table 4.3 continued

$LiNa_5N_2$	C_2	$a = 6.731$ $b = 5.944$ $c = 6.383$ $\beta = 91.18$	$a = 6.735$ $b = 5.949$ $c = 6.389$ $\beta = 91.15$
$Li_2Na_4N_2$	P4/nmm	$a = 3.895$ $c = 6.114$	$a = 4.066$ $c = 6.099$
Li_2NaN	P6/nmm	$a = 3.65$ $c = 4.6$ $\gamma = 120$	$a = 3.62$ $c = 4.716$ $\gamma = 120$
$Li_3Na_3N_2$	Pm	$a = 3.854$ $b = 3.676$ $c = 6.32$ $\beta = 90.31$	$a = 3.853$ $b = 4.208$ $c = 7.272$ $\beta = 89.85$
$Li_4Na_2N_2$	Fm-3m	$a = 5.265$	$a = 5.404$
Li_5NaN_2	P4/mmm	$a = 3.965$ $c = 5.504$	$a = 3.705$ $c = 5.186$
Li_3NaSi_6	Pnma	$a = 17.972$ $b = 3.788$ $c = 10.299$	$a = 18.021$ $b = 3.804$ $c = 10.331$
$MgAl_2Si_2$	P-3m1	$a = 4.05$ $c = 6.74$	$a = 4.08$ $c = 6.69$
$MgB_{12}C_2$	C2/c	$a = 7.27$ $b = 8.78$ $c = 7.28$ $\beta = 105.33$	$a = 7.26$ $b = 8.77$ $c = 7.25$ $\beta = 105.32$
$Mg_2B_{24}C$	P-4n2	$a = 8.94$ $c = 5.07$	$a = 8.96$ $c = 5.09$
$MgB_{12}H_{12}$	C2/m	$a = 11.689$ $b = 8.712$ $c = 6.907$ $\beta = 122.47$	$a = 11.687$ $b = 8.711$ $c = 6.905$ $\beta = 122.5$
$MgB_{12}Si_2$	Pnma	$a = 10.98$ $b = 6.11$ $c = 8.36$	$a = 11.03$ $b = 6.13$ $c = 8.39$
MgC_4N_6	Pnnm	$a = 6.171$ $b = 7.17$ $c = 7.404$	$a = 6.443$ $b = 7.289$ $c = 7.429$
Mg_7TiH_{16}	Fm3m	$a = 9.564$	$a = 9.341$
N_2BH_7	Pbcn	$a = 9.53$ $b = 5.12$ $c = 13.01$	$a = 9.768$ $b = 5.237$ $c = 12.672$
$N_2B_{10}H_{18}$	Pnma	$a = 18.096$ $b = 7.373$ $c = 7.223$	$a = 18.237$ $b = 7.528$ $c = 7.284$
$N_3B_3H_6$	$P4_32_12$	$a = 5.428$ $c = 16.279$	$a = 5.63$ $c = 17.223$

Table 4.3 continued

$N_3B_3H_{12}$	Pbcm	a = 4.403 b = 12.21 c = 11.227	a = 4.442 b = 12.382 c = 11.272
$N_4B_9H_{11}$	$P2_1/c$	a = 8.318 b = 5.951 c = 19.265 β = 95.3	a = 8.611 b = 6.263 c = 20.044 β = 94.6
$N_4B_{10}H_8$	C2/c	a = 11.411 b = 6.658 c = 13.058	a = 11.945 b = 7.373 c = 15.268 α = 91.09
$N_4B_{10}H_{22}$	C2/c	a = 7.7 b = 7.7 c = 9.772 α = 83.872 β = 83.872 γ = 82.307	a = 7.813 b = 7.229 c = 9.473 α = 77.29 β = 76.99 γ = 82.3
NH_3BH_3	Pmn21	a = 5.395 b = 4.887 c = 4.986	a = 5.356 b = 4.796 c = 4.921
$(NH_4)_2B_{12}H_{12}$	Fm-3	a = 10.88	a = 10.79
$(NH_2)CN$	Pbca	a = 6.856 b = 6.628 c = 9.147	a = 6.726 b = 6.597 c = 8.916
NH_4HCN_2	$P2_12_12$	a = 6.44 b = 6.58 c = 7.4	a = 6.38 b = 6.5 c = 7.3
$Na_5Al_3H_{14}$	P4/mnc	a = 6.769 c = 10.289	a = 6.7 c = 10.2
$NaBH_4$	Fm-3m	a = 6.15	a = 6.02
$NaBH_4$	P-42_1c	a = 4.35 c = 5.86	a = 4.31 c = 5.82
$Na_2(B_{10}H_{10})$	P121/n1	a = 10.2828 b = 13.0218 c = 6.6734 β = 93.754	a = 9.846 b = 12.153 c = 8.104 β = 93.074
$Na_3(BN_2)$	$P2_1/c$	a = 5.717 b = 7.931 c = 7.883 β = 111.32	a = 5.737 b = 7.966 c = 7.9 β = 111.29
$Na_3C_6N_9$	$P2_1/c$	a = 11.048 b = 23.381 c = 3.516 β = 97.913	a = 11.397 b = 24.101 c = 3.937 β = 97.913

Table 4.3 continued

Sc_2AlC	P63/MMC	a = 3.2275 c = 14.8729 γ = 120	a = 3.2849 c = 15.0425 γ = 120
Ti_2AlC	$P6_3/mmc$	a = 2.97 c = 13.22	a = 3.07 c = 13.71
Ti_6Si_2B	P-62m	a = 6.802 c = 3.338 γ = 120	a = 6.777 c = 3.312 γ = 120
$V_{12}Al_3C_8$	P63/MCM	a = 5.0882 c = 22.9830 γ = 120	a = 5.0651 c = 22.6375 γ = 120
V_5SiB_2	I4/mcm	a = 5.81 c = 10.79	a = 5.774 c = 10.762
$AlNC_3H_{10}$	$P2_1/c$	a = 5.428 b = 9.9076 c = 9.9632 β = 99.254	a = 5.379 b = 11.302 c = 10.271 β = 99.2
BCH_5N_2	$Pna2_1$	a = 7.973 b = 6.445 c = 6.976	a = 7.986 b = 6.515 c = 7.103
$B_{10}C_6H_{30}N_2$	$P2_1/c$	a = 8.369 b = 16.663 c = 11.989 β = 100.34	a = 8.586 b = 17.002 c = 12.249 β = 100.67
$B_{20}C_3H_{30}N_2$	$P2_12_12_1$	a = 10.334 b = 10.873 c = 17.524	a = 10.449 b = 11.199 c = 17.78
BC_4KN_4	$I4_1/a$	a = 6.976 c = 14.21	a = 7.151 c = 14.563
$CH_3NH_2BH_3$	Pnma	a = 11.1 b = 6.58 c = 4.92	a = 11.07 b = 6.35 c = 4.88
$Ca(NH_2BH_3)_2$	C121	a = 9.10 b = 4.37 c = 6.44 β = 93.19	a = 9.12 b = 4.29 c = 6.34 β = 93.1
$KAl(NH_2)_4$	$C222_1$	a = 10 b = 5.8 c = 10.14	a = 10.2 b = 5.82 c = 10.142
$K_5C_2HN_4$	P4/ncc	a = 9.095 c = 11.029	a = 9.225 c = 11.202
$KCaN_3H_6$	$P2_1/c$	a = 6.767 b = 11.68 c = 6.624 β = 106.7	a = 6.797 b = 11.834 c = 6.797 β = 106.82

Table 4.3 continued

$K(HCN_2)$	$P2_12_12_1$	$a = 7.087$ $b = 9.09$ $c = 9.014$	$a = 7.229$ $b = 9.172$ $c = 9.158$
K_2LiAlH_6	R-3m	$a = 5.62$ $c = 27.4$	$a = 5.62$ $c = 27.31$
$KLi_3(NH_2)_4$	$I4_1/amd$	$a = 7.238$ $c = 23.956$	$a = 8.208$ $c = 23.699$
$KLi_7N_8H_{16}$	$I4_1/a$	$a = 7.18$ $c = 44.39$	$a = 7.678$ $c = 46.545$
$K_2Li(NH_2)_3$	P42/m	$a = 6.872$ $c = 11.706$	$a = 6.866$ $c = 11.726$
$K_2Mg(NH_2)_4$	$P2_1/c$	$a = 7.455$ $b = 7.024$ $c = 13.545$ $\beta = 105.6$	$a = 7.255$ $b = 7.255$ $c = 13.626$ $\beta = 105.25$
K_2NaAlH_6	$P2_1/c$	$a = 5.733$ $b = 5.754$ $c = 8.128$ $\beta = 89.97$	$a = 5.743$ $b = 5.7492$ $c = 8.0934$ $\beta = 89.99$
$K_2Na(NH_2)_3$	P42/m	$a = 7.3514$ $c = 13.1285$	$a = 7.5143$ $c = 13.3144$
$K_3Si_6N_{11}H_6$	$P4_332$	$a = 10.789$	$a = 10.797$
$LiAlMg_{10}H_{24}$	P121	$a = 8.9885$ $b = 8.9848$ $c = 4.4846$ $\beta = 89.655$	$a = 8.9147$ $b = 8.9417$ $c = 4.4493$ $\beta = 89.65$
$Li(B(CN)_4)$	P43m	$a = 7.8494$ $\alpha = \beta = \gamma = 60$	$a = 7.7822$ $\alpha = \beta = \gamma = 60$
$Li_2Ca(NH)_2$	P-3m1	$a = 3.57$ $c = 5.95$	$a = 3.58$ $c = 5.84$
$LiK(BH_4)_2$	Pnma	$a = 7.91$ $b = 4.49$ $c = 13.84$	$a = 7.78$ $b = 4.43$ $c = 13.72$
$Li(NH_2BH_3)$	Pbca	$a = 7.11$ $b = 13.93$ $c = 5.15$	$a = 6.92$ $b = 13.52$ $c = 5.07$
$(Li(NH_3)_4)_2(B_6H_6)(NH_3)_2$	P21/c	$a = 7.483$ $b = 11.871$ $c = 10.6047$ $\beta = 95.371$	$a = 7.3965$ $b = 11.649$ $c = 10.4489$ $\beta = 95.21$
$LiNa_2AlH_6$	P21/c	$a = 5.165$ $b = 5.251$ $c = 7.339$	$a = 4.777$ $b = 4.715$ $c = 6.613$
$LiNa_2(NH_2)_3$	$P4_2/m$	$a = 6.28$ $c = 11.15$	$a = 6.17$ $c = 10.90$

Table 4.3 continued

$LiSc(BH_4)_4$	P-42c	a = 6.08 c = 12.03	a = 6.45 c = 11.95
$Mg(BH_4)_2(NH_3)_2$	Pbca	a = 17.49 b = 9.41 c = 8.73	a = 17.73 b = 9.35 c = 8.68
$(NH_4)B(CN)_4$	I41/a	a = 7.132 c = 14.745	a = 7.453 c = 14.617
$NaAl(NH_2)_4$	$P2_1/c$	a = 7.328 b = 6.047 c = 13.151 β = 94.04	a = 6.565 b = 6.353 c = 15.362 β = 94.3
$NaB(CN)_4$	Fd-3mZ	a = 11.68	a = 11.874
$Si_2C_7H_{18}N_2$	$P2_1/c$	a = 9.71 b = 11.11 c = 11.88 β = 102.3	a = 10.143 b = 11.599 c = 12.422 β = 103.1
$VC_8H_{24}N_4$	P-1	a = 8.29 b = 12.016 c = 13.835 α = 75.662 β = 79.404 γ = 84.966	a = 8.637 b = 12.503 c = 14.479 α = 75.89 β = 79.47 γ = 85.3
$LiAlC_4H_{16}N_4$	$I4_1$	a = 14 c = 9.275	a = 14.128 c = 9.571
$LiSi_3C_9H_{27}N_2$	P-1	a = 8.776 b = 9.579 c = 21.949 α = 100.84 β = 92.18 γ = 115.67	a = 9.077 b = 9.875 c = 22.544 α = 101.16 β = 91.95 γ = 115
$Si_2B_2C_{12}H_{37}N_5$	$P2_1/c$	a = 15.785 b = 11.966 c = 11.804 β = 102.19	a = 16.2 b = 12.212 c = 12.205 β = 102.3

4.4 Single-step Reactions

Our thermodynamic calculations identified 74 promising single-step reactions that are predicted to have 15 kJ/mol $H_2 \leq \Delta U_0 \leq 75$ kJ/mol H_2 and that release ≥ 6.0 wt.% H_2. These 74 reactions are shown in Table 4.2. An initial way to consider this set of reactions is to compare them to the 43 single-step reactions that were identified in the earlier calculations by Alapati et

al.[8] Only 17 of these 43 reactions appear among the 74 reactions listed in Table 4.4; 26 of the reaction mixtures identified by Alapati et al. are predicted by our more complete database to not satisfy the screening criteria listed above. Almost all of these 26 reactions involve either $LiBH_4$ or $Mg(BH_4)_2$, which are now predicted to react via $B_{12}H_{12}$-containing intermediates that were unknown at the time of Alapati et al.'s work. The importance of these intermediates has been discussed in a number of recent reports.[7, 13, 14, 16] 57 of the reactions identified by our calculations were not encountered in the calculations of Alapati et al. because they include one or more compounds that were not included in the database used in those calculations.

The 74 reactions listed in Table 4.4 were found by calculations that consider systems that are able to reach perfect thermodynamic equilibrium in an environment where H_2 is the only possible gas species. To discuss these reactions, it is useful to divide them into several classes that are arranged by our expectations for how reasonable these assumptions are. We first consider reactions that involve species that include $B_{12}H_{12}$; 13 reactions include species of this type. These reactions do not include any refractory materials or carbon (see below). None of the reactions involving $B_{12}H_{12}$ species were predicted by Alapati, Johnson, and Sholl with our previous database, since the database did not include any metal closoboranes.[8] The reaction mixtures found in our calculations are consistent with those already reported by Ozolins *et al.* for $LiBH_4$, $Ca(BH_4)_2$, $Mg(BH_4)_2$, $MgH_2/MgB_{12}H_{12}$, $LiBH_4/Mg(BH_4)_2$, and $Mg(BH_4)_2/Ca(BH_4)_2$[7] and Kim *et al.* for $LiSc(BH_4)_4$.[15] There are also several experimental reports related to the mixtures of $LiBH_4$, $Ca(BH_4)_2$, $Mg(BH_4)_2$, $MgH_2/MgB_{12}H_{12}$, and $LiBH_4/Mg(BH_4)_2$.[13, 14, 16, 28-36] Unfortunately, most experimental studies indicate metal closoboranes are very kinetically stable, meaning that reactions involving any $B_{12}H_{12}$ species are typically not reversible.[7, 37] This observation suggests that the 13 reactions involving $MB_{12}H_{12}$ (M = Li, Mg, Ca, and K) would be undesirable from a practical point of view.

The reactions involving $B_{12}H_{12}$ species illustrate one way in which a reaction that is thermodynamically feasible may be strongly limited by kinetic effects. It is reasonable to suspect that similar kinetic limitations could limit the viability of reactions whose reactants or products

are known to be refractory. Among the materials we considered, BN, TiB_2, ScB_2, AlN, VN, CaB_6, and V_2N can all be characterized as refractory materials because they have melting temperatures ≥ 2000 °C.[38-44] 39 of the reactions listed in Table 4.4 involve one or more of these species. Ten of the 39 reactions were already predicted by Alapati, Johnson, and Sholl:[8] $2LiH+LiNH_2+BN$, $2LiBH_4+ScH_2$, $2LiBH_4+TiH_2$, $2LiBH4+Mg(NH_2)_2$, $ScH_2+Mg(BH_4)_2$, $3LiBH_4+TiN$, $12LiH+3Mg(NH_2)_2+4BN$, $2ScN+3Mg(BH_4)_2$, $2TiN+3Mg(BH_4)_2$ and, $4LiH+3LiNH_2+VN$. There are also relevant theoretical reports showing the same reaction schemes as our current prediction for $CaH_2/CaB_{12}H_{12}$, $ScH_2/Ca(BH_4)_2$, and $TiH_2/Ca(BH_4)_2$.[7, 9, 45] A few experimental reports support the idea that refractory materials make reactions involving them irreversible.[46, 47] Purewal et al. experimentally examined hydrogen absorption and desorption behavior in $LiBH_4/ScH_2$ system.[46] Due to the stability of ScH_2 and ScB_2, $LiBH_4$ did not react with ScH_2. Yang et al. experimentally studied $LiBH_4/TiH_2$, another reaction system included in this category.[47] Similar to Purewal et al., they observed that $LiBH_4$ decomposed to release H_2 without reacting with TiH_2. They also examined the reversibility of $LiBH_4/CaH_2$ system and concluded that the system was not reversible due to the kinetic stability of CaB_6.

The reactions we have discussed above are likely to be impractical because of kinetic limitations. It is also possible that some of the reactions predicted by our calculations may differ from experimental observations because of the formation of non-H_2 gases at equilibrium. This issue was discussed in detail in recent work that reported thermodynamic calculations for a small number of metal hydrides that included a wide range of potential gas species, not just H_2.[20] One class of chemical mixtures highlighted in that work was those that involve C. In these mixtures the thermodynamically stable states at low temperatures often involved high levels of CH_4. It appears in general to be incorrect to assume that calculations that do not allow for the presence of CH_4 can predict the correct thermodynamic equilibrium states when carbon is present in the reaction mixture. For this reason, we have separated the 19 reactions in Table 4.4 that involve carbon either as graphitic C or as part of a compound such as KC_8.

The discussion of the potential role of methane in reaction mixtures involving C could

lead to the conclusion that it would be better to simply exclude all C-containing materials from the materials considered in our calculations. We feel, however, that it is better to report the results involving these compounds because the kinetic implications of mixing metal hydrides and carbon experimentally are not yet clear. There are recent reports showing that nanoporous carbons can improve reaction kinetics in metal hydride systems.[48-52] Berseth et al., for example, examined the interaction between carbon nanostructures and $NaAlH_4$ and concluded that the carbon materials could improve the dehydrogenation reaction of $NaAlH_4$.[49] These experiments indicated that the nanostructured C did not react with the metal hydride. In interpreting experiments of this kind, however, it is important to be aware of the potential reactions that can occur between metal hydrides and carbon supports.

Table 4.4: Promising single-step reactions divided into six categories. ΔU_0 and ΔS_{conf} represent the changes of the reaction enthalpy at 0 K and the configurational entropy. The configurational entropy is only listed in cases where this quantity is not zero. The enthalpy changes at 0 K for reactions involving $LiBH_4$ used the DFT total energy of ortho-$LiBH_4$.

Interesting reactions (3 reactions)	**wt.%**	**ΔU_0 ($T\Delta S_{conf}$) (kJ/mol H_2)**
$MgH_2 \rightarrow Mg+H_2$	7.66	64.7
$LiH+2LiNH_2+KBH_4 \rightarrow Li_3BN_2+KH+4H_2$	7.48	43.6 (-7.2)
$2MgH_2+Mg(NH_2)_2 \rightarrow Mg_3N_2+4H_2$	7.4	26
Reactions involving $B_{12}H_{12}$ species (13 reactions)	**wt.%**	**ΔU_0 ($T\Delta S_{conf}$) (kJ/mol H_2)**
$LiBH_4 \rightarrow (5/6)LiH+(1/12)Li_2B_{12}H_{12}+(13/12)H_2$	10.03	62.1
$4LiBH_4+5Si+10Mg(BH_4)_2 \rightarrow 5Mg_2Si+2Li_2B_{12}H_{12}+36H_2$	9.46	41
$5Si+12Mg(BH_4)_2 \rightarrow 5Mg_2Si+2MgB_{12}H_{12}+36H_2$	9.21	43.6
$5Si+10Mg(BH_4)_2+2Ca(BH_4)_2 \rightarrow 5Mg_2Si+2CaB_{12}H_{12}+36H_2$	8.85	41.2
$2LiBH_4+5Mg(BH_4)_2 \rightarrow 5MgH_2+Li_2B_{12}H_{12}+13H_2$	8.36	43.1
$5Si+10Mg(BH_4)_2+4KBH_4 \rightarrow 5Mg_2Si+2K_2B_{12}H_{12}+36H_2$	8.1	37.3 (-2.9)
$Mg(BH_4)_2 \rightarrow (5/6)MgH_2+(1/6)MgB_{12}H_{12}+(13/6)H_2$	8.09	47.1
$LiSc(BH_4)_4 \rightarrow (2/5)LiBH_4+ScH_2+(3/10)Li_2B_{12}H_{12}+(22/5)H_2$	7.97	24.1
$5Mg(BH_4)_2+Ca(BH_4)_2 \rightarrow 5MgH_2+CaB_{12}H_{12}+13H_2$	7.72	43.1
$5MgH_2+MgB_{12}H_{12} \rightarrow 6MgB_2+11H_2$	7.45	62.1
$5Mg(BH_4)_2+2KBH_4 \rightarrow 5MgH_2+K_2B_{12}H_{12}+13H_2$	6.94	38 (-4)
$Ca(BH_4)_2 \rightarrow (5/6)CaH_2+(1/6)CaB_{12}H_{12}+(13/6)H_2$	6.26	57.4
$LiH+3Ca(BH_4)_2 \rightarrow 3CaH_2+(1/2)Li_2B_{12}H_{12}+(13/2)H_2$	6.03	56.5

Table 4.4 continued

Reactions involving refractory materials (BN, TiB_2, ScB_2, AlN, VN, CaB_6, V_2N) (39 reactions)	**wt.%**	**ΔU_0 ($T\Delta S_{conf}$) (kJ/mol H_2)**
$27N_2BH_7+AlNC_3H_{10} \rightarrow AlN+27BN+(3/2)C_2H_{18}N_{18}+86H_2$	13.08	65.6
$(NH_4)_2B_{12}H_{12} \rightarrow 10B+2BN+10H_2$	11.33	44
$5LiSc(BH_4)_4+2(NH_4)_2B_{12}H_{12} \rightarrow 5ScB_2+4BN+(5/2)Li_2B_{12}H_{12}+45H_2$	9.95	15
$20SiC+19(NH_4)_2B_{12}H_{12} \rightarrow 38BN+20SiB_3+10B_{13}C_2+190H_2$	9.16	40.8
$2LiBH_4+ScH_2 \rightarrow 2LiH+ScB_2+4H_2$	8.91	49.7
$2LiBH_4+TiH_2 \rightarrow 2LiH+TiB_2+4H_2$	8.63	22.2
$ScB_2+(NH_4)_2B_{12}H_{12} \rightarrow ScB_{12}+2BN+10H_2$	8.25	41.5
$9ScH_2+Si+9Mg(BH_4)_2 \rightarrow 7MgH_2+Mg_2Si+9ScB_2+38H_2$	8.18	37.3
$2LiBH_4+Mg(NH_2)_2 \rightarrow MgH_2+2LiH+2BN+4H_2$	8.07	20.6
$ScH_2+Mg(BH_4)_2 \rightarrow MgH_2+ScB_2+4H_2$	7.99	37.5
$BN+LiSc(BH_4)_4 \rightarrow (1/5)LiBH_4+ScN+(2/5)Li_2B_{12}H_{12}+(26/5)H_2$	7.7	22.8
$3Mg(NH_2)_2+4NaBH_4 \rightarrow 4NaH+Mg_3N_2+4BN+12H_2$	7.55	34.4 (-8.8)
$11LiH+25LiNH_2+AlB_{12} \rightarrow AlN+12Li_3BN_2+(61/2)H_2$	7.51	56
$41ScH_2+4VB_2+40Mg(BH_4)_2 \rightarrow 40MgH_2+41ScB_2+2V_2B_3+161H_2$	7.42	37.2
$10Si+3(NH_4)_2B_{12}H_{12} \rightarrow 6BN+10SiB_3+30H_2$	7.42	38.7
$3LiBH_4+TiN \rightarrow 3LiH+TiB_2+BN+(9/2)H_2$	7.13	35.9
$NaAl(NH_2)_4 \rightarrow AlN+NaN_3+4H_2$	7.07	16.2
$ScH_2+Ca(BH_4)_2 \rightarrow CaH_2+ScB_2+4H_2$	6.91	46.8
$3LiNH_2+2KBH_4 \rightarrow Li_3BN_2+BN+2KH+6H_2$	6.84	41.6 (-9.7)
$56LiH+21Mg(NH_2)_2+4V_2N \rightarrow 8Li_7N_4V+7Mg_3N_2+70H_2$	6.75	47.9
$TiH_2+Ca(BH_4)_2 \rightarrow CaH_2+TiB_2+4H_2$	6.74	19.3
$12LiH+3Mg(NH_2)_2+4BN \rightarrow 4Li_3BN_2+Mg_3N_2+12H_2$	6.65	54.2
$LiNH_2+NaBH_4 \rightarrow LiH+NaH+BN+2H_2$	6.63	19.4 (-11.3)
$5LiSc(BH_4)_4+2MgB_{12}H_{12} \rightarrow 5ScB_2+2Mg(BH_4)_2+(5/2)Li_2B_{12}H_{12}+29H_2$	6.58	21.6
$ScH_2+2NaBH_4 \rightarrow 2NaH+ScB_2+4H_2$	6.58	67.5 (-19.8)
$39LiNH_2+2AlB_{12} \rightarrow 2AlN+13Li_3BN_2+11BN+39H_2$	6.5	59.5
$2ScN+3Mg(BH_4)_2 \rightarrow 3MgH_2+2ScB_2+2BN+9H_2$	6.48	43.1
$5NaBH_4+2(NH_4)_2B_{12}H_{12} \rightarrow 4BN+(5/2)Na_2(B_{10}H_{10})+(35/2)H_2$	6.47	26.7 (-6.7)
$TiH_2+2NaBH_4 \rightarrow 2NaH+TiB_2+4H_2$	6.42	40 (-15.1)
$Mg(NH_2)_2+Ca(BH_4)_2 \rightarrow MgH_2+CaH_2+2BN+4H_2$	6.39	17.7
$2TiN+3Mg(BH_4)_2 \rightarrow 3MgH_2+2TiB_2+2BN+9H_2$	6.35	19.5
$2LiH+LiNH_2+BN \rightarrow Li_3BN_2+2H_2$	6.33	49.1
$CaH_2+CaB_{12}H_{12} \rightarrow 2CaB_6+7H_2$	6.3	61.8
$3Mg(NH_2)_2+4KBH_4 \rightarrow Mg_3N_2+4BN+4KH+12H_2$	6.29	46.9 (-10.3)
$8ScH_2+2V_2B_3+9Mg(BH_4)_2 \rightarrow 9MgH_2+8ScB_2+4VB_2+35H_2$	6.24	37.1
$13CaH_2+CaSi_2+14CaB_{12}H_{12} \rightarrow 2Si+28CaB_6+97H_2$	6.13	60.6
$4LiH+3LiNH_2+VN \rightarrow Li_7N_4V+5H_2$	6.09	37.4
$ScB_2+4BN+3LiSc(BH_4)_4 \rightarrow 4ScN+(3/2)Li_2B_{12}H_{12}+15H_2$	6.05	21.9
$MgH_2+3BN+2MgB_{12}H_{12} \rightarrow 3MgB_9N+13H_2$	6.05	58.6

Table 4.4 continued

Reactions involving C (19 reactions)	wt.%	ΔU_0 ($T\Delta S_{conf}$) (kJ/mol H_2)
$LiBH_4+C \rightarrow LiBC+2H_2$	11.93	45.1
$2C+Mg(BH_4)_2 \rightarrow MgB_2C_2+4H_2$	10.34	43.1
$20C+13(NH_4)_2B_{12}H_{12} \rightarrow 26BN+10B_{13}C_2+130H_2$	10.27	35.2
$2C+Ca(BH_4)_2 \rightarrow CaB_2C_2+4H_2$	8.6	56.8
$VC_8H_{24}N_4 \rightarrow 7C+VN+NH_4HCN_2+(19/2)H_2$	8.42	22.8
$214C+607Mg(BH_4)_2+100Ca(BH_4)_2 \rightarrow 500MgH_2+107MgB_2C_2+100CaB_{12}H_{12}+1728H_2$	8.23	42.4
$C+KBH_4+K(NH_2)(NH_3)_2 \rightarrow BN+K_2CN_2+6H_2$	7.8	26.8 (-3.8)
$2LiH+2C+Ca(BH_4)_2 \rightarrow CaH_2+2LiBC+4H_2$	7.35	42.2
$4LiH+3Mg(NH_2)_2+2C \rightarrow 2Li_2CN_2+Mg_3N_2+8H_2$	7.17	47.8
$2C+K(NH_2)(NH_3)_2 \rightarrow (1/3)K_3C_6N_9+4H_2$	7.12	68.4
$LiH+C+NaBH_4 \rightarrow NaH+LiBC+2H_2$	6.98	62.9 (-19)
$2LiNH_2+C \rightarrow Li_2CN_2+2H_2$	6.96	31.4
$266C+100KBH_4+383Ca(BH_4)_2 \rightarrow 250CaH_2+133CaB_2C_2+50K_2B_{12}H_{12}+1182H_2$	6.75	53.4 (-2.6)
$MgH_2+2C+Ca(BH_4)_2 \rightarrow CaH_2+MgB_2C_2+4H_2$	6.71	52.4
$14Li_3Na(NH_2)_4+5Na_2CN_2+16NH_4HCN_2 \rightarrow 21Li_2CN_2+24NaN_3+96H_2$	6.71	64.6
$2C+MgB_{12}H_{12} \rightarrow MgB_{12}C_2+6H_2$	6.36	64.3
$16LiNH_2+KC_8 \rightarrow 8Li_2CN_2+KH+(31/2)H_2$	6.22	31.7
$7NaNH_2+2NH_4HCN_2 \rightarrow 2Na_2CN_2+3NaN_3+12H_2$	6.18	62.8
$Li_3Na(NH_2)_4+2C \rightarrow (3/2)Li_2CN_2+(1/2)Na_2CN_2+4H_2$	6.11	32.6

The discussion above described how 71 of the 74 single step reactions identified by our thermodynamic calculations are unlikely to be of practical interest for reversible H_2 storage. Of the remaining 3 reactions that meet our screening criteria, one is the direct decomposition of MgH_2. It is well known that the reaction enthalpy of this reaction is too high to allow H_2 release at the temperatures desirable in a mobile storage device[53-56]. The observation that the DFT-predicted reaction enthalpy lies towards the upper bound of the range of reaction enthalpies we used in our screening is consistent with this fact. This leaves two single-step reactions that do not suffer from any of the possible disadvantages listed above, one with a 2:1:1 mixture of $LiNH_2$, LiH, and KBH_4, and the other with a 2:1 mixture of MgH_2 and $Mg(NH_2)_2$. Both of these reactions release ~7.4 wt.% H_2 at completion.

The reaction between MgH_2 and $Mg(NH_2)_2$ forming Mg_3N_2 with H_2 release has been analyzed in several previous computational studies.[4, 8, 57] Akbarzadeh, Ozolins, and Wolverton computed the free energy for this reaction using DFT.[4] We performed similar calculations after computing the VDOS for each solid compound in the reaction, and our results are entirely consistent with those of Akbarzadeh, Ozolins, and Wolverton. A van't Hoff plot based on our DFT-calculated free energies is shown in Fig. 4.2. The predicted reaction temperature for the $MgH_2/Mg(NH_2)_2$ mixture at a H_2 pressure of 1 bar is 160 K, in good agreement with the value (130 K) reported by Akbarzadeh, Ozolins, and Wolverton.[4] An important feature of Fig. 4.2 is that is indicates the (large) range of H_2 pressures that are associated with an uncertainty of ±10 kJ/mol H_2. This is the typical uncertainty that is associated with DFT-calculated reaction free energies for metal hydride decomposition reactions where comparisons with detailed experimental data have been possible.[2, 12, 55]

The 2:1 mixture of MgH_2 and $Mg(NH_2)_2$ was studied in ball milling experiments by Hu et al..[57] As predicted by computational studies, they observed that Mg_3N_2 was produced with the release of a stoichiometric amount of H_2 (7.4 wt.%). Very low levels of NH_3 (~1 ppm) were detected. Hu et al. described the thermodynamics of this process using tabulated thermodynamic data, and estimated that the heat of reaction at 298 K was 3.5 kJ/mol H_2. This is in reasonable agreement with our DFT-calculated result ($\Delta H_{298\ K}$ = 15.6 kJ/mol H_2). No experimental information appears to be available regarding the reversibility of this reaction. Figure 4.2 indicates that large H_2 pressures would be necessary to reverse the reaction at room temperature or above.

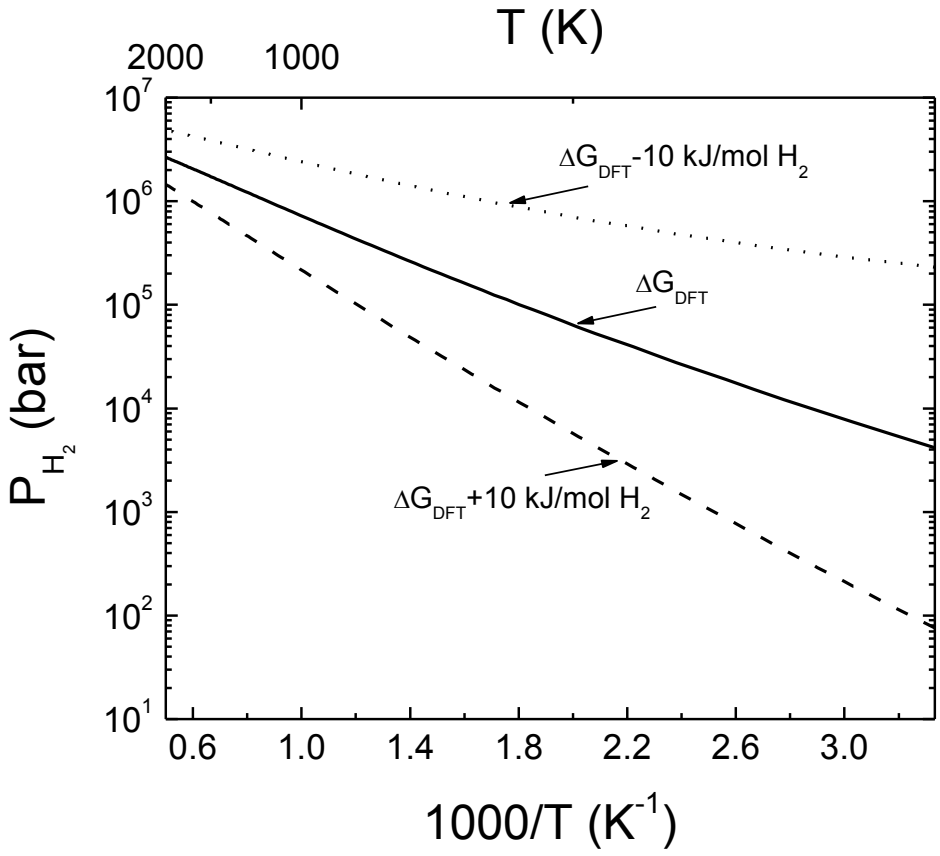

Figure 4.2: A van't Hoff plot for $2MgH_2 + Mg(NH_2)_2 \rightarrow Mg_3N_2 + 4H_2$. The dotted (dashed) line represents the upper (lower) bound of the van't Hoff plot when an uncertainty of ±10 kJ/mol H_2 in the DFT-calculated reaction free energy is considered.

The other promising single-step reaction is the reaction of a 2:1:1 mixture of $LiNH_2$, LiH, and KBH_4, which is predicted to react in a single step forming solid Li_3BN_2 and KH along with gaseous H_2. This reaction has, to the best of our knowledge, not been considered in any earlier experimental or computational studies. This calculated 0 K reaction enthalpy change for this reaction is 43.6 kJ/mol H_2. We computed the VDOS for each solid compound in this reaction in order to analyze the free energy for the reaction. When we consider the vibrational and entropic contributions, our calculation predicts $\Delta H_{300\ K}$ = 28.1 kJ/mol H_2 and $\Delta S_{vib,300\ K}$ (the reaction vibrational entropy change at 500 K) = 116.3 J/K/mol H_2, giving $\Delta G_{300\ K}$ = -6.8 kJ/mol H_2. As

discussed above, the partial disorder of H atoms in α-KBH_4 means that the configurational entropy (S_{conf}) associated with this disorder should be considered to completely describe the reaction thermodynamics. If we use an estimate for the configurational entropy based on complete disorder among the partially occupied sites[1], $T\Delta S_{conf}$ at 300 K is -3.5 kJ/mol H_2. As discussed in Chapter 3, this approach is likely to overestimate the entropy associated with site disorder in KBH_4.[1] Therefore, the resulting reaction free energy change including the configurational entropy effect would be -3.3 kJ/mol H_2. The van't Hoff plot based on these calculations is shown in Fig. 4.3. This figure shows that this reaction has the reaction temperatures of 300 ~ 420 K at H_2 pressures of 1 ~ 100 bar, indicating that H_2 would be released at the appropriate temperatures and H_2 pressures for reversible hydrogen storage applications. As with Fig. 4.2, we show uncertainty estimates in Fig. 4.3 that emphasize how the imprecision associated with DFT calculations leads to a rather large uncertainty in predicted H_2 pressures. Despite this unavoidable uncertainty, the thermodynamic properties of this reaction suggest that it is a good candidate for experimental studies.

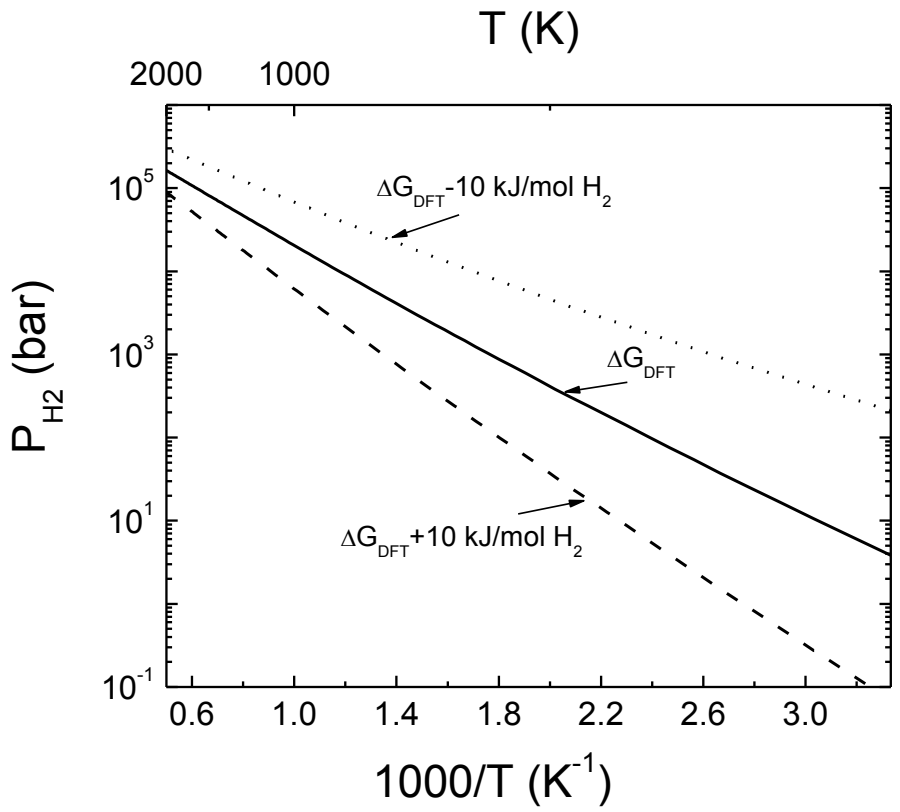

Figure 4.3: Similar to Fig. 4.2, but for $2LiNH_2 + LiH + KBH_4 \rightarrow Li_3BN_2 + KH + 4H_2$.

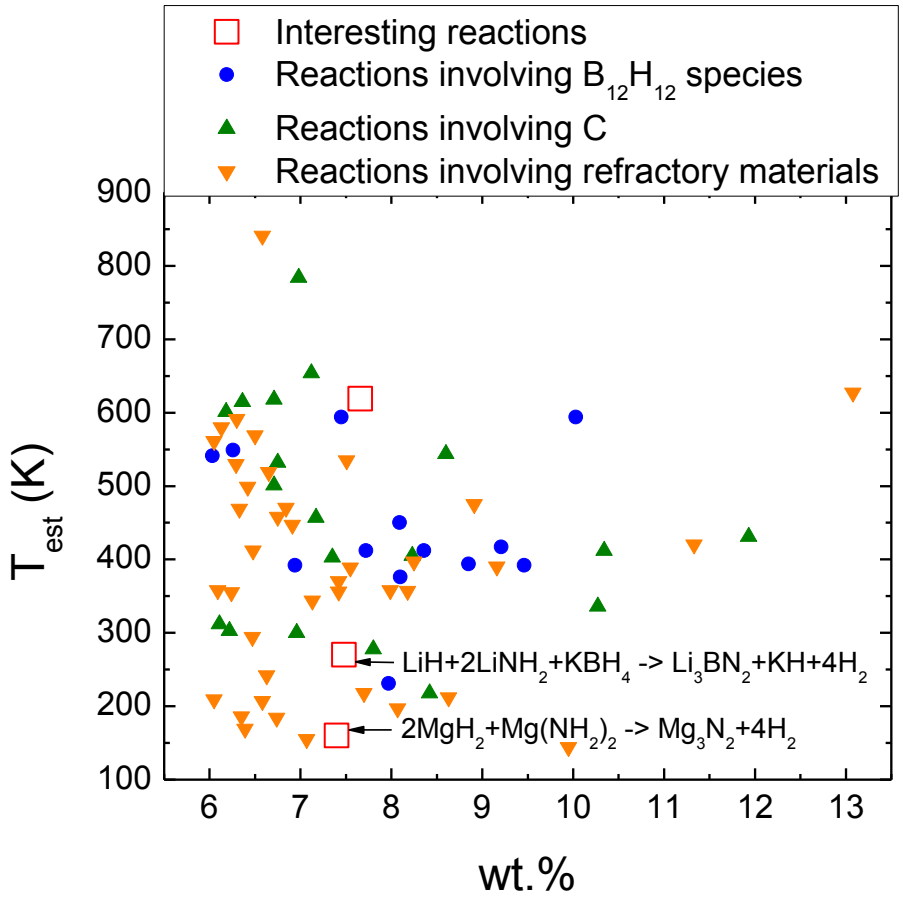

Figure 4.4: The estimated temperature (T_{est}) as a function of H_2 capacity (wt.%) for the 74 promising single-step reactions described in Table 4.4.

We summarize the main results from this section visually in Fig. 4.4 by plotting the estimated reaction temperature for a H_2 pressure of 1 bar as a function of the H_2 capacity of each single step reaction. For all of the reactions except the two shown in Figs. 4.2 and 4.3, the reaction temperature, T_{est}, was estimated using

$$T_{est}\,(\mathrm{K}) = \Delta U_0/(\Delta S - R) \qquad (4.3)$$

ΔU_0 and ΔS are the reaction enthalpy at 0 K and reaction entropy associated with site disorder when this phenomenon is relevant and R is the gas constant. The equation neglects the contributions of the vibrational energies and PV term to the free energies of solid compounds.[10,

[12, 58] The reaction temperatures of $MgH_2/Mg(NH_2)_2$ and $LiNH_2/LiH/KBH_4$ mixtures for a H_2 pressure of 1 bar were taken from the van't Hoff plots in Figs. 4.2 and 4.3. The detailed figures for the separate collection of the reactions included in each list of Table 4.4 are given from Fig. 4.5 to Fig. 4.8.

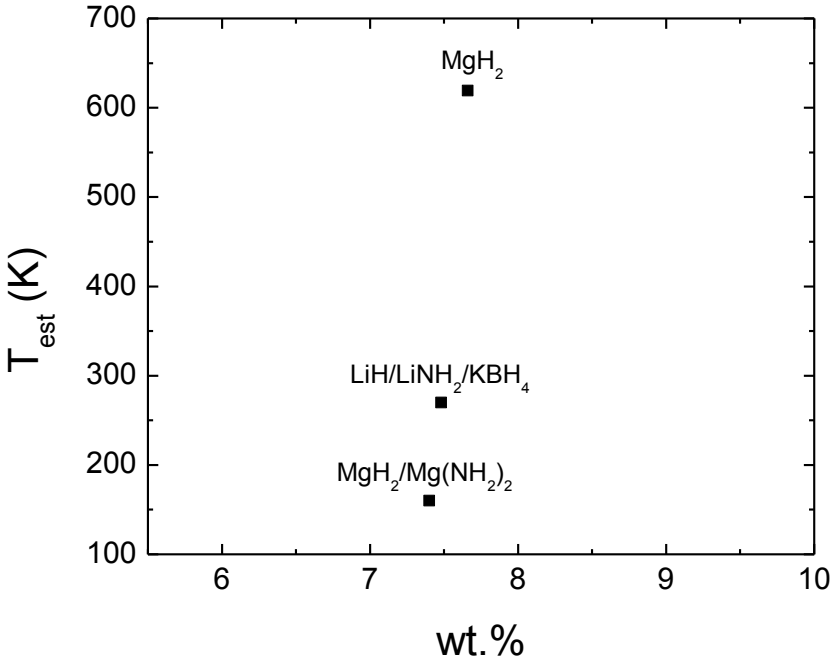

Figure 4.5. The estimated temperature (T_{est}) as a function of H_2 capacity (wt.%) for the "interesting reactions" in Table 4.4.

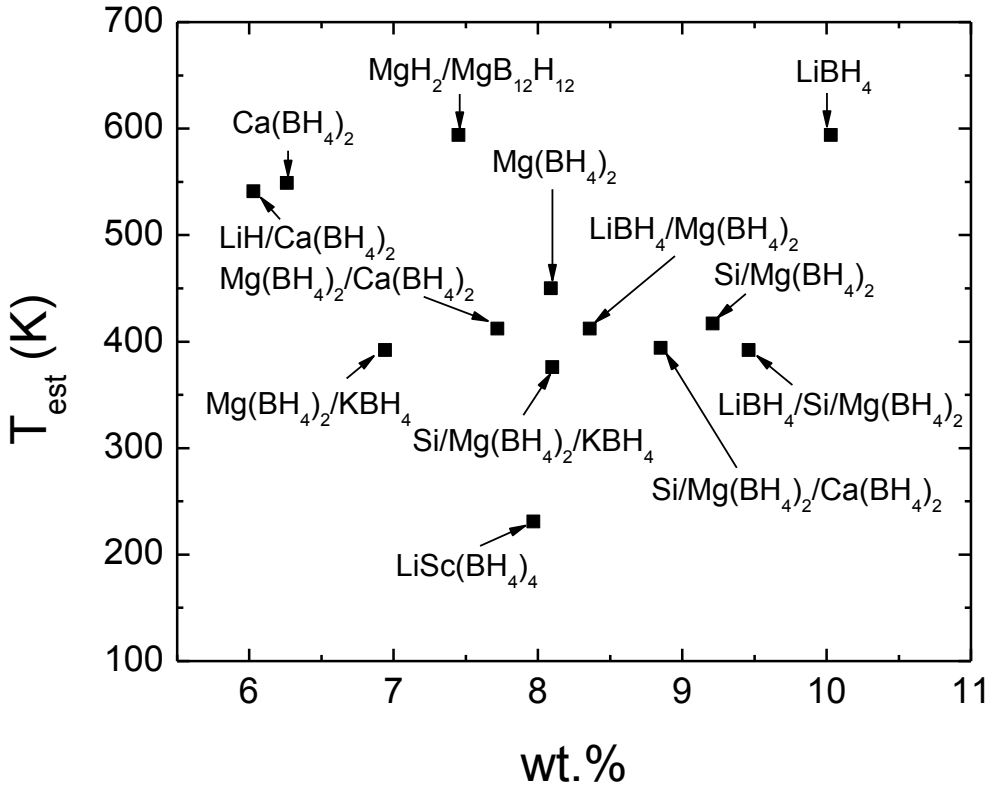

Figure 4.6. The estimated temperature (T_{est}) as a function of H_2 capacity (wt.%) for thirteen reactions involving $B_{12}H_{12}$ species in Table 4.4.

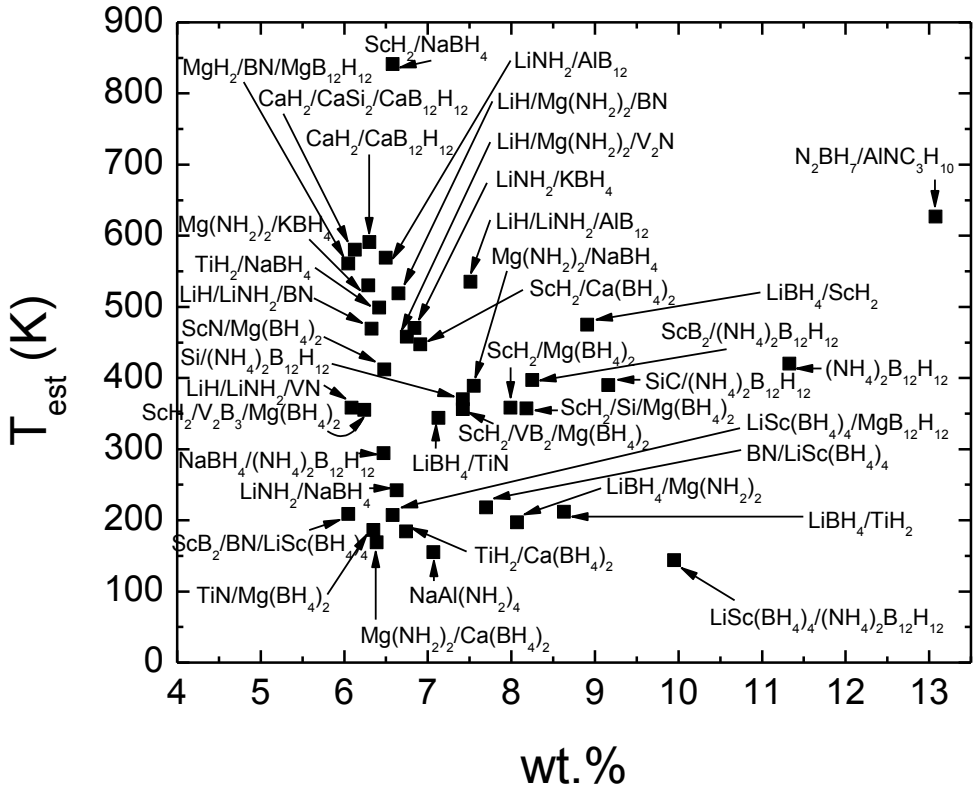

Figure 4.7. The estimated temperature (T_{est}) as a function of H_2 capacity (wt.%) for the 39 reactions involving refractory materials in Table 4.4.

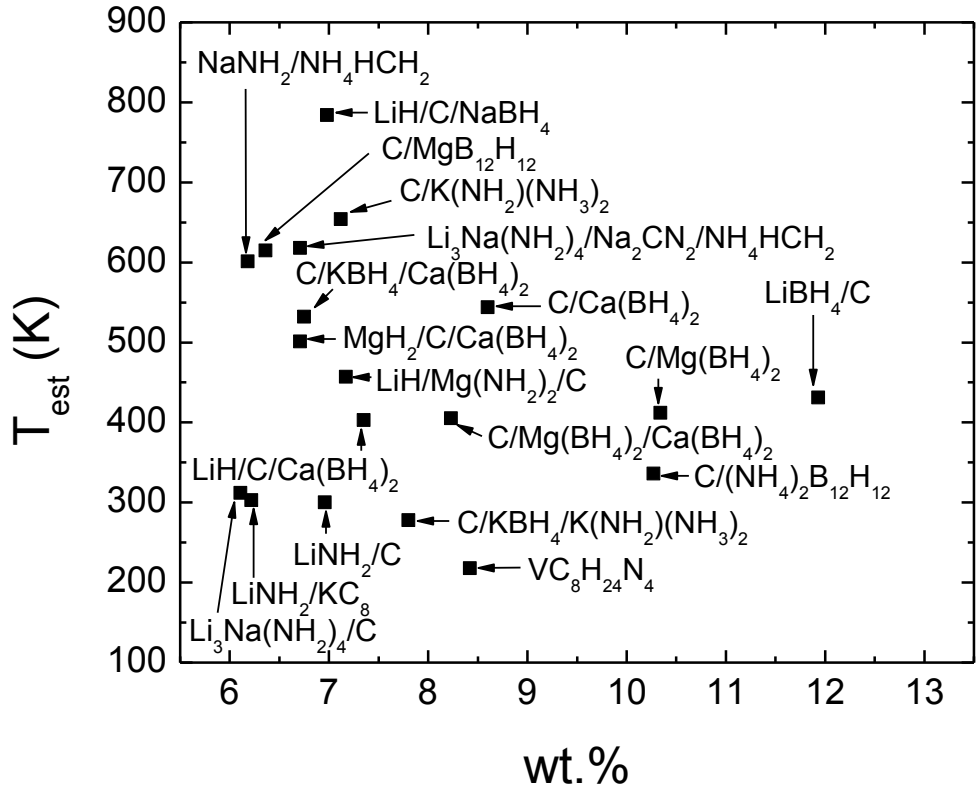

Figure 4.8. The estimated temperature (T_{est}) as a function of H_2 capacity (wt.%) for the nineteen reactions involving C in Table 4.4.

4.5 Multi-step Reactions

We now turn to the possibility of finding multi-step reactions with useful properties for reversible H_2 storage. We examined all of the reaction mixtures defined in section 4.2 to detect multi-step reactions in which every step satisfied $15 \leq \Delta U_0 \leq 75$ kJ/mol H_2 and the total H_2 release from the combined reaction steps was > 6.0 wt.% H_2. This initially generated more than 10^5 candidate reaction mixtures, but this large number contains a much smaller number of distinct reaction schemes. To illustrate this concept, consider the reaction of a mixture of *x* moles of Li_3AlH_6 and *y* moles of MgH_2. For a range of *x* and *y*, our thermodynamic calculations show

that this mixture reacts in two steps as follows:

$$x\ Li_3AlH_6 \rightarrow 3x\ LiH + x\ Al + 1.5x\ H_2 \quad (4.4)$$

$$y\ MgH_2 + x\ Al \rightarrow (x/30)\ Al_{30}Mg_{23} + (y - 23x/30)\ MgH_2 + (23x/30)\ H_2 \quad (4.5)$$

The overall H_2 capacity of this pair of reactions varies depending on how much MgH_2 remains unreacted in the second step. In all families of reactions like this, we chose the net stoichiometry of the mixture to maximize the H_2 capacity. Applying this approach reduces the number of distinct multi-step reactions to ~1000.

In the two step reaction above, the second reaction uses a product from the first reaction as a reactant. We will refer to this situation as a reaction that is linked by an intermediate compound. Examples also exist where two or more independent reactions can be combined to increase the overall H_2 capacity relative to one reaction alone. An example of this concept is that reaction of a 10:1:6:2 mixture of MgH_2:$NaMgH_3$:$Mg(NH_2)_2$:$KMgH_3$. This mixture evolves via three reactions that do not use reactants from lower temperature reactions in the higher temperature reactions. The first step, in which a 10:5 ratio of MgH_2 and $Mg(NH_2)_2$ react, releases 5.14 wt.% H_2 relative to the overall mixture. The two additional steps both release 0.514 wt.% H_2, meaning that the net H_2 release from the multi-step process is > 6 wt.%.

The individual reactions that are predicted to take place within multi-step reactions could suffer from practical drawbacks for the same reasons discussed in the preceding section. To reflect these issues, we further filtered the multi-step reactions to exclude any reactions that involve carbon in any form or the refractory materials BN, TiB_2, ScB_2, AlN, VN, CaB_6, V_2N, VB_2, and V_5Si_3. In addition, we excluded multi-step reactions including any step with reaction enthalpy at 0 K higher than 60 kJ/mol H_2. This filtering of our results led to 23 distinct multi-step reactions, which are listed in Tables 4.5 and 4.6. Table 4.5 (4.6) lists the examples that are (are not) linked by intermediate compounds. In general, $LiBH_4$ undergoes the phase transition from the low temperature orthorhombic phase to the high temperature hexagonal phase at 381 K[59-61], so that the orthorhombic phase has lower DFT total energy than the hexagonal phase. It implies that if a reaction involving $LiBH_4$ as a reactant occurs at a temperature higher than 381 K, the 0

K reaction enthalpy change calculated using the DFT energy of the orthorhombic phase will be overestimated. If a low temperature step in a multi step reaction corresponds to the case just described, the step may have higher 0 K reaction enthalpy change than a high temperature step in the same multi step reaction. Because all the reaction steps involving $LiBH_4$ listed in these tables correspond to this case, we used the DFT total energy of hexagonal $LiBH_4$ to calculate 0 K reaction enthalpy changes of them.

Table 4.5: Multi-step reactions where one or more single step reactions are linked with intermediate compounds. (ΔG_{max} - ΔG_{min}) is the difference of ($\Delta U_0 - T\Delta S_{conf}$) between the first step and final step in a multi-step reaction. The enthalpy changes at 0 K of $LiBH_4$ involved reactions were obtained using the DFT total energy of the hexagonal phase of $LiBH_4$.

Class I (reactions having (ΔG_{max}- ΔG_{min}) ≤ 30 kJ/mol H_2 and not involving $B_{12}H_{12}$ species)				
No.	**Reaction**	**wt.%**	**ΔU_0 ($T\Delta S_{conf}$) (kJ/mol H_2)**	**ΔG_{max}- ΔG_{min} (kJ/mol H_2)**
1	Entire reaction $36MgH_2+19Mg(NH_2)_2+2KMgH_3 \rightarrow 19Mg_3N_2+2KH+76H_2$	7.12		21.2
	1st step $36MgH_2+18Mg(NH_2)_2 \rightarrow 18Mg_3N_2+72H_2$	6.748	26	
	2nd step $0.5Mg(NH_2)_2+2KMgH_3 \rightarrow 0.5Mg_3N_2+K_2MgH_4+2H_2$	0.187	38.6	
	3rd step $0.5Mg(NH_2)_2+K_2MgH_4 \rightarrow 0.5Mg_3N_2+2KH+2H_2$	0.187	47.2	
2	Entire reaction $13MgH_2+NaMgH_3+9Mg(NH_2)_2+4KMgH_3 \rightarrow NaH+9Mg_3N_2+4KH+36H_2$	6.23		21.2
	1st step $13MgH_2+6.5Mg(NH_2)_2 \rightarrow 6.5Mg_3N_2+26H_2$	4.498	26	
	2nd step $NaMgH_3+0.5Mg(NH_2)_2 \rightarrow NaH+0.5Mg_3N_2+2H_2$	0.346	31.3	
	3rd step $Mg(NH_2)_2+4KMgH_3 \rightarrow Mg_3N_2+2K_2MgH_4+4H_2$	0.692	38.6	
	4th step $Mg(NH_2)_2+2K_2MgH_4 \rightarrow Mg_3N_2+4KH+4H_2$	0.692	47.2	

Table 4.5 continued

3	Entire reaction $1.58Li_3AlH_6+1.2MgH_2 \rightarrow 4.75LiH+0.02Al+0.05Al_{30}Mg_{23}+3.58H_2$	6.17		28.1
	1^{st} step $1.58Li_3AlH_6 \rightarrow 4.75LiH+1.58Al+2.38H_2$	4.097	28.8	
	2^{nd} step $1.2MgH_2+1.56Al \rightarrow 0.05Al_{30}Mg_{23}+1.2H_2$	2.07	56.9	
Class II (reactions having (ΔG_{max}- ΔG_{min}) ≥ 30 kJ/mol H_2 and not involving $B_{12}H_{12}$ species)				
1	Entire reaction $5.67Li_3AlH_6+8MgH_2 \rightarrow 17LiH+0.47Al_{12}Mg_{17}+16.5H_2$	6.45		30.3
	1^{st} step $5.67Li_3AlH_6 \rightarrow 17LiH+5.67Al+(17/2)H_2$	3.323	28.8	
	2^{nd} step $4.34MgH_2 +3.67Al \rightarrow 0.19Al_{30}Mg_{23}+4.34H_2$	1.698	56.9	
	3^{rd} step $3.66MgH_2 +0.19Al_{30}Mg_{23} \rightarrow 0.47Al_{12}Mg_{17}+3.66H_2$	1.429	59.1	
2	Entire reaction $9Li_3AlH_6+Al+Si+12MgH_2 \rightarrow 27LiH+Mg_2Si+0.22Al_{30}Mg_{23} +0.3Al_{12}Mg_{17}+25.5H_2$	6.01		30.8
	1^{st} step $0.33Li_3AlH_6+0.67Al+Si \rightarrow AlLiSi+H_2$	0.236	28.3	
	2^{nd} step $8.67Li_3AlH_6 \rightarrow 26LiH+8.67Al+13H_2$	3.063	28.8	
	3^{rd} step $2MgH_2+AlLiSi \rightarrow LiH+Al+Mg_2Si+1.5H_2$	0.353	40.7	
	4^{th} step $7.67MgH_2+10Al \rightarrow 0.33Al_{30}Mg_{23}+7.67H_2$	1.806	56.9	
	5^{th} step $2.33MgH_2+0.12Al_{30}Mg_{23} \rightarrow 0.3Al_{12}Mg_{17}+2.33H_2$	0.55	59.1	
3	Entire reaction $10Li_3AlH_6+9MgH_2+ScH_2 \rightarrow 30LiH+Al_3Sc+0.05Al_{30}Mg_{23} +0.47Al_{12}Mg_{17}+25H_2$	6.13		31.9
	1^{st} step $3Li_3AlH_6+ScH_2 \rightarrow 9LiH+Al_3Sc +5.5H_2$	1.348	27.2	
	2^{nd} step $7Li_3AlH_6 \rightarrow 21LiH+7Al +10.5H_2$	2.574	28.8	
	3^{rd} step $5.37MgH_2+7Al \rightarrow 0.24Al_{30}Mg_{23}+5.37H_2$	1.316	56.9	
	4^{th} step $3.64MgH_2+0.19Al_{30}Mg_{23} \rightarrow$	0.891	59.1	

Table 4.5 continued

	$0.47Al_{12}Mg_{17}+3.64H_2$			
4	Entire reaction $9Li_3AlH_6+7MgH_2+VH_2 \rightarrow 27LiH+0.69Al_3V+0.05Al_{45}V_7+0.41Al_{12}Mg_{17}+21.5H_2$	6		42.4
	1^{st} step $3Li_3AlH_6+VH_2 \rightarrow 9LiH+Al_3V+5.5H_2$	1.536	15.1	
	2^{nd} step $3.43Li_3AlH_6+Al_3V \rightarrow 10.29LiH+0.15Al_{45}V_7+5.15H_2$	1.436	27.2	
	3^{rd} step $2.57Li_3AlH_6 \rightarrow 7.72LiH+2.57Al+3.86H_2$	1.077	28.8	
	4^{th} step $1.97MgH_2+2.57Al \rightarrow 0.09Al_{30}Mg_{23}+1.97H_2$	0.551	56.9	
	5^{th} step $5.03MgH_2+0.09Al_{30}Mg_{23}+0.1Al_{45}V_7 \rightarrow 0.41Al_{12}Mg_{17}+0.69Al_3V+5.03H_2$	1.404	57.5	
Class III (reactions involving $B_{12}H_{12}$ species)				
1	Entire reaction $24LiBH_4+KBH_4 \rightarrow 20.84LiH+1.59Li_2B_{12}H_{12}+0.5K_2B_{12}H_{12}+27.09H_2$	9.47		13.9
	1^{st} step $24LiBH_4 \rightarrow 20LiH+2Li_2B_{12}H_{12}+26H_2$	9.088	47.2	
	2^{nd} step $KBH_4+0.42\ Li_2B_{12}H_{12} \rightarrow 0.84LiH+0.5K_2B_{12}H_{12}+1.09H_2$	0.379	31.7 (-29.4)	
2	Entire reaction $178LiBH_4+10Ca(BH_4)_2+42KBH_4+Li_2B_{12}H_{12} \rightarrow 180LiH+10CaH_2+21K_2B_{12}H_{12}+260H_2$	7.49		13.9
	1^{st} step $178LiBH_4 \rightarrow 148.35LiH+14.85Li_2B_{12}H_{12}+192.85H_2$	5.556	47.2	
	2^{nd} step $3.35LiH+10Ca(BH_4)_2 \rightarrow 10CaH_2+1.65Li_2B_{12}H_{12}+21.65H_2$	0.624	56.5	
	3^{rd} step $42KBH_4+17.5Li_2B_{12}H_{12} \rightarrow 35LiH+21K_2B_{12}H_{12}+45.5H_2$	1.311	31.7 (-29.4)	

Table 4.6: Multi-step reactions in which individual reactions are not linked by intermediate compounds. The enthalpy changes at 0 K of $LiBH_4$ involved reactions were obtained using the DFT total energy of the hexagonal phase of $LiBH_4$.

Class I (reactions having (ΔG_{max}- ΔG_{min}) ≤ 10 kJ/mol H_2)				
No.	**Reaction**	**wt.%**	**ΔU_0 ($T\Delta S_{conf}$) (kJ/mol H_2)**	**ΔG_{max}- ΔG_{min} (kJ/mol H_2)**
1	Entire reaction $6LiBH_4+15Mg(BH_4)_2+MgH_2+8Si \rightarrow 8Mg_2Si+3Li_2B_{12}H_{12}+55H_2$	9.31		1.6
	1st step $MgH_2+0.5Si \rightarrow 0.5Mg_2Si+H_2$	0.169	37.6	
	2nd step $6LiBH_4+15Mg(BH_4)_2+7.5Si \rightarrow 7.5Mg_2Si+3Li_2B_{12}H_{12}+54H_2$	9.136	39.2	
2	Entire reaction $18.33Si+40Mg(BH_4)_2+4Ca(BH_4)_2 \rightarrow 18.33Mg_2Si+3.33MgB_{12}H_{12}+4CaB_{12}H_{12}+132H_2$	9.01		2.4
	1st step $10Si+20Mg(BH_4)_2+4Ca(BH_4)_2 \rightarrow 10Mg_2Si+4CaB_{12}H_{12}+72H_2$	4.914	41.2	
	2nd step $8.33Si+20Mg(BH_4)_2 \rightarrow 8.33Mg_2Si+3.33MgB_{12}H_{12}+60H_2$	4.095	43.6	
3	Entire reaction $5MgH_2+10Si+15Mg(BH_4)_2+6KBH_4 \rightarrow 10Mg_2Si+3K_2B_{12}H_{12}+59H_2$	7.69		2.6
	1st step $5MgH_2+2.5Si \rightarrow 2.5Mg_2Si+5H_2$	0.652	37.6	
	2nd step $7.5Si+15Mg(BH_4)_2+6KBH_4 \rightarrow 7.5Mg_2Si+3K_2B_{12}H_{12}+54H_2$	7.042	37.3 (-2.87)	
4	Entire reaction $35Si+80Mg(BH_4)_2+8KBH_4 \rightarrow 35Mg_2Si+10MgB_{12}H_{12}+4K_2B_{12}H_{12}+252H_2$	8.86		3.5
	1st step $10Si+20Mg(BH_4)_2+8KBH_4 \rightarrow 10Mg_2Si+4K_2B_{12}H_{12}+72H_2$	2.532	37.3 (-2.9)	
	2nd step $25Si+60Mg(BH_4)_2 \rightarrow 25Mg_2Si+10MgB_{12}H_{12}+180H_2$	6.329	43.6	
5	Entire reaction $16LiBH_4+28.33Si+60Mg(BH_4)_2 \rightarrow 28.33Mg_2Si+8Li_2B_{12}H_{12}+3.33MgB_{12}H_{12}+204H_2$	9.38		4.5
	1st step $16LiBH_4+20Si+40Mg(BH_4)_2 \rightarrow 20Mg_2Si+8Li_2B_{12}H_{12}+144H_2$	6.622	39.2	
	2nd step	2.759	43.62	

Table 4.6 continued

	$8.33Si+20Mg(BH_4)_2 \rightarrow 8.33Mg_2Si+3.33MgB_{12}H_{12}+60H_2$			
6	Entire reaction $25MgH_2+NaMgH_3+13Mg(NH_2)_2 \rightarrow NaH+13Mg_3N_2+52H_2$	7.28		5.3
	1st step $25MgH_2+12.5Mg(NH_2)_2 \rightarrow 12.5Mg_3N_2+50H_2$	6.996	26	
	2nd step $NaMgH_3+0.5Mg(NH_2)_2 \rightarrow NaH+0.5Mg_3N_2+2H_2$	0.28	31.3	
7	Entire reaction $4MgH_2+47Si+108Mg(BH_4)_2 \rightarrow 47Mg_2Si+18MgB_{12}H_{12}+328H_2$	9.11		6.1
	1st step $4MgH_2+2Si \rightarrow 2Mg_2Si+4H_2$	0.111	37.6	
	2nd step $45Si+108Mg(BH_4)_2 \rightarrow 45Mg_2Si+18MgB_{12}H_{12}+324H_2$	9.002	43.6	
8	Entire reaction $2LiBH_4+MgH_2+7Mg(BH_4)_2+3.83Si \rightarrow 3.83Mg_2Si+Li_2B_{12}H_{12}+0.33MgB_{12}H_{12}+25H_2$	9.07		6.1
	1st step $MgH_2+0.5Si \rightarrow 0.5Mg_2Si+H_2$	0.363	37.6	
	2nd step $2LiBH_4+5Mg(BH_4)_2+2.5Si \rightarrow 2.5Mg_2Si+Li_2B_{12}H_{12}+18H_2$	6.533	39.2	
	3rd step $2Mg(BH_4)_2+0.83Si \rightarrow 0.83Mg_2Si+0.33MgB_{12}H_{12}+6H_2$	2.178	43.6	
9	Entire reaction $MgH_2+6Mg(BH_4)_2+Ca(BH_4)_2+3.42Si \rightarrow 3.42Mg_2Si+0.17MgB_{12}H_{12}+CaB_{12}H_{12}+22H_2$	8.6		6.1
	1st step $MgH_2+0.5Si \rightarrow 0.5Mg_2Si+H_2$	0.391	37.6	
	2nd step $5Mg(BH_4)_2+Ca(BH_4)_2+2.5Si \rightarrow 2.5Mg_2Si+CaB_{12}H_{12}+18H_2$	7.033	41.2	
	3rd step $Mg(BH_4)_2+0.42Si \rightarrow 0.42Mg_2Si+0.17MgB_{12}H_{12}+3H_2$	1.172	43.62	
10	Entire reaction $46LiBH_4+10Mg(BH_4)_2+5Si \rightarrow 35LiH+5Mg_2Si+5.5Li_2B_{12}H_{12}+81.5H_2$	9.77		8
	1st step $4LiBH_4+10Mg(BH_4)_2+5Si \rightarrow 5Mg_2Si+2Li_2B_{12}H_{12}+36H_2$	4.314	39.2	
	2nd step $42LiBH_4 \rightarrow 35LiH+3.5Li_2B_{12}H_{12}+45.5H_2$	5.452	47.2	
11	Entire reaction $12LiBH_4+MgH_2+Mg(BH_4)_2+Si \rightarrow 9.67LiH+Mg_2Si+1.17Li_2B_{12}H_{12}+17.17H_2$	9.36		9.6

Table 4.6 continued

	1st step $MgH_2+0.5Si \rightarrow 0.5Mg_2Si+H_2$	0.545	37.6	
	2nd step $0.4LiBH_4+Mg(BH_4)_2+0.5Si \rightarrow 0.5Mg_2Si+0.2Li_2B_{12}H_{12}+3.6H_2$	1.963	39.2	
	3rd step $11.6LiBH_4 \rightarrow 9.67LiH+0.97Li_2B_{12}H_{12}+12.57H_2$	6.851	47.16	
12	Entire reaction $10LiBH_4+2MgH_2+Si \rightarrow 8.33LiH+Mg_2Si+0.83Li_2B_{12}H_{12}+12.83H_2$	8.67		9.6
	1st step $2MgH_2+Si \rightarrow Mg_2Si+2H_2$	1.35	37.6	
	2nd step $10LiBH_4 \rightarrow 8.33LiH+0.83Li_2B_{12}H_{12}+10.83H_2$	7.315	47.2	
Class II **(reactions having 10 kJ/mol $H_2 \leq (\Delta G_{max}- \Delta G_{min}) \leq 20$ kJ/mol H_2)**				
1	Entire reaction $33MgH_2+17Mg(NH_2)_2+2KMgH_3 \rightarrow 17Mg_3N_2+K_2MgH_4+68H_2$	7		12.6
	1st step $33MgH_2+16.5Mg(NH_2)_2 \rightarrow 16.5Mg_3N_2+66H_2$	6.791	26	
	2nd step $0.5Mg(NH_2)_2+2KMgH_3 \rightarrow 0.5Mg_3N_2+K_2MgH_4+2H_2$	0.206	38.6	
2	Entire reaction $10MgH_2+NaMgH_3+6Mg(NH_2)_2+2KMgH_3 \rightarrow NaH+6Mg_3N_2+K_2MgH_4+24H_2$	6.17		12.6
	1st step $10MgH_2+5Mg(NH_2)_2 \rightarrow 5Mg_3N_2+20H_2$	5.14	26	
	2nd step $NaMgH_3+0.5Mg(NH_2)_2 \rightarrow NaH+0.5Mg_3N_2+2H_2$	0.514	31.3	
	3rd step $0.5Mg(NH_2)_2+2KMgH_3 \rightarrow 0.5Mg_3N_2+K_2MgH_4+2H_2$	0.514	38.6	

For convenience, the multi-step reactions in Table 4.5 are divided into three classes. Class I contains three multi-step reactions that do not involve any $B_{12}H_{12}$ species in which the difference in the calculated reaction energies between the first step and final step, (ΔG_{max} - ΔG_{min}), is lower than 30 kJ/mol H_2. This free energy includes entropy effects associated with site disorder in KBH_4 and $NaBH_4$ only, not entropy associated with the VDOS. Class II contains four multi-step reactions that do not involve any $B_{12}H_{12}$ species for which (ΔG_{max} - ΔG_{min}) is larger than 30 kJ/mol H_2. Class I is thermodynamically more desirable in hydrogen storage than Class

II because when (ΔG_{max} - ΔG_{min}) is large, a broad range of temperatures would be required for all steps in the multi-step mechanism to be relevant. Class III contains two multi-step reactions that include $B_{12}H_{12}$ species and satisfy the screening criteria stated early. These reactions release relatively large amounts of H_2 compared to the previous classes.

The seven multi-step reactions in Class I and Class II of Table 4.5 can be summarized by the two kinds of reaction schemes. The first scheme combines the destabilization reactions of $Mg(NH_2)_2$ by MgH_2, $NaMgH_3$, $KMgH_3$, or K_2MgH_4. Two of the multi-step reactions in Table 4.5 are of this type. In these two reactions, the first step involves the combination of $Mg(NH_2)_2$ and MgH_2. This single step reaction was identified above and in previous experimental and computational work.[4, 9, 57, 62, 63] K_2MgH_4 is the only compound connecting separate reaction steps in this scheme. In the second scheme, which accounts for five multi-step reactions, the first reaction is the decomposition and/or destabilization reaction of Li_3AlH_6, followed by destabilization reactions of MgH_2. For example, the net reaction predicted from the initial mixture of Li_3AlH_6 and MgH_2 with a ratio of 17:24 in Table 4.5 produces LiH and $Al_{12}Mg_{17}$ with a H_2 release of 6.45 wt.% and (ΔG_{max} - ΔG_{min}) of 30.3 kJ/mol H_2 via three single step reactions. The first step is the decomposition reaction of Li_3AlH_6 forming LiH and Al with a H_2 release of 3.323 wt.%. The second step is the destabilization reaction of MgH_2 by Al which is produced from the first step, forming $Al_{30}Mg_{23}$ with a H_2 release of 1.698 wt.%. The third step is the destabilization reaction of MgH_2 by $Al_{30}Mg_{23}$ which is produced from the second step, forming $Al_{12}Mg_{17}$ with a H_2 release of 1.429 wt.%.

The multi-step reactions in Table 4.6 are divided into two classes. Class I contains twelve multi-step reactions in which (ΔG_{max} - ΔG_{min}) is lower than 10 kJ/mol H_2. Class II contains two multi-step reactions in which (ΔG_{max} - ΔG_{min}) is between 10 kJ/mol H_2 and 20 kJ/mol H_2. They have the relatively low values of (ΔG_{max} - ΔG_{min}) compared to the multi-step reactions in Table 4.5, but most of them involve $B_{12}H_{12}$ species which appear to be undesirable for reversible hydrogen storage applications because of their kinetic stability. Basically, the multi-step reactions in Table 4.6 are the combination of two or more initial mixtures that have the separate

reaction paths. For example, the net reaction of the initial mixture of $LiBH_4$, MgH_2, and Si with the ratio of 10:2:1 in Table 4.6 produces LiH, Mg_2Si, and $Li_2B_{12}H_{12}$ with a H_2 release of 8.67 wt.% and (ΔG_{max} - ΔG_{min}) of 9.6 kJ/mol H_2 via two single step reactions.. The first step is the reaction between MgH_2 and Si to form Mg_2Si with a H_2 release of 1.35 wt.% and the second step which is the decomposition reaction of $LiBH_4$ to form LiH and $Li_2B_{12}H_{12}$ with a H_2 release of 7.315 wt.%.

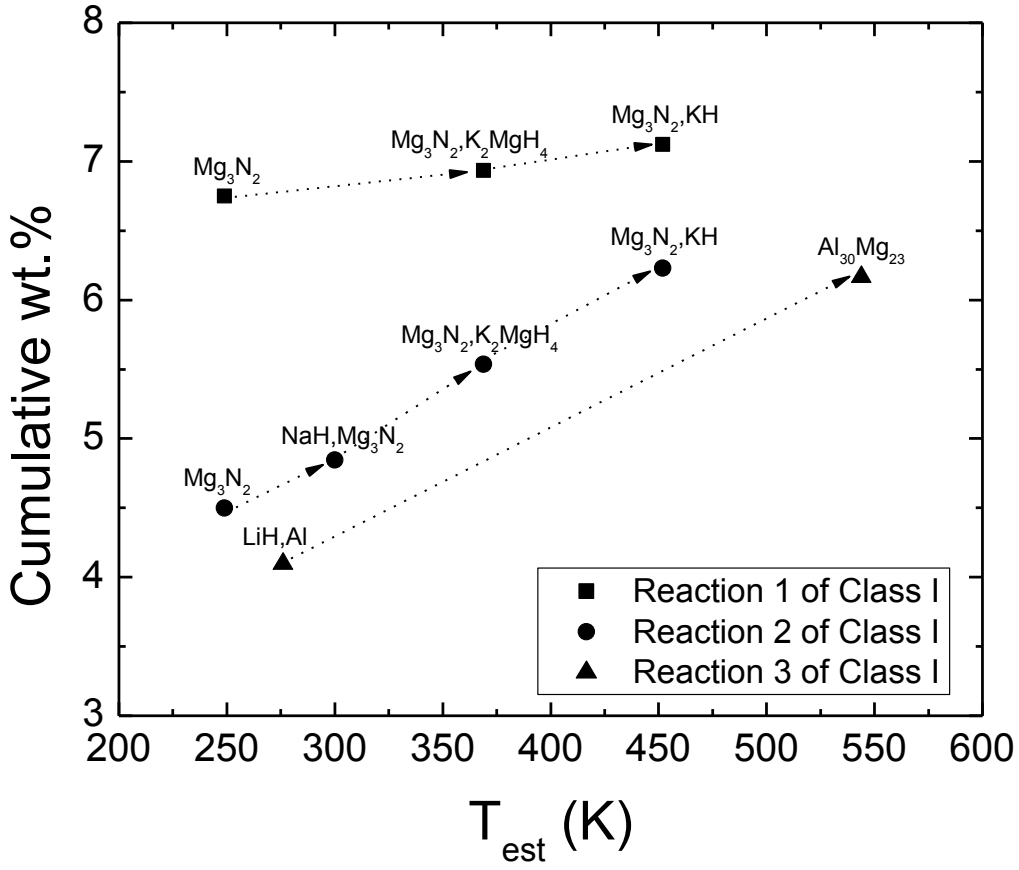

Figure 4.9: The cumulative H_2 capacity (wt.%) as a function of the estimated temperature (T_{est}) for the three reactions in Class I of Table 4.5. The compounds on each symbol represent the products at each step of a reaction.

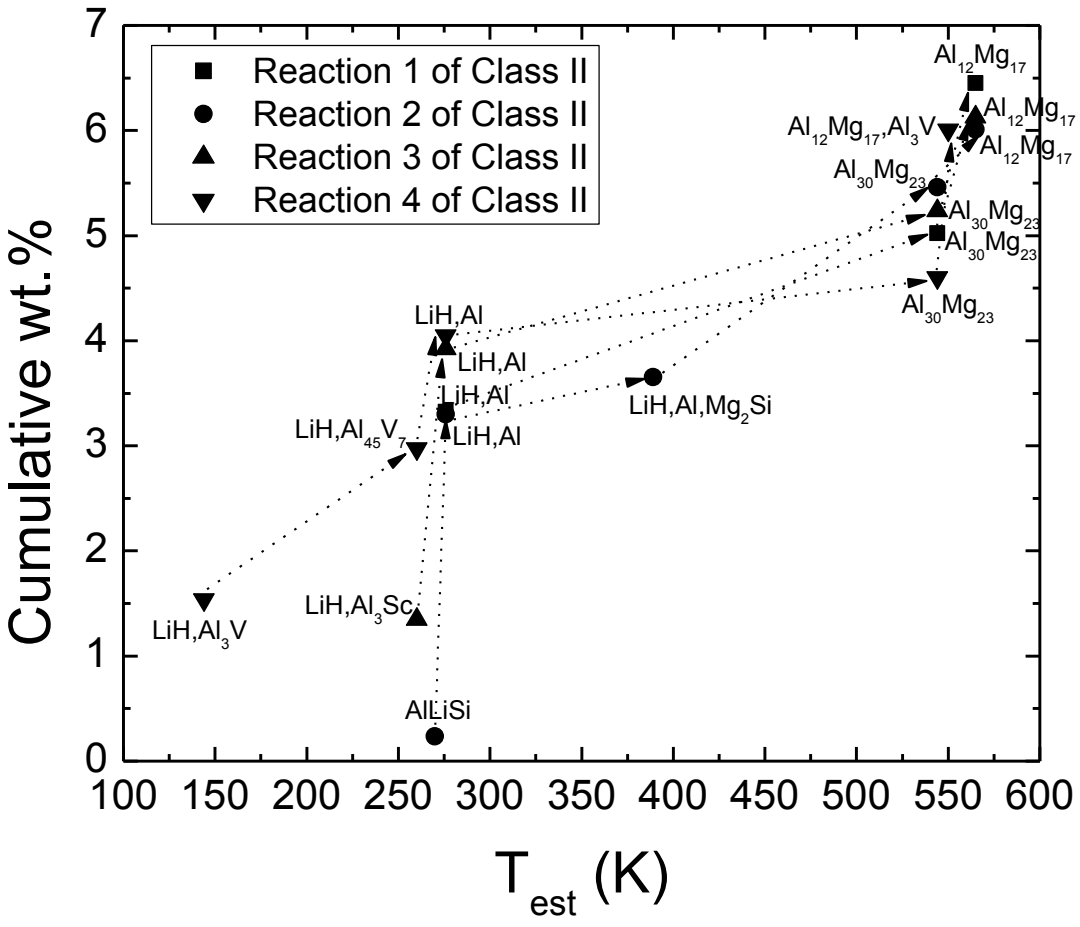

Figure 4.10: The cumulative H_2 capacity (wt.%) as a function of the estimated temperature (T_{est}) for the four reactions in Class II of Table 4.5. The compounds on each symbol represent the products at each step of a reaction.

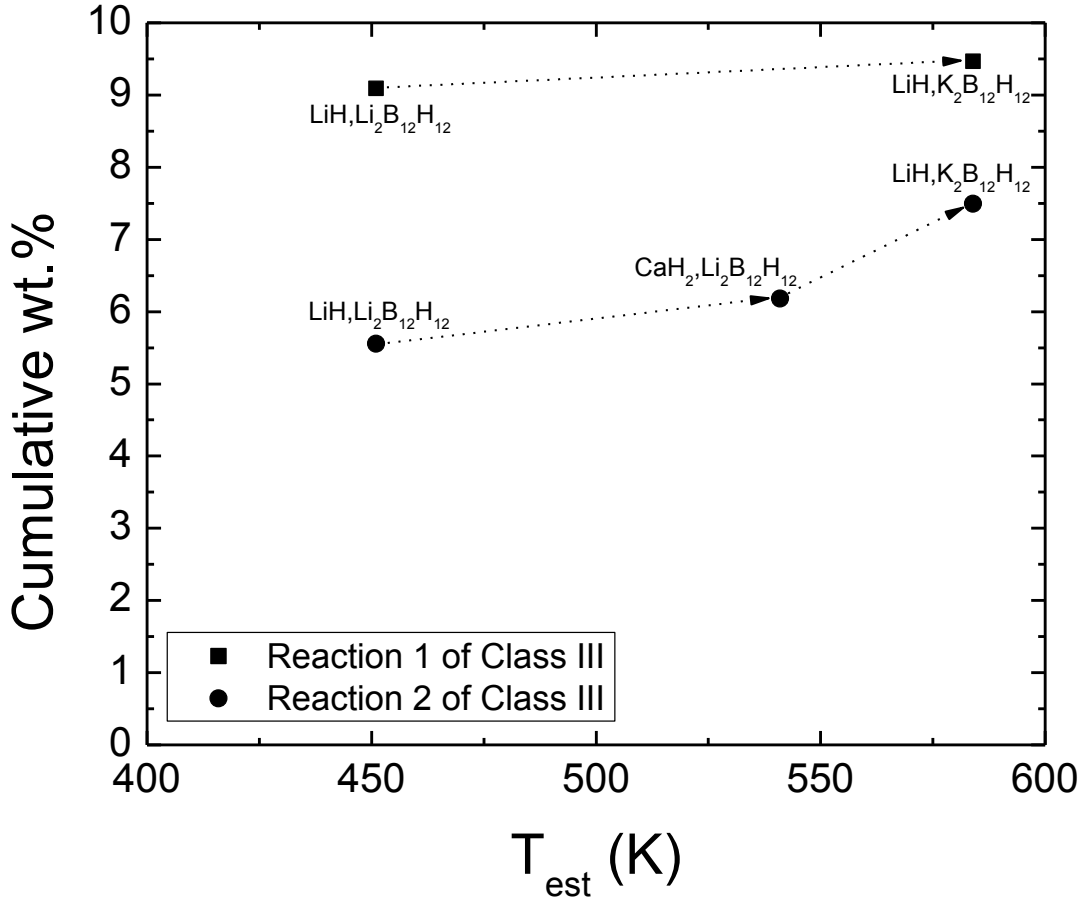

Figure 4.11: The cumulative H_2 capacity (wt.%) as a function of the estimated temperature (T_{est}) for the two reactions in Class III of Table 4.5. The compounds on each symbol represent the products at each step of a reaction.

We estimated the reaction temperature for each step of the multi-step reactions using Eqn (4.3). Figures 4.9, 4.10, and 4.11 show the cumulative H_2 capacity as a function of the estimated temperature for each step of the multi-step reactions in Table 4.5. The figures related to the reactions in Table 4.6 are given from Fig. 4.12 to Fig. 4.14. These figures illustrate the steps of each multi-step reaction. For example, in case of the reaction predicted from the initial mixture of MgH_2, $NaMgH_3$, $Mg(NH_2)_2$, and $KMgH_3$ with the ratio of 13:1:9:4 in Table 4.5 and Fig. 4.9,

the net reaction moves to the final mixture of NaH, Mg_3N_2, and KH with the ratio of 1:9:4, with a H_2 release of 6.23 wt.% via four steps. As seen in Fig. 4.9, the multi-step reaction produces Mg_3N_2, NaH/Mg_3N_2, Mg_3N_2/K_2MgH_4, and Mg_3N_2/KH in turn and H_2 is dominantly released in the first step. However, the total H_2 capacity does not reach 6.0 wt.% until the final step is completed.

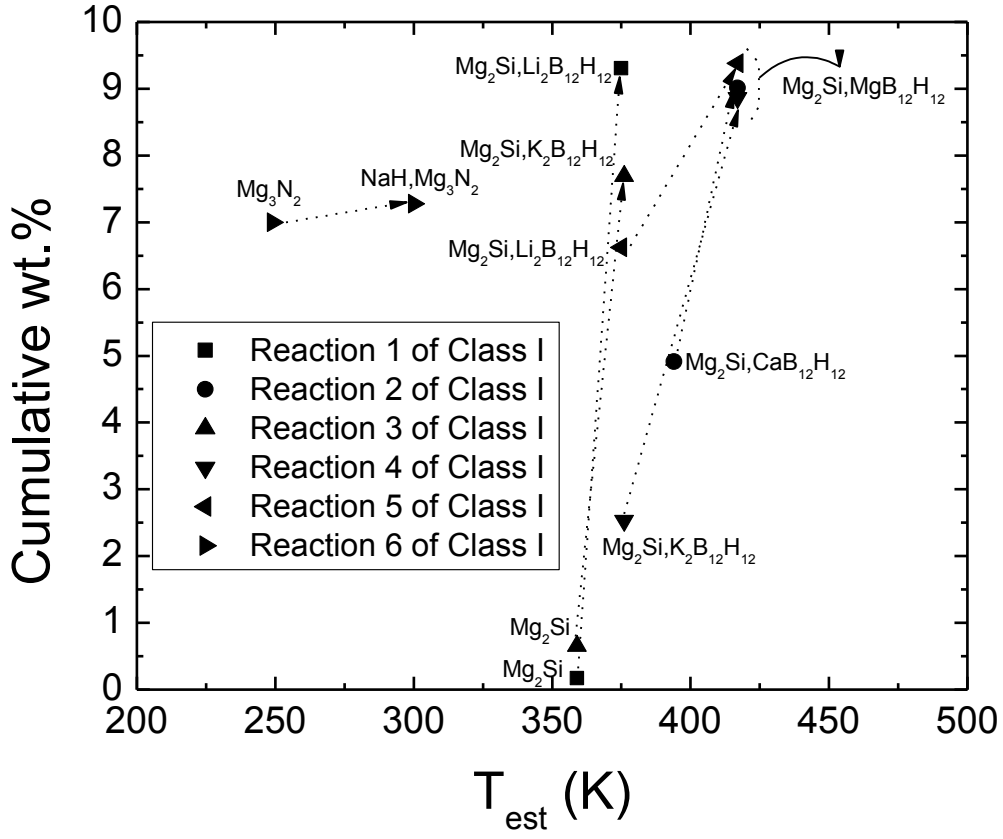

Figure 4.12. The cumulative H_2 capacity (wt.%) as a function of the estimated temperature (T_{est}) for the first six reactions in Class I of Table 4.6.

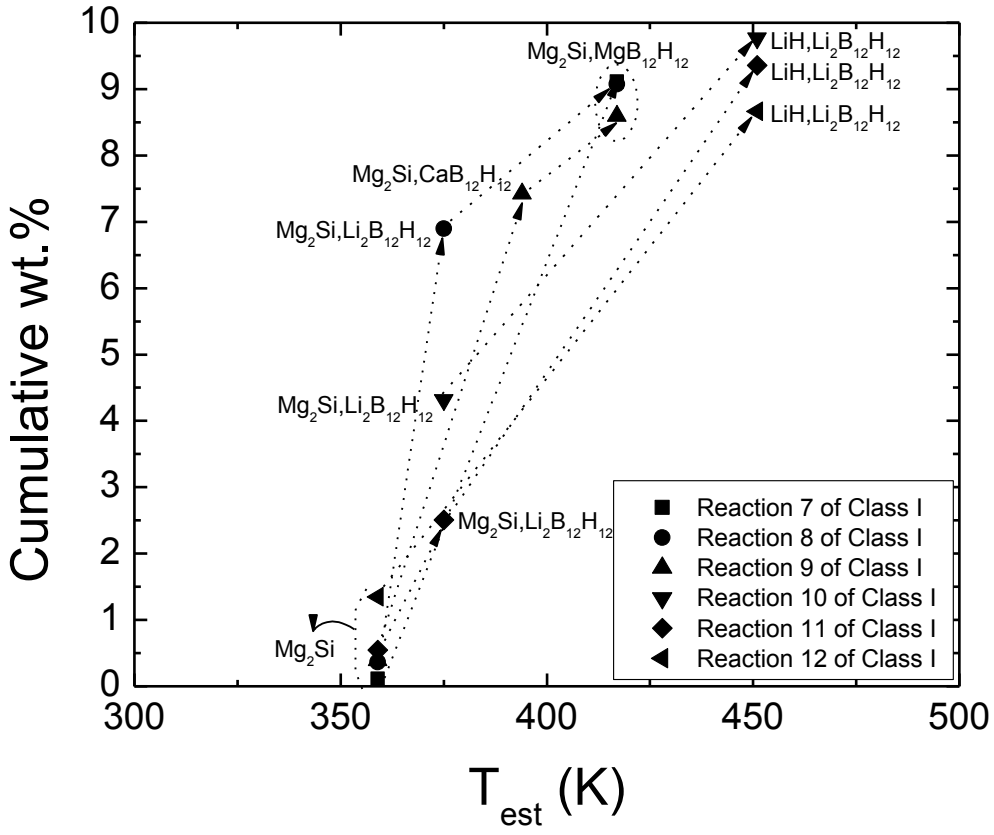

Figure 4.13. The cumulative H_2 capacity (wt.%) as a function of the estimated temperature (T_{est}) for the second six reactions in Class I of Table 4.6.

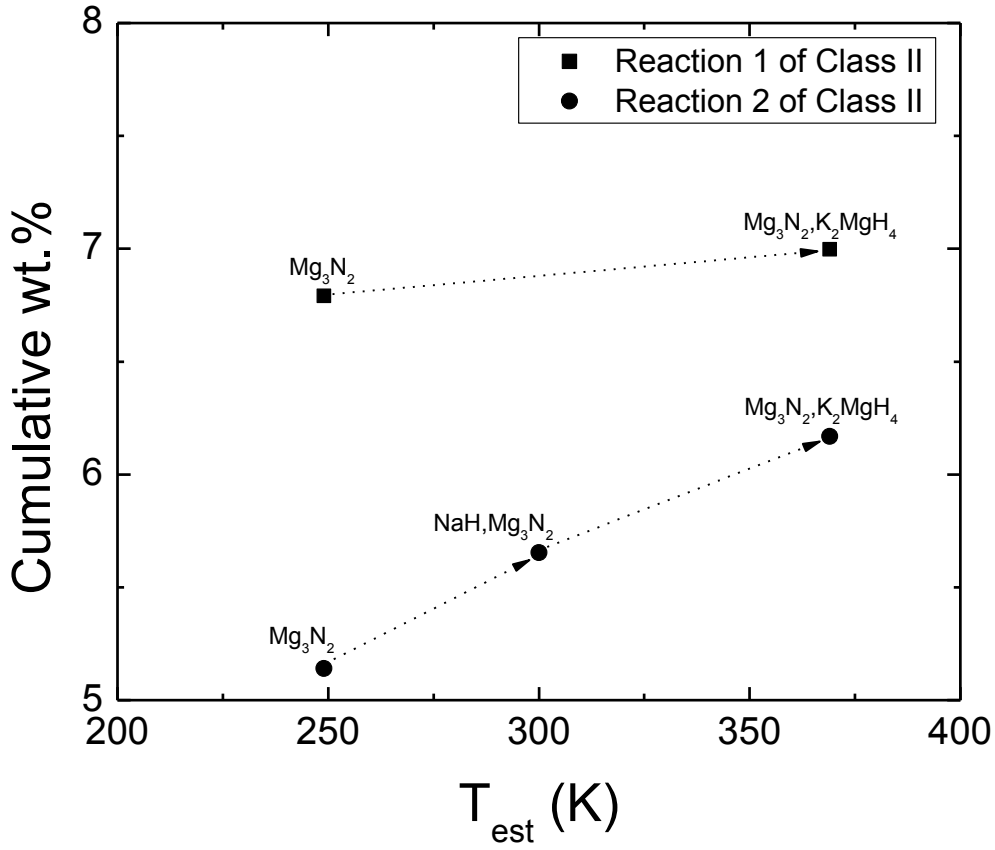

Figure 4.14. The cumulative H_2 capacity (wt.%) as a function of the estimated temperature (T_{est}) for the two reactions in Class II of Table 4.6.

4.6 Conclusions

In this chapter, we have described the largest set of thermodynamic calculations associated with reversible H_2 storage in light metal hydrides to date based on DFT total energy calculations for 359 crystalline materials. Our calculations rigorously predict the stable mixtures that are available among combinations of these materials and gaseous H_2. We have examined all single step and multi-step reactions that have 0 K reaction enthalpies (as computed using DFT) between 15 and 75 kJ/mol H_2 and release more than 6.0 wt.% H_2 at completion. These criteria

generate 74 distinct single step reactions and 23 multi-step reactions. One important conclusion from calculations of this kind is that *any* other combination of materials from the set of compounds in our database does not satisfy at least one of these criteria if used for H_2 storage.

We discussed the properties of the 74 single step reactions identified by our thermodynamic calculations in terms of how likely these reactions are to be observable and reversible in practice. The majority of these reactions include reactants that suggest that fully reversible thermodynamic equilibrium between the low and high temperature states may be challenging to achieve. This description includes reactions involving refractory materials (39 of the reactions) and species containing $B_{12}H_{12}$ groups. Reactions in both of these categories are likely to be associated with kinetic limitations. 19 of the reactions involve carbon, and these reactions are likely to be problematic for a different reason. Recent thermodynamic calculations that involve a broad range of gas phase species support the idea that the presence of carbon in a mixture of light metal hydrides is typically associated (at equilibrium) with generation of large amounts of CH_4 under some conditions.[20] Hydrocarbon generation may be strongly suppressed by kinetic limitations, as apparently occurs in studies of metal hydrides confined in nanoporous carbons[35, 48], but the existence of this reaction channel means that thermodynamic calculations that do not include CH_4 or other hydrocarbons are at best incomplete. After examining all 74 single step reactions in this way, our calculations point to two reactions as being the most interesting, the reactions of a $MgH_2/Mg(NH_2)_2$ mixture and the reaction of a $LiNH_2/LiH/KBH_4$ mixture. The former mixture has been discussed in earlier computational and experimental studies[4, 9, 57, 62, 63], but the latter reaction appears to be one that has not been examined before.

Our analysis of multi-step reactions used an efficient approach for filtering the very large number of reactions of this type that exist. Although individual reactions in the reactions paths identified in these calculations can suffer from the same reversibility problems that were discussed above for single step reactions, our calculations point to several multi-step reactions that appear to have useful properties.

4.7 REFERENCES

1. K. C. Kim and D. S. Sholl, *J. Phys. Chem. C*, 2010, **114**, 678-686.
2. J. J. Vajo, S. L. Skeith and F. Mertens, *J. Phys. Chem. B*, 2005, **109**, 3719-3722.
3. A. Ibikunle, A. J. Goudy and H. Yang, *J. Alloys Compd.*, 2009, **475**, 110-115.
4. A. R. Akbarzadeh, V. Ozolinš and C. Wolverton, *Adv. Mater.*, 2007, **19**, 3233-3239.
5. A. R. Akbarzadeh, C. Wolverton and V. Ozolins, *Phys. Rev. B*, 2009, **79**, 184102.
6. K. J. Michel, A. R. Akbarzadeh and V. Ozolins, *J. Phys. Chem. C*, 2009, **113**, 14551-14558.
7. V. Ozolins, E. H. Majzoub and C. Wolverton, *J. Am. Chem. Soc.*, 2009, **131**, 230-237.
8. S. V. Alapati, J. K. Johnson and D. S. Sholl, *J. Phys. Chem. C*, 2008, **112**, 5258-5262.
9. C. Wolverton, D. J. Siegel, A. R. Akbarzadeh and V. Ozolins, *J. Phys.: Condens. Matter*, 2008, **20**, 064228.
10. S. V. Alapati, J. K. Johnson and D. S. Sholl, *Phys. Chem. Chem. Phys.*, 2007, **9**, 1438-1452.
11. S. V. Alapati, J. K. Johnson and D. S. Sholl, *J. Alloys Compd.*, 2007, **446**, 23-27.
12. S. V. Alapati, J. K. Johnson and D. S. Sholl, *J. Phys. Chem. C*, 2007, **111**, 1584-1591.
13. J. H. Her, M. Yousufuddin, W. Zhou, S. S. Jalisatgi, J. G. Kulleck, J. A. Zan, S. J. Hwang, J. Robert C. Bowman and T. J. Udovic, *Inorganic Chemistry*, 2008, **47**, 9757-9759.
14. S. J. Hwang, J. Robert C. Bowman, J. W. Reiter, J. Rijssenbeek, G. L. Soloveichik, J. C. Zhao, H. Kabbour and C. C. Ahn, *J. Phys. Chem. C*, 2008, **112**, 3164-3169.
15. C. Kim, S.-J. Hwang, J. Robert C. Bowman, J. W. Reiter, J. A. Zan, J. G. Kulleck, H. Kabbour, E. H. Majzoub and V. Ozolins, *J. Phys. Chem. C*, 2009, **113**, 9956-9968.
16. H. W. Li, K. Miwa, N. Ohba, T. Fujita, T. Sato, Y. Yan, S. Towata, M. W. Chen and S. Orimo, *Nanotechnology*, 2009, **20**, 204013.
17. S. V. Alapati, J. K. Johnson and D. S. Sholl, *J. Phys. Chem. B*, 2006, **110**, 8769-8776.
18. *The Inorganic Crystal Structure Database (ICSD)*, http://www.fiz-informationsdienste.de/en/DB/icsd/.
19. D. S. Sholl and J. A. Steckel, *Density Functional Theory: A Practical Introduction*, John Wiley & Sons, Inc., 2008.
20. K. C. Kim, M. D. Allendorf, V. Stavila and D. S. Sholl, *Phys. Chem. Chem. Phys.*, **in press**.
21. X. Zheng, Z. Xiong, S. Qin, Y. Chua, H. Chen and P. Chen, *Int. J. Hydrogen Energy*, 2008, **33**, 3346-3350.
22. J. P. Perdew, J. A. Chevary, S. H. Vosko, K. A. Jackson, M. R. Pederson, D. J. Singh and C. Fiolhais, *Phys. Rev. B*, 1992, **46**, 6671-6687.
23. G. Kresse and J. Furthmuller, *Phys. Rev. B*, 1996, **54**, 11169-11186.
24. G. Kresse and J. Hafner, *Phys. Rev. B*, 1993, **47**, 558-561.
25. D. Vanderbilt, *Phys. Rev. B*, 1990, **41**, 7892-7895.
26. G. Kresse and D. Joubert, *Phys. Rev. B*, 1999, **59**, 1758.
27. K. Parlinski, *Software PHONON*, 2005.
28. J.-H. Kim, S.-A. Jin, J.-H. Shim and Y. W. Cho, *J. Alloys Compd.*, 2008, **461**, L20-L22.
29. M. Aoki, K. Miwa, T. Noritake, N. Ohba, M. Matsumoto, H.-W. Li, Y. Nakamori, S. Towata and S. Orimo, *Appl. Phys. A*, 2008, **92**, 601-605.

30. L.-L. Wang, D. D. Graham, I. M. Robertson and D. D. Johnson, *J. Phys. Chem. C*, 2009, **113**, 20088–20096.
31. G. L. Soloveichik, M. Andrusa, Y. Gaoa, J. C. Zhao and S. Kniajanski, *Inter. J. Hydrogen Energy*, 2009, **34**, 2144-2152.
32. Z.-Z. Fang, X.-D. Kang, P. Wang, H.-W. Li and S.-I. Orimo, *J. Alloys Compd.*, 2010, **491**, L1-L4.
33. H.-W. Li, K. Kikuchi, Y. Nakamori, N.Ohba, K. Miwa, S. Towata and S. Orimo, *Acta Mater.*, 2008, **56**, 1342-1347.
34. O. Friedrichs, J. W. Kim, A. Remhof, F. Buchter, A. Borgschulte, D. Wallacher, Y. W. Cho, M. Fichtner, K. H. Oh and A. Züttel, *Phys. Chem. Chem. Phys.*, 2009, **11**, 1515-1520.
35. S. Cahen, J. B. Eymery, R. Janot and J. M. Tarascon, *J. Power Sources*, 2009, **189**, 902-908.
36. N. Hanada, K. Chlopek, C. Frommen, W. Lohstroh and M. Fichtner, *J. Mater. Chem.*, 2008, **18**, 2611-2614.
37. A. D. Kulkarni, L.-L. Wang, D. Johnson, D. S. Sholl and K. Johnson, *submitted to J. Phys. Chem. C*.
38. L. G. Dyachkov, L. A. Zhilyakov and A. V. Kostanovskii, *Tech. Phys.*, 2000, **45**, 115-117.
39. K. Nakano, H. Matsubara and T. Imura, *Jpn. J. Appl. Phys.*, 1974, **13**, 1005-1006.
40. X. P. Hao, D. L. Cui, G. X. Shi, Y. Q. Yin, X. G. Xu, M. H. Jiang, X. W. Xu and Y. P. Li, *Mater. Lett.*, 2001, **51**, 509-513.
41. G. Levchenko, A. Lyashchenko, V. Baumer, A. Evdokimova and V. Filippov, *J. Solid State Chem.*, 2006, **179**, 2949–2953.
42. Y. I. Matrosov and V. N. Anashenko, *Metal Science and Heat Treatment*, 1971, **13**, 893-896.
43. Z. Lin, M. Guanghui and Y. Huashun, *Ceram. Int.*, 2009, **35**, 3533-3536.
44. A. N. Christensen, *Acta Cryst. B*, 1979, **35**, 2677-2678.
45. D. J. Siegel, C. Wolverton and V. Ozoliņš, *Phys. Rev. B*, 2007, **76**, 134102-134101~134106.
46. J. Purewal, S. J. Hwang, J. Robert C. Bowman, E. Rnnebro, B. Fultz and C. Ahn, *J. Phys. Chem. C*, 2008, **112**, 8481-8485.
47. J. Yang, A. Sudik and C. Wolverton, *J. Phys. Chem. C*, 2007, **111**, 19134-19140.
48. A. F. Gross, J. J. Vajo, S. L. Van Atta and G. L. Olson, *J. Phys. Chem. C*, 2008, **112**, 5651-5657.
49. P. A. Berseth, A. G. Harter, R. Zidan, A. Blomqvist, C. M. Araujo, R. H. Scheicher, R. Ahuja and P. Jena, *Nano Lett.*, 2009, **9**, 1501-1505.
50. Z. Z. Fang, P. Wang, T. E. Rufford, X. D. Kang, G. Q. Lu and H. M. Cheng, *Acta Mater.*, 2008, **56**, 6257-6263.
51. R. Campesi, F. Cuevas, E. Leroy, M. Hirscher, R. Gadiou, C. Vix-Guterl and M. Latroche, *Micropor. Mesopor. Mat.*, 2009, **117**, 511-514.
52. Y. Zhang, W.-S. Zhang, A.-Q. Wang, L.-X. Sun, M.-Q. Fan, H.-L. Chu and J.-C. S. T. Zhang, *Int. J. Hydrogen Energy*, 2007, **32**, 3976-3980.
53. P. Wang, A. M. Wang, Y. L. Wang, H. F. Zhang and Z. Q. Hu, *Scripta Mater.*, 2000, **43**, 83-87.
54. J. J. Vajo and G. L. Olson, *Scripta Mater.*, 2007, **56**, 829-834.

55. J. J. Vajo, F. Mertens, C. C. Ahn, J. Robert C. Bowman and B. Fultz, *J. Phys. Chem. B*, 2004, **108**, 13977-13983.
56. I. E. Malka, T. Czujko and J. Bystrzycki, *Int. J. Hydrogen Energy*, 2010, **35**, 1706-1712.
57. J. Hu, G. Wu, Y. Liu, Z. Xiong, P. Chen, K. Murata, K. Sakata and G. Wolf, *J. Phys. Chem. B*, 2006, **110**, 14688-14692.
58. S. V. Alapati, J. K. Johnson and D. S. Sholl, *Phys. Rev. B*, 2007, **76**, 104108.
59. J. P. Soulié, G. Renaudin, R. Cerny and K. Yvon, *J. Alloys Compd.*, 2002, **346**, 200–205.
60. S. Gomes, H. Hagemann and K. Yvon, *J. Alloys Compd.*, 2002, **346**, 206–210.
61. A. V. Skripov, A. V. Soloninin, Y. Filinchuk and D. Chernyshov, *J. Phys. Chem. C*, 2008, **112**, 18701–18705.
62. P. Chen, Z. Xiong, G. Wu, Y. Liu, J. Hu and W. Luo, *Scripta Mater.*, 2007, **56**, 817-822.
63. C. M. Araújo, R. H. Scheicher and R. Ahuja, *Appl. Phys. Lett.*, 2008, **92**, 021907.

CHAPTER 5

EXAMINING THE ROBUSTNESS OF FIRST-PRINCIPLES CALCULATIONS FOR METAL HYDRIDE REACTION THERMODYNAMICS BY DETECTION OF METASTABLE REACTION PATHWAYS

5.1 Introduction

In the previous chapter, we predicted all possible promising metal hydride mixtures by using the grand canonical linear programming method combined with our updated database about the 715 element spaces that were previously adopted by Alapati, Johnson, and Sholl.[1] Our result finally provided the completion in a series of computational examinations that had been recently performed via the linear programming method. However, we could not be free from the fact that our result was based on the first-principles calculations without considering any vibrational and entropic contributions to the relevant reactions. The main drawback was that the predicted reaction thermodynamics might be changed if a H_2 pressure is changed or the vibrational and entropic contributions are considered.

In this chapter, we describe how our predicted promising single-step reactions would be changed when the vibrational and entropic contributions to free energies are considered. Specifically, we consider thirteen chosen single-step reactions among all 74 promising single-step reactions that we previously predicted.[1] We discuss the minimum free energy paths of the chosen reactant mixtures through the examination of the possible metastable paths of the mixtures. All possible metastable paths of each mixture are examined via the modified thermodynamic calculations described below. The minimum free energy paths are identified by considering the vibrational and entropic contributions of each compound involved in each

reaction and its metastable paths.

5.2 Theoretical Approach

5.2.1 Thermodynamic Calculations

The detailed method of our thermodynamic calculations based on the grand canonical linear programming method is described by Alapati et al. and in the previous chapter.[1, 2] Here, we review the key concept related to the calculations. Our thermodynamic calculations aim to predict reaction thermodynamics at finite temperatures for a system where a solid mixture is in equilibrium state with a H_2. Here, the solid mixture is based on the database including 359 crystalline compounds within the element space of Al, B, C, Ca, K, Li, Mg, N, Na, Sc, Si, Ti, V, and H. In general, the equilibrium state between the solid mixture and H_2 is changed with temperature at a fixed H_2 pressure. The compositions of the solid mixture corresponding the equilibrium state at each temperature is rigorously and efficiently determined by a linear program which minimizes the density functional theory (DFT) based grand canonical potential of the system at a fixed temperature and a H_2 pressure of 1 bar. Our calculations detect the compositional changes of the solid mixture in the system as temperature increases to predict reaction thermodynamics. Our calculations can efficiently predict reliable reaction thermodynamics from large collection of compounds using the method just described.

The caveats associated with our thermodynamic calculations to predict reaction thermodynamics are as follows. First, our calculations cannot give any information about the possibility of reactions involving materials which are not included in the database. Second, our calculations cannot explain situations associated with the kinetic limitation experimentally observed. Third, our calculations are based on the assumption that the only gaseous species included in these calculations is H_2, so we cannot explain the possible evolution of any impurity other than H_2. In Chapter 6, we demonstrated that a total free energy minimization method can predict the possible evolution of impurity other than H_2 for several specified mixtures.[3] However,

it is not currently ready to efficiently predict reaction thermodynamics from large collection of compounds.

5.2.2 Detecting the Existence of Metastable Reaction Paths

In the method outlined above, the composition of a mixture of non-H elements in equilibrium with a specified H_2 pressure is determined at each temperature of interest. Changes in this composition as T is changed correspond to steps along a reaction path. Posing this problem at each *T* allows the equilibrium composition to be found rigorously as the outcome of a linear program.[4] We will refer to the reaction path found in this way as the equilibrium reaction path. An undesirable feature of this approach is that it cannot give any information about the existence of alternative reaction paths.

Alternative reaction paths may be important in several contexts. When calculations are based on 0 K enthalpies, it is possible that the reaction path could change once zero point energies and entropy effects are included. This situation has been referred to as "entropic stabilization".[5-7] Even if the full VDOS for every material is known, however, systematic uncertainties exist between all calculations with DFT functional and physical reality.[2, 8-10] This may make it difficult to unambiguously distinguish between several possible reaction paths with similar reaction thermodynamics using DFT calculations. Finally, experimental situations can exist where one (or more) reaction paths may face severe kinetic limitations, meaning that the reaction observed experimentally may not be the equilibrium reaction path.[2, 11, 12] For all of these reasons, it would be useful to be able to determine when alternative reaction paths exist that should be considered in addition to the equilibrium reaction path.

We have extended the computational approach outlined above to detect the existence of metastable paths of a reaction in an automated way. Let us consider the following original reaction including reactants R_1 and R_2 and products P_1 and P_2:

$$R_1 + R_2 + \ldots \rightarrow P_1 + P_2 + n_1 H_2 \quad . \tag{5.1}$$

If we temporarily remove P_1, one of the products of the reaction (5.1), from our database and

then perform the thermodynamic calculations again, we will obtain an alternative reaction mechanism:

$$R_1 + R_2 + \ldots \rightarrow P_1' + P_2' + n_2H_2 \ . \qquad (5.2)$$

By construction, the 0 K reaction enthalpy for this reaction is higher than the reaction enthalpy for reaction (5.1), so this new reaction is a metastable reaction for the starting reactants. This process can be repeated by removing a different reaction product of reaction (5.1) from the database, and repeated again by removing both solid reaction products of reaction (5.1) from the database. We will describe the three metastable reactions generated by these calculations as the first generation of the family of metastable reactions related to the original reaction.

The process of generating metastable reactions can now continue starting from the first generation reactions. For example, if we remove P_1 and P_1', one of the products of reaction (5.2), from the database and then perform the thermodynamic calculations again, we will obtain another metastable path having higher 0 K enthalpy than the reaction in Eq. (5.2):

$$R_1 + R_2 + \ldots \rightarrow P_1'' + P_2'' + n_3H_2 \ . \qquad (5.3)$$

We can also repeat this process for P_2', the other product of reaction (5.2), or both of the two products in Eq. (5.2), and proceed similarly for the other first generation metastable reactions. We refer to the reactions determined in this way as second generation reactions. This process can be continued to subsequent generations of metastable reactions.

The method defined above generates an enormous number of distinct reactions, so it is important that we can select among these reactions the relatively small number of reactions that will be physically significant. Previous DFT calculations of the kind we are using have been shown to yield reaction free energies that are accurate relative to experimental data within ±10 kJ/mol H_2.[2, 8-10] This observation suggests that if the 0 K reaction enthalpy of a metastable reaction is more than 10 kJ/mol H_2 higher than the original reaction then it is reasonable to conclude without ambiguity that it is the original reaction that is the thermodynamically stable path. For this reason, we only retained for further analysis metastable paths where the difference in 0 K reaction enthalpy between the original reaction and its metastable path is lower than 10

kJ/mol H_2.

5.3 Computational Details

All DFT calculations used the Vienna *ab initio* Simulation Package (VASP) with the PW91 generalized gradient approximation functional[13-16] and the projector augmented wave method.[17] The geometry optimization used for all crystal structures that were considered has been described previously.[1] These calculations generated a database of 359 solids whose DFT total energy was available to define 0 K reaction enthalpies. For every compound that is involved in a reaction represented in one or more van't Hoff plots below, we computed the VDOS using the PHONON code developed by Parlinski.[18] These VDOS calculations require computing the force constant matrix of each atomic interaction in a periodic material via finite difference approximations calculated from DFT total energy calculations. Because evaluating this force constant matrix requires a large number of individual total energy calculations, obtaining the VDOS is far more more computationally expensive than optimizing a material's crystal structure from experimental data. In all, we computed the VDOS for 37 of the crystalline solid among the 359 materials examined in our initial geometry optimization calculations. Once the VDOS for each species in a reaction was available, a van't Hoff plots for the reaction is given by[8]

$$P_{H2}/P_0 = \exp(-\Delta G(T)/(RT)) \tag{5.4}$$

Here, P_{H2} is the H_2 pressure, P_0 is 1 bar, $\Delta G(T)$ is the Gibbs free energy change of a reaction, and R is the gas constant.

5.4 Examining the Most Stable Paths of Thirteen Selected Single Step Reactions

In the previous chapter, our examination[1] of single step H_2 evolution reactions based on the 0 K enthalpies, ΔU_0, that can be calculated from the database of 359 solids we considered gave a total of 74 reactions with $15 \leq \Delta U_0 \leq 75$ kJ/mol H_2 and a total H_2 capacity > 6.0 wt.%. Many of these reactions however, are potentially problematic because they involve refractory compounds that are likely to be associated with poor reaction kinetics or require the presence of

carbon, which can be associated with hydrocarbon formation at equilibrium.[3] We therefore limit our attention here to the reactions that do not have involve BN, TiB_2, ScB_2, AlN, VN, CaB_6, V_2N or carbon. Three reactions among the 74 identified in our earlier calculations stood out because they satisfied all of the requirements just mentioned and in addition did not include any $B_{12}H_{12}$ species, which have also been associated with poor reaction kinetics. Among them, decomposition of MgH_2 has the high reaction enthalpy so needs the high temperature for releasing H_2. Additionally, the reaction path is clear from a number of reports.[19-22] We therefore take out from the list for our further examination. We first discuss the remaining two reactions in terms of their metastable reactions, then turn to reactions in which $B_{12}H_{12}$ species play a role.

The two most interesting reactions highlighted in Chapter 4 were the reaction of a 1:2:1 ratio of LiH, $LiNH_2$, and KBH_4 and the reaction of a 2:1 ratio of MgH_2 and $Mg(NH_2)_2$. The latter reaction has a simple interpretation in terms of the existence of potential metastable reactions; our calculations show that no metastable reactions that have reaction enthalpies within 10 kJ/mol H_2 of the original reaction. This observation gives strong evidence that the reaction path predicted by DFT for this mixture, $2MgH_2 + Mg(NH_2)_2 \rightarrow Mg_3N_2 + 4H_2$, is indeed the thermodynamically stable path. This reaction mechanism agrees with earlier experimental and computational observations.[4, 23-26]

The situation for a 1:2:1 mixture of LiH, $LiNH_2$, and KBH_4, is more complicated. Analysis of the metastable reactions for this mixture reveals 8 distinct reactions whose estimated reaction free energy lie within 10 kJ/mol H_2 of the original reaction (as characterized using 0 K enthalpies). All of these reactions are listed in Table 5.1. The calculations in Table 5.1 included an estimate for the configurational entropy associated with site disorder in KBH_4, so the reaction free energies were calculated using the 0 K DFT total energies and this configurational entropy as described in Chapter 3.[27] It is interesting to note that all but one of the 8 metastable reactions predicted in this have lower H_2 capacity than the original reaction.

Table 5.1: Metastable paths of the reaction of a 1:2:1 mixture of LiH, $LiNH_2$, and KBH_4 as characterized using 0 K reaction enthalpies.

Original reaction	**wt.%**	**ΔU_0 ($T\Delta S_{conf}$) (kJ/mol H_2)**
$LiH+2LiNH_2+KBH_4 \rightarrow Li_3BN_2+KH+4H_2$	7.48	43.6 (-7.2)
Metastable paths (8 reaction paths)	**wt.%**	**ΔU_0 ($T\Delta S_{conf}$) (kJ/mol H_2)**
$LiH+2LiNH_2+KBH_4 \rightarrow 2LiH+LiNH_2+BN+KH+2H_2$	3.74	38.2 (-14.8)
$LiH+2LiNH_2+KBH_4 \rightarrow 1.44LiH+0.78KBH_4+0.22BN+0.22KLi_7N_8H_{16}+0.44H_2$	0.83	44.2 (-15.8)
$LiH+2LiNH_2+KBH_4 \rightarrow LiH+0.8KBH_4+0.2Li_3BN_2+0.2KLi_7N_8H_{16}+0.8H_2$	1.5	46.6 (-7.5)
$LiH+2LiNH_2+KBH_4 \rightarrow LiH+0.33KBH_4+0.67Li_3BN_2+0.67KNH_2+2.67H_2$	4.99	47.4 (-7.6)
$LiH+2LiNH_2+KBH_4 \rightarrow 0.69LiH+0.23KBH_4+0.31K+0.77Li_3BN_2+0.46KNH_2+3.23H_2$	6.04	47.7 (-7.2)
$LiH+2LiNH_2+KBH_4 \rightarrow 2LiH+LiNH_2+K+BN+2.5H_2$	4.68	47.8 (-12.7)
$LiH+2LiNH_2+KBH_4 \rightarrow K+Li_3BN_2+4.5H_2$	8.42	48.3 (-6.7)
$LiH+2LiNH_2+KBH_4 \rightarrow LiH+0.43KBH_4+0.57Li_3BN_2+0.29K_2Li(NH_2)_3+2.29H_2$	4.27	48.8 (-7.7)

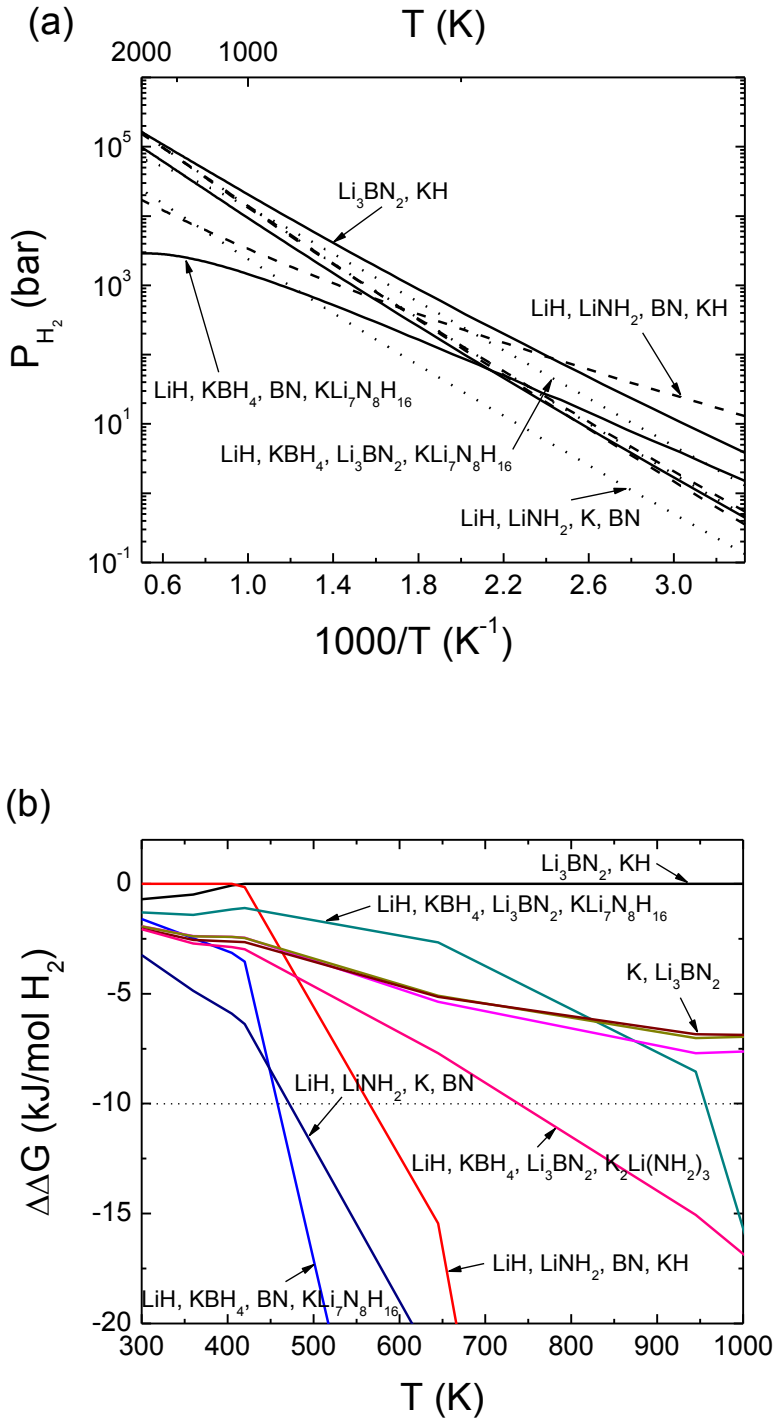

Figure 5.1: (a) van't Hoff plot for the reactions associated with a 1:2:1 mixture of LiH, $LiNH_2$, and KBH_4. Labels on the figure indicate the reaction products. (b) Gibbs free energy change of each reaction path relative to the most stable path calculated as described in the text.

To further characterize the reaction thermodynamics of the 1:2:1 mixture of LiH, $LiNH_2$, and KBH_4, we calculated the VDOS for each compound that appears in the reactions in Table 5.1. The van't Hoff plot for this set of reactions is shown in Fig. 5.1(a). The most straightforward intepretation of this figure is that for H_2 pressures higher than $10^{1.95}$ =90.1 bar, the reaction proceeds via the mechanism identified in our initial calculations, $LiH+2LiNH_2+KBH_4 \rightarrow Li_3BN_2+KH+4H_2$, releasing 7.48 wt.% H_2. At lower H_2 pressures, the reaction proceeds via a different path, $LiH+2LiNH_2+KBH_4 \rightarrow 2LiH+LiNH_2+BN+KH+2H_2$. This reaction releases only 3.74 wt.% H_2. It is useful to note that if the linear programming approach used in earlier work[4, 25, 28-30] in this area was applied to the reactions shown in Fig. 5.1, only the two reactions we have just discussed would be identified, as this approach does not identify metastable reactions.

It is useful to consider whether DFT calculations can be used to unambiguously distinguish between reaction mechanisms such as the two that were just discussed. The free energy changes calculated by DFT for reactions are necessarily imprecise because of the inexact nature of DFT functionals. Comparisons between DFT calculations of the kind we have used here and thermodynamic data from experiments for a variety of metal hydride decomposition reactions has suggested that DFT calculations are typically accurate within ±10 kJ/mol H_2.[2, 8-10, 31] This implies that we can only unambiguously distinguish between two possible reaction paths when the magnitude of the free energy difference between the two reactions is larger than 10 kJ/mol H_2. The difference between the first two reactions listed in Table 5.1, for example, is characterized by the free energy of $2LiH + LiNH_2 + BN \rightarrow Li_3BN_2 + 2H_2$. We denote this free energy by $\Delta\Delta G$. For each metastable reaction shown in Fig. 5.1, we calculated $\Delta\Delta G$ at the temperature-dependent pressure associated with the most stable reaction. The resulting free energies are shown in Fig. 5.1(b). At all temperatures shown in this figure, there are multiple reaction products whose free energy differs from the most stable products by considerably less than 10 kJ/mol H_2. This is an important observation, as it implies that DFT calculations for this system cannot make an unambiguous prediction about the expected reaction mechanism.

The ambiguity associated with identifying the thermodynamically stable reaction for the

1:2:1 LiH:$LiNH_2$:KBH_4 mixture may seem undesirable. We do not view our results this way, instead, this ambiguity contains important information about how the DFT results should be interpreted that has not been available previously. We reiterate that this is an unavoidable outcome of using DFT to predict the reaction thermodynamics, since the source of this uncertainty is simply that DFT functionals do not describe electron exchange and correlation exactly. This kind of ambiguity has largely been ignored in previous theoretical studies because calculations based on linear programming[1, 2, 4, 25, 28-30] can only identify the reaction corresponding to the minimum free energy at each state point as defined by the energies assigned to each phase. The methods we have introduced here are an efficient way to overcome this constraint and as a result draw useful physical conclusions about the robustness of the reaction paths predicted by DFT calculations.

We now move to applying the methods above to single step reactions that have been predicted in Chapter 4[1] to involve $B_{12}H_{12}$-containing species. Using the database of 359 crystalline materials described above, our calculations identified 11 single step reactions that involved one or more $B_{12}H_{12}$-containing species with a reaction enthalphy based on 0 K total energies less than 60 kJ/mol H_2. For each of these 11 reactions, metastable reactions were identified using the full database of materials as described in section 2.2. All 11 of the reactions had two or more metastable reactions as determined by the criterion defined above. For all of these metastable reactions, the VDOS of all relevant species was computed and used to produce van't Hoff plots.

We first discuss the 5:10:4 mixture of Si:$Mg(BH_4)_2$:KBH_4. The reactions associated with this mixture are listed in Table 5.2 and the van't Hoff plot for these reactions is shown in Fig. 5.2(a). If temperature and H_2 pressure are varied over the full range shown in Fig. 5.2(a), three distinct reactions are predicted to define the thermodynamically stable reaction mechanisms for this mixture. At H_2 pressures below $10^{2.4}$ bar, the reaction is predicted to favor the second mechanism listed in Table 5.2, producing $5Si+10MgH_2+2K_2B_{12}H_{12}+26H_2$, releasing 5.85 wt.% H_2. For H_2 pressures between $10^{2.4}$ and $10^{3.7}$ bar, the reaction mechanism originally identified

using 0 K reaction enthalpies is favored, producing $5Mg_2Si+2K_2B_{12}H_{12}+36H_2$, releasing 8.1 wt.% H_2. At even higher pressures, a third path that produces Si, KBH_4, Mg_2Si, and $MgB_{12}H_{12}$ is favored.

The robustness of the predictions just discussed are can be understood by examining the free energy differences shown in Fig. 5.2(b). The result is similar to Fig. 5.1(b); over the range of temperatures shown in the figure we cannot make an unambiguous conclusion about the favored reaction path based on DFT calculations.

Table 5.2: Metastable paths of the reaction of a 5:10:4 mixture of Si, $Mg(BH_4)_2$, and KBH_4 as characterized using 0 K reaction enthalpies.

Original reaction	**wt.%**	**ΔU_0 ($T\Delta S_{conf}$) (kJ/mol H_2)**
$5Si+10Mg(BH_4)_2+4KBH_4 \rightarrow 5Mg_2Si+2K_2B_{12}H_{12}+36H_2$	8.1	37.3 (-2.9)
Metastable paths (5 reaction paths)	**wt.%**	**ΔU_0 ($T\Delta S_{conf}$) (kJ/mol H_2)**
$5Si+10Mg(BH_4)_2+4KBH_4 \rightarrow 5Si+10MgH_2+2K_2B_{12}H_{12}+26H_2$	5.85	38 (-4)
$5Si+10Mg(BH_4)_2+4KBH_4 \rightarrow 0.83Si+4KBH_4+4.17Mg_2Si+1.67MgB_{12}H_{12}+30H_2$	6.75	43.6
$5Si+10Mg(BH_4)_2+4KBH_4 \rightarrow 5Si+10Mg+2K_2B_{12}H_{12}+36H_2$	8.1	44.8 (-3.1)
$5Si+10Mg(BH_4)_2+4KBH_4 \rightarrow 5.83Mg(BH_4)_2+2.33KBH_4+0.83Mg_5Si_6+0.83K_2B_{12}H_{12}+15H_2$	3.38	46.6 (-3.2)
$5Si+10Mg(BH_4)_2+4KBH_4 \rightarrow 5Si+4KBH_4+8.33MgH_2+1.67MgB_{12}H_{12}+21.67H_2$	4.88	47.1

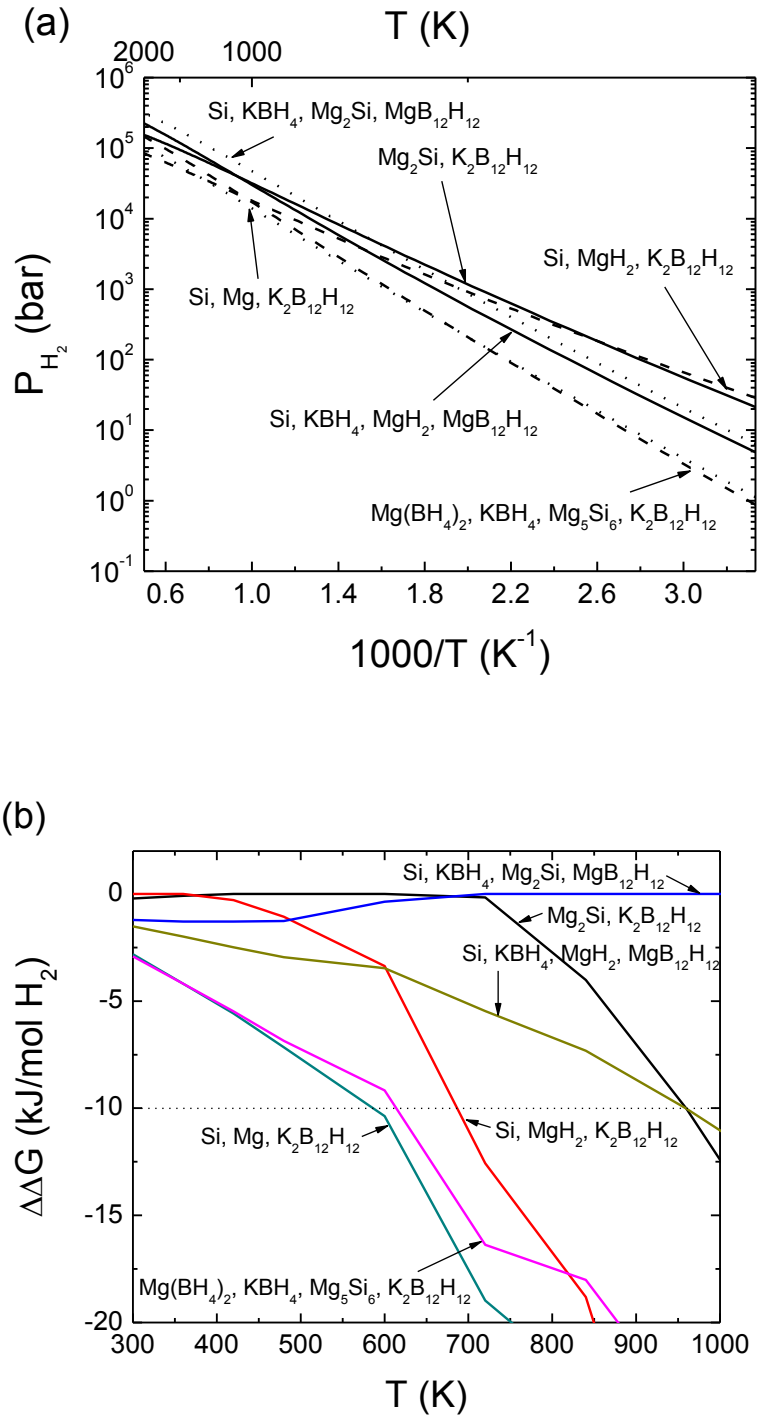

Figure 5.2: (a) van't Hoff plot for the reactions associated with a 5:10:4 mixture of Si, $Mg(BH_4)_2$, and KBH_4. Labels on the figure indicate the reaction products. (b) Gibbs free energy change of each reaction path relative to the most stable path calculated as described in the text.

We next discuss the 5:10:2 mixture of Si:$Mg(BH_4)_2$:$Ca(BH_4)_2$. This mixture is the same as the previous mixture except that KBH_4 is replaced by $Ca(BH_4)_2$. The reaction originally predicted using 0 K reaction enthalpies and its metastable paths associated with this mixture are listed in Table 5.3 and the van't Hoff plot for these reactions is shown in Fig. 5.3(a). In this mixture, as a H_2 pressure increases over the full range shown in Fig. 5.3(a), three distinct reactions are predicted as thermodynamically stable mechanisms as shown in Fig. 5.3(a). At H_2 pressures below $10^{1.1}$ bar, the second mechanism listed in Table 5.3 is the thermodynamically stable one, producing $5Si+10MgH_2+2CaB_{12}H_{12}+26H_2$, releasing 6.39 wt.% H_2. For H_2 pressures between $10^{1.1}$ and $10^{2.4}$ bar, the resulting stable reaction mechanism is the original one identified using 0 K reaction enthalpies, producing $5Mg_2Si+2CaB_{12}H_{12}+36H_2$, releasing 8.85 wt.% H_2. At higher pressures than $10^{2.4}$ bar, the third reaction mechanism is favored, producing Si, $Ca(BH_4)_2$, Mg_2Si, and $MgB_{12}H_{12}$ with a H_2 release of 7.38 wt.%. These reaction mechanisms involve kinetically stable $B_{12}H_{12}$-containing species, so that controlling a H_2 pressure cannot improve the reversibility of this mixture. The relative free energies of the reaction products from Table 5.3 are shown in Fig. 5.3(b). Once again, several of the reaction paths have free energies that are sufficiently close that their relative stability cannot be determined unambiguously from DFT.

Table 5.3: Metastable paths of the reaction of a 5:10:2 mixture of Si, $Mg(BH_4)_2$ and $Ca(BH_4)_2$ as characterized using 0 K reaction enthalpies.

Original reaction	**wt.%**	**ΔU_0 ($T\Delta S_{conf}$) (kJ/mol H_2)**
$5Si+10Mg(BH_4)_2+2Ca(BH_4)_2 \rightarrow 5Mg_2Si+2CaB_{12}H_{12}+36H_2$	8.85	41.2
Metastable paths (8 reaction paths)	**wt.%**	**ΔU_0 ($T\Delta S_{conf}$) (kJ/mol H_2)**
$5Si +10Mg(BH_4)_2+2Ca(BH_4)_2 \rightarrow 5Si+10MgH_2+2CaB_{12}H_{12}+26H_2$	6.39	43.1
$5Si+10Mg(BH_4)_2+2Ca(BH_4)_2 \rightarrow 2Ca(BH_4)_2+0.83Si+4.17Mg_2Si+1.67MgB_{12}H_{12}+30H_2$	7.38	43.6
$5Si+10Mg(BH_4)_2+2Ca(BH_4)_2 \rightarrow 5Si+2Ca(BH_4)_2+8.33MgH_2+1.67MgB_{12}H_{12}+21.67H_2$	5.33	47.1
$5Si+10Mg(BH_4)_2+2Ca(BH_4)_2 \rightarrow 5Si+10Mg+2CaB_{12}H_{12}+36H_2$	8.85	48.7
$5Si+10Mg(BH_4)_2+2Ca(BH_4)_2 \rightarrow 3Si+6Mg(BH_4)_2+2CaB_6+2Mg_2Si+24H_2$	5.9	49.1
$5Si+10Mg(BH_4)_2+2Ca(BH_4)_2 \rightarrow 3.57Si+8.57Mg(BH_4)_2+1.43CaMgSi+0.57CaB_{12}H_{12}+10.29H_2$	2.53	49.9
$5Si+10Mg(BH_4)_2+2Ca(BH_4)_2 \rightarrow 5.83Mg(BH_4)_2+1.17Ca(BH_4)_2+0.83Mg_5Si_6+0.83CaB_{12}H_{12}+15H_2$	3.69	50.5
$5Si+10Mg(BH_4)_2+2Ca(BH_4)_2 \rightarrow 5Si+2Ca(BH_4)_2+8.33Mg+1.67MgB_{12}H_{12}+30H_2$	7.38	51.2

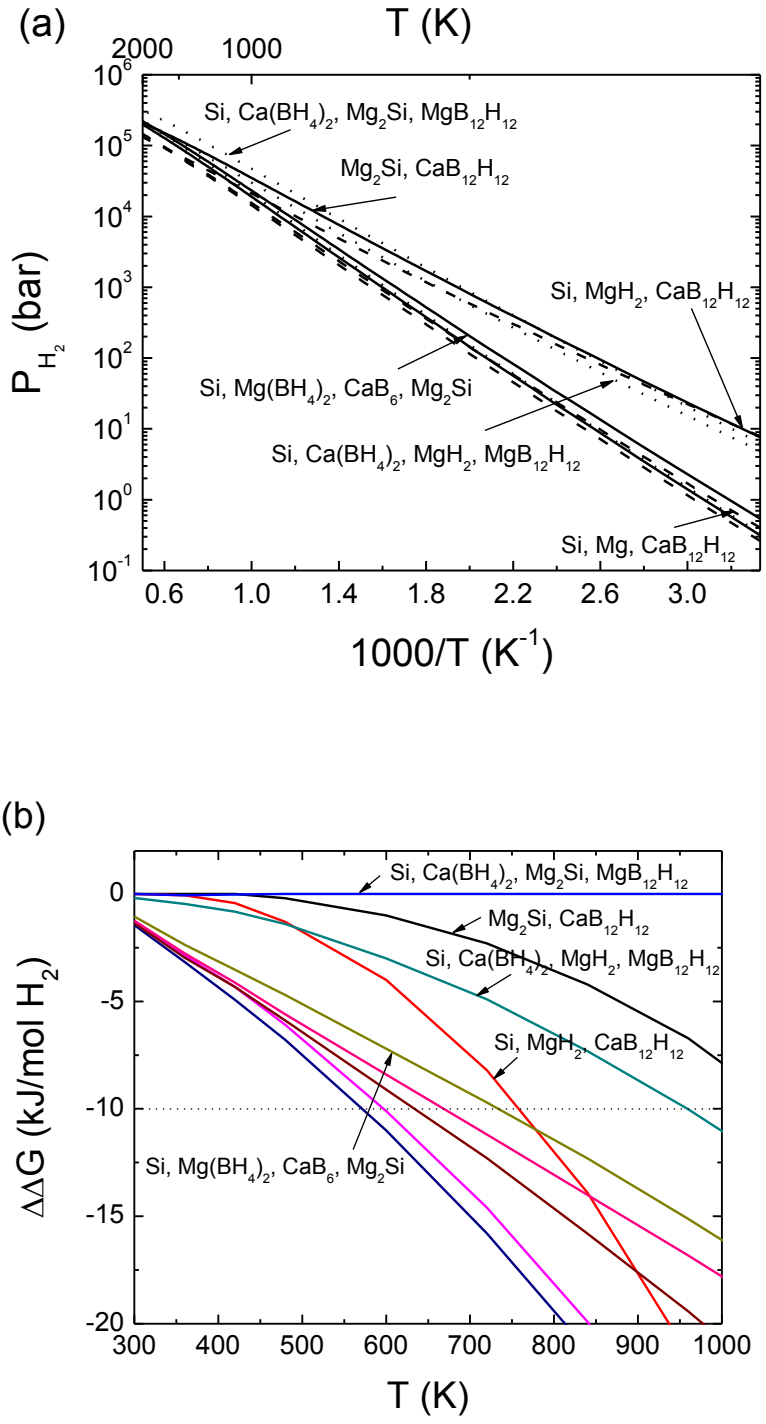

Figure 5.3: (a) van't Hoff plot for the reactions associated with a 5:10:2 mixture of Si, $Mg(BH_4)_2$ and $Ca(BH_4)_2$. Labels on the figure indicate the reaction products. (b) Gibbs free energy change of each reaction path relative to the most stable path calculated as described in the text.

The decomposition of $Ca(BH_4)_2$ is another example where our analysis of metastable reactions yields interesting results. Calculations using 0 K reaction enthalpies predict that this borohydride decomposes via $6Ca(BH_4)_2 \rightarrow 5CaH_2+CaB_{12}H_{12}+13H_2$. The two metastable reactions that are associated with this compound are listed in Table 5.4 and the associated van't Hoff plot is shown in Fig. 5.4 (a). The alternative reaction $6Ca(BH_4)_2 \rightarrow 4CaH_2 + 2CaB_6 + 20H_2$ has a reaction free energy that is very similar to the decomposition path involving $CaB_{12}H_{12}$. The van't Hoff plot predicts that the formation of $CaB_{12}H_{12}$ is favored below a H_2 pressure of $10^{1.7}$ bar, while at higher pressures the mechanism forming CaB_6 is favored. These observations are in agreement with earlier analysis of $Ca(BH_4)_2$, where one report showed $Ca(BH_4)_2$ decomposition reaction is competitive between two final mixtures[28] and another report showed that $Ca(BH_4)_2$ can be synthesized from the CaH_2 and CaB_6 at high H_2 pressures of 700 bar.[32] The relative free energies of the various reaction products from Table 5.4 are shown in Fig. 5.4(b). As might be inferred from Table 5.4 and Fig. 5.4(a), the free energy difference between the reactions involving $CaB_{12}H_{12}$ and CaB_6 are small. We would argue that the precision of DFT does not allow us to unambiguously determine which reaction products are more stable in the temperature range shown in Fig. 5.4(b).

Table 5.4: Metastable paths of the decomposition of $Ca(BH_4)_2$ as characterized using 0 K reaction enthalpies.

Original reaction	**wt.%**	**ΔU_0 ($T\Delta S_{conf}$) (kJ/mol H_2)**
$6Ca(BH_4)_2 \rightarrow 5CaH_2+CaB_{12}H_{12}+13H_2$	6.26	57.4
Metastable paths (2 reaction paths)	**wt.%**	**ΔU_0 ($T\Delta S_{conf}$) (kJ/mol H_2)**
$6Ca(BH_4)_2 \rightarrow 4CaH_2+2CaB_6+20H_2$	9.63	58.6
$6Ca(BH_4)_2 \rightarrow 3CaH_2+3CaB_4+21H_2$	10.11	63

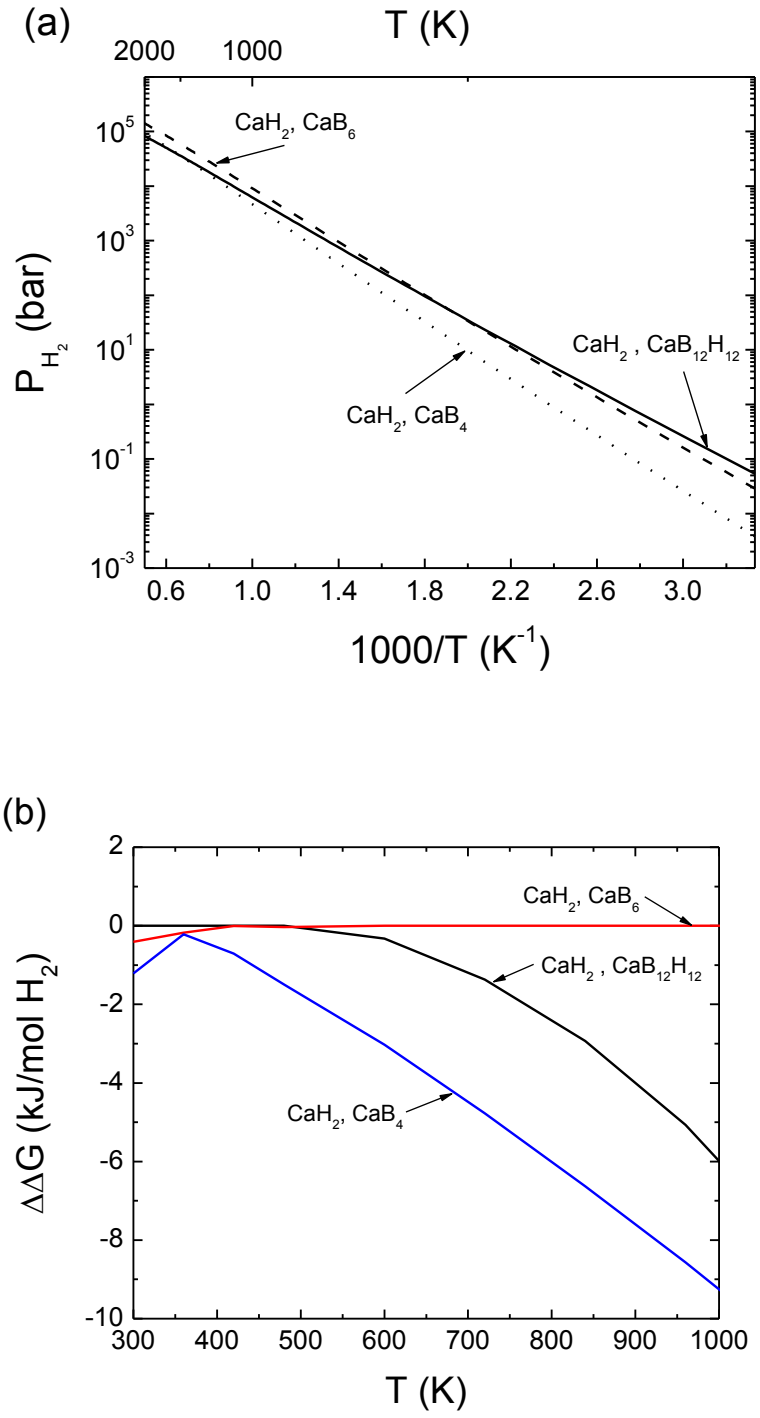

Figure 5.4: (a) van't Hoff plot for the reactions associated with the decomposition of $Ca(BH_4)_2$. Labels on the figure indicate the reaction products. (b) Gibbs free energy change of each reaction path relative to the most stable path calculated as described in the text.

The next example associated with identifying the minimum free energy path is the decomposition of $LiSc(BH_4)_4$. Table 5.5 lists the reaction originally predicted using 0 K reaction enthalpies and its metastable paths, and Fig. 5.5(a) shows the van't Hoff plot associated with the reaction mechanisms listed in Table 5.5. As a H_2 pressure increases, the van't Hoff plot predicts that the second reaction listed in Table 5.5 forming $LiBH_4$, ScB_2, and $Li_2B_{12}H_{12}$ is favored over all H_2 pressures ranged in Fig. 5.5(a). The resulting stable path is interestingly different from the reaction path predicted by Kim *et. al.*[33] They experimentally synthesized this compound and then theoretically examined its decomposition thermodynamics. Their calculations predicted that $LiSc(BH_4)_4$ would be decomposed to produce $LiBH_4$, ScH_2, and $Li_2B_{12}H_{12}$ releasing a H_2, which is exactly the same mechanism as the reaction originally predicted using 0 K reaction enthalpies. It indicates that their predicted mechanism is only based on the DFT energies of the compounds associated with the DFT energy based path and thus the vibrational and entropic contributions can be crucial to predict the exact reaction path. The relative free energies of the reaction products from Table 5.5 are shown in Fig. 5.5(b). At the upper end of the temperature range in this figure, the difference between the most stable state (as predicted by DFT) and the other states is large enough that the DFT calculations give a high degree of confidence that this identification of the stable state is unambiguous. Unfortunately, this regime occurs under conditions where the H_2 pressures are very large (cf. Fig. 5.2(a)). At lower temperatures and H_2 pressures that would be of more practical interest, the first two reactions listed in Table 5.5 are sufficiently close in free energy that they cannot be unambiguously distinguished with DFT.

The four single step reactions involving $B_{12}H_{12}$-containing species discussed above have either multiple distinct paths or only a metastable path as stable reaction mechanisms at H_2 pressures of 1 ~ 100 bar desirable for reversible hydrogen storage. The stable paths of the reactions therefore differ from the mechanisms originally predicted using 0 K reaction enthalpies at some of the H_2 pressures. On the other hand, the rest of the reactions involving $B_{12}H_{12}$-containing species have only mechanisms originally predicted using 0 K reaction enthalpies as thermodynamically stable paths at 1 ~ 100 bar. The detailed original reaction mechanisms are

listed in Table 5.6. Ozolins et al. also reported that the calculations based on the grand canonical linear programming method predicted the reaction mechanisms of $2LiBH_4+5Mg(BH_4)_2$, $5Mg(BH_4)_2+Ca(BH_4)_2$, and $Mg(BH_4)_2$ as listed in Table 5.6.[28]

Table 5.5: Metastable paths of the decomposition of $LiSc(BH_4)_4$ as characterized using 0 K reaction enthalpies.

Original reaction	**wt.%**	**ΔU_0 ($T\Delta S_{conf}$) (kJ/mol H_2)**
$10LiSc(BH_4)_4 \rightarrow 4LiBH_4+10ScH_2+3Li_2B_{12}H_{12}+44H_2$	7.97	24.1
Metastable paths (7 reaction paths)	**wt.%**	**ΔU_0 ($T\Delta S_{conf}$) (kJ/mol H_2)**
$10LiSc(BH_4)_4 \rightarrow 8LiBH_4+10ScB_2+Li_2B_{12}H_{12}+58H_2$	10.51	25.4
$10LiSc(BH_4)_4 \rightarrow 3.33LiH+10ScH_2+3.33Li_2B_{12}H_{12}+48.33H_2$	8.76	27.1
$10LiSc(BH_4)_4 \rightarrow 6.67LiH+10ScB_2+1.67Li_2B_{12}H_{12}+66.67H_2$	12.08	29.7
$10LiSc(BH_4)_4 \rightarrow 10LiBH_4+ScB_{12}+9ScB_2+60H_2$	10.87	30.8
$10LiSc(BH_4)_4 \rightarrow 10LiBH_4+10ScB_2+10B+60H_2$	10.87	31.4
$10LiSc(BH_4)_4 \rightarrow 3.33Li+10ScH_2+3.33Li_2B_{12}H_{12}+50H_2$	9.06	31.9
$10LiSc(BH_4)_4 \rightarrow 4LiBH+10ScH_2+3Li_2B_{12}H_{12}+50H_2$	9.06	32.2

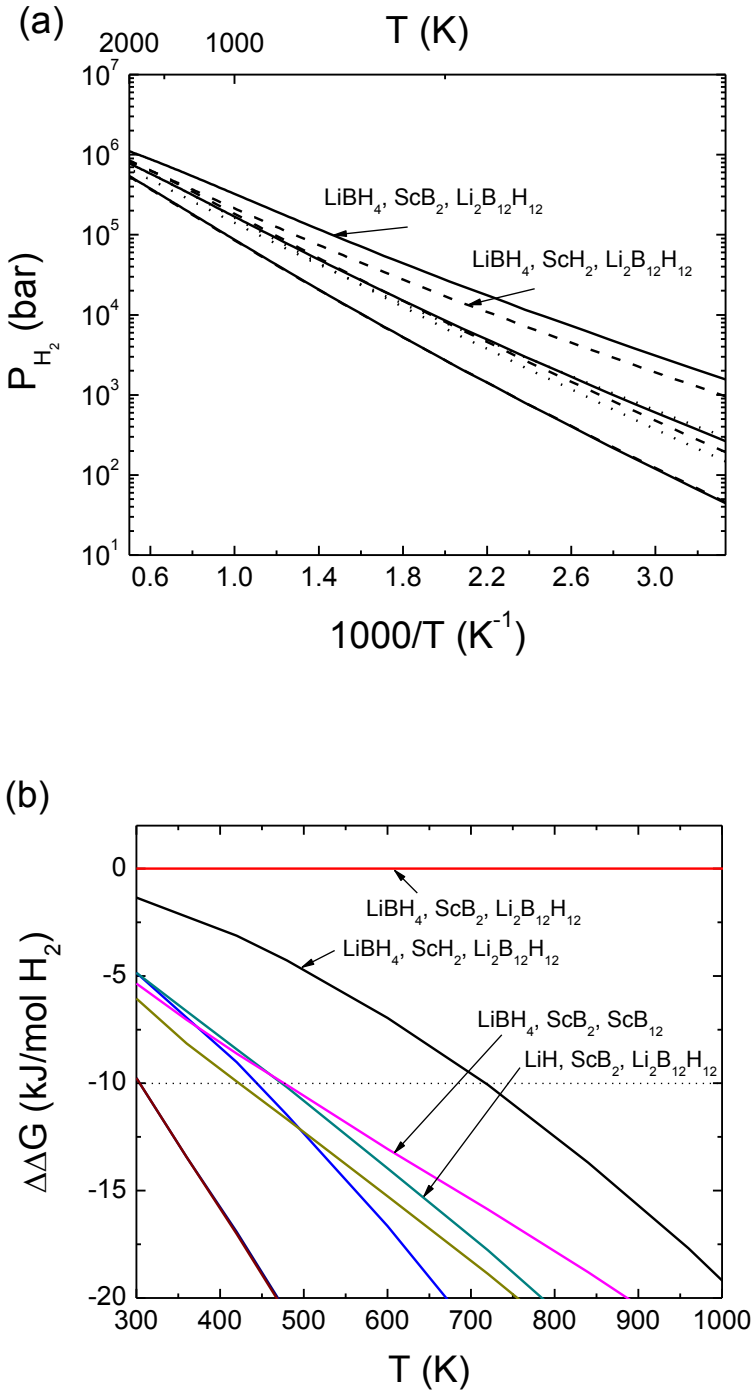

Figure 5.5: (a) van't Hoff plot for the reactions associated with the decomposition of $LiSc(BH_4)_4$. Labels on the figure indicate the reaction products. (b) Gibbs free energy change of each reaction path relative to the most stable path calculated as described in the text.

All of the reactions have two or more metastable paths and the relative stability of them are identified by considering vibrational and entropic contributions. That is, as a H_2 pressure increases, the most stable reaction paths of $LiBH_4/Si/Mg(BH_4)_2$ mixture having four metastable paths is changed from the path listed in Table 5.6 into $4LiBH_4 + 5Si + 10Mg(BH_4)_2 \rightarrow 4LiBH_4 + 0.83Si + 4.17Mg_2Si + 1.67MgB_{12}H_{12} + 30H_2$ at a H_2 pressure of $10^{2.23}$ bar which is close to the desired range of 1 ~ 100 bar. The reaction between $LiBH_4$ and $Mg(BH_4)_2$ which are two most well known borohydrides produces MgH_2 and $Li_2B_{12}H_{12}$ with the molar ratio of 5:1 at H_2 pressures below $10^{2.87}$ bar, but produces $LiBH_4$, MgH_2, and $MgB_{12}H_{12}$ with the molar ratio of 12:25:5 at higher pressures. The most stable path of $Mg(BH_4)_2/Ca(BH_4)_2$ mixture having four metastable paths is also changed at a H_2 pressure of $10^{2.94}$ bar. At a H_2 pressure below (over) $10^{2.94}$ bar the mixture produces MgH_2 and $CaB_{12}H_{12}$ with the molar ratio of 5:1 ($Ca(BH_4)_2$, MgH_2, and $MgB_{12}H_{12}$ with the molar ratio of 6:25:5). In cases of the mixtures of $Mg(BH_4)_2/KBH_4$ and $LiH/Ca(BH_4)_2$, as a H_2 pressure increases, the most stable paths are changed from their original mechanism listed in Table 5.6 into $5Mg(BH_4)_2 + 2KBH_4 \rightarrow 2KBH_4 + 4.17MgH_2 + 0.83MgB_{12}H_{12} + 10.83H_2$ and $2LiH + 6Ca(BH_4)_2 \rightarrow 2LiH + 4CaH_2 + 2CaB_6 + 20H_2$ at $10^{3.82}$ bar and $10^{3.46}$ bar, respectively. The mixtures of $Si/Mg(BH_4)_2$ and $Mg(BH_4)_2$ follow the mechanisms listed in Table 5.6 in the physically interesting range of H_2 pressures and temperatures. The relative reaction free energy changes of all reaction paths predicted by DFT calculations for each mixture listed in Table 5.6 indicate that we cannot make an unambiguous conclusion about the favored reaction path based on DFT calculations in the range of physical interest.

Table 5.6: The list of 7 reactions except for 4 reactions discussed above among the 11 single step reactions that involve one or more $B_{12}H_{12}$-containing species with a reaction enthalpy based on 0 K total energies less than 60 kJ/mol H_2.

Original reaction	wt.%	ΔU_0 ($T\Delta S_{conf}$) (kJ/mol H_2)
$4LiBH_4+5Si+10Mg(BH_4)_2 \rightarrow 5Mg_2Si+2Li_2B_{12}H_{12}+36H_2$	9.46	41
$5Si+12Mg(BH_4)_2 \rightarrow 5Mg_2Si+2MgB_{12}H_{12}+36H_2$	9.21	43.6
$2LiBH_4+5Mg(BH_4)_2 \rightarrow 5MgH_2+Li_2B_{12}H_{12}+13H_2$	8.36	43.1
$6Mg(BH_4)_2 \rightarrow 5MgH_2+MgB_{12}H_{12}+13H_2$	8.09	47.1
$5Mg(BH_4)_2+Ca(BH_4)_2 \rightarrow 5MgH_2+CaB_{12}H_{12}+13H_2$	7.72	43.1
$5Mg(BH_4)_2+2KBH_4 \rightarrow 5MgH_2+K_2B_{12}H_{12}+13H_2$	6.94	38 (-4)
$LiH+3Ca(BH_4)_2 \rightarrow 3CaH_2+0.5Li_2B_{12}H_{12}+6.5H_2$	6.03	56.5

5.5 Conclusions

In this chapter, based on the result of the promising single-step reactions that we predicted in our previous chapter[1], we first examined possible metastable paths for a few selected reactions using the first-principles calculations combined with our thermodynamic calculations. We specifically focused on the two most interesting reactions and eleven reactions involving $B_{12}H_{12}$-containing species which have lower reaction enthalpy at 0 K than 60 kJ/mol H_2. Next, we demonstrated the idea that changing the H_2 pressure can change the reaction scheme by examining the minimum free energy path from the resulting metastable paths of each reaction.

Only the mixture of $LiH/LiNH_2/KBH_4$ with the ratio of 1:2:1 among the two most interesting reactions had metastable paths within 10 kJ/mol H_2 higher than the original reaction. Specifically, the mixture had eight distinct metastable paths. Next, we identified that the minimum free energy path was changed with a H_2 pressure (the critical pressure: 90.1 bar) from the further examination based on the VDOS calculations of the compounds which were involved in the nine reaction paths. As the temperature increased, the initial mixture moved to the final mixtures of LiH, $LiNH_2$, BN, and KH below 90.1 bar and Li_3BN_2 and KH over 90.1 bar. It indicates that the reactant mixture should be controlled over 90.1 bar to avoid the production of BN, a refractory material.

All eleven reactions involving $B_{12}H_{12}$-containing species had two or more metastable

paths. However, only four of them had the minimum free energy path which was partially or totally changed to a metastable path within the range of 1 ~ 100 bar. The first mixture was Si:$Mg(BH_4)_2$:KBH_4 with the ratio of 5:10:4. As temperature increased, the mixture moved to the different final mixtures of Si, MgH_2, and $K_2B_{12}H_{12}$, Mg_2Si and $K_2B_{12}H_{12}$, and Si, KBH_4, Mg_2Si, and $MgB_{12}H_{12}$ according to a H_2 pressure. The critical points at which the reaction scheme was changed were $10^{2.4}$ bar and $10^{3.7}$ bar. The mixture therefore moved to the final mixture of Si, MgH_2, and $K_2B_{12}H_{12}$ within the range of 1 ~ 100 bar, indicating that the reaction would not be reversible. The second mixture was Si:$Mg(BH_4)_2$:$Ca(BH_4)_2$ with the ratio of 5:10:2. Similarly, as temperature increased, the mixture moved to the final mixtures of Si, MgH_2, and $CaB_{12}H_{12}$ below the H_2 pressure of $10^{1.1}$ bar, Mg_2Si and $CaB_{12}H_{12}$ at the H_2 pressure between $10^{1.1}$ bar and $10^{2.4}$ bar, and Si, $Ca(BH_4)_2$, Mg_2Si, and $MgB_{12}H_{12}$ over the H_2 pressure of $10^{2.4}$ bar. At 1 ~ 100 bar, both of two paths corresponding to the most stable paths involved $B_{12}H_{12}$ species would not be reversible. The next example was the decomposition of $Ca(BH_4)_2$. As temperature increased, it moved to the final mixtures of CaH_2 and $CaB_{12}H_{12}$ below the H_2 pressure of $10^{1.7}$ bar and CaH_2 and CaB_6 over the H_2 pressure of $10^{1.7}$ bar. It indicates that $Ca(BH_4)_2$ decomposition reaction would be competitive between two finial mixtures and $B_{12}H_{12}$ species could be disappeared by controlling the H_2 pressure. The last example was the decomposition of $LiSc(BH_4)_4$. Our calculations basically predicted that the most stable path would be not the reaction mechanism originally identified using 0 K reaction enthalpies at any H_2 pressures in full range shown the figure.

In summary, our examination shows that only four of thirteen promising single-step reactions had one of the metastable paths as the minimum free energy path at the H_2 pressure of 1 bar. Additionally two of the four reactions had the original reaction as the minimum free energy path over a certain H_2 pressure of 10 ~ 100 bar. It indicates that our DFT based thermodynamic calculations efficiently give us the reliable prediction. Although our calculations predicted the precise values associated with the transition points of the stable paths as just discussed, the relative reaction free energy changes of all possible paths for each reaction

indicated that we could not make an unambiguous conclusion about the favored reaction path based on DFT calculations at the broad range of temperatures and H_2 pressures.

5.6 REFERENCES

1. K. C. Kim, A. D. Kulkarni, J. K. Johnson and D. S. Sholl, *in preparation*.
2. S. V. Alapati, J. K. Johnson and D. S. Sholl, *J. Phys. Chem. C*, 2008, **112**, 5258-5262.
3. K. C. Kim, M. D. Allendorf, V. Stavila and D. S. Sholl, *Phys. Chem. Chem. Phys.*, **in press**.
4. A. R. Akbarzadeh, V. Ozolinš and C. Wolverton, *Adv. Mater.*, 2007, **19**, 3233-3239.
5. M. M. A. E. Claessens, F. A. M. Leermakers, F. A. Hoekstra and M. A. C. Stuart, *Langmuir*, 2007, **23**, 6315–6320.
6. S. S. Kapur and T. Sinno, *Appl. Phys. Lett.*, 2008, **93**, 221911.
7. R. Kumar and A. K. Bhuyan, *J. Biol. Inorg. Chem.*, 2009, **14**, 11-21.
8. S. V. Alapati, J. K. Johnson and D. S. Sholl, *Phys. Chem. Chem. Phys.*, 2007, **9**, 1438-1452.
9. S. V. Alapati, J. K. Johnson and D. S. Sholl, *J. Alloys Compd.*, 2007, **446**, 23-27.
10. S. V. Alapati, J. K. Johnson and D. S. Sholl, *J. Phys. Chem. C*, 2007, **111**, 1584-1591.
11. J. Yang, A. Sudik and C. Wolverton, *J. Phys. Chem. C*, 2007, **111**, 19134-19140.
12. J. Purewal, S. J. Hwang, J. Robert C. Bowman, E. Rnnebro, B. Fultz and C. Ahn, *J. Phys. Chem. C*, 2008, **112**, 8481-8485.
13. J. P. Perdew, J. A. Chevary, S. H. Vosko, K. A. Jackson, M. R. Pederson, D. J. Singh and C. Fiolhais, *Phys. Rev. B*, 1992, **46**, 6671-6687.
14. G. Kresse and J. Furthmuller, *Phys. Rev. B*, 1996, **54**, 11169-11186.
15. G. Kresse and J. Hafner, *Phys. Rev. B*, 1993, **47**, 558-561.
16. D. Vanderbilt, *Phys. Rev. B*, 1990, **41**, 7892-7895.
17. G. Kresse and D. Joubert, *Phys. Rev. B*, 1999, **59**, 1758.
18. K. Parlinski, *Software PHONON*, 2005.
19. J. J. Vajo, F. Mertens, C. C. Ahn, J. Robert C. Bowman and B. Fultz, *J. Phys. Chem. B*, 2004, **108**, 13977-13983.
20. P. Wang, A. M. Wang, Y. L. Wang, H. F. Zhang and Z. Q. Hu, *Scripta Mater.*, 2000, **43**, 83-87.
21. J. J. Vajo and G. L. Olson, *Scripta Mater.*, 2007, **56**, 829-834.
22. I. E. Malka, T. Czujko and J. Bystrzycki, *Int. J. Hydrogen Energy*, 2010, **35**, 1706-1712.
23. P. Chen, Z. Xiong, G. Wu, Y. Liu, J. Hu and W. Luo, *Scripta Mater.*, 2007, **56**, 817-822.
24. J. Hu, G. Wu, Y. Liu, Z. Xiong, P. Chen, K. Murata, K. Sakata and G. Wolf, *J. Phys. Chem. B*, 2006, **110**, 14688-14692.
25. C. Wolverton, D. J. Siegel, A. R. Akbarzadeh and V. Ozolins, *J. Phys.: Condens. Matter*, 2008, **20**, 064228.
26. C. M. Araújo, R. H. Scheicher and R. Ahuja, *Appl. Phys. Lett.*, 2008, **92**, 021907.
27. K. C. Kim and D. S. Sholl, *J. Phys. Chem. C*, 2010, **114**, 678-686.
28. V. Ozolins, E. H. Majzoub and C. Wolverton, *J. Am. Chem. Soc.*, 2009, **131**, 230-237.
29. A. R. Akbarzadeh, C. Wolverton and V. Ozolins, *Phys. Rev. B*, 2009, **79**, 184102.
30. K. J. Michel, A. R. Akbarzadeh and V. Ozolins, *J. Phys. Chem. C*, 2009, **113**, 14551-14558.
31. S. V. Alapati, J. K. Johnson and D. S. Sholl, *J. Phys. Chem. B*, 2006, **110**, 8769-8776.
32. E. Ronnebro and E. H. Majzoub, *J. Phys. Chem. B*, 2007, **111**, 12045-12047.

33. C. Kim, S.-J. Hwang, J. Robert C. Bowman, J. W. Reiter, J. A. Zan, J. G. Kulleck, H. Kabbour, E. H. Majzoub and V. Ozolins, *J. Phys. Chem. C*, 2009, **113**, 9956-9968.

CHAPTER 6

PREDICTING IMPURITY GASES AND PHASES DURING HYDROGEN EVOLUTION FROM COMPLEX METAL HYDRIDES

6.1 Introduction*

From Chapter 3 to Chapter 5, we have focused on the search for mixtures of materials whose reaction thermodynamics are more favorable than the individual reactants.[1] First-principles calculations have played a useful role in searching for mixtures with promising characteristics. These calculations can predict the free energy of metal hydride decomposition with a precision of approximately ±10 kJ/mol H_2, a precision that is high enough to make useful predictions in screening of materials.[1-13] The calculations in earlier chapters are based on the grand canonical linear programming methods that rigorously and efficiently determine the thermodynamic equilibrium state from a library of compounds with known energies.[1, 12-15] This approach has been used to examine enormous numbers of reactant mixtures with the aim of identifying mixtures that will reversibly store large amounts of H_2.[1, 6-15]

To date, the linear programming methods mentioned above have assumed that H_2 is the *only* gaseous species formed during heating of the reactant mixture. This assumption is reasonable when the aim of the calculation is to place an upper bound on the H_2 storage capacity of a mixture of interest. In practice, however, the evolution of gaseous species other than H_2 can have a decisive influence on the value of a complex hydride mixture. Fuel cell catalysts are extremely sensitive to poisoning by NH_3, so emission of even trace amounts of NH_3 will be problematic in fuel cell applications.[16, 17] Any reactant mixture containing B has potential to emit boranes or other toxic or reactive B-containing gases. Similarly, reaction mixtures containing C could form gaseous hydrocarbons. If produced in large quantities, any of these gases could

*The contents of this chapter have also appeared in < K. C. Kim, M. D. Allendorf, V. Stavila and D. S. Sholl, *Phys. Chem. Chem. Phys*, in press>.

consume reactants that would otherwise be treated as available for H_2 evolution in any calculation that considers only H_2 as a gaseous product.

In this chapter, we show how thermodynamic data from density functional theory (DFT) calculations can be combined with standard thermochemical methods to predict the evolution of non-H_2 gases from metal hydride mixtures. We consider a variety of hydrides and hydride mixtures that are either well characterized experimentally, are known to evolve gases other than H_2, and/or were identified by earlier theoretical calculations as potentially attractive destabilized systems.

The approach we describe in this chapter, in which the Gibbs free energy is minimized to obtain the composition of the system at thermodynamic equilibrium, adds an important capability to the suite of theoretical methods that can be applied to describe the properties of mixtures involving metal hydrides. Such calculations will be useful, for example, in focusing attention on reactant mixtures that are associated with low levels of gaseous impurities. In addition, the thermodynamic equilibrium approach will be valuable in elucidating the mechanisms by which metal hydrides react because it makes it possible to judge whether the impurity gases observed in experiments are the result of full thermodynamic equilibrium among the products, or in contrast, are in a nonequilibrium state due to the existence of kinetic barriers limiting the creation of one or more reaction products.

6.2 Computational Details

Thermodynamic calculations were performed using the FactSage program version 6.0, a free-energy minimization code designed to model complex multi-phase equilibria.[18, 19] Computations were performed assuming a fixed temperature and fixed total pressure. Thermodynamic data, in the form of heats of formation and entropies (both at 298 K) are required for each species that is included in the calculations, as well as a polynomial fit representing the species' heat capacity as a function of temperature. For gas-phase and liquid species data were obtained from the Fact 5.3 and Elements databases, which contain data from

the JANAF Thermochemical Tables.[20, 21] Data for the metal hydrides of interest, however, are largely unavailable in standard sources or in the databases included in the FactSage package. Consequently, these data were obtained from DFT calculations, as described below. Two exceptions to this description are MgH_2 and LiH, for which data in the JANAF Tables were used because DFT does not accurately predict the known energy of formation for these compounds. The complete set of species that were included in our thermodynamic calculations is listed in Table 6.1.

All DFT calculations were performed with the PW91 generalized gradient approximation (GGA) functional using the Vienna ab initio simulation package (VASP).[22-25] The core electrons of each atom were described by the projector augmented wave (PAW) method.[26] We used a conjugate gradient method for optimization of all materials. A cutoff energy of 425 eV was used in all calculations. Geometries were relaxed until the forces on all atoms were less than 0.03 eV $Å^{-1}$.

Our DFT calculations optimized the bulk crystal structure of each material of interest for supercells comprised of 1×1×1 unit cells of all solid compounds listed in Table 6.1 (except MgH_2). In general, the experimentally reported crystal structure was used as the starting point for these calculations.[27] The crystal structures of $Li_2B_{12}H_{12}$ and $MgB_{12}H_{12}$, which are possible intermediates in reactions involving $LiBH_4$ and $Mg(BH_4)_2$, were taken from the structures observed by Her *et al.*[28] and predicted by Ozolins *et al.*[7], respectively. A Monkhorst-Pack mesh of 8×8×8 *k*-points was used for almost all compounds. For a few systems having large unit cells, we used smaller number of *k*-points. Based on the optimized structures, we computed the Vibrational Density of States (VDOS) calculations of all solid compounds using the PHONON code developed by Parlinski.[29] The enthalpy of formation, entropy, and heat capacity of each solid compound was then defined using the DFT total energies and VDOS.[30] We fitted the heat capacity of each solid compound using

$$H = aT^3 + bT^2 + cT + d \qquad (6.1)$$

Here H is the heat capacity, T is the temperature in K, and a, b, c, and d are fitting parameters. The complete thermodynamic data set, in the form of polynomial coefficients suitable for use in FactSage, are reported in Table 6.2.

Table 6.1: The gaseous, liquid, and solid species considered in our thermodynamic calculations using FactSage.

Gaseous species				
N-containing gases				
N	N_2	N_3	NH	NH_2
NH_3	N_2H_4	HNNH	HCN	LiN
MgN	CN	C_2N	CNN	$(CN)_2$
C_4N_2	CH_3NH_2	CH_3NC	C_2H_5N	$(CH_3)_2NH$
$CH_3N_2H_3$	$(CH_3)_2N_2H_2$			
C-containing gases				
C	C_2	C_3	C_4	C_5
CH	CH_2	CH_3	CH_4	C_2H
C_2H_2	C_2H_3	C_2H_4	C_2H_5	C_2H_6
C_3H_6	C_3H_8	C_4H_2	C_4H_{10}	C_5H_{10}
C_5H_{12}	C_6H_6			
B-containing gases				
B	B_2	BH	BH_2	BH_3
BH_4	BH_5	B_2H	B_2H_2	B_2H_3
B_2H_4	B_2H_5	B_2H_6	B_3H_7	B_3H_9
B_4H_4	B_4H_{10}	B_4H_{12}	B_5H_9	B_5H_{11}
B_6H_{10}	B_8H_{12}	B_9H_{15}	$B_{10}H_{14}$	BN
BC	$B_3H_6N_3$			
Other gases				
H	H_2	Li	Li_2	LiH
Mg	Mg_2	MgH	Ar	
Liquid species				
N-containing liquids				
N_2H_4	HN_3	CH_3NH_2	CH_3NC	$(CH_3)_2NH$
$CH_3N_2H_3$	$(CH_3)_2N_2H_2$			
B-containing liquids				
B	B_5H_9	$B_{10}H_{14}$	$B_3H_6N_3$	B_4C
Other liquids				
Mg	Li	LiH		
Solid species				
N-containing solids				
$LiNH_2$	Li_2NH	Li_2CN_2	Li_3N	Mg_3N_2
NH_4N_3	$C_2N_4H_4$			
C-containing solids				
C	Li_2C_2	MgC_2	Mg_2C_3	
B-containing solids				
B	$LiBH_4$	LiBC	$Mg(BH_4)_2$	MgB_2C_2
MgB_9N	MgB_2	MgB_4	$MgB_{12}H_{12}$	$Mg(B_6)_2$
BN	B_4C	$B_{10}H_{14}$	$Li_2B_{12}H_{12}$	
Other solids				
Li	Mg	LiH	MgH_2	

Table 6.2: The coefficients of Eq. (6.1) for each compound considered.

Compound		*a*	*b*	*c*	*d*
$LiBH_4$	Orthorhombic	3.636541×10^{-7}	-7.11204×10^{-4}	0.4462118	-8.95918
	Hexagonal	-2×10^{-8}	2×10^{-9}	0.091519	34
MgH_2	$T \leq 300$ K	-8.302866×10^{-7}	2.416685×10^{-4}	0.123194	-1.885627
	300 K $\leq T$	4.911733×10^{-8}	-1.531973×10^{-4}	0.1752424	-4.697331
LiH	$T \leq 300$ K	-1.712594×10^{-6}	8.053210×10^{-4}	2.885563×10^{-3}	-0.5188577
	300 K $\leq T$	5.986921×10^{-8}	-1.595036×10^{-4}	0.1508835	-4.673983
MgB_2	$T \leq 300$ K	-3.543290×10^{-6}	1.642266×10^{-3}	-1.440233×10^{-2}	-0.6620203
	300 K $\leq T$	9.609885×10^{-8}	-2.434423×10^{-4}	0.2147273	4.50789
$LiNH_2$	$T \leq 300$ K	-2.837013×10^{-6}	1.124962×10^{-3}	7.291100×10^{-2}	-1.100816
	300 K $\leq T$	5.888579×10^{-8}	-1.466699×10^{-4}	0.1393837	17.52205
Li_2NH	$T \leq 300$ K	-4.063113×10^{-6}	1.655448×10^{-3}	7.932981×10^{-2}	-1.63127
	300 K $\leq T$	9.426549×10^{-8}	-2.316938×10^{-4}	0.2016655	22.55682
LiBC	$T \leq 300$ K	-3.004132×10^{-6}	1.518113×10^{-3}	-5.469920×10^{-2}	0.10208
	300 K $\leq T$	9.171260×10^{-8}	-2.441465×10^{-4}	0.2309884	-8.896635
MgB_4	$T \leq 300$ K	-2.352285×10^{-6}	1.164151×10^{-3}	6.345771×10^{-2}	-0. 9585945
	300 K $\leq T$	1.352889×10^{-7}	-3.590979×10^{-4}	0.3383136	-12.02963
BN	$T \leq 300$ K	-2.450190×10^{-7}	3.516906×10^{-4}	-2.781613×10^{-2}	0.3744896
	300 K $\leq T$	6.755135×10^{-8}	-1.901316×10^{-4}	0.1925282	-25.78044
$Mg(BH_4)_2$	$T \leq 300$ K	-4.379487×10^{-7}	-4.664635×10^{-4}	0.5317298	-4.475003
	300 K $\leq T$	3.772146×10^{-8}	-1.781348×10^{-4}	0.3227687	21.49815
MgB_9N	$T \leq 300$ K	-3.528169×10^{-6}	2.060964×10^{-3}	0.1392271	-1.419138
	300 K $\leq T$	3.359269×10^{-7}	-9.054726×10^{-4}	0.8699687	-56.54753
B	$T \leq 500$ K	-7.4354698×10^{-8}	1.164462×10^{-6}	0.06480096	-5.2
	500 K $\leq T$	-1.0546979×10^{-9}	2.764462×10^{-6}	0.00970096	13.8
Li_2CN_2	$T \leq 300$ K	-4.706116×10^{-6}	1.815788×10^{-3}	0.1500075	-2.596693
	300 K $\leq T$	9.866718×10^{-8}	-2.588153×10^{-4}	0.2464586	29.49204
Li_2C_2	$T \leq 300$ K	-5.873775×10^{-6}	2.170881×10^{-3}	0.1236201	-3.188169
	300 K $\leq T$	6.431751×10^{-8}	-1.647615×10^{-4}	0.1518167	43.7241
$Mg(NH_2)_2$	$T \leq 300$ K	-3.500502×10^{-6}	1.410608×10^{-3}	0.1093911	-1.739497
	300 K $\leq T$	8.929321×10^{-8}	-2.264943×10^{-4}	0.2267766	16.32941
MgB_2C_2	$T \leq 300$ K	-2.863707×10^{-6}	1.321984×10^{-3}	7.442171×10^{-2}	-1.751908
	300 K $\leq T$	1.328548×10^{-7}	-3.663483×10^{-4}	0.36284	-15.06061
$MgB_{12}H_{12}$	$T \leq 500$ K	5.261138×10^{-7}	-1.733499×10^{-3}	1.695737	-96.93459
	500 K $\leq T$	2.663488×10^{-7}	-8.230325×10^{-4}	0.9874182	63.06564
$Li_2B_{12}H_{12}$	300 K $\leq T$	6.465948×10^{-7}	-1.755604×10^{-3}	1.778746	-148.3633

6.3 Pressure Dependence on Reaction Thermodynamics

For each hydride considered in this investigation, we performed calculations at constant pressure for three different total pressures: 1, 10, and 100 atm. In all examples except one ($Mg(BH_4)_2$), the same overall reaction mechanism is observed at each pressure and the primary effect of changing the pressure is to shift the temperature at which the reactions of interest occur. By considering the factors that dictate the temperature of these reactions, it is possible to display

the results for multiple total pressures on a single plot. To do this we write the Gibbs' free energy change for a reaction as:

$$\Delta G \approx \left[\Delta U_0 + \Delta U_{vib} + P\Delta V\right] - T\left[\Delta S - \alpha\right] \qquad (6.2)$$

Here ΔU_0 and ΔU_{vib} are the DFT total energy change and contributions from the VDOS of the reaction, ΔS is the entropic change of the reaction, ΔV is the volumetric change associated with solid materials of the reaction, and α indicates the fact that the rotational and translational energies and the PV contribution associated with the gaseous phase of the reaction are proportional to T. Equation (6.2) is approximate because ΔU_{vib} and ΔS are not perfectly independent of T; this fact is incorporated into our detailed calculations but is not critical for the scaling analysis described below. We are typically interested in determining the transition temperature for which this free energy change is zero for a specified total pressure. The dependence of this transition temperature is shown schematically in Fig. 6.1(a), where it can be seen that higher pressures yield higher transition temperatures.

The data in Fig. 6.1(a) can be replotted so that the results for all three pressures meet at one point when $\Delta G = 0$, by rewriting Eq. (6.2) as

$$\Delta G \approx \left[\Delta U_0 + \Delta U_{vib} + P\Delta V\right] - \left(P^a\left(\Delta S - \alpha\right)\right)\frac{T}{P^a} \qquad (6.3)$$

Here a is the coefficient that collapses the three lines to a single point when $\Delta G = 0$. This scaling coefficient is different for each reaction that is considered. In some of the examples presented below, we use this scaling (and report the resulting scaling coefficient) to show results from multiple total pressures on a single figure.

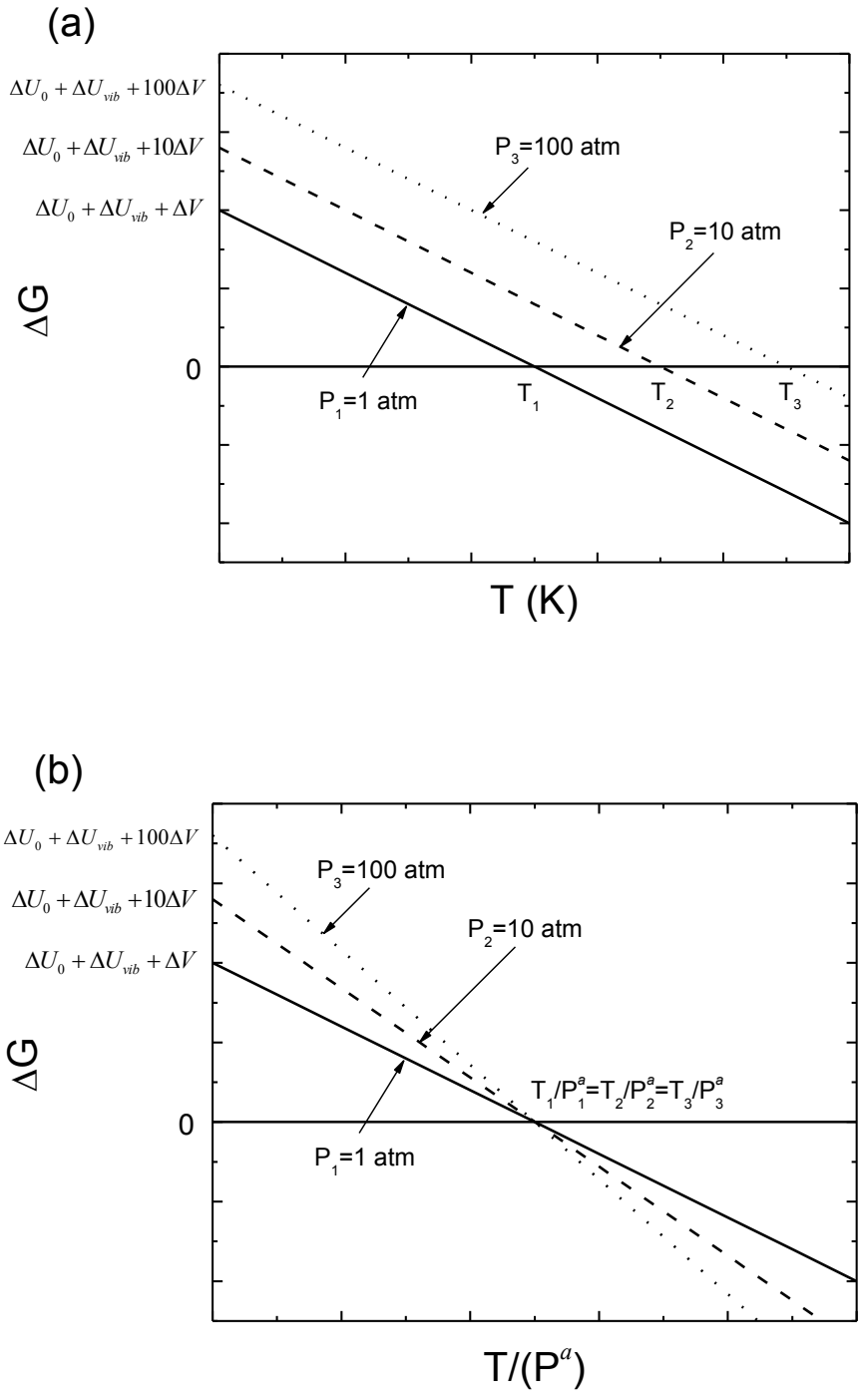

Figure 6.1: A schematic illustration of the Gibbs' free energy changes of a reaction (a) at three different total pressures as a function of temperature, and (b) replotted to collapse the transition temperature for each pressure to a single point.

6.4 Reaction Thermodynamics of $LiNH_2$ and $LiNH_2$ + LiH

We first illustrate our approach by modeling $LiNH_2$, the decomposition of which has been thoroughly investigated.[31-45] Recent experiments demonstrate that pure $LiNH_2$ decomposes to form Li_2NH with evolution of NH_3, while a 1:1 mixture of $LiNH_2$ and LiH produces Li_2NH without evolution of any gases other than H_2.[31-45] Yao *et al.* reported an onset of decomposition for pure $LiNH_2$ at ~ 573 K and 1 atm, using thermogravimetry (TG), differential scanning calorimetry (DSC), and mass spectrometry (MS) to monitor the composition of the gas phase.[31] At 653 K the sample melts, leading to additional release of NH_3. These authors also examined the reaction of $LiNH_2$ and LiH and proposed a mechanism in which LiH exothermically captures NH_3 evolved by the decomposition of $LiNH_2$, forming Li_2NH.

In this hydride system, as well as in the others discussed in this chapter, we computed the equilibrium composition for fixed temperatures in the range 300 - 1000 K and fixed total pressures of 1, 10, and 100 atm. The initial composition was either 1 mol of $LiNH_2$ or 1 mol $LiNH_2$ + 1 mol LiH. The resulting mixture of gas, liquid, and solid phases as a combined function of temperature and pressure is shown in Fig. 6.2. The calculated transition temperature for each system as the pressure is varied from 1 atm to 150 atm using FactSage is shown in Fig. 6.3. The most important reaction for each of the seven systems in Fig 6.3 is shown in Table 6.3. All species containing any combination of Li, N, and H that are listed in Table 6.1 were included in these calculations.

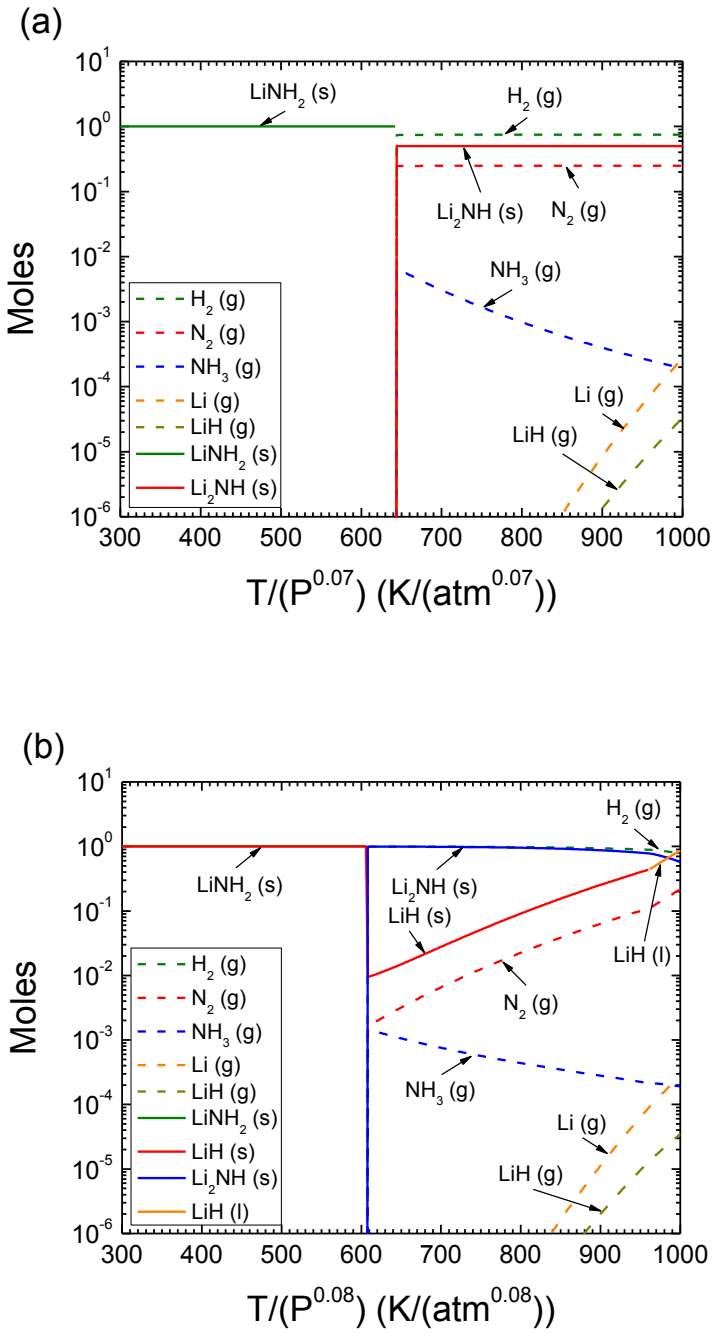

Figure 6.2: Predicted equilibrium composition (moles) of the gaseous and condensed-phase species corresponding to (a) 1 mole $LiNH_2$ and (b) $LiNH_2$ + LiH. For clarity, results are only shown for a total pressure of 1 atm.

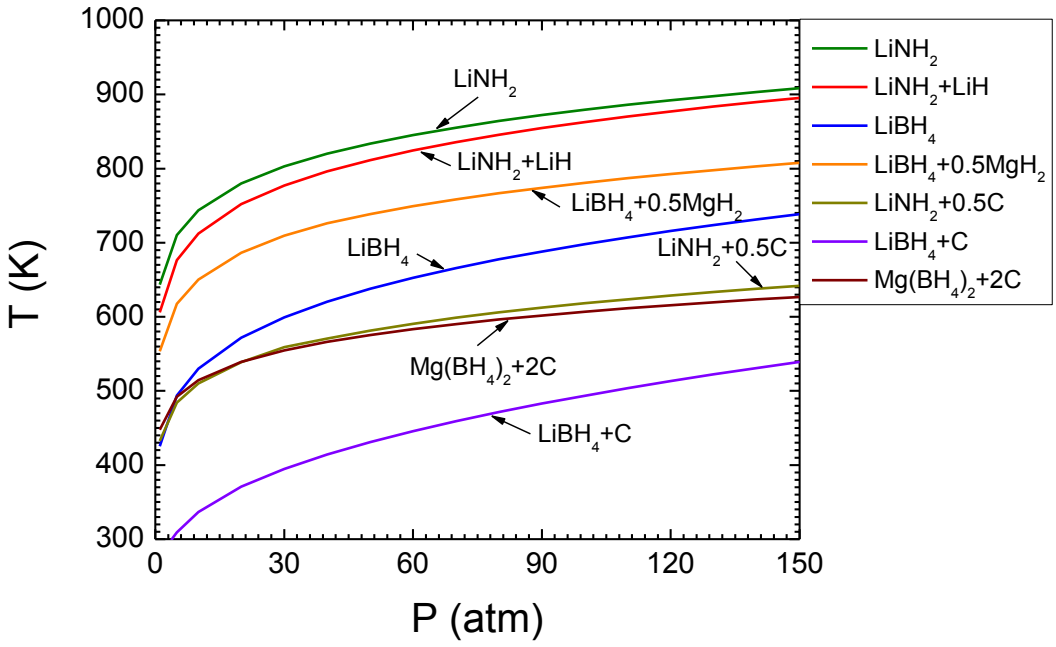

Figure 6.3: The calculated reaction temperatures of seven systems as a function of total pressure.

Table 6.3: The single step reactions considered in Fig. 6.3.

System	Nominal reaction
$LiNH_2$	$LiNH_2 \rightarrow \frac{1}{2}Li_2NH+\frac{1}{4}N_2+\frac{3}{4}H_2$
($LiNH_2$ + LiH)	$LiNH_2+LiH \rightarrow Li_2NH+H_2$
$LiBH_4$	$LiBH_4 \rightarrow \frac{5}{6}LiH+\frac{1}{12}Li_2B_{12}H_{12}+\frac{13}{12}H_2$
($LiBH_4$ + MgH_2)	$Li_2B_{12}H_{12}+6MgH_2 \rightarrow 2LiH+6MgB_2+11H_2$
($LiNH_2$ + C)	$LiNH_2+\frac{1}{2}CH_4 \rightarrow \frac{1}{2}Li_2CN_2+2H_2$
($LiBH_4$ + C)	$10LiH+Li_2B_{12}H_{12}+12CH_4 \rightarrow 12LiBC+35H_2$
($Mg(BH_4)_2$ + C)	$\frac{9}{4}MgB_2C_2+5MgH_2+MgB_{12}H_{12} \rightarrow \frac{33}{4}MgB_2+\frac{9}{2}CH_4+2H_2$

For pure $LiNH_2$, the calculations (Fig. 6.2(a)) predict that $LiNH_2$ decomposes to form

Li_2NH, with a phase change predicted at 644 K (1 atm) that shifts to higher temperatures as the pressure increases. This behavior is in agreement with the experimental literature.[31, 38, 41] The reaction produces N_2 and H_2 in the gas phase in a 1:3 ratio, with minor amounts (mole fraction ≤ 0.007) of NH_3 also forming. The same result is predicted by our calculations at higher total pressures. This disagrees with the experimental result, where the primary gas evolved is NH_3, with smaller amounts of H_2 and N_2 also forming.[31, 38, 41] To determine the reason for the predominance of N_2 over NH_3 predicted by our model, we examined the thermodynamic equilibrium for mixtures of N_2, H_2, and NH_3 (with no other species present). As seen in Fig. 6.4, at temperatures > 450 K a mixture of N_2 and H_2 is thermodynamically more stable than NH_3. For example, the molar ratio of N_2 to NH_3 predicted at the $LiNH_2$ decomposition temperature is 37.4, 14.1, and 5.6 at 644 K (1 atm), 744 K (10 atm), and 880 K (100 atm), which is the same value as that predicted for the $N_2/H_2/NH_3$ equilibrium. This analysis strongly suggests that the experimentally observed production of NH_3 during decomposition of $LiNH_2$ is the result of a kinetic barrier to the formation of N_2.

To further test this hypothesis we recomputed the $LiNH_2$ equilibrium excluding N_2 from the calculation. The results from these calculations, which are shown in Fig. 6.5, simulate the existence of an infinite kinetic barrier to N_2 formation. As seen in Fig. 6.5, NH_3 is the dominant gas phase product in this limit, with minor amounts (mole fraction ≤ 0.001) of H_2 also forming. This brings the calculations into qualitative agreement with the experimental results of Yao *et al.*[31] and indirectly supports the hypothesis that formation of N_2 is kinetically limited. However, the decomposition temperature in this limit shifts upward by 170 K to 815 K, a value much higher than the observations of Yao *et al.*. In the experiments conducted by Yao *et al.*, melting of $LiNH_2$ was observed at 653 K, followed by a strong increase in NH_3 production at higher temperatures. Our calculations did not include the formation of liquid-phase $LiNH_2$, because we do not have adequate thermodynamic data for this state. Recall that when N_2 is included in our calculation the decomposition temperature is much closer to the experimental value. This outcome suggests that reaction kinetics determine the product channel in this process without

affecting the thermodynamic stability of $LiNH_2$.

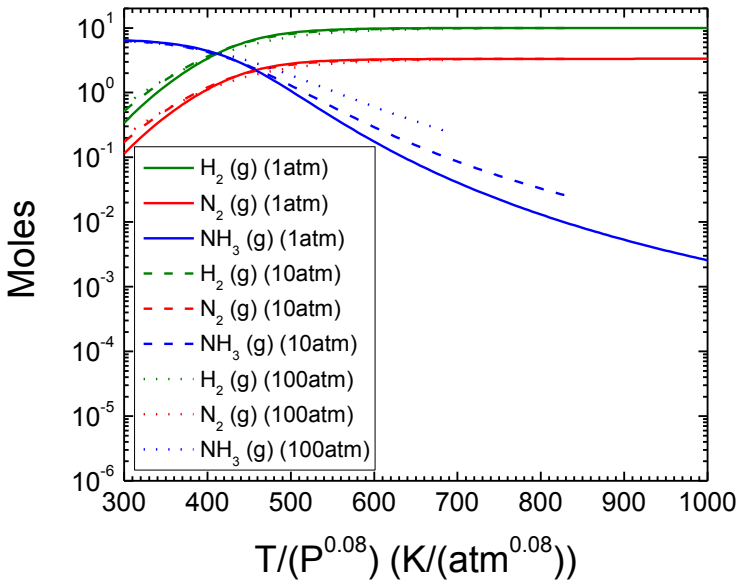

Figure 6.4: The gas phase equilibria of the $N_2/H_2/NH_3$ mixture (gases alone) at a combined function of temperature and pressure, using an input composition of 6.67 moles NH_3. The plots represent three cases of 1, 10, and 100 atm.

The results of our calculations for $LiNH_2$ + LiH are shown in Fig. 6.2(b) and they agree well with experimental observations. In particular, they indicate that $LiNH_2$ reacts with LiH to form Li_2NH and H_2.[31, 32, 36, 38, 40-42] A phase change is predicted at 608 K (1 atm), which shifts to higher temperatures as the pressure increases. Experimentally, this phase change is observed at ~560 K, below the melting point of $LiNH_2$.[31, 32, 36, 38, 41] Our model does not predict significant amounts of gas-phase species other than H_2 (NH_3 and N_2 mole fraction ≤ 0.001), consistent with experimental observations made with MS.[31, 32, 36, 38, 41] Interestingly, at 1 atm and ~980 K, slightly above the melting point of LiH, Li_2NH becomes unstable relative to H_2, N_2, and LiH, a process that has not been observed experimentally[31, 32, 36, 38, 41]. This prediction again suggests that a significant kinetic barrier to N_2 formation exists. Overall, the thermodynamic equilibrium

of the $LiNH_2$ + LiH system can be described by the following scheme:

$$LiNH_2(s) \rightarrow \frac{1}{2}Li_2NH(s) + \frac{1}{4}N_2(g) + \frac{3}{4}H_2(g) \quad (6.4)$$

$$\frac{1}{4}N_2(g) + \frac{3}{4}H_2(g) + LiH(s) \rightarrow \frac{1}{2}Li_2NH(s) + H_2(g) \quad (6.5)$$

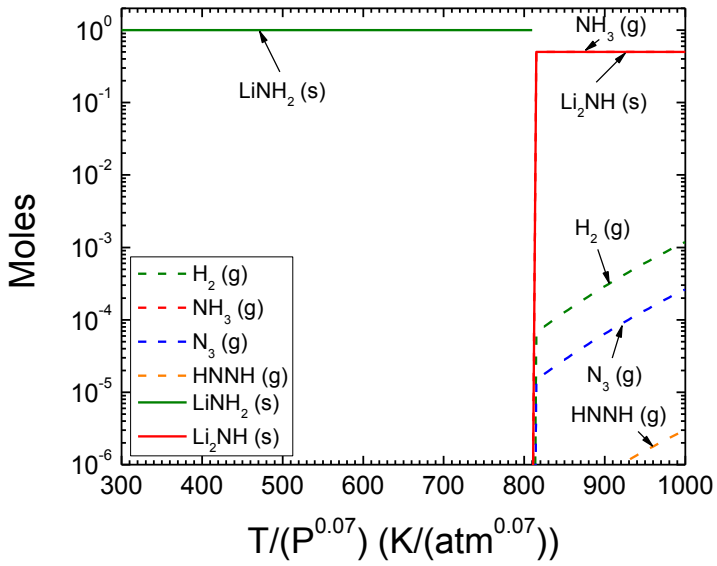

Figure 6.5: The moles of the gaseous and solid/liquid species of $LiNH_2$ decomposition reaction when excluding N_2 from our database. This figure is represented into a combined function of temperature and pressure (1 atm).

6.5 Reaction Thermodynamics of $LiBH_4$ and $LiBH_4 + MgH_2$

We now discuss $LiBH_4$, another well-known complex hydride that has been experimentally investigated due to its high H_2 capacity.[46-52] Several destabilization approaches have been proposed for mixtures involving $LiBH_4$.[47-49, 51, 52] In this section, we consider $LiBH_4$ destabilization by MgH_2, a well-studied reaction.[47] In a separate section below we discuss destabilization of $LiBH_4$ by the addition of carbon. As before, we computed the equilibrium

composition of each system of interest for temperatures of 300 – 1000 K and fixed total pressures of 1, 10, and 100 atm. The initial composition was either 1 mol of $LiBH_4$ or ($LiBH_4$ + $0.5MgH_2$).

According to the available experimental data on pure $LiBH_4$ and $LiBH_4$ + $0.5MgH_2$ mixtures, no gases other than H_2 evolve upon heating.[46, 47] In the absence of any additives, most investigators report that $LiBH_4$ decomposition produces LiH and B, along with H_2.[47-49, 52-54] Recently, there have been reports suggesting that $Li_2B_{12}H_{12}$ is also formed as an intermediate during the decomposition reaction.[7, 28, 55-59] This assertion relies on experimental data[57-59] indicating that the observed intermediates have vibrational or NMR spectra close to those of $[B_{12}H_{12}]^{2-}$ species. In the case of $LiBH_4$ + $0.5MgH_2$, Vajo *et al.* experimentally observed that this reaction produces LiH and MgB_2 without formation of any intermediates.[47] In their study, mass spectrometric analysis of the desorbed gas using a residual gas analyzer (RGA) detected only H_2.

Our computed equilibrium compositions for pure $LiBH_4$ are shown in Fig. 6.6(a). They predict that $LiBH_4$ decomposes to form LiH, $Li_2B_{12}H_{12}$, and H_2 via an overall reaction that can be written as:

$$\mathrm{LiBH_4(s)} \rightarrow \frac{5}{6}\mathrm{LiH(s)} + \frac{1}{12}\mathrm{Li_2B_{12}H_{12}(s)} + \frac{13}{12}\mathrm{H_2(g)} \qquad (6.6)$$

The decomposition reaction is predicted to occur at 426 K (1 atm), shifting to higher temperatures as the total pressure increases. At higher temperature (~952 K at 1 atm), $Li_2B_{12}H_{12}$ decomposes to form LiH, B, and H_2 by

$$\mathrm{Li_2B_{12}H_{12}(s)} \rightarrow 2\mathrm{LiH(l)} + 12\mathrm{B(s)} + 5\mathrm{H_2(g)} \qquad (6.7)$$

These transition temperatures agree with the computational predictions by Ozolins *et al.* from calculations that only considered H_2 as a potential gas phase product.[7] Our calculations did not include liquid $LiBH_4$, but the first predicted phase change at P = 1 atm occurs well below the experimentally observed melting point of $LiBH_4$ (560 K). This indicates that including the liquid species in our calculations should not alter the decomposition pathway.

A key prediction of our calculations is that no gases other than H_2 evolve during $LiBH_4$

decomposition except for small amounts of LiH, Li, Li_2, and BH_3 (mole fraction $\leq 4 \times 10^{-4}$). These species are only observed for temperatures > 400 K higher than the transition temperature for the first reaction step above. This implies that accumulation of these gases by repeated dehydrogenation-rehydrogenation reaction cycles should be negligible.

The decomposition process for $LiBH_4$ described in Eqs. (6.6) and (6.7) differs from the mechanism deduced from a number of experiments[47, 49, 52, 54] and examined in earlier theoretical calculations,[2, 3, 5, 6] which employs a single-step decomposition of $LiBH_4$ into a mixture of LiH, B, and H_2.[1] Recent NMR experiments by Hwang *et al.*[60], however, support the idea that $Li_2B_{12}H_{12}$ appears as a decomposition product of $LiBH_4$, although the experimental evidence indicates that this species is amorphous rather than crystalline.[1]

It is interesting to note that $LiBH_4$ incorporated into nanoporous carbon scaffolds decomposes at a considerably lower temperature than a hydride film deposited on a graphite surface.[61] Gross *et al.* found that this temperature decrease is associated with a substantial drop in the activation energy for hydrogen desorption. In addition, these investigators suggest that interactions of the confined particles with the pore walls of the scaffold contribute to improved desorption kinetics by changing the free energy of the decomposition reaction.[61] The results of Gross *et al.* and our predicted decomposition pathways suggest that changes in both the thermodynamics and kinetics of decomposition occur when $LiBH_4$ is confined within nanopores. Gross *et al.* found that confined $LiBH_4$ decomposes in a single step described by $LiBH_4 \rightarrow LiH + B + 1.5H_2$, with no evidence for $Li_2B_{12}H_{12}$ found in NMR. This indicates that either the thermodynamic stability of $Li_2B_{12}H_{12}$ is dramatically reduced by nanoconfinement or an alternative kinetic pathway is activated that bypasses its formation. The latter possibility is supported by experiments and calculations indicating that interactions with fullerene and carbon nanotube surfaces can weaken the Al-H bonds in $NaAlH_4$, leading to faster H_2 desorption kinetics.[62]

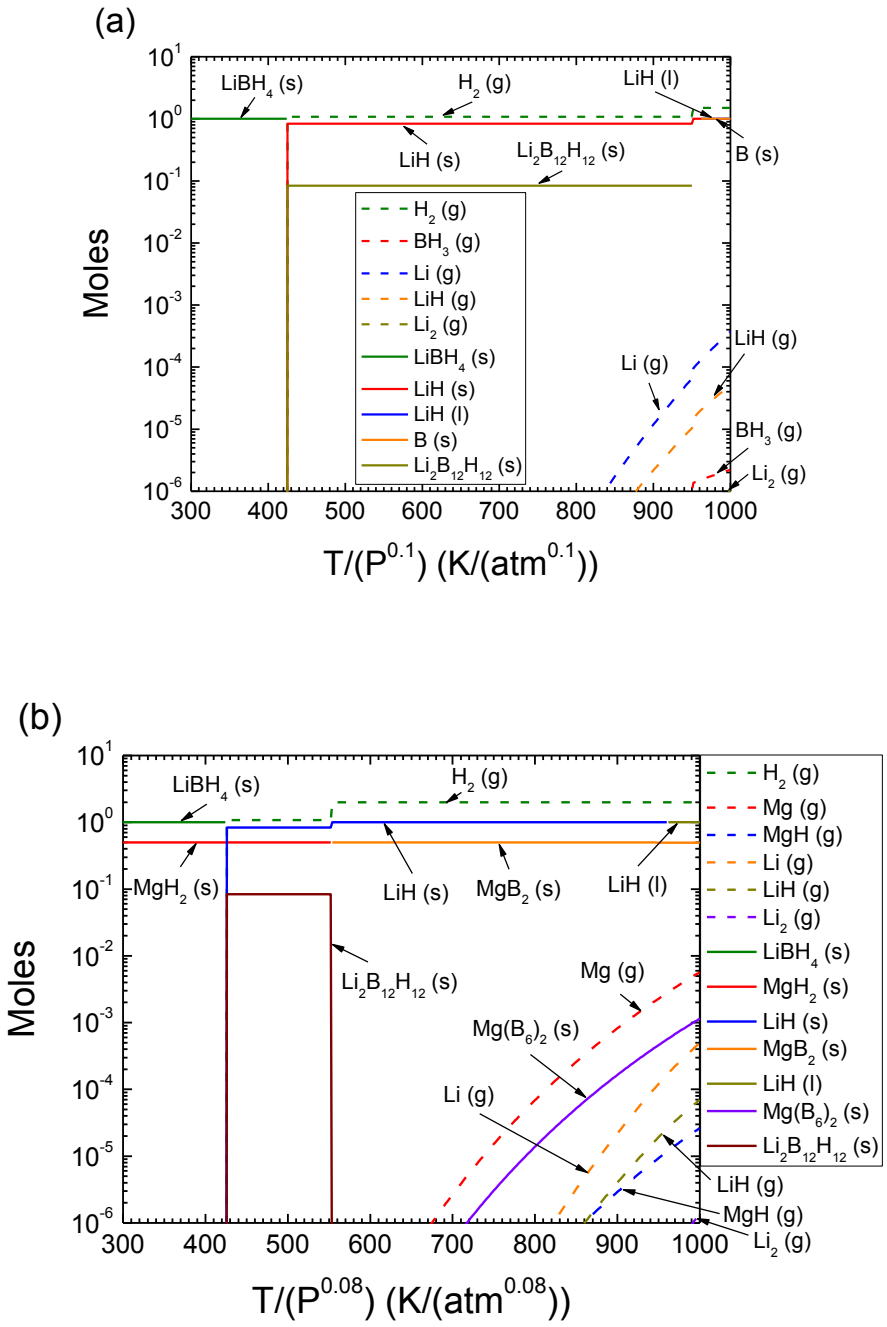

Figure 6.6: Predicted equilibrium composition (moles) of the gaseous and condensed-phase species corresponding to (a) 1 mole $LiBH_4$ and (b) $LiBH_4$ + 0.5MgH_2. For clarity, results are shown for the situation of a fixed total pressure of 1 atm.

Another feature of the $LiBH_4$ system is that although $LiBH_4$ contains boron, a potential

source of boranes, no significant amounts of impurity gases evolve, in agreement with the experimental observations.[46, 47] This is due to the relative thermodynamic stability between the mixture of solid B, gaseous H_2, and boranes. Boranes have a positive formation energy, as seen from the values of BH_3 (106.7 kJ/mol at 298.15 K) and B_2H_6 (41 kJ/mol at 298.15 K),[63] indicating that these compounds are unstable relative to their elements. Therefore, boranes should not evolve during $LiBH_4$ decomposition. The agreement between experiment and theory in this case indicates that the formation of solid boron and H_2 is not impeded by large kinetic barriers.

When MgH_2 and $LiBH_4$ are mixed in a 1:2 ratio, the lowest temperature reaction predicted by our calculations is identical to Eq. (6.6). That is, the presence of MgH_2 has no effect on this reaction. At a pressure of 1 atm, however, the $Li_2B_{12}H_{12}$ produced by this reaction becomes unstable at 554 K, resulting in more complete dehydrogenation than in the absence of MgH_2. The resulting mixture of gas, liquid, and solid phases is shown in Fig. 6.6(b). At 554 K and 1 atm, $Li_2B_{12}H_{12}$ is predicted to react with MgH_2 to form LiH, MgB_2, and H_2 with a phase change described by the overall reaction:

$$Li_2B_{12}H_{12}(s)+6MgH_2(s)\rightarrow 2LiH(s)+6MgB_2(s)+11H_2(g) \qquad (6.8)$$

This reaction is the only example we encountered for which changing the total pressure alters the reaction mechanism. At the highest pressure we considered (100 atm), MgH_2 decomposes at 782 K, so the reaction above is replaced by a reaction in which $Li_2B_{12}H_{12}$ reacts with Mg to form LiH and MgB_2 at higher temperature (800 K). The multi-step reaction path at 1 atm pressure and the related transition temperatures are in agreement with the computational predictions by Ozolins *et al*.[7] Liquid-phase MgH_2 is not included in our modeling, but this should have little effect since the dehydrogenation reactions occur at a temperature below the melting point of MgH_2.[47] Our thermodynamic analysis does not predict formation of $MgB_{12}H_{12}$. This is in agreement with experimental observations.[47] Similar to the system containing only $LiBH_4$, the mixture of MgH_2 and $LiBH_4$, generates almost no gases other than H_2 except at temperatures high enough that

trace amounts of gaseous Mg, Li, LiH, and similar species exist.

The behavior of 1:2 mixtures of MgH_2 and $LiBH_4$ as a function of H_2 pressure have been examined experimentally by Pinkerton *et al.*[64] In these experiments, formation of MgB_2 as a product of dehydrogenation was only observed in experiments where the H_2 pressure exceeded a few bar. In experiments performed at reduced pressure, decomposition of $LiBH_4$ to form LiH was observed without formation of MgB_2. Pinkerton *et al.* concluded that a H_2 pressure > 3 bar is necessary to suppress direct decomposition of $LiBH_4$ so that destabilization by MgH_2 can occur. Our results, and those of Ozolins *et al.*[7], support a rather different view of this reaction: at thermodynamic equilibrium and at all H_2 pressures, $LiBH_4$ undergoes direct decomposition to form $Li_2B_{12}H_{12}$ at a temperature lower than that at which any of the boron in this system can react with MgH_2 to form MgB_2. This implies that the variations in reaction mechanism observed by Pinkerton *et al.* originate from kinetic limitations, not thermodynamics. This conclusion was anticipated by Pinkerton *et al.*, who state that the phase diagram developed from their experiments reflects both thermodynamic and kinetic boundaries.

6.6 Evolution of CH_4 in Reactions involving C

We now turn to the reaction thermodynamics of several systems that involve carbon. There are two related motivations to consider examples of this kind. First, the calculations of Alapati *et al.* identified a number of systems in which elemental carbon was predicted to destabilize metal hydrides to yield reactions with favorable thermodynamics and high H_2 capacity.[6] These calculations predicted, for example, that C destabilizes $LiNH_2$, $LiBH_4$, and $Mg(BH_4)_2$. As highlighted earlier, however, these calculations assumed that the only gas-phase product was H_2. This is obviously problematic given that many gaseous hydrocarbons are very stable. One objective of the calculations below is to understand what role these hydrocarbons play in mixtures of metal hydrides with elemental carbon.

A second motivation is that a number of recent studies explored confinement of metal hydrides inside porous carbons.[61, 65-67] These experiments provide examples of improved reaction

kinetics and cycling capacity relative to experiments with bulk samples of the same metal hydrides. In general, the results are interpreted by viewing the porous carbon as an inert scaffold that does not participate in any way in the chemical reactions that occur, although Berseth *et al.* conclude based on a combination of experiments and theory that carbon nanomaterials can serve as catalysts for hydride decomposition.[62] The reactions predicted by Alapati *et al.* involving combinations of metal hydrides and C and the reaction mechanisms we examine below, however, raise the possibility that under true equilibrium conditions it may not be possible to view the scaffold in this way.

We first discuss the 1:2 mixture of $LiNH_2$ and C; results of our equilibrium calculations are shown in Fig. 6.7(a). In calculations that included only H_2 as a possible gaseous species, Alapati *et al.* predicted this mixture would react as follows[6]: $LiNH_2 + 0.5\ C \rightarrow 0.5\ Li_2CN_2 + H_2$. It is immediately clear from Fig. 6.7(a) that this prediction is incorrect; at 300 K, approximately equal amounts of H_2 and CH_4 are present when the system is in equilibrium. If the temperature of the mixture is increased without loss of gases from the system, the CH_4 that is stable at 300 K is replaced by H_2 and solid Li_2CN_2. At a pressure of 1 atm, the equilibrium mixture includes only small amounts of CH_4 at 350 K, while at temperatures above 430 K, the CH_4 mole fraction is less than 10 ppm. Minor amounts of other gases such as N_2, NH_3, Li, and LiH (mole fraction $\leq 1 \times 10^{-4}$) are present at much higher temperatures.

The results in Fig. 6.7(a) demonstrate that a large reduction in the temperature at which H_2 evolves during hearing can be achieved through the addition of C (Fig. 6.2(a)). The fact that the low temperature state of the system involves all of a critical reactant in the process (C) being in a gaseous state, however, could pose a significant challenge to designing a process that actually uses this mixture. If gaseous CH_4 was released at any point during use of this system, carbon would be irreversibly lost and the reaction thermodynamics at all later times would be different than the results from Fig. 6.7(a). Aside from the loss of reactant, the presence of CH_4 in any H_2 delivered from a system of this kind could potentially create problems associated with coking of anodes in fuel cells.

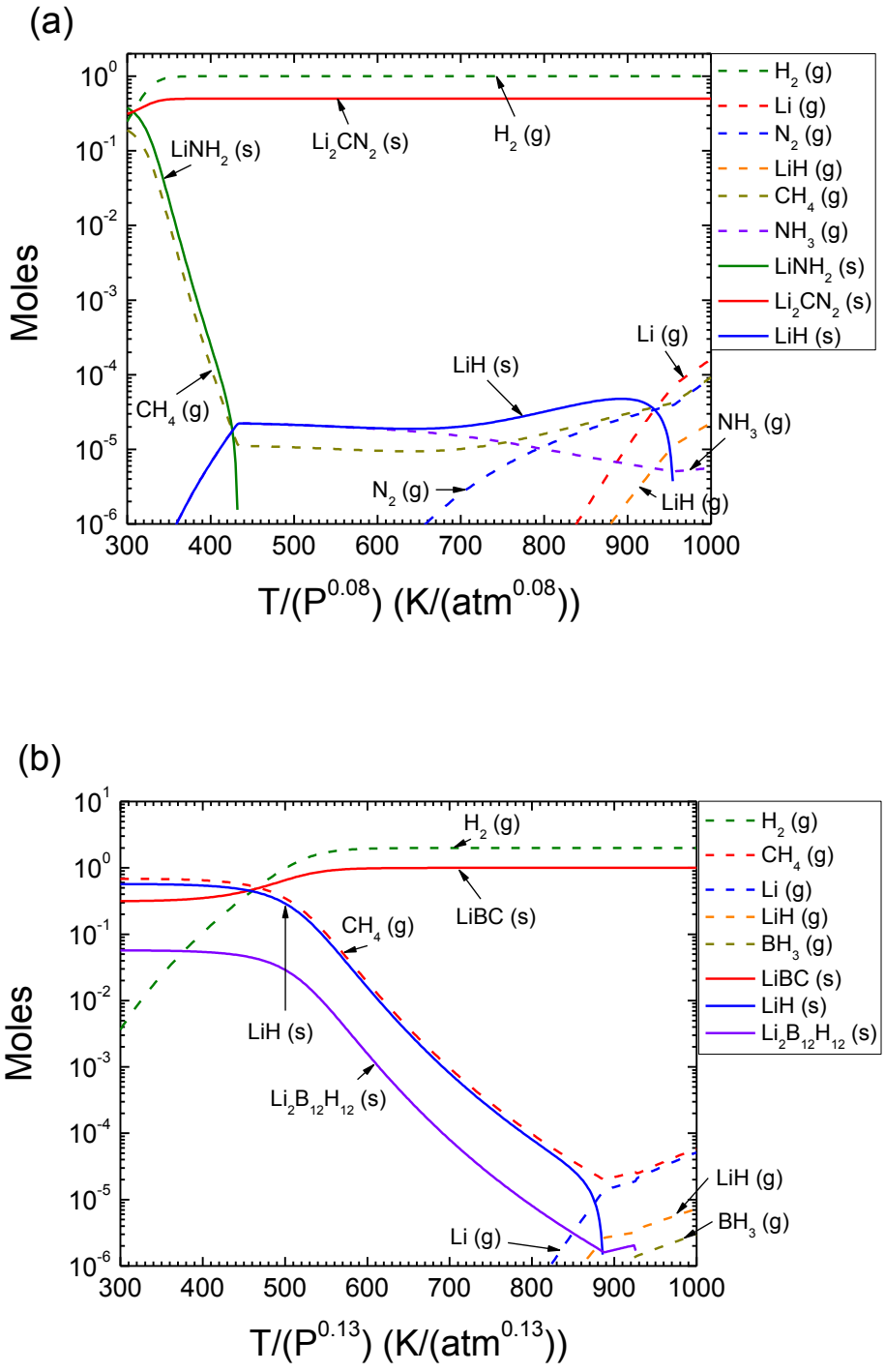

Figure 6.7: Predicted equilibrium composition (moles) of the gaseous and condensed-phase species corresponding to $LiNH_2$ + 0.5C (a) and $LiBH_4$ + C (b). Results are displayed as a combined function of temperature and pressure (for clarity, we only show the case of 1 atm).

The equilibrium behavior for a 1:1 mixture of $LiBH_4$ and C is shown in Fig. 6.7(b), and in many respects it is similar to the $LiNH_2$/C mixture. At 300 K and 1 atm, essentially all of the C in the system is in the form of CH_4. An interesting aspect of this example is that $LiBH_4$ is not seen at equilibrium under any of the conditions we examined. At 300 K, the dominant solids are LiH and a smaller amount of LiBC, while at elevated temperatures LiBC is essentially the only remaining solid. Only very small amounts of $Li_2B_{12}H_{12}$ exist. Reasonably high levels of CH_4 are present at equilibrium over a wider temperature range than was seen with $LiNH_2$/C; at a pressure of 1 atm the mole fraction of CH_4 is > 0.01 for all temperatures below 630 K. No gases other than CH_4 and H_2 are seen for this mixture at anything above trace levels.

It is possible, indeed, likely, that kinetic barriers limit the formation or conversion of CH_4 when metal hydrides are mixed with carbon. We note in this context that Gross *et al.* detected small amounts of methane (<0.2 wt.%) in experiments where decomposition of $LiBH_4$ within a carbon aerogel was monitored with FTIR spectroscopy.[61] We performed calculations to mimic the existence of a severe kinetic barrier for CH_4 formation by removing this species and all other hydrocarbons from the set of compounds that were considered. When this is done, H_2 is essentially the only gaseous product across the entire temperature range we considered, and the reactions proceed as predicted by Alapati *et al.*. If CH_4 is removed from these calculations but other hydrocarbons are not, then formation of aliphatic hydrocarbons with higher molecular weight than methane is predicted. Even in situations where some CH_4 is formed, it is unlikely that the conversion of CH_4 to H_2 and other products at the relatively low temperatures that are predicted by our calculations can proceed without severe kinetic limitations; development of catalysts that activate methane at low temperatures is an important challenge that has received considerable attention.[68]

We finally turn to the combination of $Mg(BH_4)_2$ and C. The thermodynamic properties of $Mg(BH_4)_2$ have been thoroughly investigated.[28, 55, 59, 69-73] $Mg(BH_4)_2$ is less stable than $LiBH_4$, but still decomposes at temperatures considered too high for vehicular hydrogen storage. Investigations of $Mg(BH_4)_2$ have therefore focused on destabilizing the material.[5-7] Alapati *et al.*

computationally predicted that $Mg(BH_4)_2$ can be destabilized by C.[6] Specifically, a 1:2 mixture of $Mg(BH_4)_2$ and C was predicted to react as follows:

$$Mg(BH_4)_2(s)+2C(s) \rightarrow MgB_2C_2(s)+4H_2(g) \quad (6.9)$$

As in the previous examples, those calculations did not include the possibility of gas-phase species other than H_2 or the formation of a $[B_{12}H_{12}]^{2-}$-containing condensed phase. Subsequent experiments made it clear that $MgB_{12}H_{12}$ forms during decomposition of $Mg(BH_4)_2$.[7, 69, 70]

Before examining the thermodynamic equilibrium of the $Mg(BH_4)_2$ + C, we first consider pure $Mg(BH_4)_2$. The resulting predictions for $Mg(BH_4)_2$ decomposition are shown in Fig. 6.8(a) and show that the hydride should decompose to form MgH_2, $MgB_{12}H_{12}$, and H_2 at 300 K by the following scheme:

$$Mg(BH_4)_2(s) \rightarrow \frac{5}{6}MgH_2(s)+\frac{1}{6}MgB_{12}H_{12}(s)+\frac{13}{6}H_2(g) \quad (6.10)$$

The formation of $MgB_{12}H_{12}$ agrees with experimental[70, 74, 75] and computational observations.[7] The predicted decomposition temperature of this species is also in agreement with the computational predictions by Ozolins *et al.*[7], but experiments indicate that higher temperatures are needed before this species is seen. At 520 K and 1 atm pressure, our calculations predict that the $MgB_{12}H_{12}$ compound becomes unstable in combination with MgH_2:

$$5MgH_2(s)+MgB_{12}H_{12}(s) \rightarrow 6MgB_2(s)+11H_2(g) \quad (6.11)$$

Our calculations do not include liquid MgH_2 or $Mg(BH_4)_2$, but we know of no experimental evidence that these phases are relevant under the conditions we considered.

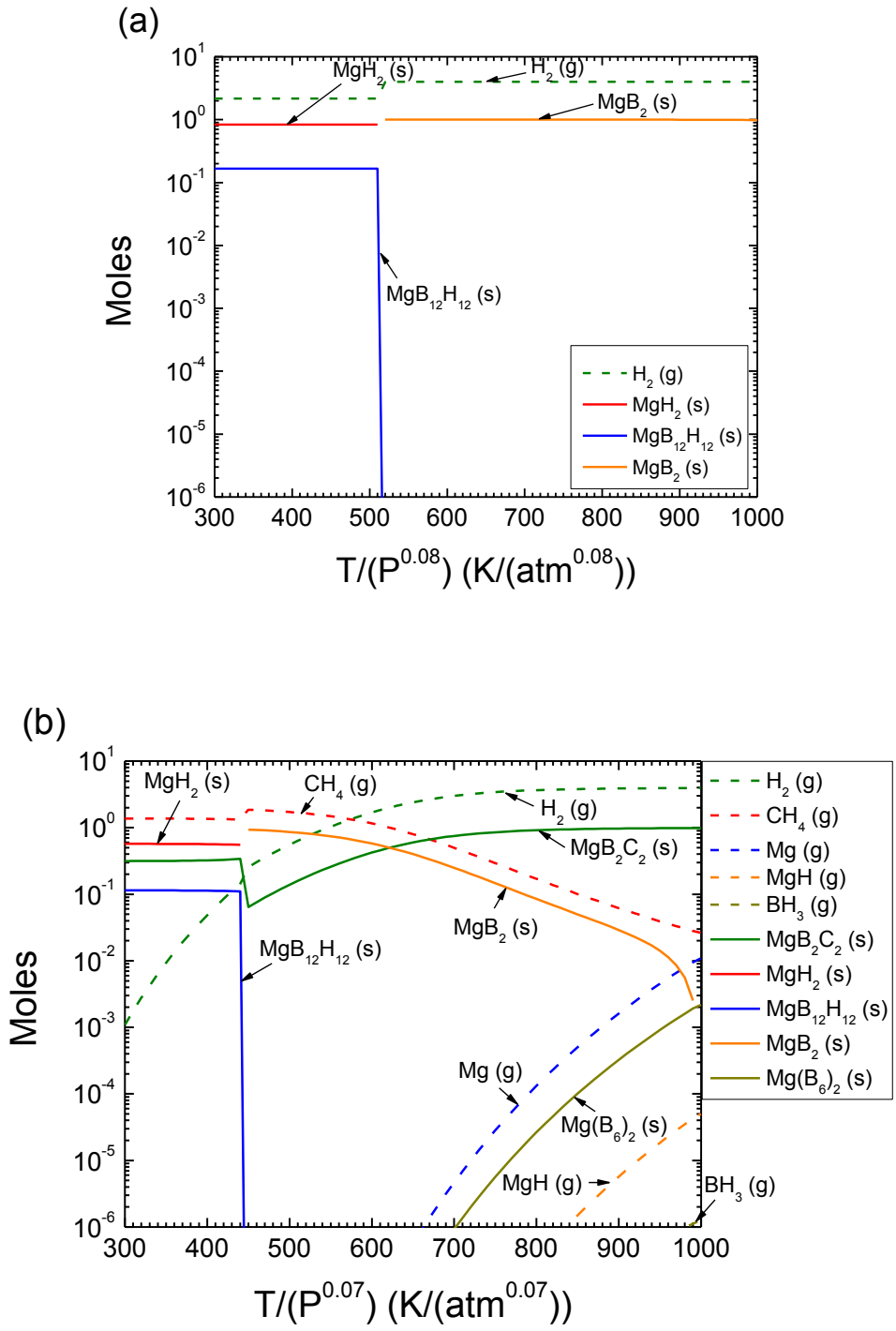

Figure 6.8: Predicted equilibrium composition (moles) of the gaseous and condensed-phase species corresponding to (a) $Mg(BH_4)_2$ and (b) $Mg(BH_4)_2$ + 2C (b). Results are displayed as a combined function of temperature and pressure (for clarity, we only show the case of 1 atm).

In a 1:1 mixture of $Mg(BH_4)_2$ and C, most of the C at 300 K and 1 atm is present as CH_4, although some solid MgB_2C_2 also exists, as shown in Fig. 6.8(b). Unlike the other two examples involving C discussed above, an appreciable amount of CH_4 (mole fraction ≥ 0.009) is present at all conditions that we examined. The presence of C in the system reduces the temperature at which $MgB_{12}H_{12}$ converts to other species. At 1 atm, this temperature reduction is ~60 K for the 1:1 mixture shown in Fig. 6.8(b). At elevated temperatures, most of the Mg in this mixture is present as MgB_2C_2, with only minor amounts of MgB_2. Almost no gases other than H_2 and CH_4 are predicted to exist below 600 K (at 1 atm total pressure), and at higher temperatures the only other gases are trace levels of Mg, MgH, and BH_3. The relatively high levels of CH_4 that we predict to be in equilibrium with this mixture suggest that even if complete equilibrium could be obtained in a practical setting it would be very difficult to use this mixture as a storage medium that could be cycled many times and that would generate relatively pure H_2.

6.7 Conclusions

In this chapter, we described the thermodynamic equilibrium including the possible evolution of gases other than H_2 in hydride systems based on $LiNH_2$, $LiBH_4$, $Mg(BH_4)_2$ and their mixtures with LiH, MgH_2, or C. Although the majority of research on materials for reversible storage of H_2 has focused on issues associated with favorable thermodynamics and hydrogen capacity as studied in earlier chapters, the generation or absence of gaseous impurities from any storage system could be decisive in the value of such a system in practical settings. The studies in earlier chapters that have applied first-principles calculations to searching for metal hydrides and their mixtures with attractive properties for reversible storage have typically assumed that H_2 is the only gas phase product. The approach we have introduced in this chapter couples first-principles (DFT) methods, which are used to obtain the thermodynamic properties of solid phases of interest, and free energy minimization incorporating a broad range of gaseous and liquid species to obtain a comprehensive thermodynamic picture of the metal hydride decomposition chemistry. This concept will be a valuable addition to computational efforts

designed to aid development of reversible storage applications by screening large numbers of materials.

One useful way to categorize the systems we have studied is to assess the purity of H_2 that is available at equilibrium in each case. To this end, we define *R* to be the fraction of H_2 that is observed at equilibrium relative to the amount of H_2 that would be predicted in the gas phase if H_2 was the only gaseous species considered in a thermodynamic calculation. The variation in *R* as a function of temperature at 1 atm pressure is shown for each system we considered in Fig. 6.9. The nominal reactions used to examine the amount of H_2 predicted in the gaseous phase if H_2 is the only gaseous species considered in a thermodynamic calculation are shown in Table 6.4. For $LiNH_2$, $LiBH_4$, and 2 $LiBH_4$ + MgH_2, *R* is very close to 1; that is, these examples are associated with very low levels of gas-phase impurities. The mixture $LiNH_2$ + LiH, in contrast, generates an appreciable level of N_2 and NH_3 when $LiNH_2$ decomposes, especially at temperatures above 700 K. All three of the mixtures we considered that included C, namely 2$LiNH_2$ + C, $LiBH_4$ + C, and $Mg(BH_4)_2$ + C, are associated with very impure H_2 except at high temperatures because of the strong thermodynamic stability of CH_4.

All of our calculations were performed for closed systems at constant pressure as a function of temperature. We showed that a relatively simple scaling of the pressure and temperature values can be used in almost all cases to condense the results from calculations at varying pressures. To make detailed comparisons between calculations of this type and specific experiments, care must be taken to describe the overall pressure history of the experiments. This pressure history can differ strongly from a single, constant pressure.[64, 76] Equally importantly, comparisons of this kind must account for the net removal of gases from the control volume if experiments are performed under dynamic vacuum or similar conditions. It would of course be helpful in experimentally assessing the issues we raise in this chapter if the practice of analyzing the composition of gases generated by heating of a metal hydride mixture was more widespread, instead of assuming that all weight loss is due to H_2.

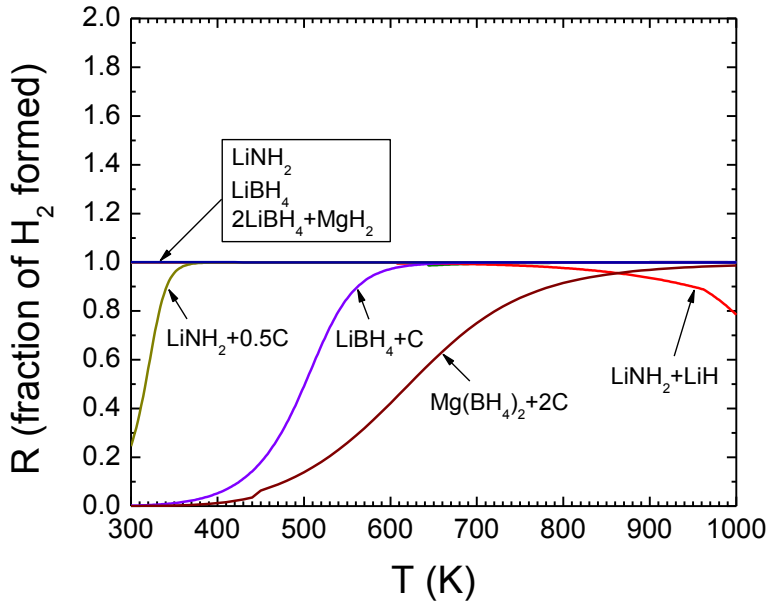

Figure 6.9: Mole fraction of H_2 predicted by our equilibrium calculations normalized with the H_2 available from the nominal reactions listed in Table 6.4 as a function of temperature for the seven systems considered in the chapter.

Table 6.4: The nominal reaction schemes of the seven systems considered in Fig. 6.9.

System	Nominal reaction
$LiNH_2$	$LiNH_2 \rightarrow 0.5Li_2NH+0.25N_2+0.75H_2$
($LiNH_2$ + LiH)	$LiNH_2+LiH \rightarrow Li_2NH+H_2$
$LiBH_4$	$LiBH_4 \rightarrow \frac{5}{6}LiH+\frac{1}{12}Li_2B_{12}H_{12}+\frac{13}{12}H_2$
	$Li_2B_{12}H_{12} \rightarrow 2LiH+12B+5H_2$
($LiBH_4$ + 0.5MgH_2)	$LiBH_4 \rightarrow \frac{5}{6}LiH+\frac{1}{12}Li_2B_{12}H_{12}+\frac{13}{12}H_2$
	$Li_2B_{12}H_{12}+6MgH_2 \rightarrow 2LiH+6MgB_2+11H_2$
($LiNH_2$ + C)	$LiNH_2+0.5C \rightarrow 0.5Li_2CN_2+H_2$
($LiBH_4$ + C)	$LiBH_4+C \rightarrow LiBC+2H_2$
($Mg(BH_4)_2$ + C)	$Mg(BH_4)_2+2C \rightarrow MgB_2C_2+4H_2$

Our results rely on the prediction of thermodynamic properties of a number of solids

using DFT calculations. The accuracy of these calculations for metal hydrides and related materials have been discussed extensively, but the most salient point is that the inexactness of DFT exchange-correlation functionals implies that these calculations are associated with unavoidable uncertainty. Estimates based on comparisons with well characterized experimental systems suggest that the DFT calculations we have used here give reaction free energies that are accurate within ±10 kJ/mol.[2-8] None of the key findings we report in this chapter appear to be sensitive to this uncertainty.

Reactions involving light metal hydrides and their mixtures are frequently affected by significant kinetic limitations. Even in materials that have been extensively studied, such as $NaAlH_4$, there is still considerable uncertainty associated with the detailed mechanisms that underlie these limitations. This situation greatly limits the possibility of rationally selecting catalysts or material treatment strategies that can enhance reaction kinetics. Our calculations only describe thermodynamic equilibrium, so it may superficially seem that using them to understand materials that are likely to be subject to kinetic limitations is problematic. We have shown, however, that equilibrium calculations can provide useful insight about the reaction mechanisms associated with light metal hydrides. To give just one example, our calculations indicate that the experimentally observed evolution of NH_3 during heating of $LiNH_2$ is not the equilibrium reaction path for this material. Instead, ammonia is formed during this process because the kinetics of forming N_2, which is a stable reaction product at equilibrium, from the solid are extremely slow. An additional unexpected result obtained from our calculations concerns the origin of nanoscale effects resulting from confinement of hydrides within nanoporous scaffolds. Our thermodynamic data are strictly applicable only to bulk species. However, comparison of experimental data obtained from bulk $LiBH_4$ and infiltrated carbon aerogels with the equilibrium prediction points to a major change in the reaction kinetics as a result of nanoconfinement. Such insights can focus future experiments and modeling to help establish the origins of nanoscale hydride destabilization.

6.8 REFERENCES

1. K. C. Kim and D. S. Sholl, *J. Phys. Chem. C*, 2010, **114**, 678-686.
2. S. V. Alapati, J. K. Johnson and D. S. Sholl, *J. Phys. Chem. B*, 2006, **110**, 8769-8776.
3. S. V. Alapati, J. K. Johnson and D. S. Sholl, *Phys. Chem. Chem. Phys.*, 2007, **9**, 1438-1452.
4. S. V. Alapati, J. K. Johnson and D. S. Sholl, *J. Alloys Compd.*, 2007, **446**, 23-27.
5. S. V. Alapati, J. K. Johnson and D. S. Sholl, *J. Phys. Chem. C*, 2007, **111**, 1584-1591.
6. S. V. Alapati, J. K. Johnson and D. S. Sholl, *J. Phys. Chem. C*, 2008, **112**, 5258-5262.
7. V. Ozolins, E. H. Majzoub and C. Wolverton, *J. Am. Chem. Soc.*, 2009, **131**, 230-237.
8. D. J. Siegel, C. Wolverton and V. Ozolins, *Phys. Rev. B*, 2007, **76**, 134102.
9. C. Wolverton and V. Ozolins, *Phys. Rev. B*, 2007, **75**, 064101.
10. D. J. Siegel, C. Wolverton and V. Ozolins, *Phys. Rev. B*, 2007, **75**, 014101.
11. B. Magyari-Kope, V. Ozolins and C. Wolverton, *Phys. Rev. B*, 2006, **73**, 220101.
12. K. C. Kim, A. D. Kulkarni, J. K. Johnson and D. S. Sholl, *in preparation*.
13. K. C. Kim, A. D. Kulkarni, J. K. Johnson and D. S. Sholl, *in preparation*.
14. A. R. Akbarzadeh, C. Wolverton and V. Ozolins, *Phys. Rev. B*, 2009, **79**, 184102.
15. A. R. Akbarzadeh, V. Ozolins and C. Wolverton, *Adv. Mater.*, 2007, **19**, 3233-3239.
16. Y. Nagahara, S. Sugawara and K. Shinohara, *J. Power Sources*, 2008, **182**, 422-428.
17. R. Halseid, P. J. S. Vie and R. Tunold, *J. Power Sources*, 2006, **154**, 343-350.
18. C. W. Bale, P. Chartrand, S. A. Degterov, G. Eriksson, K. Hack, R. B. Mahfoud, J. Melanqon, A. D. Pelton and S. Petersen, *CALPHAD*, 2002, **26**, 189-228.
19. M. D. Allendorf, R. B. Diver, N. P. Siegel and J. E. Miller, *Energy Fuels*, 2008, **22**, 4115-4124.
20. M. W. Chase, C. A. Davies, J. R. Downey, D. J. Frurip, R. A. Mcdonald and A. N. Syverud, *J. Phys. Chem. Ref. Data*, 1985, **14**, 1-926.
21. M. W. Chase, C. A. Davies, J. R. Downey, D. J. Frurip, R. A. Mcdonald and A. N. Syverud, *J. Phys. Chem. Ref. Data*, 1985, **14**, 927-1856.
22. J. P. Perdew, J. A. Chevary, S. H. Vosko, K. A. Jackson, M. R. Pederson, D. J. Singh and C. Fiolhais, *Phys. Rev. B*, 1992, **46**, 6671-6687.
23. G. Kresse and J. Hafner, *Phys. Rev. B*, 1993, **47**, 558-561.
24. G. Kresse and J. Furthmuller, *Phys. Rev. B*, 1996, **54**, 11169-11186.
25. D. Vanderbilt, *Phys. Rev. B*, 1990, **41**, 7892-7895.
26. G. Kresse and D. Joubert, *Phys. Rev. B*, 1999, **59**, 1758.
27. The Inorganic Crystal Structure Database (ICSD), http://www.fiz-informationsdienste.de/en/DB/icsd/.
28. J. H. Her, M. Yousufuddin, W. Zhou, S. S. Jalisatgi, J. G. Kulleck, S. J. H. Jason A. Zan, J. Robert C. Bowman and T. J. Udovic, *Inorg. Chem.*, 2008, **47**, 9757-9759.
29. K. Parlinski, *Software PHONON*, 2005.
30. G. J. Ackland, *J. Phys.: Condens. Matter.*, 2002, **14**, 2975-3000.
31. J. H. Yao, C. Shang, K. F. Aguey-Zinsou and Z. X. Guo, *J. Alloys Compd.*, 2007, **432**, 277-282.
32. L. L. Shaw, R. Ren, T. Markmaitree and W. Osborn, *J. Alloys Compd.*, 2008, **448**, 263-271.

33. S. Orimo, Y. Nakamori, G. Kitahara, K. Miwa, N. Ohba, T. Noritake and S. Towata, *Appl. Phys. A*, 2004, **79**, 1765-1767.
34. Y. Song and Z. X. Guo, *Phys. Rev. B*, 2006, **74**, 195120.
35. J. F. Herbst and J. L. G. Hector, *Phys. Rev. B*, 2005, **72**, 125120.
36. S. Isobe, T. Ichikawa, K. Tokoyoda, N. Hanada, H. Leng, H. Fujii and Y. Kojima, *Thermochimica Acta*, 2008, **468**, 35-38.
37. M. Gupta and R. P. Gupta, *J. Alloys Compd.*, 2007, **446-447**, 319-322.
38. P. Chen, Z. Xiong, J. Luo, J. Lin and K. L. Tan, *J. Phys. Chem. B*, 2003, **107**, 10967-10970.
39. H. Y. Leng, T. Ichikawa, S. Hino and H. Fujii, *J. Alloys Compd.*, 2008, **463**, 462-465.
40. Y. Nakamori and S. Orimo, *Mater. Sci. Eng. B*, 2004, **108**, 48-50.
41. T. Ichikawa, N. Hanada, S. Isobe, H. Leng and H. Fujii, *J. Phys. Chem. B*, 2004, **108**, 7887-7892.
42. J. Z. Hu, J. H. Kwak, Z. Yang, W. Osborn, T. Markmaitree and L. L. Shaw, *J. Power Sources*, 2008, **181**, 116-119.
43. K. F. Aguey-Zinsou, J. Yao and Z. X. Guo, *J. Phys. Chem. B*, 2007, **111**, 12531-12536.
44. S. Ikeda, N. Kuriyama and T. Kiyobayashi, *Inter. J. Hydrogen Energy*, 2008, **33**, 6201-6204.
45. T. Kar, S. Scheiner and L. Li, *J. Mol.Struc. THEOCHEM*, 2008, **857**, 111-114.
46. A. Zuttel, S. Rentsch, P. Fischer, P. Wenger, P. Sudan, P. Mauron and C. Emmenegger, *J. Alloys Compd.*, 2003, **356-357**, 515-520.
47. J. J. Vajo, S. L. Skeith and F. Mertens, *J. Phys. Chem. B*, 2005, **109**, 3719-3722.
48. A. Ibikunle, A. J. Goudy and H. Yang, *J. Alloys Compd.*, 2009, **475**, 110-115.
49. O. Friedrichs, J. W. Kim, A. Remhof, F. Buchter, A. Borgschulte, D. Wallacher, Y. W. Cho, M. Fichtner, K. H. Oh and A. Züttel, *Phys. Chem. Chem. Phys.*, 2009, **11**, 1515-1520.
50. R. L. Corey, D. T. Shane, J. Robert C. Bowman and M. S. Conradi, *J. Phys. Chem. C*, 2008, **112**, 18706-18710.
51. X. Y. Juan Xu, Zhiqing Zou, Zhilin Li, Zhu Wu, Daniel L. Akins and Hui Yang, *Chem. Commun.*, 2008, 5740-5742.
52. Z.-Z. Fang, X.-D. Kang, P. Wang and H. M. Cheng, *J. Phys. Chem. C*, 2008, **112**, 17023-17029.
53. Y. Nakamori, K. Miwa, A. Ninomiya, H. Li, N. Ohba, S. I. Towata, A. Zuttel and S. I. Orimo, *Phys. Rev. B*, 2006, **74**, 045126.
54. M. Au, W. Spencer, A. Jurgensen and C. Zeigler, *J. Alloys Compds.*, 2008, **462**, 303-309.
55. A. Zuttel, A. Borgschultea and S. I. Orimo, *Scr. Mater.*, 2007, **56**, 823-828.
56. N. Ohba, K. Miwa, M. Aoki, T. Noritake, S. I. Towata, Y. Nakamori, S. Orimo and A. Zuettel, *Phys. Rev. B*, 2006, **74**, 075110.
57. S. I. Orimo, Y. Nakamori, N. Ohba, K. Miwa, M. I. Oaki, S. Towata and A. Zuttel, *Appl. Phys. Lett.*, 2006, **89**, 021920.
58. S. J. Hwang, J. Robert C. Bowman, J. W. Reiter, J. Rijssenbeek, G. L. Soloveichik, J. C. Zhao, H. Kabbour and C. C. Ahn, *J. Phys. Chem. C*, 2008, **112**, 3164-3169.
59. S. Cahen, J. B. Eymery, R. Janot and J. M. Tarascon, *J. Power Sources*, 2009, **189**, 902-908.
60. S. J. Hwang, J. Robert C. Bowman, J. W. Reiter, J. Rijssenbeek, G. L. Soloveichik, J. C. Zhao, H. Kabbour and C. C. Ahn, *J. Phys. Chem. C*, 2008, **112**, 3164-3169.

61. A. F. Gross, J. J. Vajo, S. L. Van Atta and G. L. Olson, *J. Phys. Chem. C*, 2008, **112**, 5651-5657.
62. P. A. Berseth, A. G. Harter, R. Zidan, A. Blomqvist, C. M. Araujo, R. H. Scheicher, R. Ahuja and P. Jena, *Nano Lett.*, 2009, **9**, 1501-1505.
63. http://webbook.nist.gov/chemistry/.
64. F. E. Piinkerton, M. S. Meyer, G. P. Meisner, M. P. Balogh and J. J. Vajo, *J. Phys. Chem. C*, 2007, **111**, 12881-12885.
65. Z. Z. Fang, P. Wang, T. E. Rufford, X. D. Kang, G. Q. Lu and H. M. Cheng, *Acta Mater.*, 2008, **56**, 6257-6263.
66. R. Campesi, F. Cuevas, E. Leroy, M. Hirscher, R. Gadiou, C. Vix-Guterl and M. Latroche, *Micropor. Mesopor. Mat.*, 2009, **117**, 511-514.
67. Y. Zhang, W.-S. Zhang, A.-Q. Wang, L.-X. Sun, M.-Q. Fan, H.-L. Chu and J.-C. S. T. Zhang, *Int. J. Hydrogen Energy*, 2007, **32**, 3976-3980.
68. M. Schlangen and H. Schwarz, *Dalton Trans.*, 2009, 10155-10165.
69. H. W. Li, K. Kikuchi, Y. Nakamori, N.Ohba, K. Miwa, S. Towata and S. Orimo, *Acta Mater.*, 2008, **56**, 1342-1347.
70. G. L. Soloveichik, M. Andrusa, Y. Gaoa, J. C. Zhao and S. Kniajanski, *Inter. J. Hydrogen Energy*, 2009, **34**, 2144-2152.
71. M. J. Ingleson, J. P. Barrio, J. Bacsa, A. Steiner, G. R. Darling, J. T. A. Jones, Y. Z. Khimyak and M. J. Rosseinsky, *Angew. Chem. Int. Ed.*, 2009, **48**, 2012-2016.
72. T. Matsunagaa, F. Buchtera, P. Maurona, M. Bielmana, Y. Nakamoric, S. Orimoc, N. Ohbad, K. Miwad, S. Towatad and A. Züttel, *J. Alloys Compd.*, 2008, **459**, 583-588.
73. H. W. Li, K. Miwa, N. Ohba, T. Fujita, T. Sato, Y. Yan, S. Towata, M. W. Chen and S. Orimo, *Nanotechnology*, 2009, **20**, 204013.
74. N. Hanada, K. Chlopek, C. Frommen, W. Lohstroh and M. Fichtner, *J. Mater. Chem.*, 2008, **18**, 2611-2614.
75. H. W. Li, K. Kikuchi, T. Sato, Y. Nakamori, N. Ohba, M. Aoki, K. Miwa, S. Towata and S. Orimo, *Mater. Trans.*, 2008, **49**, 2224-2228.
76. X. Wan, T. Markmaitree, W. Osborn and L. L. Shaw, *J. Phys. Chem. C*, 2008, **112**, 18232-18243.

CHAPTER 7

CONCLUSIONS

Metal hydride is a good candidate for H_2 storage applications in the sense that it can strongly store hydrogen in atomic form with high H_2 capacity. However, unfavorable thermodynamics and poor kinetics of metal hydrides should be solved for the use of hydrogen as fuel of on board applications.[1-11] Based on the idea that kinetics of metal hydrides can be enhanced by adding catalysts[4, 12, 13] or controlling a particle size[4, 8, 14-18], we have only described the issue of metal hydride thermodynamics in this thesis. Indeed, a number of reports showed the positive effect of catalysts and controlled particle size on a reaction rate. Bogdanovic et al. used Ti as a catalyst to improve kinetics of $NaAlH_4$ decomposition reaction.[13] Li et al. showed that the reduction of Mg particle size leaded to the shortened diffusion length of H in the particle so improved kinetics.[8] On the other hand, thermodynamics of metal hydrides are determined by the type of materials associated with a reaction. It indicates that unfavorable thermodynamics of a metal hydride mixture can be only improved by using a combination of any other materials having favorable thermodynamics.

In this thesis, we showed that the thermodynamic examinations of metal hydrides could be approachable on the various points of view. We first approached metal hydride study focusing on the improvement of their thermodynamics. In Chapter 2, we discussed about the relation between the particle size of simple metal hydrides and thermodynamics of their decomposition reactions. From Chapter 3 to Chapter 5, our thermodynamic calculations based on the grand canonical linear programming method could screen many promising metal hydride mixtures having favorable thermodynamics and releasing a H_2 via single or multi step. We also identified minimum free energy paths for the selected promising mixtures through the consideration of vibrational and entropic contributions. We next approached metal hydride study in another point of view. In Chapter 6, we showed that reaction thermodynamics could be quite different when

the impurity gases other than H_2 were present. This study was focused on the examination of the thermodynamic equilibrium of all phases at each temperature and a fixed total pressure. The examination provided the thermodynamic relation of $N_2/H_2/NH_3$ mixture.

The main idea of this thesis is that combinations of promising metal hydride mixtures can be rigorously and efficiently screened from large collection of possible mixtures through our grand canonical linear programming method combined with the density functional theory (DFT) calculations. We started with finding promising single-step reactions associated with three metal hydrides ($LiK(BH_4)_2$, KBH_4, and $NaBH_4$) in Chapter 3. Although most of the predicted single-step reactions produced undesirable compounds, it is noticeable that our method efficiently screened all possible reactions involving one of the three metal hydrides. Another main conclusion of this study was that $LiK(BH_4)_2$ was predicted to be unstable at almost all temperatures. Based on the result, our study was extended to a much larger number of mixtures in Chapter 4. All of our thermodynamic examinations in Chapter 4 were performed based on the updated database. Our calculations predicted 74 promising single step reactions categorized by several classes. First, we identified 52 single step reactions involving the kinetically stable $B_{12}H_{12}$ containing species or refractory materials which made the reactions irreversible. Second, we identified 19 single step reactions involving graphite, C including materials, or KC_8 in which our prediction may differ from experimental observations due to the formation of non-H_2 gases at equilibrium state. Third, we found three interesting single step reactions which did not have any of the undesirable compounds discussed above. Among the interesting reactions, the mixture of $LiNH_2$:LiH:KBH_4 with the ratio of 2:1:1 was a good candidate for reversible hydrogen storage applications in the sense that the reaction would release a sufficient amount of H_2 at desirable temperatures and H_2 pressures in spite of the DFT uncertainty. Our calculations additionally identified 23 promising metal hydride mixtures releasing H_2 via multi step. Seven of them included steps linked with one or more intermediate compounds, while the rest of them included independent steps without linking. This examination shows the new approach associated with predicting promising metal hydride mixtures using a linear program.

Our ultimate purpose in examining thermodynamics of promising metal hydride mixtures was to identify minimum free energy paths at finite temperatures. However, the reaction paths of the promising mixtures predicted in Chapter 4 were the most stable paths predicted using 0 K reaction enthalpy changes at a H_2 pressure of 1 bar. It was therefore possible that the most stable paths might be changed with H_2 pressure or according to the vibrational and entropic contributions to the free energy. We identified the most stable free energy paths for thirteen promising single-step reactions chosen in the list of the 74 promising single-step reactions as stated in Chapter 5. Eight of the thirteen promising reactions had reaction mechanisms predicted using 0 K reaction enthalpy changes as the most stable free energy paths at H_2 pressures of 1 ~ 100 bar, demonstrating that our grand potential approach efficiently provided the reliable reaction thermodynamics without the consideration of the vibrational and entropic contributions. One interesting example discussed in Chapter 5 was the mixture of $LiNH_2$:LiH:KBH_4 with the ratio of 2:1:1. As discussed in Chapter 5, this reaction had two distinct stable paths with H_2 pressures, indicating that H_2 pressure should be maintained within the range of 90.1 ~ 100 bar to release a sufficient amount of H_2 without producing any undesirable compounds at temperatures desirable for reversible hydrogen storage applications. Although our examination precisely specified the most stable paths of reactant mixtures at varied H_2 pressures as just described, the relative reaction free energy changes of all possible paths for each reaction indicated that we could not make an unambiguous conclusion about the favored reaction path based on DFT calculations at the broad range of temperatures and H_2 pressures.

As stated early, our main strategy for improving thermodynamics of metal hydrides in Chapters 3, 4, and 5 was to find bulk metal hydrides or their mixtures having favorable thermodynamics. However, we were eager to improve thermodynamics by controlling a particle size along with the focus on the bulk phase reactions of metal hydrides. We specifically carried out the thermodynamic examination with seven simple metal hydrides to identify the relation between the particle size and the reaction temperature as stated in Chapter 2. Mainly, we identified that the trend of the reaction temperature of each seven particle according to the

particle size was characterized by total surface energy difference between the metal hydride form and the metal form of each particle. We identified through the additional charge analysis that the trend was intimately related to the ionicity of metal-hydrogen bond in the metal hydrides.

We provided another point of view for thermodynamics of metal hydrides in Chapter 6. In this chapter, we focused on demonstrating the possible evolution of the impurity gases other than H_2 instead of predicting promising reaction thermodynamics involving metal hydrides with the pure H_2. We used the FactSage program[19, 20] to examine the thermodynamic equilibrium of a system including gas, liquid, and solid phases of interest at each temperature and a fixed pressure. The change of the thermodynamic equilibrium with temperature provided reaction schemes involving the impurity gases. Our examination basically provides two conclusions. First, even though the mixture of N_2 and H_2 is thermodynamically favored rather than NH_3, the kinetic limitation of N_2 evolution leads to the evolution of NH_3 in real reaction systems. Second, methane is very stable phase at low temperatures, so the evolution of methane in C-involving systems would be inevitable. These two conclusions lead to the expectation of the same results in the similar systems such as $Mg(NH_2)_2$, KNH_2, $Ca(BH_4)_2$+2C, and $MgB_{12}H_{12}$+C.

This thesis only focused on reaction thermodynamics of metal hydrides. Therefore, it did not provide any information associated with reaction kinetics even though understanding the reaction kinetics of metal hydrides is one of the main focuses in hydrogen storage study. To understand the reaction kinetics, the mechanisms related to the dissociation of H_2 and diffusion of H should be figured out. Recently, Hao and Sholl identified the H defect – induced diffusion mechanism in MgH_2 and $NaMgH_3$.[21] They reported that H diffusion was dominated by the system of charged defects and the diffusivity of H depended on the defect formation energy and the activation barrier of a diffusion path of the defect. This report shows that first-principles calculations can help to examine kinetics of H diffusion in metal hydride systems. The study on the dissociation of H_2 would be also possible by examining hydrogen spillover on the catalyst based systems from first-principles calculations.[22]

7.1 REFERENCES

1. J. Graetz, J. J. Reilly, J. G. Kulleck and R. C. Bowman, *J. Alloys Compd.*, 2007, **446**, 271-275.
2. F. E. Pinkerton, *J. Alloys Compd.*, 2005, **400**, 76-82.
3. A. Sudik, J. Yang, D. Halliday and C. Wolverton, *J. Phys. Chem. C*, 2007, **111**, 6568-6573.
4. T. Vegge, *Phys. Chem. Chem. Phys.*, 2006, **8**, 4853-4861.
5. J. Graetz and J. J. Reilly, *Scripta Materialia*, 2007, **56**, 835-839.
6. M. Aoki, K. Miwa, T. Noritake, G. Kitahara, Y. Nakamori, S. Orimo and S. Towata, *Appl. Phys. A*, 2005, **80**, 1409.
7. S. Li, P. Jena and R. Ahuja, *Phys. Rev. B*, 2006, **74**, 132106-132104.
8. W. Li, C. Li and H. M. J. Chen, *J. Am. Chem. Soc.*, 2007, **129**, 6710-6711.
9. O. M. Løvvik and S. M. Opalka, *Phys. Rev. B*, 2005, **71**, 054103.
10. J. Lu, Z. Z. Fang and H. Y. Sohn, *Inorg. Chem.*, 2006, **45**, 8749-8754.
11. S. V. Alapati, J. K. Johnson and D. S. Sholl, *J. Phys. Chem. C*, 2008, **112**, 5258-5262.
12. W. Luo and K. J. Gross, *J. Alloys Compd.*, 2004, **385**, 224.
13. B. Bogdanovíc and M. Schwickardi, *J. Alloys Compd.*, 1997, **253-254**, 1.
14. A. F. Gross, J. J. Vajo, S. L. Van Atta and G. L. Olson, *J. Phys. Chem. C*, 2008, **112**, 5651-5657.
15. M. Fichtner, J. Engel, O. Fuhr, O. Kircher and O. Rubner, *Mater. Sci. Eng. B*, 2004, **108**, 42-47.
16. A. Pundt, *Adv. Eng. Mat.*, 2004, **6**, 11-21.
17. S. Bouaricha, J.-P. Dodelet, D. Guay, J. Huot and R. Schulz, *J. Maters. Res*, 2001, **16**, 2893.
18. J. Huot, G. Liang and R. Schulz, *Appl. Phys. A*, 2001, **72**, 187.
19. C. W. Bale, P. Chartrand, S. A. Degterov, G. Eriksson, K. Hack, R. B. Mahfoud, J. Melanqon, A. D. Pelton and S. Petersen, *CALPHAD*, 2002, **26**, 189-228.
20. M. D. Allendorf, R. B. Diver, N. P. Siegel and J. E. Miller, *Energy Fuels*, 2008, **22**, 4115-4124.
21. S. Hao and D. S. Sholl, *Appl. Phys. Lett.*, 2008, **93**, 251901.
22. A. J. Du, S. C. Smith, X. D. Yao and G. Q. Lu, *J. Phys. Chem. B*, 2005, **109**, 18037-18041.